University of Kentucky
UKnowledge

Theses and Dissertations--Earth and Environmental Sciences

Earth and Environmental Sciences

2017

THE OLIGOCENE WEST ELK BRECCIA: EVIDENCE FOR MASSIVE VOLCANIC DEBRIS AVALANCHES IN THE EASTERN GUNNISON RIVER VALLEY, WEST-CENTRAL COLORADO, U.S.A.

Patrick J. Whalen
University of Kentucky, PatrickJamesWhalen@gmail.com
Digital Object Identifier: https://doi.org/10.13023/ETD.2017.162

Right click to open a feedback form in a new tab to let us know how this document benefits you.

Recommended Citation

Whalen, Patrick J., "THE OLIGOCENE WEST ELK BRECCIA: EVIDENCE FOR MASSIVE VOLCANIC DEBRIS AVALANCHES IN THE EASTERN GUNNISON RIVER VALLEY, WEST-CENTRAL COLORADO, U.S.A." (2017). *Theses and Dissertations--Earth and Environmental Sciences*. 47.
https://uknowledge.uky.edu/ees_etds/47

This Master's Thesis is brought to you for free and open access by the Earth and Environmental Sciences at UKnowledge. It has been accepted for inclusion in Theses and Dissertations--Earth and Environmental Sciences by an authorized administrator of UKnowledge. For more information, please contact UKnowledge@lsv.uky.edu.

STUDENT AGREEMENT:

I represent that my thesis or dissertation and abstract are my original work. Proper attribution has been given to all outside sources. I understand that I am solely responsible for obtaining any needed copyright permissions. I have obtained needed written permission statement(s) from the owner(s) of each third-party copyrighted matter to be included in my work, allowing electronic distribution (if such use is not permitted by the fair use doctrine) which will be submitted to UKnowledge as Additional File.

I hereby grant to The University of Kentucky and its agents the irrevocable, non-exclusive, and royalty-free license to archive and make accessible my work in whole or in part in all forms of media, now or hereafter known. I agree that the document mentioned above may be made available immediately for worldwide access unless an embargo applies.

I retain all other ownership rights to the copyright of my work. I also retain the right to use in future works (such as articles or books) all or part of my work. I understand that I am free to register the copyright to my work.

REVIEW, APPROVAL AND ACCEPTANCE

The document mentioned above has been reviewed and accepted by the student's advisor, on behalf of the advisory committee, and by the Director of Graduate Studies (DGS), on behalf of the program; we verify that this is the final, approved version of the student's thesis including all changes required by the advisory committee. The undersigned agree to abide by the statements above.

Patrick J. Whalen, Student

Dr. Frank Ettensohn, Major Professor

Dr. Edward Woolery, Director of Graduate Studies

THE OLIGOCENE WEST ELK BRECCIA: EVIDENCE FOR MASSIVE VOLCANIC DEBRIS AVALANCHES IN THE EASTERN GUNNISON RIVER VALLEY, WEST-CENTRAL COLORADO, U.S.A.

THESIS

A thesis submitted in partial fulfillment of the
requirements for the degree of Master of Science in the
College of Arts and Sciences
at the University of Kentucky

By

Patrick Whalen

Lexington, Kentucky

Director: Dr. Frank Ettensohn, Professor of Geology

Lexington, Kentucky

2017

Copyright © Patrick James Whalen, 2017

ABSTRACT OF THESIS

THE OLIGOCENE WEST ELK BRECCIA: EVIDENCE FOR MASSIVE VOLCANIC DEBRIS AVALANCHES IN THE EASTERN GUNNISON RIVER VALLEY, WEST-CENTRAL COLORADO, U.S.A.

The West Elk Breccia has been studied since the late 1800's with many interpretations regarding its origin. One unrecognized possibility is that parts of it are debris-avalanche deposits. This study has recognized evidence for this interpretation at three scales: volcano scale, outcrop scale, and intra-outcrop scale. At the volcano scale, a scarp in the old volcano reveals underlying Mesozoic bedrock, suggesting sector collapse. At the outcrop scale, megablocks of the original edifice, up to hundreds of meters in length, have atypical orientations and are surrounded by a gravel matrix. At the intra-outcrop scale, jigsaw-fit fracturing and rip-up clasts are common in distal deposits, which are documented in analogous debris-avalanche deposits. Similar to the debris-avalanche deposit at Mt. Shasta, medial-to-distal-matrix volcaniclast content decreases by 23%; Paleozoic and Mesozoic clasts increase by 5%; and the size of megablocks decreases. The geochemical and petrographic signatures reveal breccia blocks composed of pyroxene-andesite, a more silicic matrix facies, and the andesitic-to-dacitic East Elk Creek Tuff, all compositions that corroborate previous work on this northern extension of the San Juan volcanic field. Measured sections in the 100-km² study area allow for an estimation of total formation volume of approximately 8.5 km^3.

KEYWORDS: volcanic debris avalanches, debris flows, volcaniclastics, megaclasts, jigsaw fractures, volcanic breccia

Patrick Whalen

March 30, 2017

THE OLIGOCENE WEST ELK BRECCIA: EVIDENCE FOR MASSIVE VOLCANIC DEBRIS AVALANCHES IN THE EASTERN GUNNISON RIVER VALLEY, WEST-CENTRAL COLORADO, U.S.A.

By

Patrick James Whalen

Dr. Frank Ettensohn

Director of Thesis

Dr. Edward Woolery

Director of Graduate Studies

March 30, 2017

ACKNOWLEDGMENTS

I am indebted to my advisor, Dr. Frank Ettensohn, for his sincere guidance, patience, passion, and expertise. My committee, Drs. Mike McGlue and Dave Moecher, were also incredibly patient, having listened to painful early interpretations. Dr. Alan Stork at Western State Colorado University provided good conversation and insight. I owe many thanks to my field assistant, Jason Orr, who worked tirelessly with me and maintained a positive attitude despite frequent thunderstorms. Dr. James Vallance at the Cascade Volcano Observatory gratefully provided literature and insight that served this investigation well. Jason Backus at the Kentucky Geological Survey was very helpful in the preparation and analysis of samples for bulk-rock geochemistry. The entire Earth and Environmental Science department at the University of Kentucky and the local Earth science community were very supportive. Finally, I am indebted to my family and friends who have earned my loyalty and to whom I owe a great deal.

This work was funded by a teaching assistantship from the Department of Earth and Environmental Sciences at the University of Kentucky, grants from the Geological Society of America, the Society for Sedimentary Geologists (SEPM), and the Colorado Scientific Society. Partial funding for meeting presentations and thin-sections were provided by the Department's Brown-McFarlan Fund and the Ferm Fund. Other support came from Drs. Mike McGlue and Ryan Thigpen, who provided employment during non-fieldwork time in the summer of 2016.

TABLE OF CONTENTS

LIST OF TABLES

LIST OF FIGURES

CHAPTER 1: Introduction

1.1 Motivation

On May 18, 1980, a catastrophic failure of the north flank of Mt. St. Helens Washington (U.S.A.) led to a lateral blast, debris avalanche, and many debris flows, all of which characterized this as a historic eruption. The cause was a partial collapse of the volcano and release of an enormous amount of pressure from the magma chamber (Glicken, 1996). A huge eruption and debris avalanche ensued. Although the event was catastrophic and several lives were lost, the situation would have been much worse had geoscientists from the Cascade Volcano Observatory not warned the public when the threat of eruption was imminent.

Eruptions with mass casualties, unfortunately, are not uncommon phenomena. For example, the Nevado del Ruiz volcano in Colombia erupted on November 13, 1985. Pyroclastic flows combined with melted snow and ice to form a voluminous lahar (Pierson et al., 1990). The combination of an ice-capped summit, large-volume eruption, and seismic shaking caused a liquefied debris flow that buried the unsuspecting town of Armero. The resulting death toll was nearly 23,000 (Pierson et al., 1990).

Although terribly devastating, these eruptions have spurred investigations of sedimentary processes at volcanoes and resulted in much new knowledge about volcanoes across the globe. Geologists are now turning to the geologic record to uncover the history of eruptions at ancient volcanoes, and hence, better prepare for future events. Although eyewitness observations from active volcanoes yield much useful data for understanding the evolution of such volcanic eruptions, volcaniclastic events like that at

Mt. St. Helens are rare on human time scales. It is just as important that the earth science community continue to develop knowledge of these processes from the geologic record as well. This is already being done in the Cascade Range where hazard maps have been developed for the most threatening volcanoes (Fig. 1.1). This study aims to add to the growing knowledge of volcanic sedimentation, particularly from an ancient volcanic terrane, the West Elk Mountains of west-central Colorado.

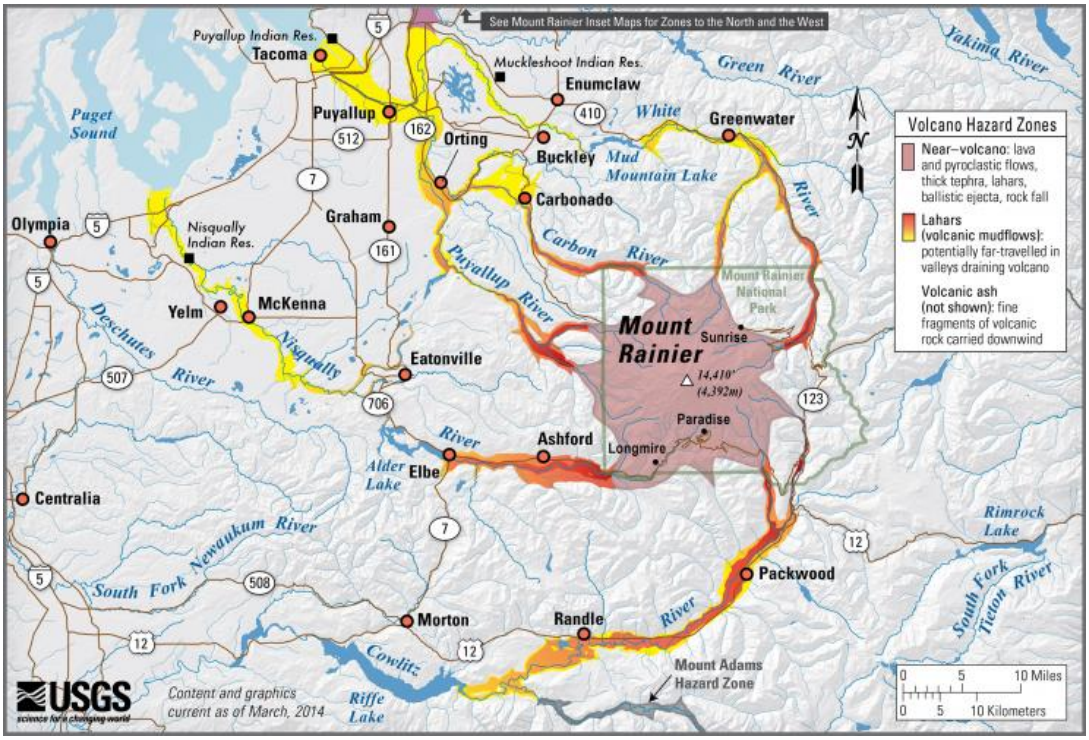

Figure 1.1. Basic ground-hazard map for communities near Mt. Rainier in northern Washington. The map was developed from studies of volcanic deposits (https://volcanoes.usgs.gov/observatories/cvo/hazards.html; accessed 12/21/16).

1.2 Study Location and Setting

The West Elk Breccia is a widely distributed volcaniclastic deposit centered on an Oligocene volcanic center in the West Elk Mountains of west-central Colorado in the southern Rocky Mountain Physiographic Province (Fig. 1.2). The West Elk range is composed of many laccoliths and fossil volcanic vents west of the Elk and Sawatch ranges of central Colorado (Fig. 1.2). Ohio Creek drains the region between the West Elk Mountains and the Flat Top and Red Mountain areas. Flat Top and Red Mountain divide the drainage of Ohio Creek and the head of the Gunnison River near Almont, Colorado (Fig. 1.2). At the northern edge of the town of Gunnison, Ohio Creek drains into the Gunnison River. Due east of Gunnison and parallel to U.S. 50, Tomichi Creek drains the southwestern Sawatch Range and southern Elk Mountains before emptying into the Gunnison River southwest of Gunnison. South of the Gunnison River and Tomichi Creek are the central San Juan Mountains, including Cochetopa Pass and Ouray (Fig. 1.2). About 65-miles west of Gunnison is the town of Montrose and the start of the Colorado Plateau physiographic province (Fig. 1.3).

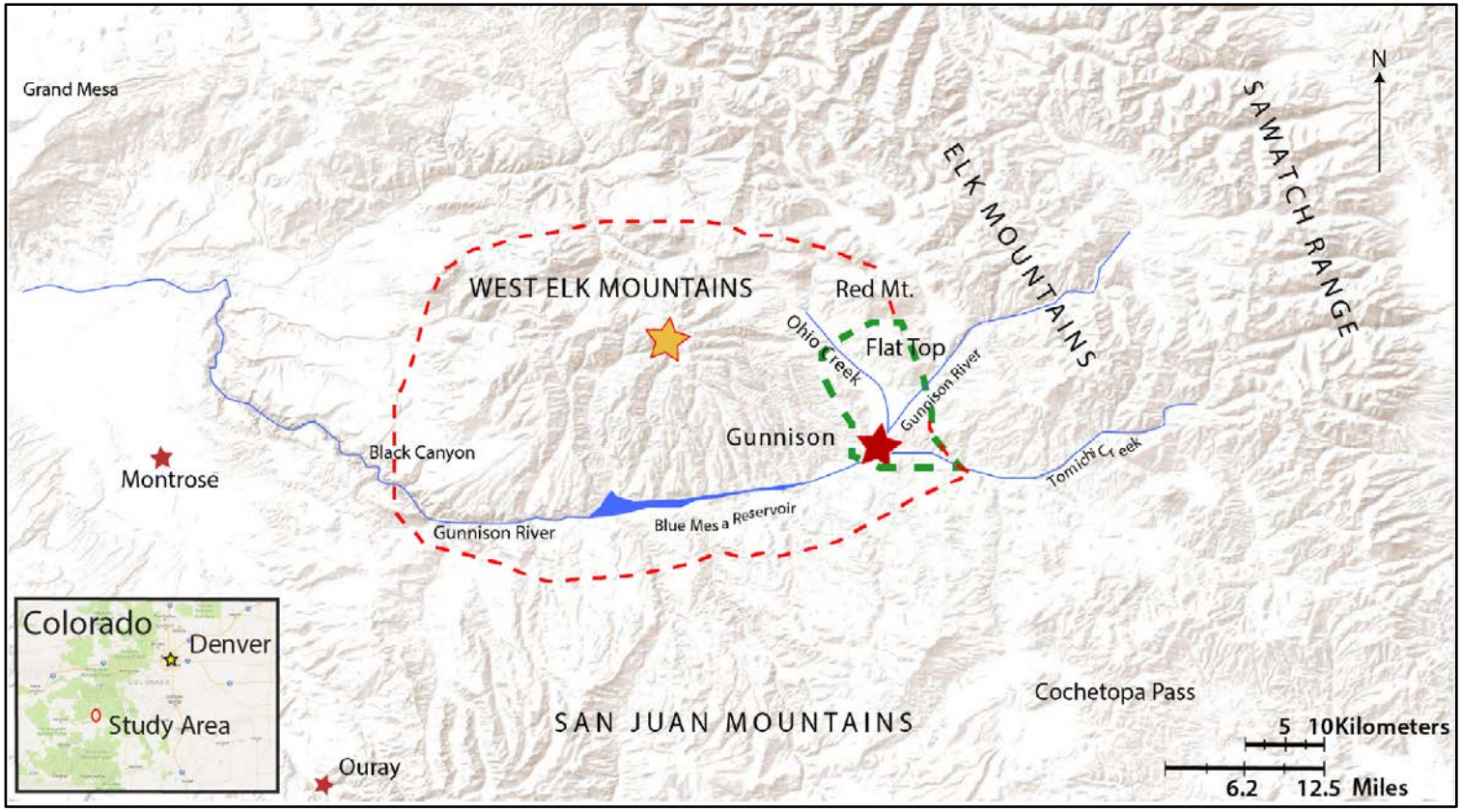

Figure 1.2. General distribution of the West Elk Breccia (red, dashed line) and study area (green, dashed line). The volcanic center is marked by the yellow star.

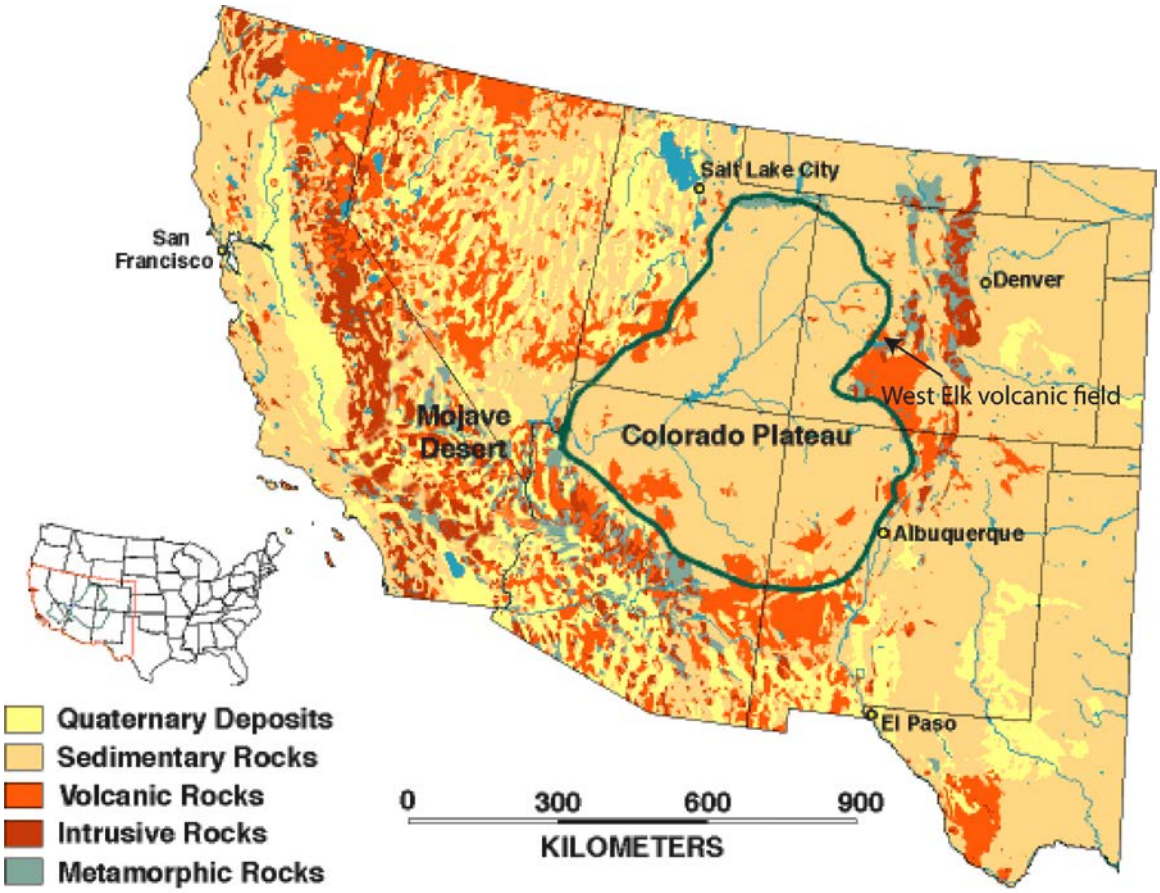

Figure 1.3. Regional setting during the Cenozoic Era for the southwestern U.S. Note the West Elk volcanic field near the eastern margin of the Colorado Plateau. The mountainous area east of the Colorado Plateau (red, orange and blue colors) largely comprise the Southern Rocky Mountain physiographic province (modified from http://higheredbcs.wiley.com/legacy/college/levin/0471697435/chap_tut/chaps/chapter 15-04.html; accessed 2-10-17).

1.3 Previous Work

Hayden (1874) made the first observations of the "eruptive geology" of the Elk and West Elk mountains. Some early workers believed that the tuffaceous conglomerate seen in the distal deposits relative to the volcanic center (Fig. 1.4), with poorly sorted cobbles and boulders, was glacial till and noted striations on rocks as evidence (Atwood

and Atwood, 1926). Van Houten (1957) reevaluated the "Gunnison Tillite," as it was then known, and showed that striations like these could be formed from clast-on-clast abrasion during debris-flow transport. Van Houten (1957) also noted the abundance of volcaniclasts, common volcanic minerals, and even pumice. Many geologic quadrangles have been mapped in the field area (e.g., Gunnison and Signal Peak quadrangles), and wherever mapped, the West Elk Breccia has primarily been shown as one unit (Hansen, 1971; Hedlund and Olson, 1973, 1974; Hedlund, 1974). Stork et al. (2006, 2007) have also mapped the West Elk Breccia as a single unit, but differentiated several Tertiary gravel units on the Gunnison and Signal Peak geologic quadrangle maps, including a gravel unit in the West Elk Breccia. Hansen (1965), in his detailed report on the local geology, referred to the West Elk Breccia as coming from a wide variety of sources and even suggested, "…explosive destruction of previously formed volcanic cones…," as a source for the enormous volume of material seen in the Black Canyon area. It is now widely accepted that the West Elk Breccia is volcaniclastic with a source located in the West Elk Mountains (Stork et al., 2006, 2007; Williams and Chronic, 2014). Coven et al., (1999) radiometrically dated the West Elk Breccia via Ar-Ar dating of plagioclase crystals from breccia and dikes near the volcanic center. They report an age of 30 Ma ± 0.5 Ma (Coven et al., 1999).

These early workers accepted a sequential, layered aggradation of material for emplacement of the West Elk Breccia. Workers like Hansen (1965), Hedlund and Olson (1973), Gaskill et al. (1981) and Stork et al. (2006, 2007) have described the West Elk Breccia in the Gunnison River valley as a series of heterolithologic breccias of mudflow

or lahar origin. They noted variations in the layers, such as pyroclastic, mud-flow, and debris-flow units.

Figure 1.4. Upper: Photograph by Atwood and Atwood (1926) the white line marks what they believed was the contact between the lower Gunnison Tillite and the upper volcanic tuff. Interestingly the contact does not include a large block of "volcanic tuff" or volcanic breccia (black line and arrow) at the base of the large outcrop. **Lower:** Modern photo of the same outcrop showing a close-up view from an area on the right-hand side of the Atwoods' photo with the "contact" marked by the black line. Note the large block of volcanic tuff (volcanic breccia) at the lower right.

Gaskill et al. (1981) completed the most extensive study of the West Elk Breccia. They identified three primary facies: a basal cone facies, a chaotic facies, and a volcaniclastic facies (Fig. 1.5). The basal cone facies shows little evidence of primary extrusive flow emplacement and is entirely intrusive breccia of basaltic andesite and diorite composition. The chaotic facies may represent early cone formation and volcaniclastic deposition with a heterogeneous mixture of lava and breccia flows. The volcaniclastic facies occupies the greatest volume and area, and Gaskill et al. (1981) described it as, "…gently dipping, crudely layered tuff breccias, local ash beds, laharic breccias, lava flows, minor tuffaceous conglomerate and epiclastic deposits." The distal deposits of this study would fall into the volcaniclastic facies of Gaskill et al. (1981). They described these rocks as being petrographically similar to the basal cone facies, having thicknesses up to 500 m. They suggested that some proximal deposits could be subdivided into four or more mappable units.

Lipman (1970, 1978) and Lipman et al. (1969) have detailed the geochemistry and petrologic evolution of the San Juan volcanic field, of which the West Elk volcanic field is a part. They noted that there was an early intermediate phase, which includes the West Elk Breccia, which was followed by a potassic or silicic phase (ignimbrite sheets of the San Juan calderas), and a final bimodal phase of mafic and felsic deposition and emplacement (Lipman et al., 1969) that includes the Miocene Hinsdale Basalt, which overlies the West Elk Breccia on Flat Top and Red Mountain (Fig. 1.2).

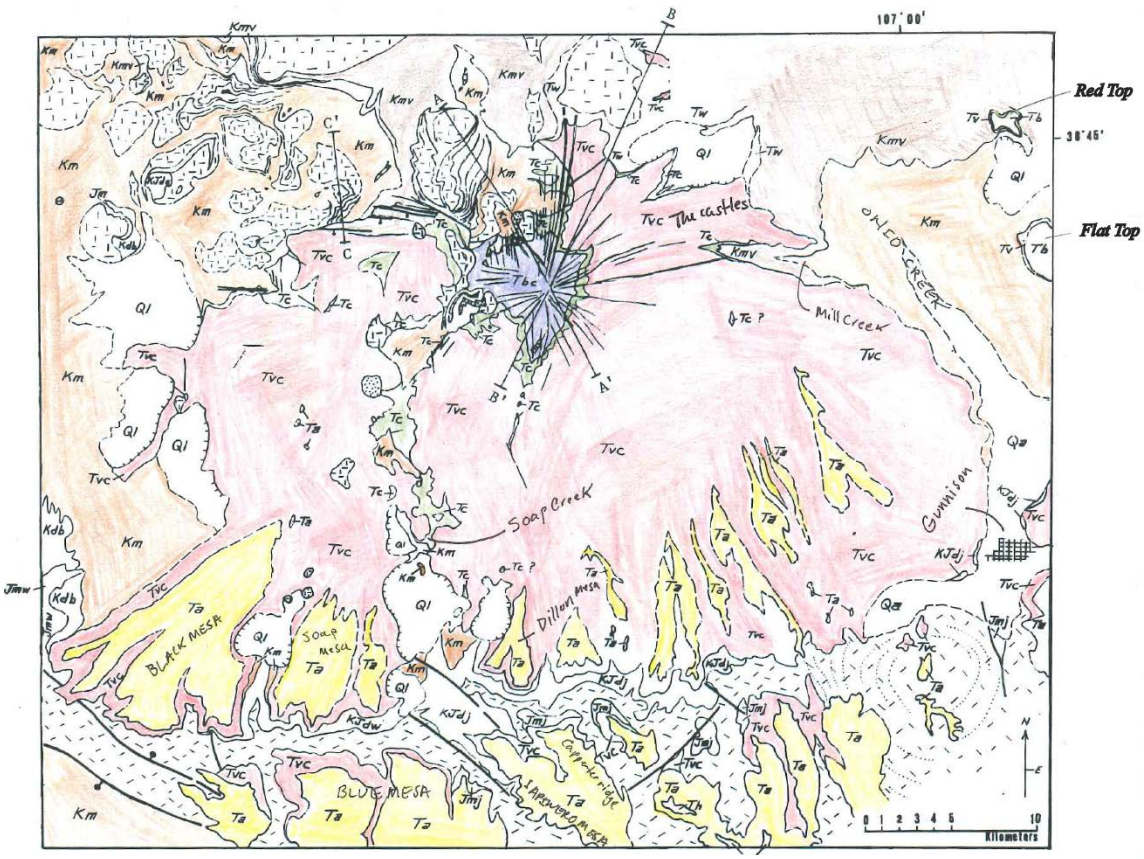

Figure 1.5. The West Elk Volcanic field after Gaskill et al. (1981). The volcaniclastic facies (Tvc - red) covers the greatest area. The basal cone facies (Tbc - purple) and the chaotic facies (Tc - green) are only partly exhumed where recent glaciation and incision have carved through the thick volcaniclastic facies. This is the most detailed map of the formation's distribution, but quadrangle maps in the vicinity of Gunnison provide greater detail of the bedrock geology (e.g., Stork et al., 2006, 2007).

1.4 Problem

In general, past studies of ancient volcaniclastics, like the West Elk Breccia, have been limited by the lack of modern analogs. Relatively recent events, such as the collapse at Mt. St. Helens in 1980, where post-deposition investigations have been coupled with detailed before-and-after eye-witness accounts, provide an analog for understanding the depositional processes behind volcaniclastics in the rock record (e.g., Glicken, 1996).

Thus, volcaniclastics in the rock record, like the West Elk Breccia, need a thorough evaluation, and in many cases re-evaluation. Although many workers have made important contributions to the understanding of volcaniclastics in the West Elk volcanic field, a more nuanced approach, considering modern volcanic events, is needed. The eastern Gunnison River valley holds many peculiar textural and depositional features such as high-angle bedding and irregular contacts. This work aims to improve on the understanding of how these rocks were deposited in parts of the eastern Gunnison River valley.

1.5 Structural and Tectonic Setting

The field area lies in a structurally complex region at the intersection of the Southern Rocky Mountains and the San Juan volcanic field. Faulting and folding have been the norm for this portion of the North American Craton as far back as 1.8 Ga. Repeated orogenic events have created a basement-fault system of aligned uplifts (Fig. 1.6). The oldest faults run northeast–southwest and align with the Colorado Mineral Belt, an economically significant source of metals from the mid-19th century to the present day. The younger basement faults run nearly perpendicular to this trend and have been associated with the Olympia-Wichita Lineament identified by Baars and Stevenson (1981). Laramide reactivation along this lineament is responsible for many of the major basement uplifts in the study area (Fig. 1.7).

In addition, these structures have been reactivated throughout geologic history and are reflected in many Paleozoic and Mesozoic stratigraphic and structural interpretations (Fig. 1.8). Workers have suggested the connection between the intersection of these lineaments and San Juan volcanism (Baars and Stevenson, 1981; Chronic and Williams, 2014; Fillmore, 2011).

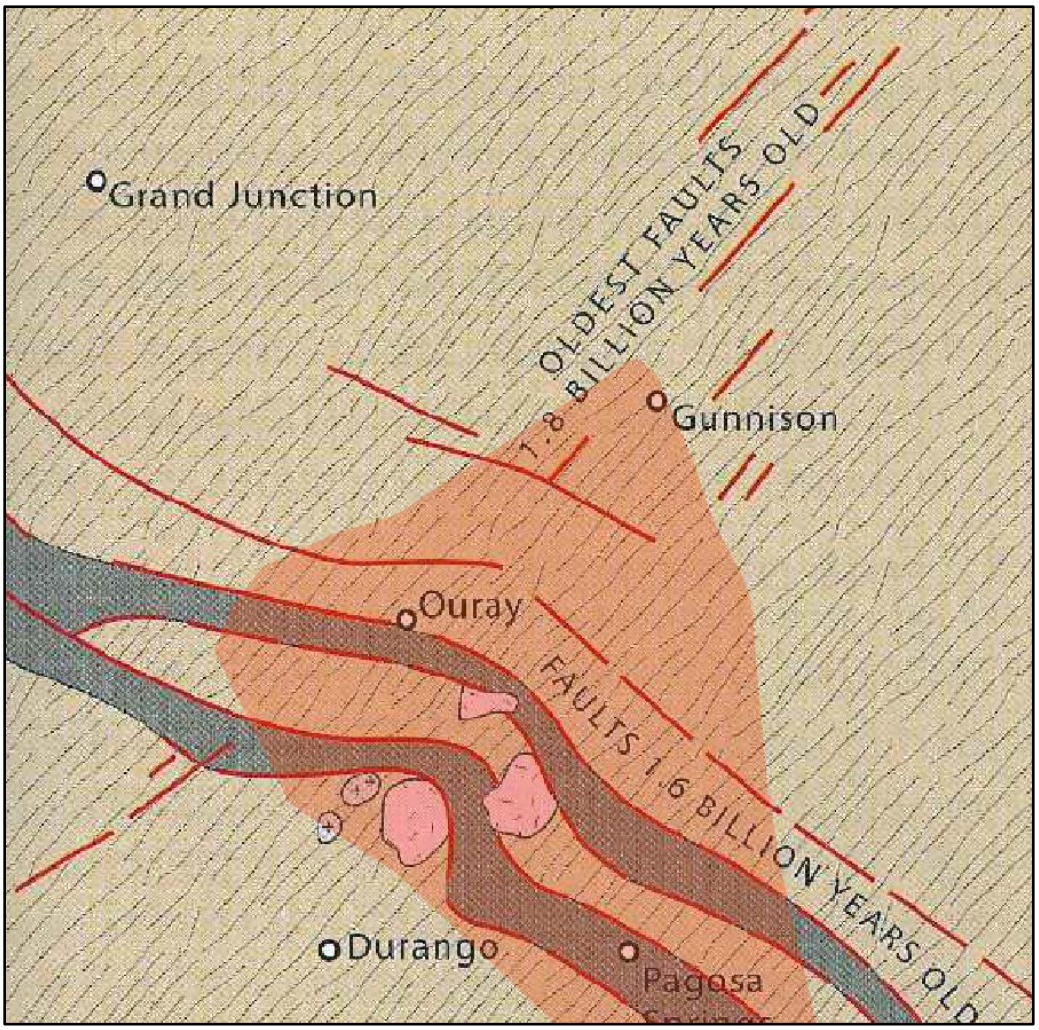

Figure 1.6. The San Juan volcanic field (red shaded area) lies at the intersection of two major Precambrian fault zones orthogonal to one another, the older zone trends to the northeast and is part of the Colorado Mineral Belt. The West Elk volcanic field is the northern extension of this larger field and is located west of Gunnison. Gray zones represent Precambrian rift basins and pink shaded areas are granitic rocks of Early Proterozoic age (after Williams and Chronic, 2014).

The source of Laramide melting and subsequent igneous activity in the Southern Rocky Mountains and San Juan Mountains is thought to be related to the partial melting of the crust during flat-slab subduction of the Farallon plate (Fig. 1.9). The decreased angle of subduction is thought to have resulted from the movement of the mid-oceanic spreading center toward the subduction zone (Fillmore, 2011). The hot subducting plate had decreased time to become cold, hydrated and dense. Thus, the Farallon plate was hot and buoyant when incorporated into the mantle, and hence, the shallow subduction angle (Fillmore, 2011). Others have suggested the Rio Grande rift as a source for mantle-derived magma and corresponding volcanism in the San Juans and West Elks, as well as laccolith emplacement throughout the area (D. Coleman, 2016, oral communication).

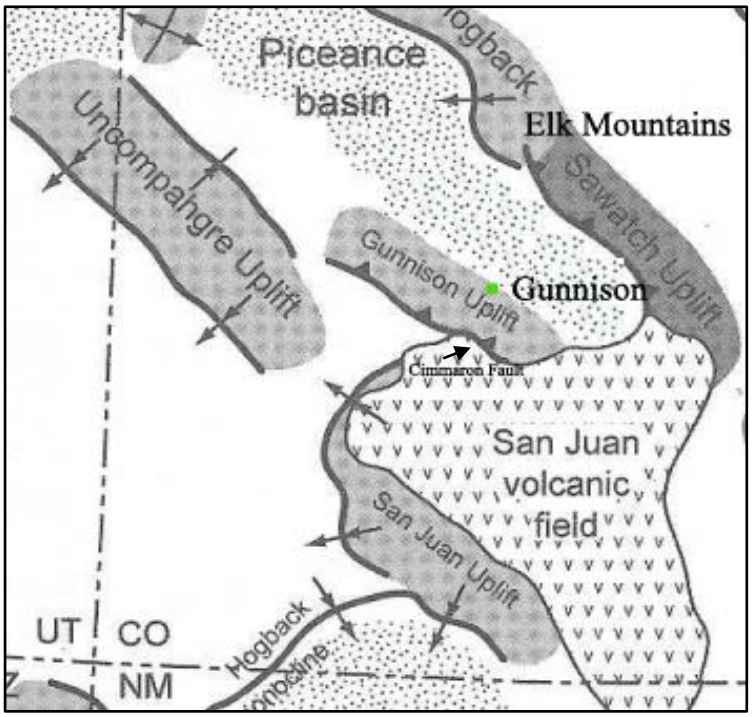

Figure 1.7. Laramide structures in the study area. Note the Cimmaron fault bounds the Gunnison Uplift to the south. Also, note, the prominent northwest–southeast structural trend that characterizes the regional Olympia-Wichita Lineament of Baars and Stevenson (1981) (modified after Fillmore, 2011).

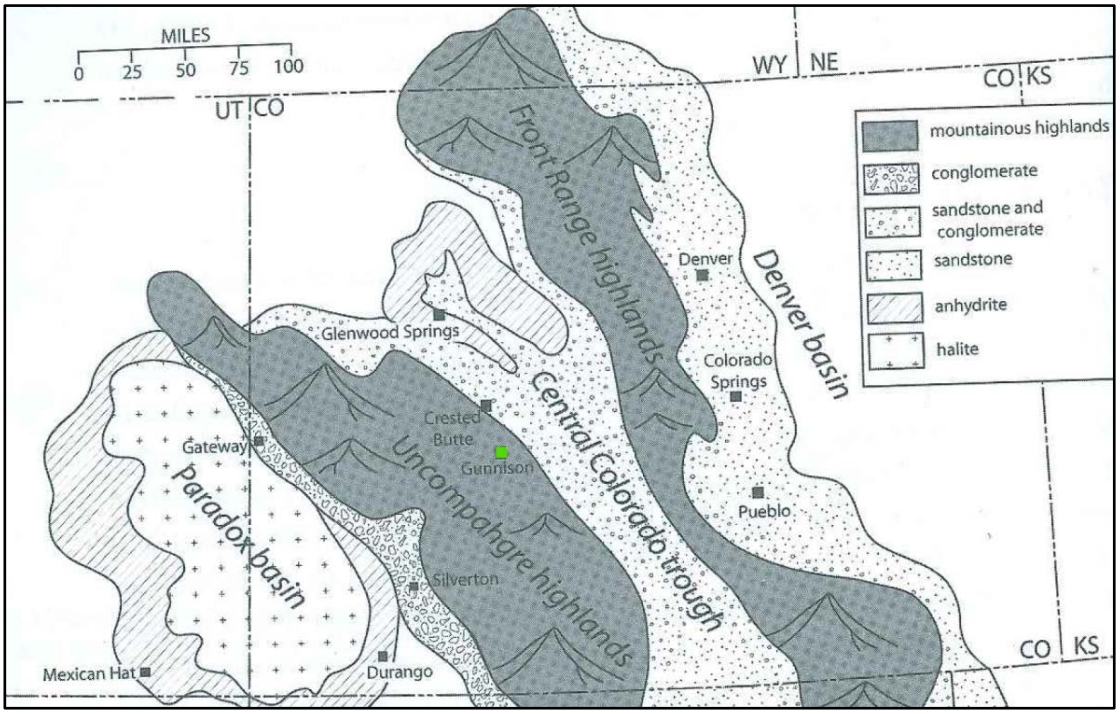

Figure 1.8. Location of Gunnison (approximate field area) relative to general lithofacies and structural setting of the Pennsylvanian Ancestral Rockies. Note the northwest-southeast orientation of the structural highlands and basins (modified after Fillmore, 2011).

In the more accepted scenario, the Laramide Orogeny was a result of the flat-slab subduction of the Farallon plate, which initiated around 65 Ma during latest Cretaceous time (Fig. 1.7). This tectonic event produced uplifts in the Sawatch, Elk and Front ranges. These areas had previously been uplifted and subsequently beveled during the "Ancestral Rockies" event in Pennsylvanian and Permian time (Hansen, 1965; Fig. 1.8).

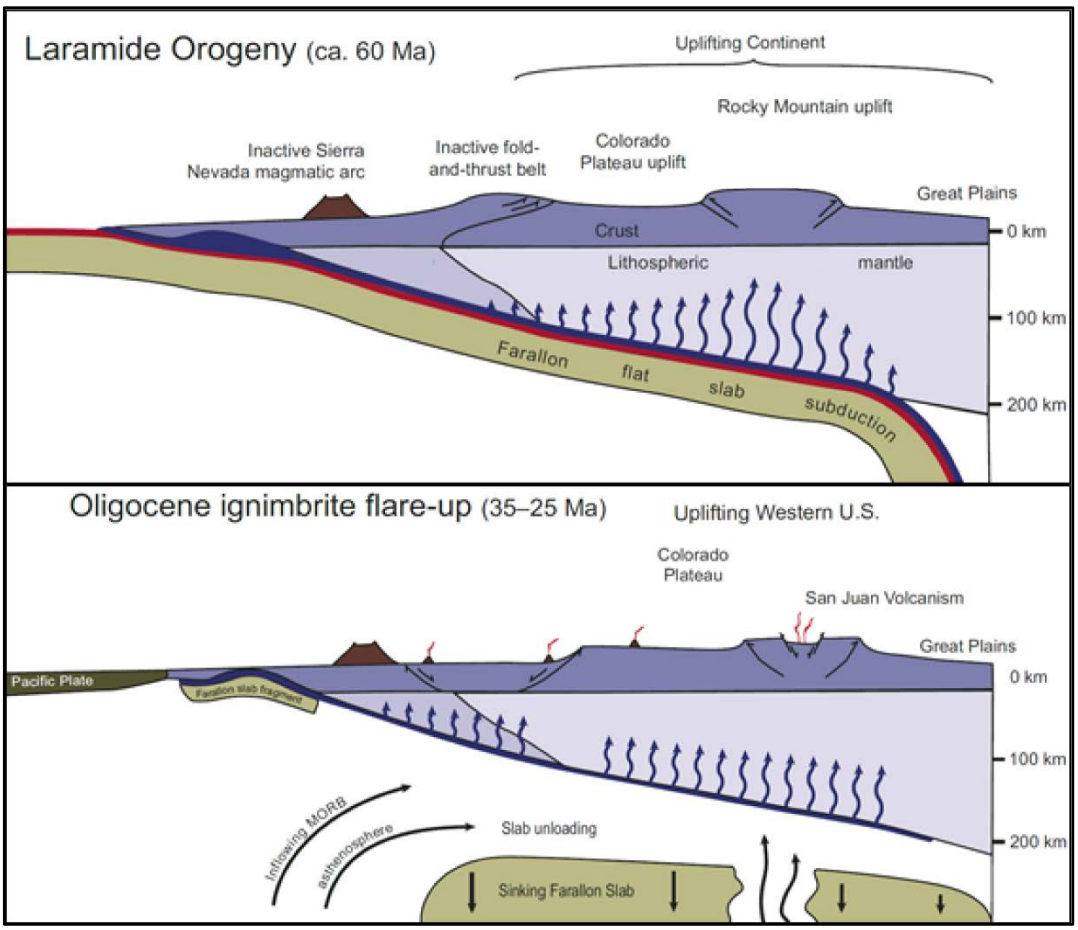

Figure 1.9. The foundering of the Farallon plate**,** following flat-slab subduction, leads to extensive volcanism in the San Juan Mountains (after Crossey et al., 2009).

As mentioned before, the field area is not new to tectonic activity, and the many paleostructures that converge in the region are evidence. As such, the bedrock stratigraphy varies from outcrop-to-outcrop over short, lateral distances. The two major structures affecting Cenozoic stratigraphy (Fig. 1.10) in the study area are the Laramide Piceance Basin and the Gunnison Uplift (Fig. 1.7). The oldest rocks in study area are the Black Canyon Gneiss (1,800 Ma) and associated schists (Fig. 1.10). These rocks represent a long island arc that was accreted onto the Wyoming Province (Halka and Chronic, 2002). Next, the Pikes Peak Granite was intruded throughout the region at

around 1.1 Ga. After these intrusions, there was a period of quiescence and erosion in which the highlands were beveled. The Late Cambrian Sawatch Sandstone, which outcrops outside of the field area in the Elk Mountains, is the first evidence of deposition after intrusion of the Pikes Peak Granite. The deposition of the cross-bedded beach sands of the Sawatch Sandstone was followed by widespread shallow-sea incursions from Ordovician to Mississippian times. The Ordovician Manitou Limestone, Harding Sandstone, Freemont Dolomite, Devonian Chafee Formation, and Mississippian Leadville Limestone record many millions of years of shallow-sea transgression and regression.

These Paleozoic rocks were probably deposited in the field area on a beveled Precambrian surface, but were eroded following the Pennsylvanian–Permian uplift of the Ancestral Rockies (Fig. 1.10). During this time, two ranges, Uncompaghria and Frontrangia, dominated the southern Rocky Mountains (Fig. 1.8). The field area lay on part of Uncompaghria and thus, has no Paleozoic rocks; yet these rocks outcrop only a few miles to the east in the Elk Mountains. Following early Mesozoic erosion of the Pennsylvanian–Permian Ancestral Rockies, incursion of sand seas, or ergs, brought thick, Mesozoic white sands with high-angle cross beds from the southwest into the field area. The Late Jurassic Junction Creek Formation represents this event. The area became wet as the Jurassic Period progressed and a great alluvial plain, represented by the Morrison Formation, covered what is now the Rocky Mountains. During this time, dinosaurs roamed the plains. Many fossils such as *Apatosaurus* can be found in the red and green sandstones and mudstones of the Morrison Formation in the field area (Ettensohn, personal communication, 2016). The Western Interior Seaway, an epicontinental sea that

extended from the Gulf of Mexico to the Arctic dominated the Cretaceous Period. Widespread mudstone deposition during this time is represented by the Mancos Shale, which outcrops in the field area. As the Cretaceous progressed, the seas retreated and gave way to fluvial and swamp environments as recorded as the sandstones and coals of the Cretaceous Mesa Verde Formation. In addition, by this time, subduction of the Farallon Plate had begun and the Laramide Orogeny was initiated. Elevation of the Gunnison Uplift along the Cimmaron Fault in the field area caused some Mesozoic units to be eroded, and hence locally, the Oligocene West Elk Breccia directly overlies the Precambrian basement (Fig. 1.7).

As the Laramide Orogeny progressed, uplift and folding led to generation of the Piceance Basin, on which the eastern section of the field area partly lies. The Piceance Basin is a northward-plunging Laramide downwarp between the Uncompaghre, Elk Range, Sawatch and Gunnison uplifts (Fig. 1.7). To the north in distal portions of the basin, thick lacustrine shales of the Green River Formation are found (Fillmore, 2011). In the field area, the Eocene Wasatch Formation records local erosion of the uplifting Laramide structures in the form of sandstones and conglomerates (Gaskill et al., 1987). During Eocene time (approximately 50 Ma), the Gunnison River drained the southern Sawatch Range and Elk Mountains and probably flowed continuously northwest into the large lakes in northern Colorado and northeastern Utah (Hansen, 1965).

Volcanism began during late Eocene to middle Oligocene time with lavas and tuffs of intermediate composition (Lipman et al., 1969). The West Elk Breccia is part of this early intermediate range of rocks that were erupted throughout the San Juan region. Many laccoliths and dikes are also emplaced in the field area during this time,

particularly north of the West Elk volcano. As these intrusions and subsequent volcanism occurred, the Gunnison River was forced to shift southward. After the early intermediate volcanism, large caldera-forming eruptions occurred to the south of the field area, in which thick ignimbrite sheets were deposited in the San Juan region and within the field area. The ignimbrite deposition caused the Gunnison River to shift north again, eventually settling into its present-day position. Volcanism continued throughout the Tertiary Period with widespread bimodal volcanic eruptions of basalt and rhyolite, including the Miocene Hinsdale Basalt that forms the summit of Red Mountain and Flat Top, and which locally overlies the West Elk Breccia in the field area (Lipman et al., 1969).

Tectonic activity did not end in late Tertiary time, because rotation of the Colorado Plateau led to local uplift and pronounced jointing throughout the region. It also caused or contributed to the rifting in the San Luis valley of south-central Colorado, part of the larger Rio Grande rift. During the past two million years, extensive erosion has largely been accomplished by Pleistocene glaciers that formed cirques in the high peaks of the West Elk Mountains, leaving glacial moraines in the valleys below. Erosion and uplift during late Tertiary and Quaternary time also contributed greatly to the erosion of the Black Canyon of the Gunnison, which in many places is deeper than it is wide and one of the deepest canyons in the country (Hansen, 1965).

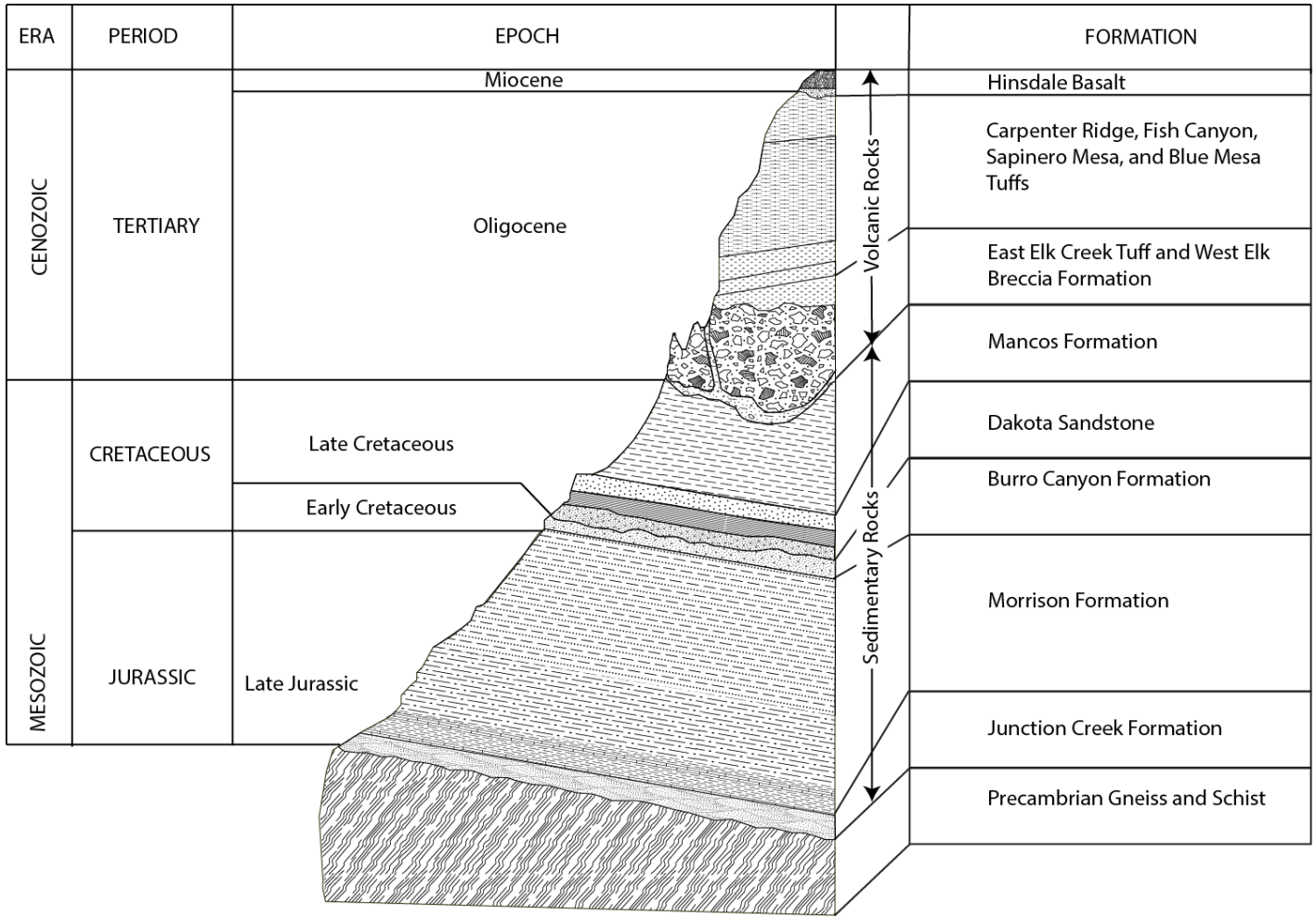

Figure 1.10. Idealized stratigraphic column in the study area. In some instances, where local Cenozoic channels incise the soft Mesozoic section, the West Elk Breccia lies on the basement or lower Mesozoic units (after Hansen, 1965).

1.6 Paleogeography and Paleoclimatic Framework

Based on evidence from the latest Eocene Florissant fossil beds, lake fossils from the Oligocene Creede caldera, and fossils from the Oligocene Pitch Pinnacle Formation in the southern Sawatch Range, climate in the area was interpreted to have been subalpine, as has been suggested for the nearby Creede caldera deposits (Wolfe and Schorn, 1989). Wolfe et al. (1998) estimated that the Creede caldera was at 40°N latitude; therefore, the West Elk Breccia has not substantially changed its latitude since Oligocene time. Larsen (2000) reported mean annual-temperature estimates (MAT) during deposition, based on the Climate-Leaf Analysis Multivariate Program (CLAMP), for the Florissant beds, the Pitch Pinnacle Formation and the Creede caldera (Fig. 1.11). Paleoclimatic data for the Eocene–Oligocene climatic shift was gathered by Barton (2010) and summarized in Table 1. This information suggests a mean annual temperature from 13–4°C, suggesting that the West Elk area probably exhibited an overall temperate to subalpine climate.

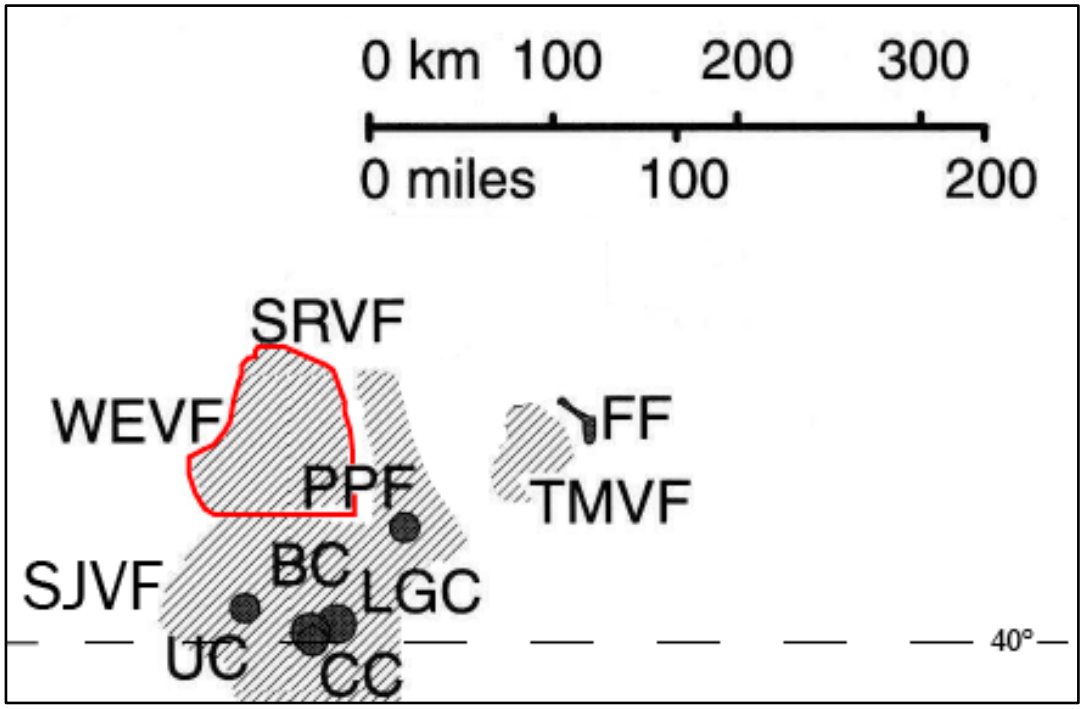

Figure 1.11. Paleolatitude and basins of late Eocene and early Oligocene time. FF = Florissant fossil beds, BC = Bachelor caldera, LGC = La Garita caldera, UC = Uncompaghre caldera, CC = Creede caldera, PPF = Pitch Pinnacle Formation, TMVF = Ten Mile volcanic field, SJVF = San Juan volcanic field, SRVF = Sawatch Range volcanic field, outlined in red WEVF = West Elk volcanic field (modified from Larsen, 2000).

Table 1: Estimates of Climatic Variables
(after Barton, 2010)

Site	MAT (°C) ± 3.6 °C	MAR T (°C) ± 5.1 °C	MAP (cm)	Elevation (km)	Age (Ma)
Florissant	10.51	12.04	74.79	4.36	34.0
Pitch-Pinnacle	13.33	14.1	136.35	3.16	29.0–33.7
Creede (non-subalpine)	8.75	22.42	43.7	2.99	26.3–26.9
Creede (Subalpine)	4.2–4.5	22.42	43.7	4.45	26.3–26.9
West Elk Breccia	13.33–4.2	n/a	n/a	4.05	30.0 ±0.5

1.7 Procedures

This study focuses on an area of about 100 km^2 in the eastern Gunnison River valley and Tomichi Creek drainages. The aim of this study is to better understand the sedimentological and stratigraphic relationships of the West Elk Breccia in distal settings. Extensive roadcut exposures occur west of Gunnison on U.S. 50 (Fig. 1.12). Because of the poor competency of much of this unit, outcrops are poor and scarce. A few choice exposures, for example, the cliffs directly west of town called the "Palisades," are the best outcrops available. Extensive erosion by streams and glaciers after deposition of the volcaniclastics has led to sometimes diffuse remnants of this voluminous deposit. Although there are good roadcuts and outcrop exposures along the Blue Mesa Reservoir and U.S. 50 west of Gunnison, examination of deposits across the entire depositional area of the West Elk Breccia, some 1,000 km^2, was impossible for this study.

The study area was effectively 100 km^2 and to effectively characterize the distal deposits, outcrops were examined for sedimentological and compositional characteristics: the Munsell color of the matrix, estimates of the matrix composition (based on accessory minerals and color) along with the percentage of clasts (greater than sand-sized), rounding and angularity, composition of clasts, sedimentary structures, fossils and other distinguishing features were recorded. Samples of the different outcrops were collected for thin-sections and wavelength-dispersive x-ray analysis. The bulk-rock elemental composition of many facies was determined, followed by identification of petrographic textures and modal analysis of thin-sections relating to each of the facies examined. Samples of tuffaceous conglomerate were analyzed for grain-size distribution on clasts less than 32 mm (-4ϕ) max-length. Finally, stratigraphic and basic geologic principles

were used to interpret the mechanisms of deposition for these deposits. All of this collected data can be found in Appendices A–E.

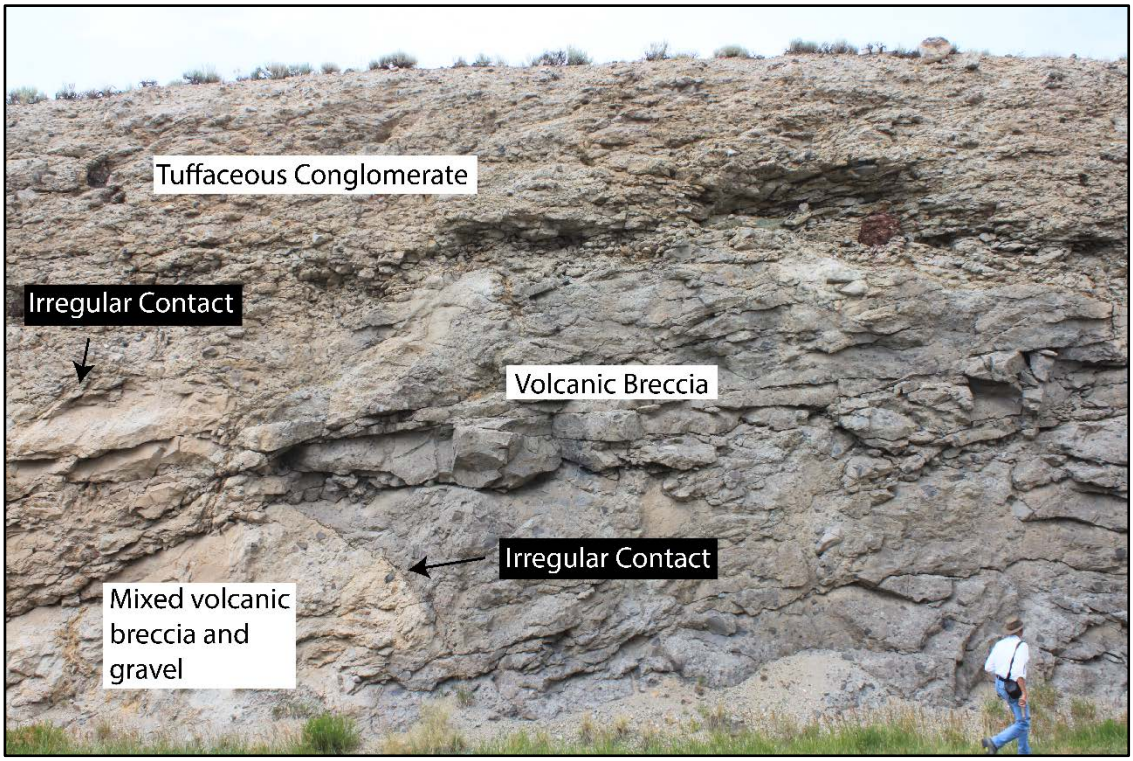

Figure 1.12. One of many excellent roadcuts along U.S. 50, about 4 km (2.5 miles) east of Gunnison, CO (WP 0010, see Appendix A for a list of waypoints and geographic coordinates). Lithofacies, are juxtaposed at peculiar sharp angles in the lower left part of the photo.

CHAPTER 2: Terminology and Definitions

As with all sedimentary rocks, various textural and sedimentary structures preserved in the rocks can provide insight into the depositional setting and flow rheology represented therein. Although pyroclastic rocks are not necessarily typical sedimentary rocks, they are composed of clasts and as such, can show common sedimentary rock structures, like graded bedding and cross bedding (Fig. 2.1). On the other hand, they show many features and structures that are not typical of other sedimentary rocks. The following discussion outlines these unique deposits and the sedimentary structures and features therein.

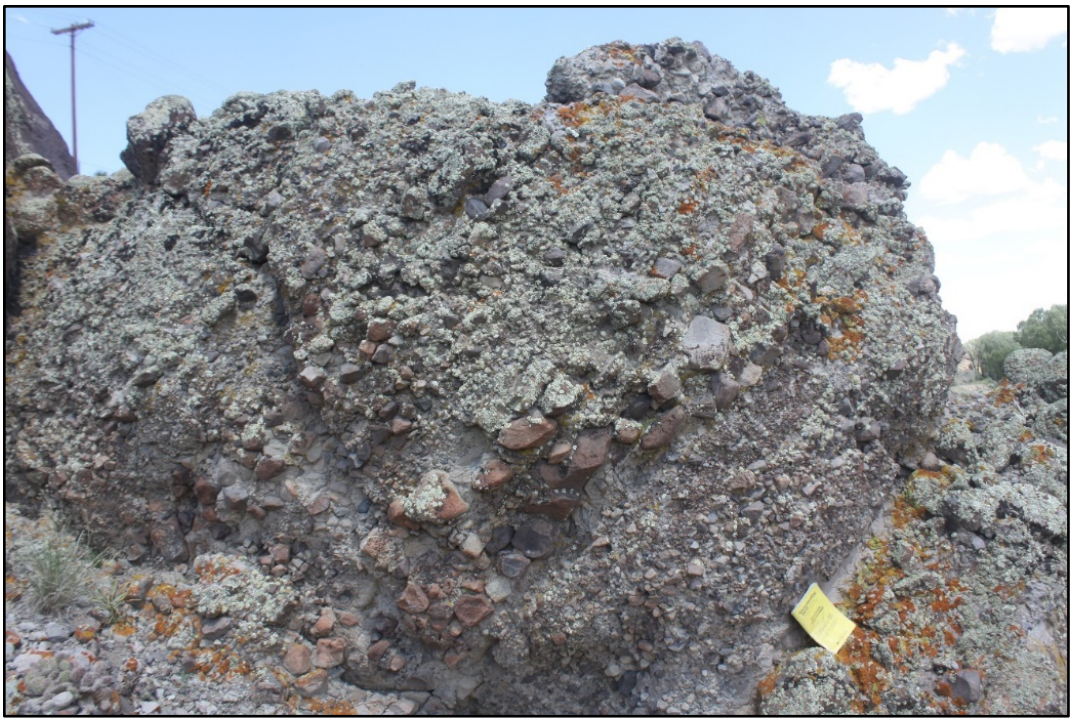

Figure 2.1. Outcrop of West Elk Breccia showing inversely to normally graded beds dipping at a high angle. This outcrop is east of the town of Gunnison, CO, on U.S. 50 near WP 203.

2.1 Tephra Fall

Tephra fall consists of ash-to-bomb-size particles that fall from the air because of explosive eruption and ejection into the atmosphere. Tephra fall may consist of crystals, vitric (glass) shards, and lithic clasts of pre-solidified magma or country rock. Tephra deposits, when solidified, become tuffs, lapilli tuffs, welded tuffs, pumice, and scoria.

2.2 Pyroclastic Flows and Nuée Ardente (Block-and-Ash-Flow) Deposits

Pyroclastic flows, which many West Elk Breccia deposits represent, originate from explosive eruptions of hot ash, gas, and molten rock (Fig. 2.2). Alternatively, sticky or viscous lavas of continental volcanoes develop steep lava domes that pile up until they

Figure 2.2. Volcano Mayon in the Philippines erupted ash and blocks of lava that cascaded down the slopes as pyroclastic flows during the 1984 eruption (photo courtesy of the USGS; http://volcanoes.usgs.gov/Imgs/Jpg/Mayon/32923351-020_caption.html; accessed 2-20-2017).

become unstable and collapse. The result is incandescent lava blocks avalanching down the slopes of a volcano in a chaotic mixture of rock, gas and ash (Fig. 2.2).

A pyroclastic-flow deposit may have a variety of sedimentary textures, such as normal to inverse grading, although bedding is typically massive to crudely layered (Fischer and Schmincke, 1984). In general, these flows consist of poorly to moderately sorted, angular and monolithologic clasts in an ash matrix. These flows commonly contain prismatically jointed bombs that may be rounded and several meters in diameter (Fig. 2.3). Pyroclastic flows with clasts greater than 26 cm (10 in) are called block-and-ash flows (http://volcanoes.usgs.gov/vsc/glossary/block_and_ash_flow.html).

Figure 2.3. A prismatically jointed bomb in the West Elk Breccia near WP 169. These contraction fractures are fragile and represent *in situ* cooling. As such, they are indications of an eruption (Fischer and Schmincke, 1984; Francis and Self, 1987).

Such chaotic flows produce deposits much like debris-flow deposits, but sorting, grading, and matrix composition may permit the differentiation of pyroclastic-flow and debris-flow deposits.

2.3 The Debris-Avalanche-to-Hyperconcentrated-Flow Continuum

Sedimentation, other than normal stream flow, pyroclastic flow, and tephra fall on volcanoes, occurs within a continuum that falls between debris avalanches and hyperconcentrated flows (Smith and Lowe, 1981) (Fig. 2.4). Flows tend to transform from one type to another during down-stream transport, depending on down-stream

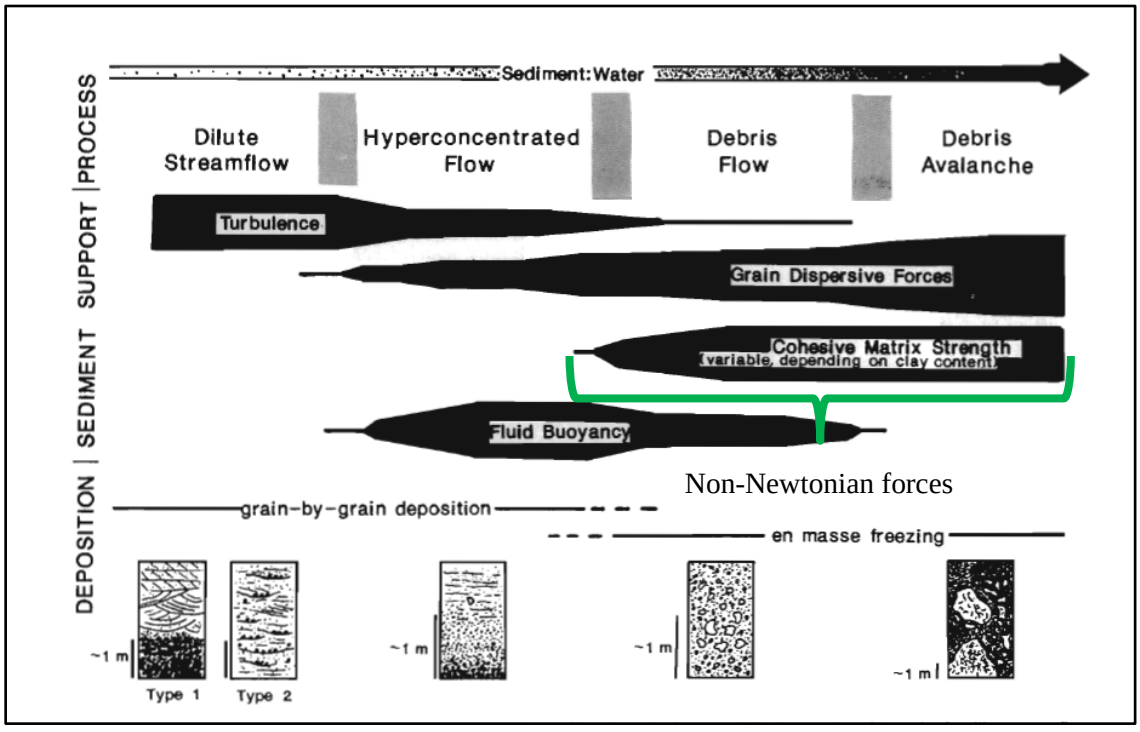

Figure 2.4. Dilute streamflow to debris avalanche, the end members of a flow continuum. Note the deposit characteristics, including typical cross-bed sedimentary structures in dilute-streamflow deposits and massive poorly sorted deposits with meter-sized clasts of debris-avalanche deposits (Smith and Lowe, 1981).

gradient and the amount of water involved in transporting the material. For example, the

Osceola mudflow initiated as a debris avalanche from a landslide on part of the summit of Mt. Rainier (Vallance and Scott, 1997). Within a few kilometers of the source area, the avalanche gained enough water and epiclastic material to become a debris flow. This flow traveled nearly 100 km to the Puget Sound (Vallance and Scott, 1997). Such transitions in flow properties inherently leave sedimentary deposits with a variety of structures and expressions (Fig. 2.5). Understanding the relationships between transitions in flow properties is an important part of interpreting depositional mechanisms.

2.4 Hyperconcentrated Stream Flow

The concentration of sediment in water determines the type of flow described in Figure 2.4. Hyperconcentrated flows have a concentration of between 20 and 50% sediment (Vallance, 2001); they are the result of a transitional turbulent-to-laminar flow and have some measurable yield strength. As such, they may contain cross bedding, normally graded beds, and massive beds (Smith and Lowe, 1981) (Fig. 2.5).

2.5 Lahars

"Lahar" is an Indonesian term that generally means any flow along the continuum between hyperconcentrated-to-debris that occurs on a volcano. Here, I consider lahars to reflect debris flows with non-Newtonian properties and sediment concentrations between 50–60% (Vallance, 2001; Smith and Lowe, 1981). Lahars are common phenomenon on stratovolcanoes, but they are typically small-volume, localized events that are not eruption related. Those that are eruption-related and have significant water have the

potential to be high-volume destructive events (e.g., Nevado Del Ruiz eruption and lahar in 1985). The long run-out potential and erosive nature of lahars make these sorts of flows particularly intriguing. Lahars often have elevated pore pressures equivalent to lithostatic pressure. This elevated fluid pressure provides resistance to shearing and allows the flow to maintain energy for great distances and to flow on even very low gradients. Lahars with enough momentum have traveled 10's of kilometers or more from their source.

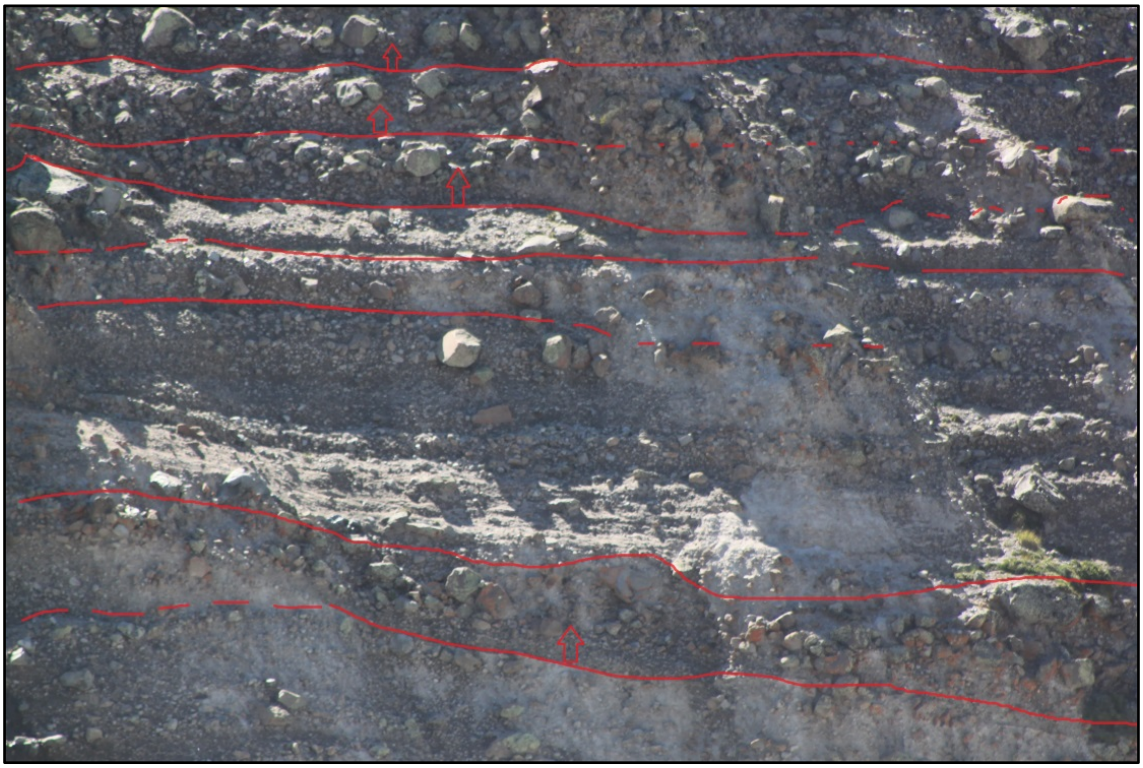

Figure 2.5. Inversely graded beds near the West Elk volcanic center at Storm Pass, Colorado (12500' elevation).

2.6 Debris Avalanche

As the late P.W. Francis accurately noted, some of the tallest mountains in the solar system are volcanos (e.g., Olympus Mons). Why then, are stratovolcanoes on Earth not the tallest mountains? It has to do with the erosion of these enormous self-constructed piles of volcanic material. The events that occurred at Mt. St. Helens on May 18, 1980 initiated the first major exploration of edifice evolution on stratovolcanoes. While debris-avalanches and catastrophic eruptions like those at Mt. St. Helens are rare and less frequent than lahars, Tost et al. (2015) suggested that sector collapses, or partial collapses on stratovolcanoes occur between 2–14 times during the active lifetime of the volcano (10–500 k.y.). In Japan, Ui et al. (1986) reported that at least 49% of active stratovolcanoes have debris-avalanche deposits. Recent work has focused on identifying these deposits and characterizing the mechanisms involved in transport and initiation.

2.7 Hummocky Topography

Volcanic debris-avalanche deposits have distinct telltale characteristics. Hummocky topographic expression is the most well-recognized of these characteristics (Fig. 2.6). After a sector has avalanched down the steep slopes of the volcano and spread out onto the ring plain below, the large blocks of the volcano that slid away from the edifice are left standing high above the plain. Hummocks can be 10’s of meters tall and kilometers in length. Despite being a telltale feature of Quaternary and Holocene debris-avalanche deposits, hummocks may be nonexistent or obscured due to secondary lahars, erosion and burial by later deposits (e.g., Malone, 1995). Along the western margin of

Ohio Creek are partially exhumed and preserved hummocks (Fig. 2.7). This string of hummocks emanates from the Palisades further to the south.

Figure 2.6. The Pleistocene debris-avalanche deposit in Shasta Valley, California, exhibits hummocky topography; blocks of the volcano were dispersed over an area of 675 km^2 and traveled more than 40 km (25 miles) from the summit (Crandell, 1989).

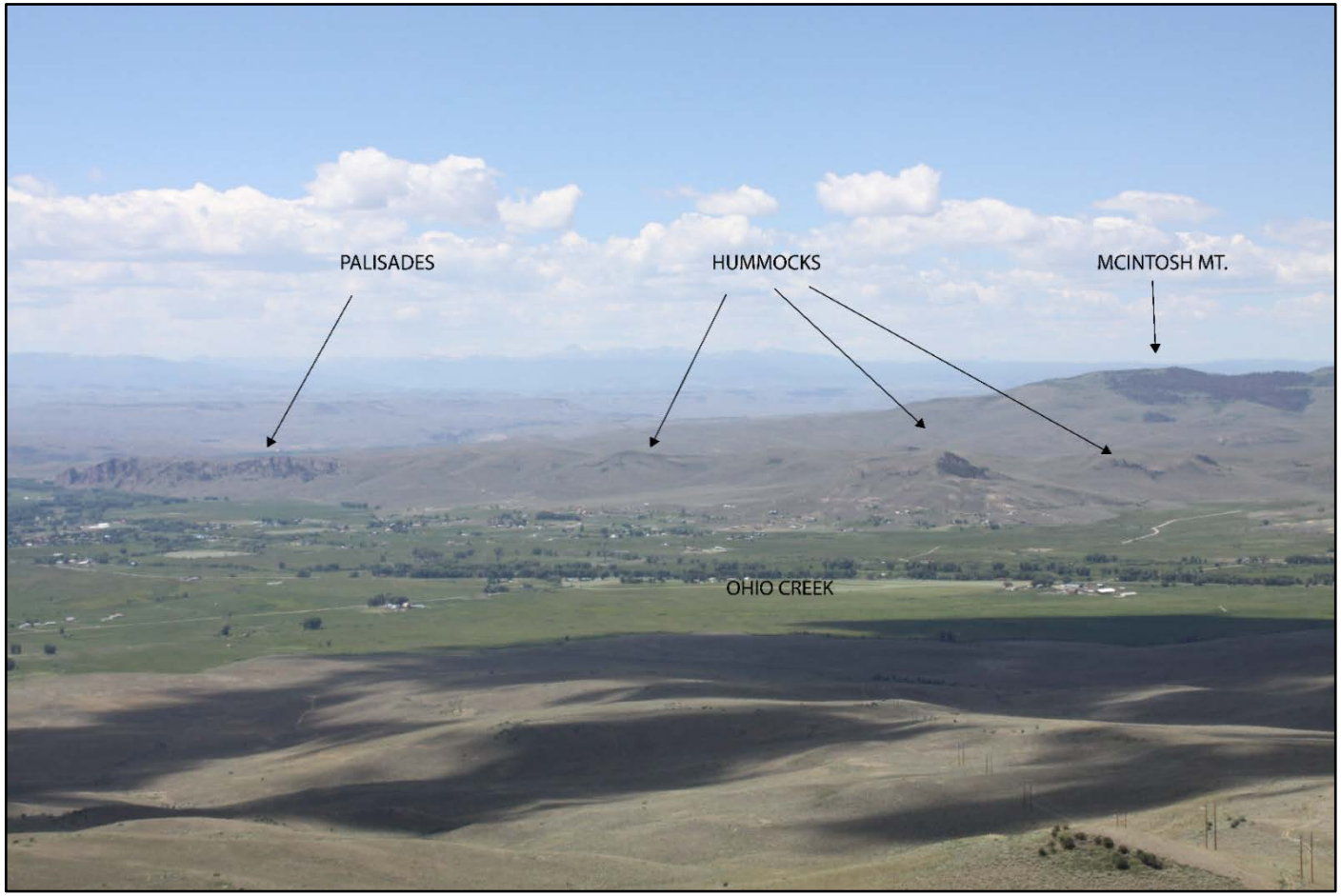

Figure 2.7. Hummocky topography displayed in the West Elk Breccia along Ohio Creek. Resistant volcanic breccia is partly to wholly surrounded by tuffaceous conglomerate and rests on the Cretaceous Mancos Shale. This view is to the southwest from near Almont Peak. These hummocks likely filled a paleovalley, whereas the present-day Ohio Creek was a paleohigh built on the Dakota and Mancos formations. Thus, this exposure represents a unique example of reversal of topography.

2.8 Megaclasts (Megablocks)

The hummocks of a debris avalanche consist of fragments of the original volcanic cone. These fragments are mostly intact pieces of the edifice that are typically encased in a matrix of fine volcaniclastic material. Megaclasts, as described by Palmer et al. (1991), are, "… all components of the deposit greater than 1-meter maximum size that are bounded by an outer surface and show an internal lithological homogeneity (Fig. 2.8)." In contrast, Vallance (written communication, 2016) described megaclasts as, "large inclusions of other material that are 5-meters or more across (written communication, 2016)." In either case, these clasts are "boulder size", or greater than -8ϕ in the Wentworth (1922) classification scheme. Because one meter is much larger than the lower bound (256 mm) for boulders (in the Wentworth scale), it is used for this study; importantly, any megaclast is a large inclusion of material distinct from a surrounding matrix. Size and composition of megaclasts vary. Primarily, they are composed of volcanic material and may be intact pieces of stratified volcaniclastic debris (Fig. 2.9). Alternatively, they may also contain alluvial material, pieces of bedrock, or alluvial rafts (Fig. 2.10). Vallance and Scott (1997) identified several of these megaclasts of "loose gravel."

Figure 2.8. The megaclast pictured here is a well-indurated breccia with angular pyroclastic material (dark-colored) in a distinct domain. Encasing this megaclast is a matrix of poorly indurated tuffaceous stream-gravel conglomerate. Note the blue-handled hammer at the right edge of the megaclast (blue oval). This clast is located nearly 38 km from the volcanic center, near way point 089.

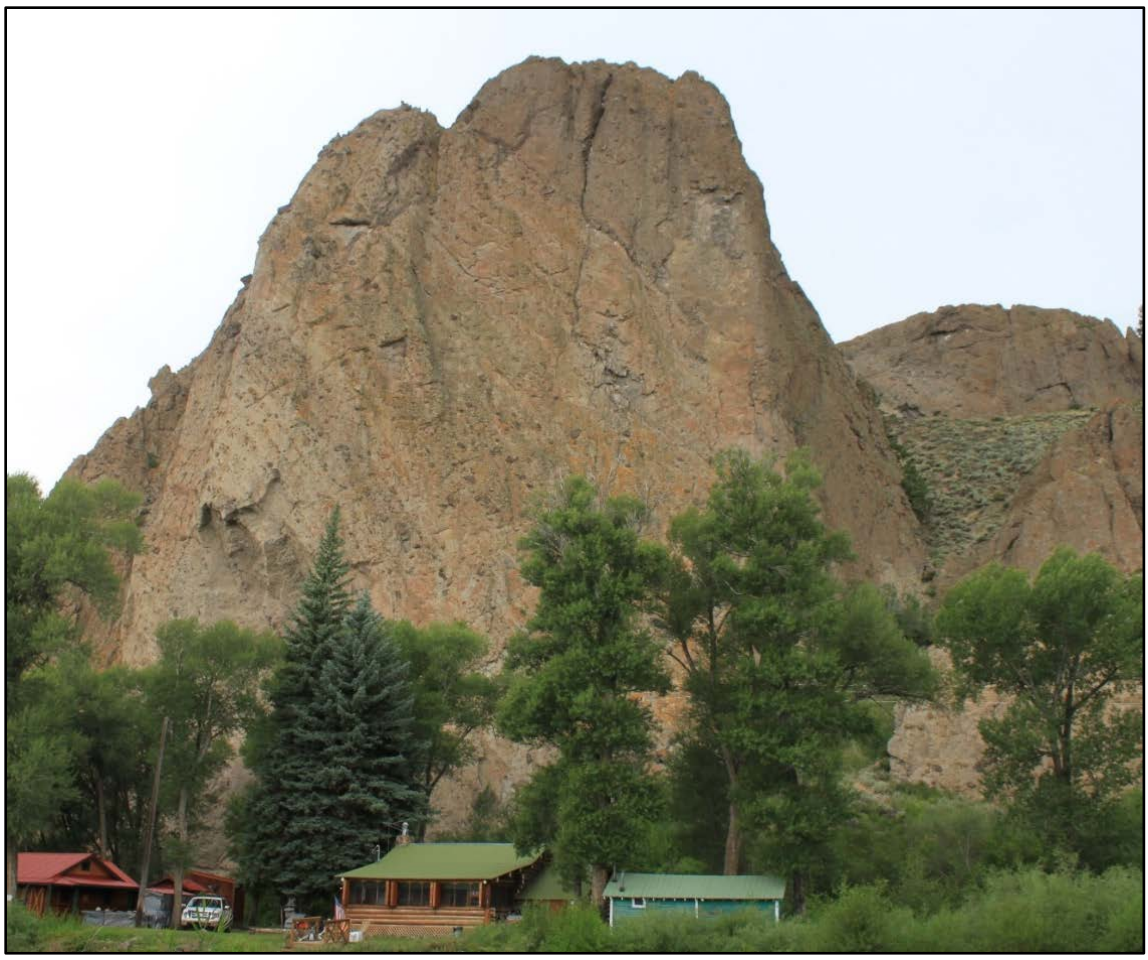

Figure 2.9. The Palisades, west of Gunnison on the Gunnison River, expose massive megaclasts with intact original beds of alternating blocky and fine volcaniclasts, originally deposited near the volcanic center. The exposure represents a single megaclast with beds that dip at an unusually high angle toward the northwest and the volcanic center.

Figure 2.10. An alluvial raft in a roadcut east of Gunnison on U.S. 50, near way point 090. An alluvial raft is a megaclast of stratified alluvium in a debris-flow deposit. The material that composes the raft is unaltered, and as such, displays original stratigraphy. Like other megaclasts, alluvial rafts are distinguished by an internal domain (unconsolidated and stratified sand and alluvium in this case) separated from a surrounding matrix (here, a polymict tuffaceous conglomerate).

2.9 Exotic or Foreign Alluvium

Volcanic debris flows can occur anywhere gravity or an explosive eruption prevails over resisting forces. Depending on the energy, water saturation and travel path of a volcanic debris flow, the incorporation of foreign or non-volcanic material may occur (Fig. 2.11). Vallance (2000) described the incorporation of secondary material by lahars as “bulking.” It is especially common for long-runout lahars to incorporate alluvium during downstream transport.

A long-runout lahar is generally one that travels 10's of kilometers from the source. Such flows may originate from an eruption or during the transformation of a debris avalanche to a debris flow, and all can potentially bulk-up on alluvium. In describing the Pleistocene-age debris-avalanche deposits in Shasta Valley, Crandell (1989) noted the increase in "other rocks" within the matrix facies. The so-called "other rocks" consist of alluvium, tephra fall, lacustrine deposits, and even fossils. Crandell (1989) noted that pebbles in the deposit are entirely of Mt. Shasta origin within 22 km from the summit of the present volcano, and that the percentage of rocks from Mt. Shasta decreases with distance from the source while the "other rocks" increase in abundance.

Figure 2.11. A megablock of sandstone measuring 9.5 ft. x 7.5 ft. (2.9 m x 2.3 m) and a smaller block of black shale (at left of the sandstone) in a roadcut. These clasts were likely derived from local Mesozoic bedrock. This location is east of Gunnison on U.S. 50 at WP 0010.

2.10 Volcanic Matrix Material

In volcanic debris flows and debris avalanches, a heterogeneous mixture of various sized volcaniclasts and other material may form from the abrasion, shearing and fracturing of volcaniclasts, addition of material that is erupted coevally with the mass movement, and through the bulking up with foreign alluvium. Workers have described

such heterogeneous and unstratified mixtures of volcanic and exotic material in debris-avalanche deposits as matrix facies (Crandell, 1989; Malone, 1995; Glicken, 1996). Such a phase seems to be associated with most wet volcanic debris avalanches. In essence, the matrix phase of a debris avalanche is all the material that becomes mixed together as the mostly dry, granular flow of large megaclasts bulks-up with more water and sediment.

2.11 Jigsaw Fracturing

Jigsaw fracturing describes a texture in some mass-movement deposits characterized by jigsaw-like pieces of a puzzle that fit together (Fig. 2.12). During a landslide or large mass movement, solid material, commonly hot rock, dilates and depressurizes resulting in volume expansion and the fracturing of the clasts (Shreve 1968; Glicken, 1996; Roverato et al., 2014). The process commonly involves the exhumation of previously deposited material (in this case, volcaniclasts) with subsequent volume expansion (Glicken, 1996), like exfoliation observed in exhumed granitic rocks. This process can occur in both volcanic and non-volcanic settings and at a variety of scales (Figs. 2.12, 2.13). Ui (1983) suggested that such fracturing is a common feature in volcanic debris-

Figure 2.12. Jigsaw fracturing of volcaniclasts along Tomichi Creek, near “W Mountain”. Clasts were dilated, fractured and subsequently filled with matrix.

avalanche deposits. Complementary jigsaw pieces may show little translational or rotational movement from transport, indicating a lack of turbulence during laminar or plug flow. Plug flow describes a type of flow without turbulence, in which deposition of debris occurs *en masse*.

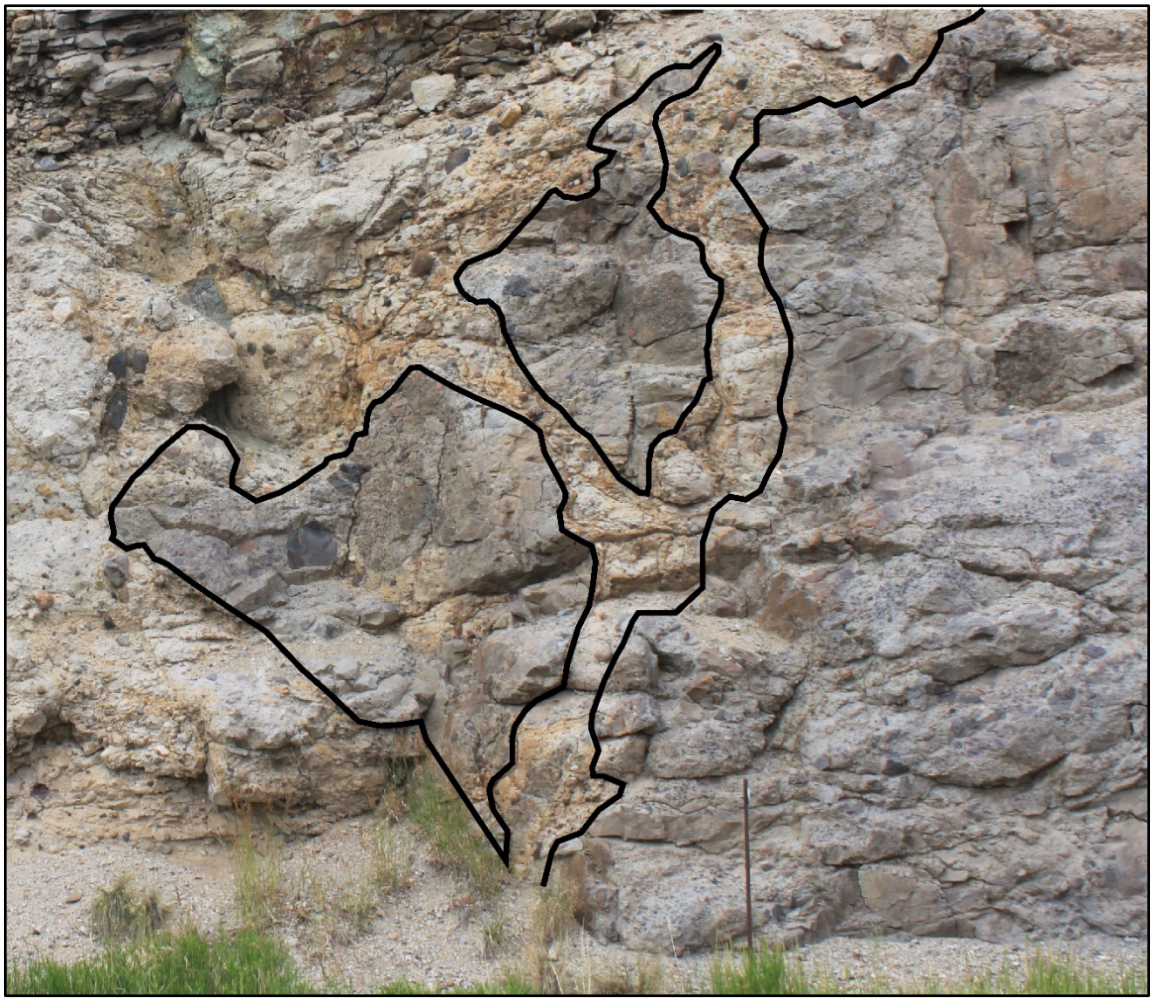

Figure 2.13. Jigsaw fracturing of a megaclast; fractured and filled with orangeish, oxidized matrix composed of stream gravel among other clastic debris. Note the highway reflector (approximately three feet or one meter in height) at bottom for scale. From a roadcut on U.S. 50 east of Gunnison, CO, WP 0010.

2.12 Inversely Graded Basal Beds

Due to a variety of forces on individual grains and grain-size heterogeneity within a flowing mass, lahar and debris-flow deposits often exhibit inversely graded bedding (Figs. 2.1, 2.5). Vallance (2000) suggested the idea of kinetic sieving to explain how different sized particles of the same composition are systematically segregated. Larger particles are moved up or down in the flowing mass by a process called squeeze expulsion. Squeeze expulsion is a result of grain-to-grain interactions, and thus, shear forces may move grains upward or downward. As clasts are expelled upward, a large void develops below these larger grains, and through percolation smaller particles from higher parts of the flow rapidly infill these voids. This process of expulsion and percolation results in the tendency for large particles to appear as if they float on lower, finer parts of the flow. In summary, the combination of squeeze expulsion and percolation may result in a kinetic-sieving process and deposits with inverse grading (Figs. 2.1, 2.5).

2.13 Massive and Unstratified Beds

Volcaniclastic deposits may or may not display bedding (Fig. 2.14). Vallance (written communication, 2014) indicated that debris-avalanche deposits are typically more than 20-meters thick. In contrast, "… lahars are less thick (not more than 20 m as a rule)" (Vallance, written communication, 2014). Zernack et al. (2009) observed that granular debris-avalanche deposits are not stratified. They display undulatory and

irregular surfaces due to the heterogeneity of the flowing mass.

Figure 2.14. Volcaniclastic deposits displaying massive bedding in outcrop. This outcrop is in the lower East Elk Creek drainage near WP 202.

2.14 Clastic Dikes or Fracture-Fill

Crandell et al. (1984) and Glicken (1996) made some of the first descriptions of clastic dikes observed in debris-avalanche deposits in seminal work at Mt. Shasta and Mt. St. Helens. These workers observed fractures filled with stream gravel and a volcanic matrix material. During transport of megaclasts, jigsaw fractures, and voids fill with the matrix phase of the flow (Fig. 2.15)

Figure 2.15. Fracture fill at the base of the Palisades (Fig 2.9); a heterogeneous mixture of stream gravel and volcaniclasts filled a fracture in darker gray volcaniclastic rock.

2.15 Rip-Up Clasts

Many deposits in the stream gravel facies contain rip-up clasts of the Cretaceous Mancos (Fig. 2.16) and the Jurassic Morrison formations. The preservation of these clasts is an indication that the flow had contact with the underlying sedimentary sequence and is a good indicator that these flows were non-turbulent. On the other hand, if these flows were turbulent and non-laminar, it is unlikely that these soft, brittle shales would have been preserved intact in the distal deposits of West Elk Breccia (Zernack et al., 2009).

Figure 2.16. Angular rip-up clasts of the Cretaceous Mancos Shale (white outlines) and sheared blocks of Jurassic Morrison Formation (bottom of channel) in a roadcut, approximately five miles (8 km) east of Gunnison on U.S. 50.

CHAPTER 3: Data and Results

3.1 Field Observations

The primary and preliminary objectives of this study were to characterize and map the distribution of the West Elk Breccia. Measurements and descriptions provided more than 14 lithofacies. These measured sections are described in detail in Appendix A. The lithofacies display characteristic sedimentary features and textures. Despite 14-unique lithofacies, lateral variation is so great and complex that stratigraphic analysis and

mapping are impossible, and hence, three lithofacies were identified: I. breccia facies and II. matrix facies and inconspicuous facies, III. mixed facies, was observed in many of the roadcuts along U.S. 50. The mixed facies is less resistant to weathering than the breccia facies despite similar clast compositions, and thus, is less apparent in outcrop (Fig. 3.1). From these descriptions and measurements, stratigraphic correlations were attempted (Fig. 3.2).

The distribution of West Elk Breccia deposits reflects a large area around the volcanic center, probably several hundred to several thousand square kilometers. How much of the deposit outside of the study area, which has the same depositional history as the West Elk Breccia in the study area, remains to be uncovered. The total volume of the West Elk Breccia is likely hundreds of cubic kilometers. Within the study area, if an average thickness based on Appendix A is assumed, the volume of the West Elk Breccia deposits is estimated to have been approximately $8.5\ km^3$. In comparison, Crandell (1989) estimated that the volcanic debris-avalanche deposits from the ancestral Mt. Shasta included more than $45\ km^3$, and Malone (1995) estimated that the volume of deposits from an Eocene volcanic debris avalanche originating at Sunlight Peak in the Absaroka Range to be $100\ km^3$.

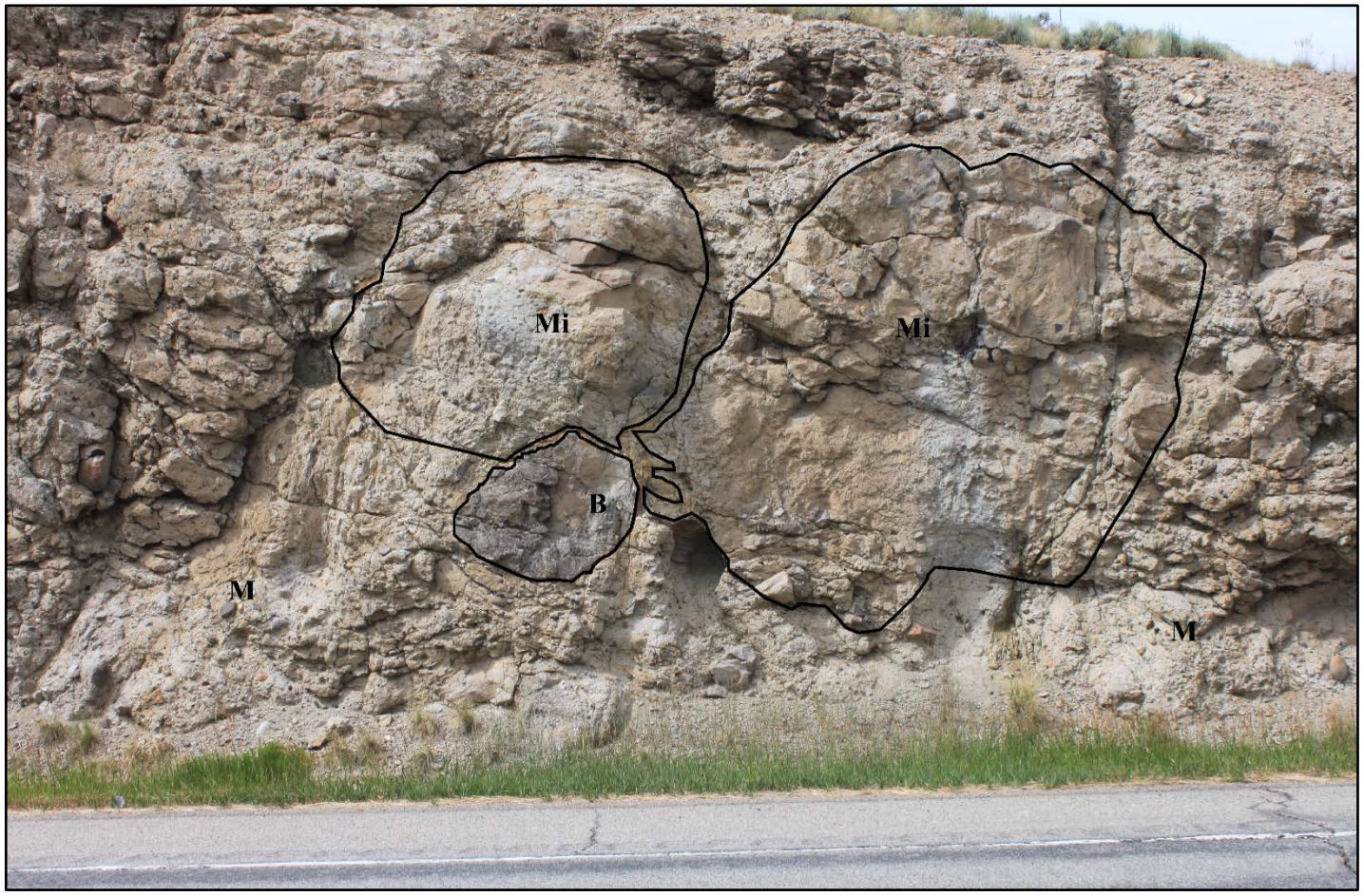

Figure 3.1. Mixed facies (Mi), two very inconspicuous subrounded megablocks of a poorly indurated volcanic breccia–coarse volcanic sandstone are intermixed with tuffaceous stream gravel (M) and a more conspicuous and smaller rounded block of volcanic breccia (B). This roadcut is at WP 0010 east of Gunnison on U.S. 50.

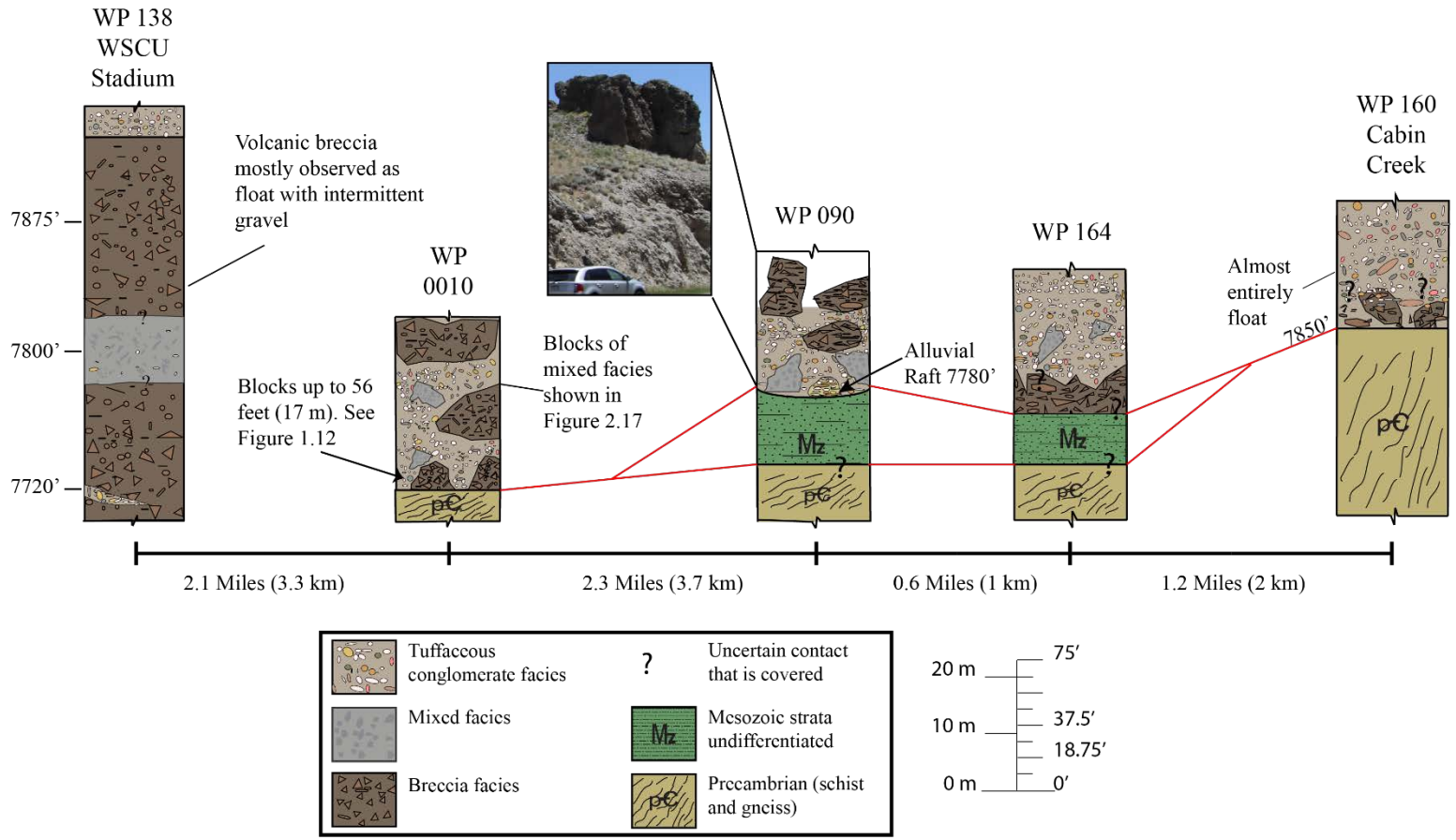

Figure 3.2 a. Measured section correlation along U.S. 50 and Tomichi Creek east of Gunnison, Colorado. Note the inconsistencies in lateral distribution of facies. Megaclasts of the breccia facies decease in size to the east, away from the volcanic center. Also, note the increasing elevation of the basement rocks to the east marking the basin margin.

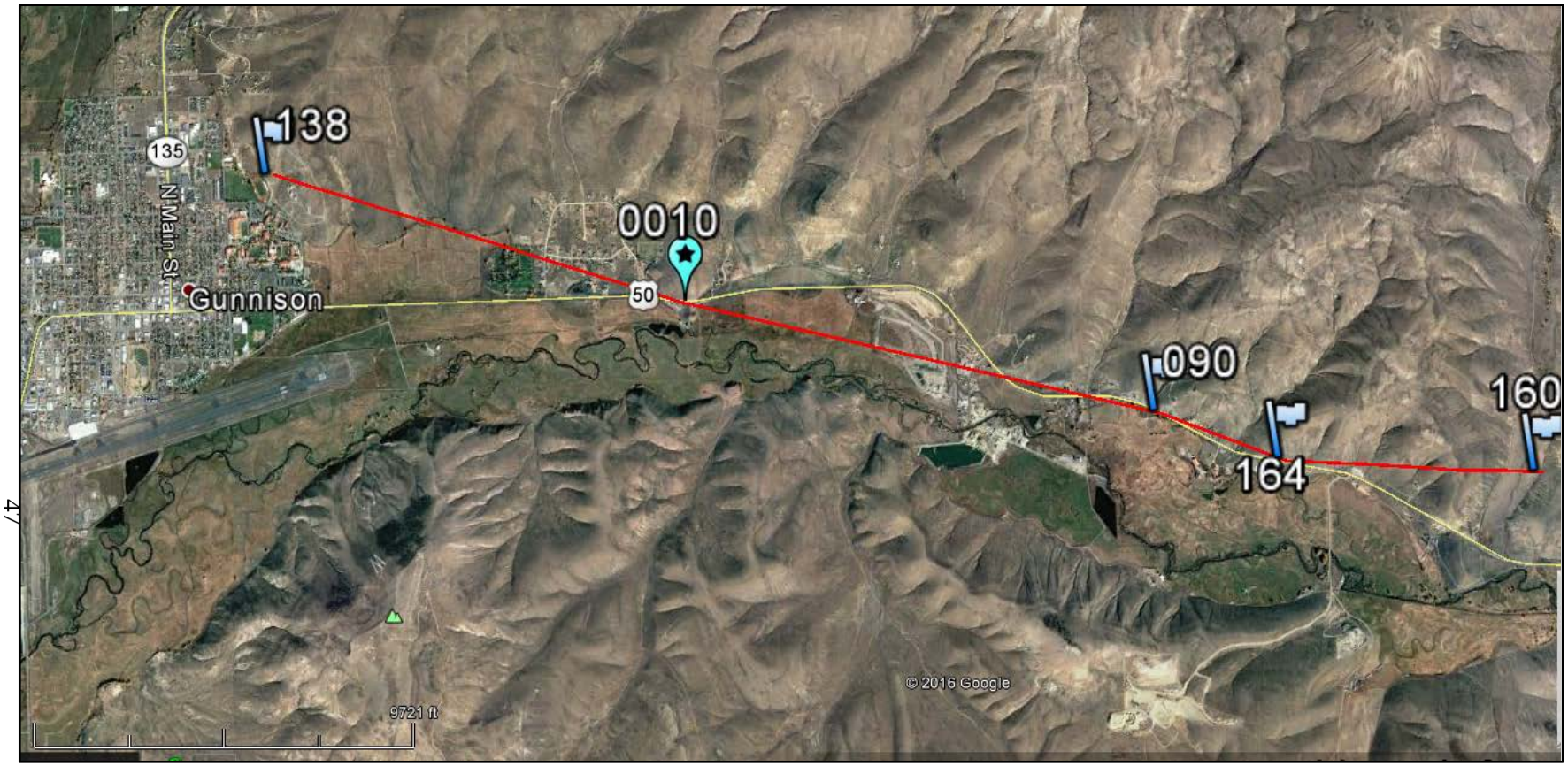

Figure 3.2 b. Map view showing waypoint location of measured sections and stratigraphic correlation line. Waypoint with black star represents a location where a sample was collected for geochemistry.

3.2 Geochemistry

Using detailed field descriptions as a guide, more than 80 samples were collected and 29 of these samples were analyzed for bulk-rock geochemistry (see Appendix B). A range of lithologies, including well-indurated volcanic breccia, lapilli tuff, vitric tuff, and soft tuffaceous conglomerate samples were collected from different elevations and at different distances from the purported source, with a focus on sampling the matrix of all lithologies (Fig. 3.3). Sample preparation for all samples, despite variations in lithology, was the same.

Samples were prepared for wavelength dispersive x-ray fluorescence (WD-XRF) analysis. Samples were crushed by hand using a sledgehammer to remove visible clasts and obtain gravel-size fragments of the matrix. Clasts of primary volcanic material were removed to limit the bias by any individual volcaniclast. The crushed sample was then disk milled in a Bico disk mill to produce a fine powder. A Carver hydraulic press was used to coalesce the milled powders. Boric acid was poured around the pressed sample, and the combination was compacted at high pressure (35 kpsi) to form a cohesive solid pellet. Major, minor and trace element abundances were collected using a Bruker-AXS S4 Pioneer XRF spectrometer housed at the Kentucky Geological Survey.

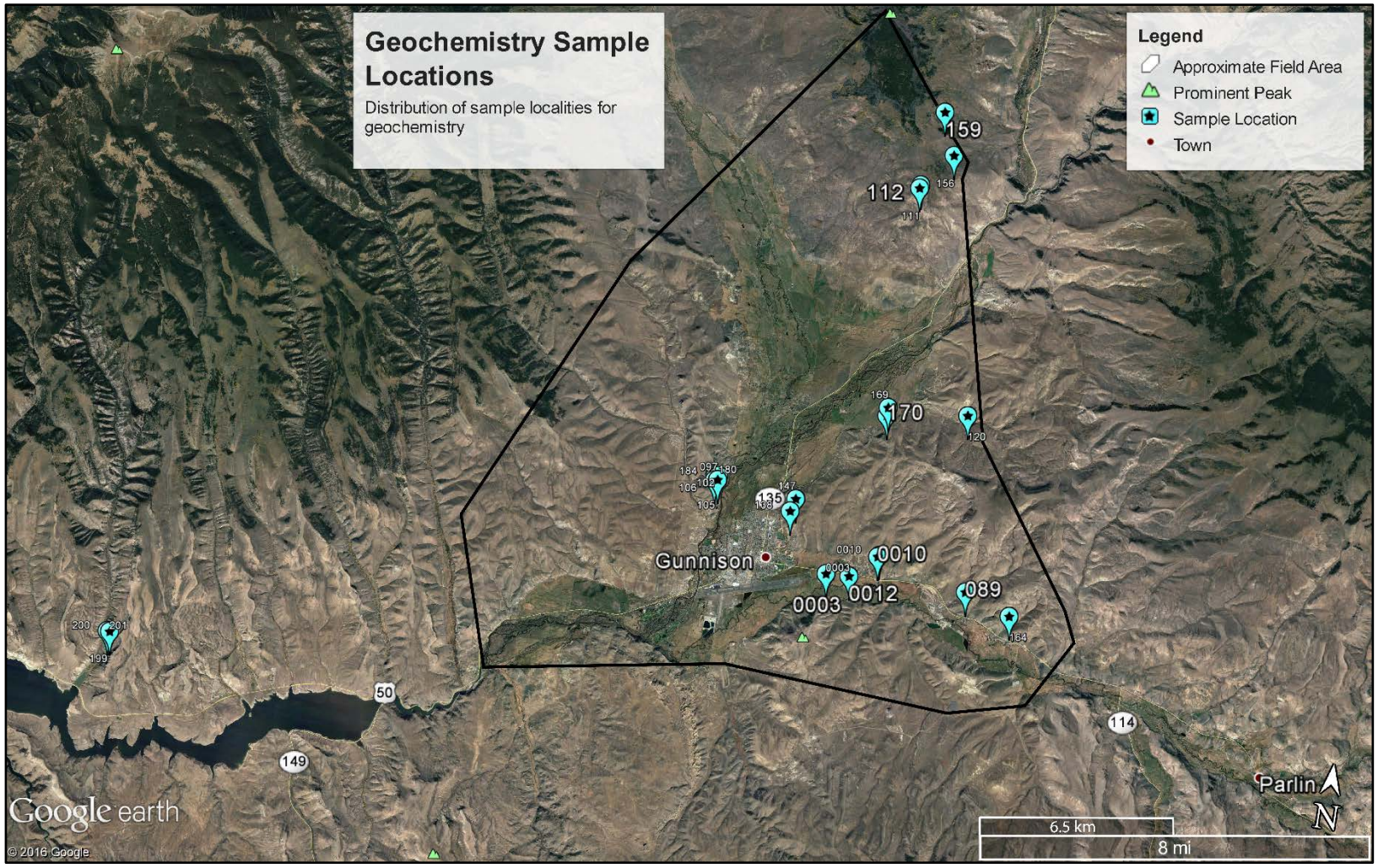

Figure 3.3. Approximate field area (black outline) and location of sample sites for geochemical analysis.

Eight standards with were used to develop correction coefficients: carbonaceous shale (Sarm 41), granite (MGT-1), greywacke (OU-10), andesite (AMH-1, AGV-2, MGL-AND), trachyandesite (AGV-1), and basalt (BCR-2), (see Appendix B). Scanning the standards and plotting the counts during a trial against known weight percentages reveals a line of best fit, which yields a calibration coefficient for components of interest (Fig. 3.4).

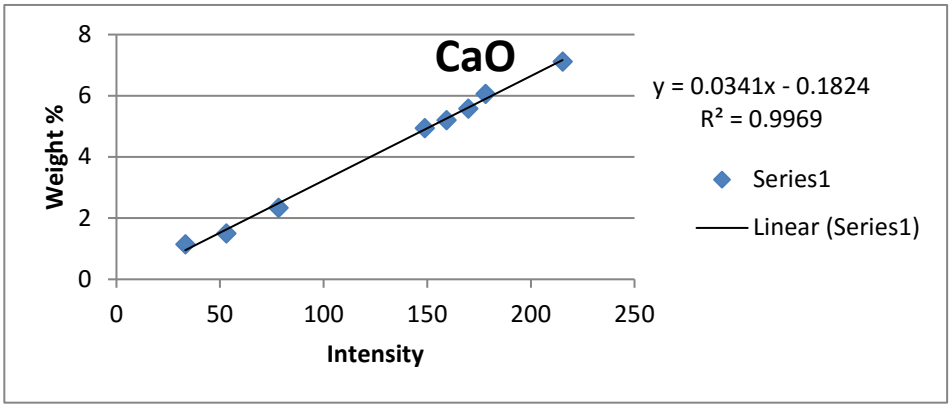

Figure 3.4. Example of CaO calibration.

3.2.1 Results

The majority of rocks analyzed are andesitic (Fig. 3.5). These data corroborate earlier geochemical studies that demonstrate early volcanism in the San Juan volcanic field, of which the West Elk Breccia is a part, are on average intermediate in composition (Fig. 3.6). Appendix B contains the complete results and sample locations.

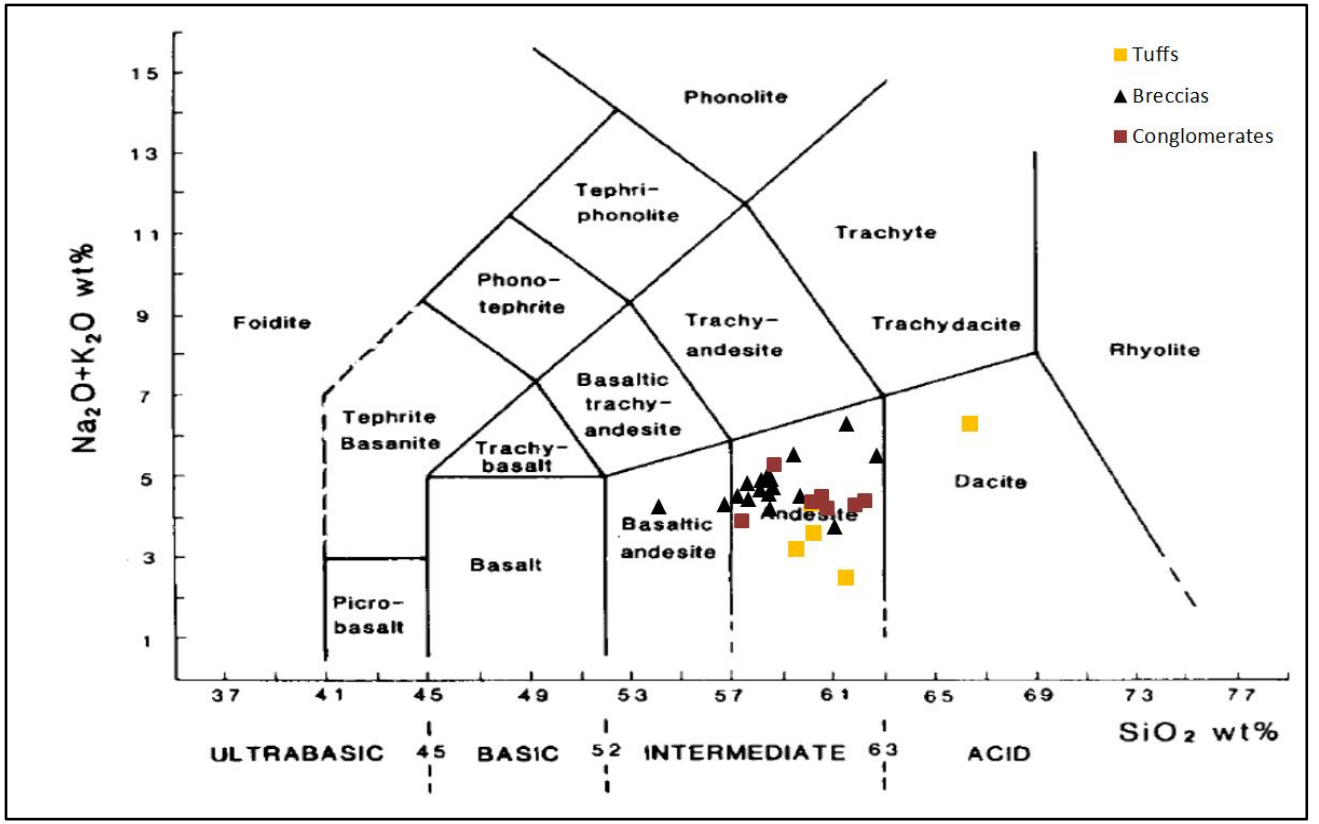

Figure 3.5. Plot of geochemical results from WD-XRF analysis with IUGS igneous-rock-classification scheme background (Le Maitre et al., 2002,). The intermediate classification corroborates earlier work referred to by Lipman et al., (1970). Tuffs refer to the East Elk Creek Tuff, a late West Elk deposit of partly devitrified lapilli and lithic tuff. The conglomerate refers to the poorly consolidated matrix phase of the West Elk Breccia, which consists of tuffaceous conglomerate found primarily in distal deposits. The breccia samples represent well-indurated volcanic-breccia samples composed entirely of volcanic material.

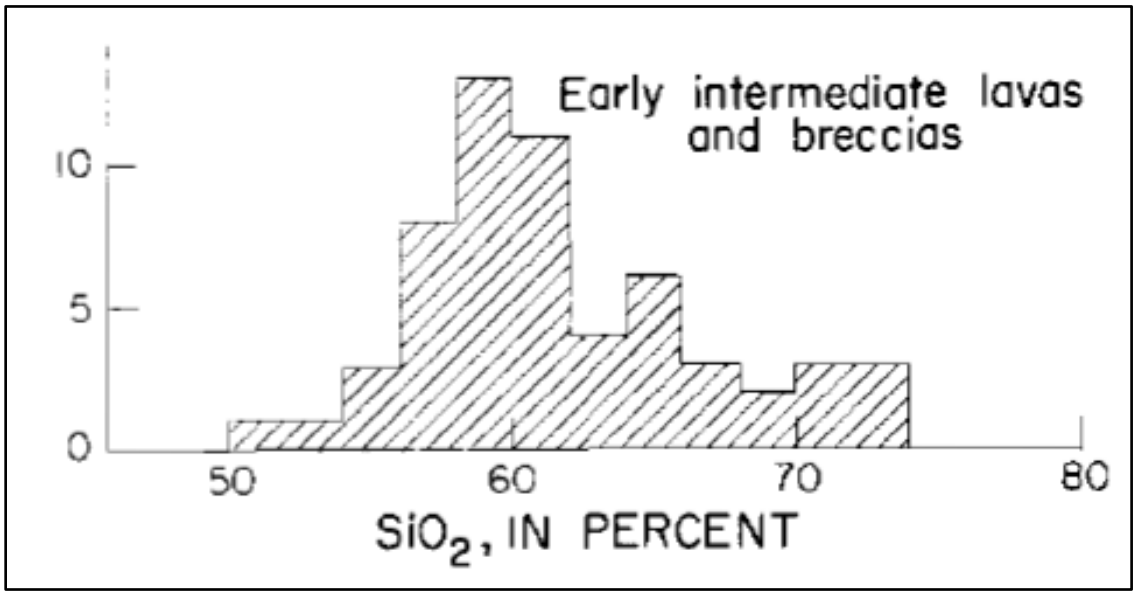

Figure 3.6. Composition of early intermediate lava and breccia samples from the San Juan volcanic field (Lipman et al., 1970).

3.3 Petrography

Despite many years of mapping and field studies by geologists, very little is known about what the West Elk Breccia is at the outcrop-to-microscopic scales. For instance, no one has reported any petrographic data on these deposits. These voids in knowledge have motivated the following questions: How do the lithologies, primarily the well-indurated breccias and the tuffaceous conglomerates, vary in framework-grain composition and texture? Can stratigraphy be verified by petrography?

Along with the measurements and descriptions recorded during the 2015 field season, I collected more than 80 samples from outcrops and roadcuts. Of these, I selected 28 for thin-sections. My objectives were to correlate units identified during the 2015 field season using framework composition or texture and identify exotic, non-volcanic matrix

in well-indurated volcanic breccias. I was motivated to investigate the latter of these objectives because of the presence of tuffaceous conglomerate in fracture fills (Fig. 2.15) and between massive outcrops of well-indurated breccia. Considering the unusual occurrence of these conglomerates, it was not clear whether the breccias are allochthonous megaclasts or represent discrete post-conglomerate debris-flow events with small-volume deposition.

Breccias, tuffaceous conglomerates and East Elk Creek samples were analyzed for principle-framework sedimentary-grain composition, matrix and cement composition, grain shapes and rounding, sorting, and size ranges (Appendix C). The composition of each specimen is based on three components in the thin-section: lithics, crystals, and vitrics (glass) (Fig. 3.7), although hand sample identification may be different considering grain size.

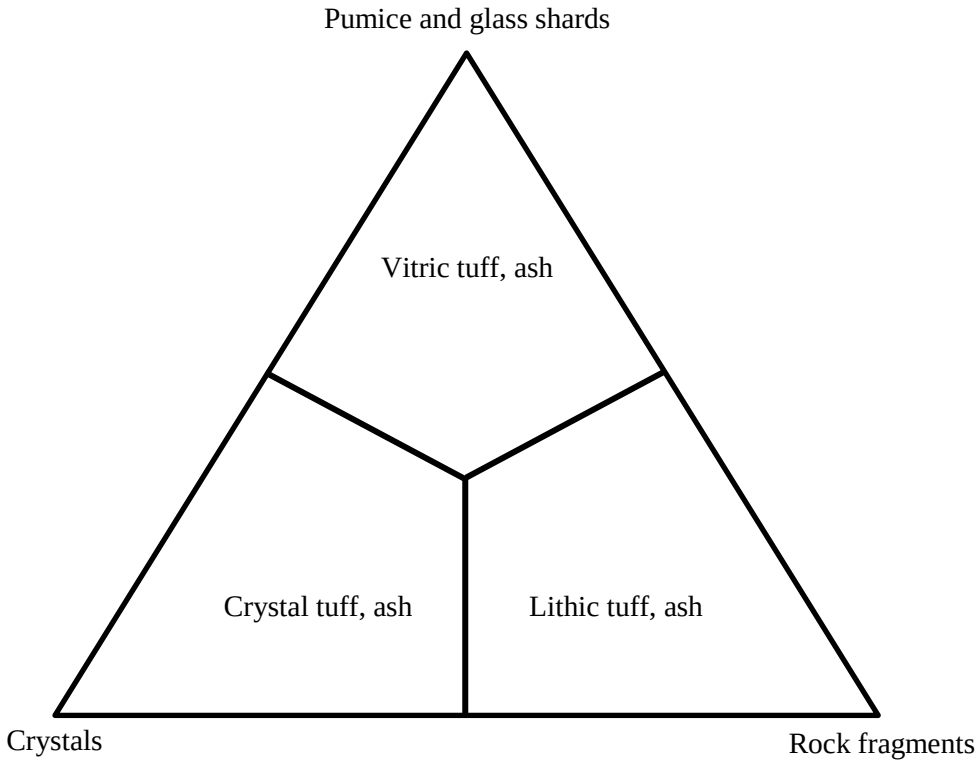

Figure 3.7. Ternary diagram, dividing tuffaceous rocks into three categories based on relative abundance of crystals, lithics, and glass (modified from Prothero and Schwab, 2014). This classification is modified and used to classify thin-section samples of the West Elk Breccia in Appendix C (http://www.sandatlas.org/tuff/#2).

3.3.1 Results

Petrographic analysis revealed that the well-indurated volcanic breccias contain only volcaniclasts in a matrix of lithics, vitrics, and subhedral to anhedral crystals of plagioclase and pyroxene (Fig. 3.8). The results of the petrographic analysis are summarized by Table 2. The tuffaceous conglomerates are composed of primarily alluvial material with a volcaniclastic matrix (Fig. 3.9). On average samples from the matrix facies are estimated to contain 32% crystals, 28% glass, and 41% lithics. Mixed

facies thin-sections are estimated to contain an average of 36% lithics, 33% crystals, and 31% glass. Samples from the East Elk Creek Tuff, the Oligocene tuff thought to have originated from the West Elk volcanic center, are estimated to contain, on average, 64% glass, 25% crystals, and 11% lithics.

TABLE 2: Average Formation and Facies Crystal Content			
	Lithics (%)	Crystals (%)	Glass (%)
Formation	28	33	39
breccia	31	31	38
matrix	41	32	28
mixed	36	33	31
EEC Tuff	11	25	64

All samples were plotted on a single ternary diagram and summarize the results of petrographic analysis (Fig. 3.10). Many samples exhibit secondary growth of calcite cement from the alteration of volcanic minerals. The complete results of this analysis are listed in Appendix C.

Petrographic analysis indicates that the volcanic breccias are distinct from the tuffaceous conglomerates in composition of framework grains. The volcanic breccias do not reveal any non-volcanic alluvial clasts in the framework. They are primarily composed of rounded-to-angular volcaniclastic fragments of intermediate lavas with abundant plagioclase and some pyroxene crystals (Fig. 3.8). Crystals not contained within volcanic fragments tend to be abraded and highly angular.

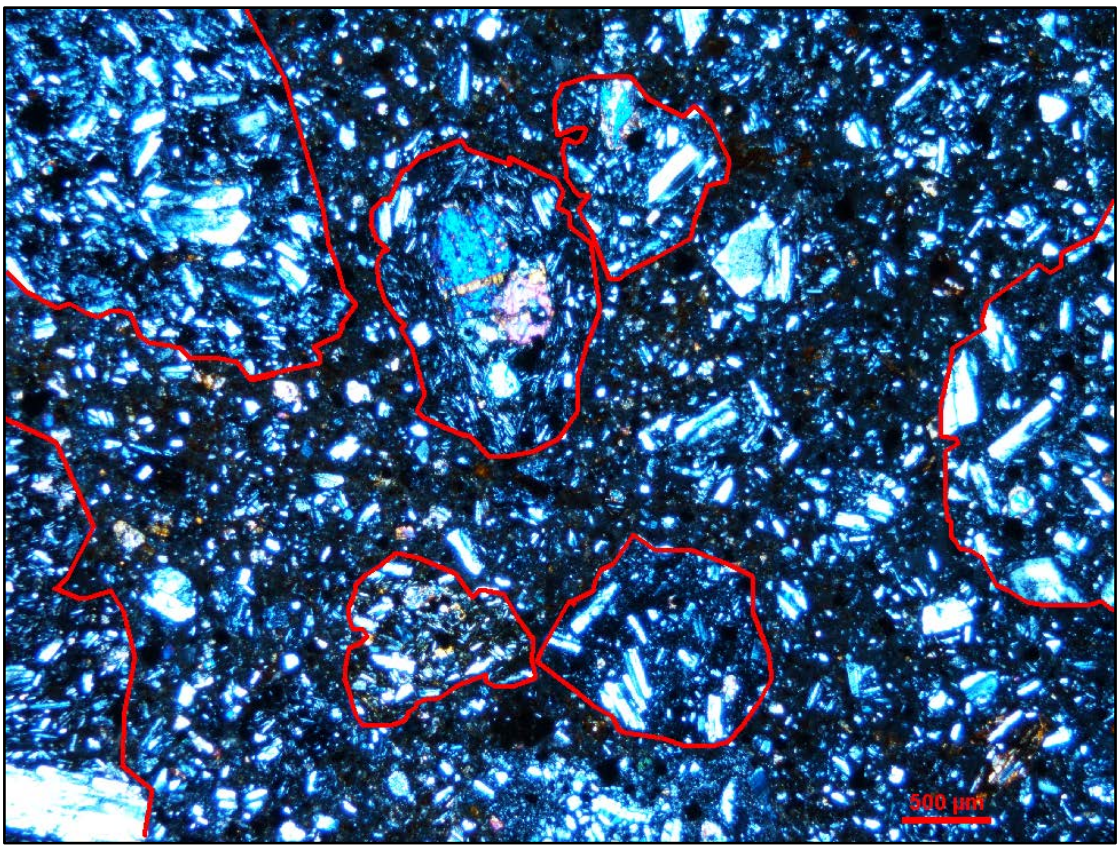

Figure 3.8. Photomicrograph in cross-polarized light of sample number 07221504, a well-indurated volcanic breccia from the upper section of the Palisades. Lithics are outlined in red (not all lithics are outlined) and separated by a matrix of glass and angular crystals. Note size range of lithic volcaniclastic grains; the scale bar is 500µm (full results in Appendix C).

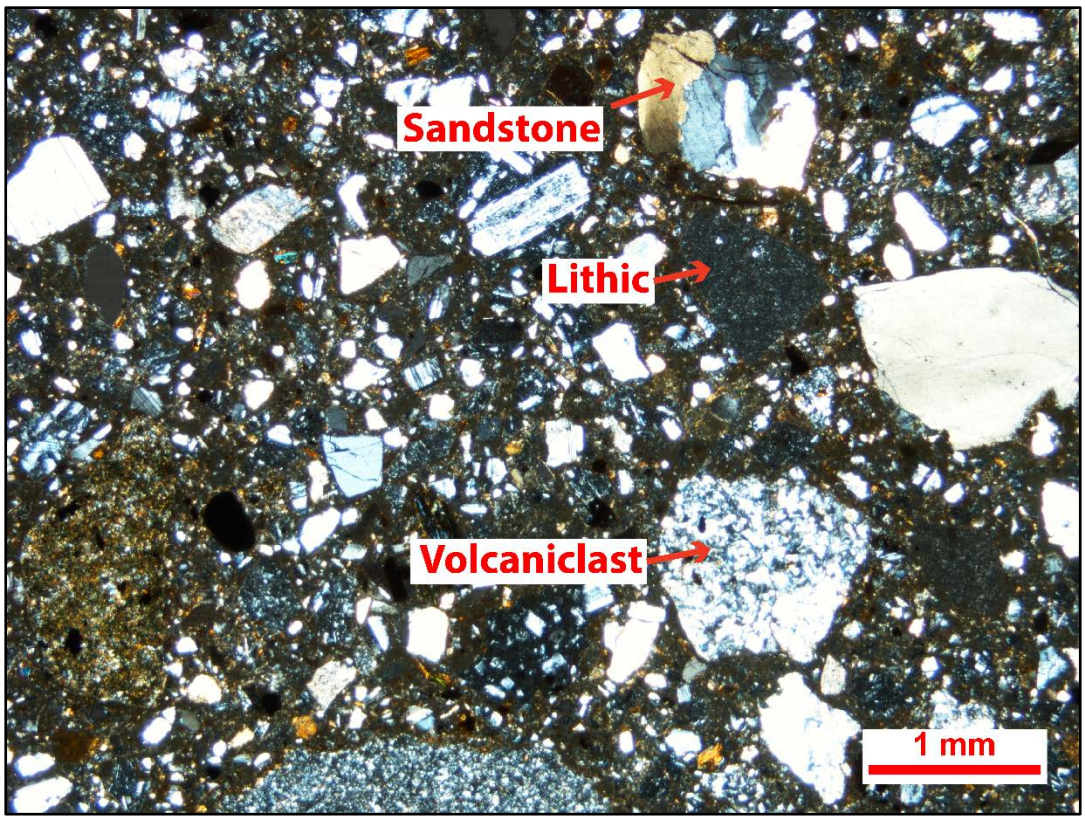

Figure 3.9. Photomicrograph in cross-polarized light of sample number 08091502, a tuffaceous conglomerate. Note the range in rounding and angularity. Among angular and subrounded volcaniclasts are rounded sandstone grains with undulatory extinction and fine-grained exotic lithic clasts.

Detailed analysis would be required to determine subtle differences in volcanic-breccia deposits for the confirmation of time-equivalent strata. In any case, the well-indurated breccias are composed of primarily volcaniclasts, crystals, and a glassy matrix. In contrast, the tuffaceous conglomerates contain a matrix of fine lithics composed of exotic alluvium and volcanic fragments, suggesting that they partially mixed with or bulked up on alluvium during transport.

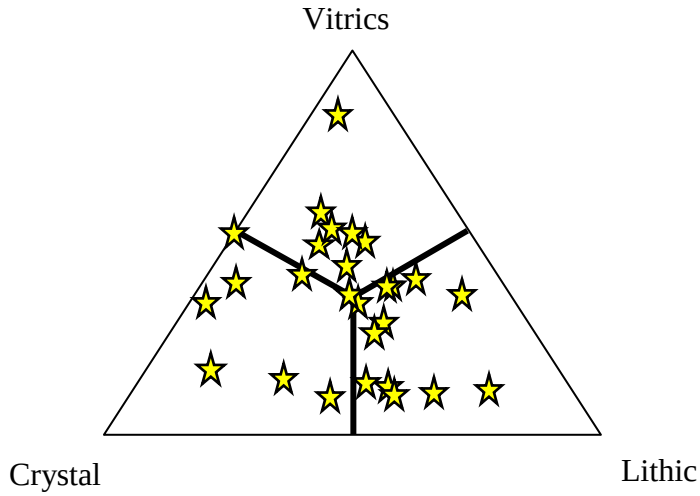

Figure 3.10. Composite results of petrographic analysis and modal estimates for all West Elk Breccia and East Elk Creek Tuff samples. The majority of the plots for petrographic samples fall within the lithic sector of the ternary diagram.

3.4 Grain-Size Analysis

To further characterize and understand the West Elk Breccia, matrix-facies samples were analyzed for grain-size distribution. If a measurable depreciation in grain size is a function of distance from the source, decreases in coarse material should appear in more distal grain-size data. Such a pattern would corroborate the proposed transport direction of flow(s) and may also elucidate information about how the flow(s) transformed in space. Furthermore, this work may provide the basis for discerning the most effective methods in future matrix-facies analyses.

Samples were collected from a total of 14 locations for grain-size analysis (Fig. 3.11). Approximately one-gallon samples were gathered at each outcrop at varying locations within the outcrop. In general, the collection, preparation, and sieving processes were kept constant with only minor variation in the disaggregation process. To prepare for dry sieving, samples were carefully crushed by hand using a standard 16-oz sledge hammer. Samples were then placed in approximately 1–2 gallons of tap water and further disaggregated for 10 minutes, using either a metal table spoon or an ultrasonic homogenizer (Fig. 3.12). After this initial disaggregation process, samples were left to sit for 24 to 48 hours. After allowing the samples to settle, excess water was carefully removed and the samples were dried for 24 hours. After drying, samples were carefully added to a nested-sieve set. Any clast or aggregate greater than 32 millimeters was removed before sieving. I used eight U.S. Standard sieves from -4 to 3 phi sizes at approximately one-phi intervals to separate the samples. In one instance, sieve sizes from U.S. Standard no. 5–325 were used (see Appendix E for details). I used an automatic shaker machine to sieve the samples for 10 minutes each. After sieving, samples were carefully weighed twice and the weights were recorded.

Figure 3.11. Distribution of waypoints where samples were collected for grain-size analysis. Complete results are listed in Appendix E.

Figure 3.12. Showing samples that have been crushed and are being soaked after agitation with the ultrasonic homogenizer shown in the foreground. The model is an Omni-Ruptor 250. The tuffaceous-conglomerate matrices broke down moderately well in tap water after crushing and agitation.

3.4.1 Results

The data suggest a primarily polymodal trend in grain size with positive skew as shown by the composite histogram (Fig. 3.13). Although the samples are very poorly sorted (high variation in peaks to tails), there appears to be a consistent peak in the -2 to -1, granule (Wentworth), phi-size class, which appears in almost every sample. A second, less pronounced peak appears at the 1–2 phi size range. A third peak or partial peak in some samples occurs in the fraction of the matrix sample that is finer than the 4-phi size classification. The alluvial-raft sample, which was not lithified, was unimodal and non-skewed (Fig. 3.14) and provides a control for comparison with the tuffaceous-conglomerate samples.

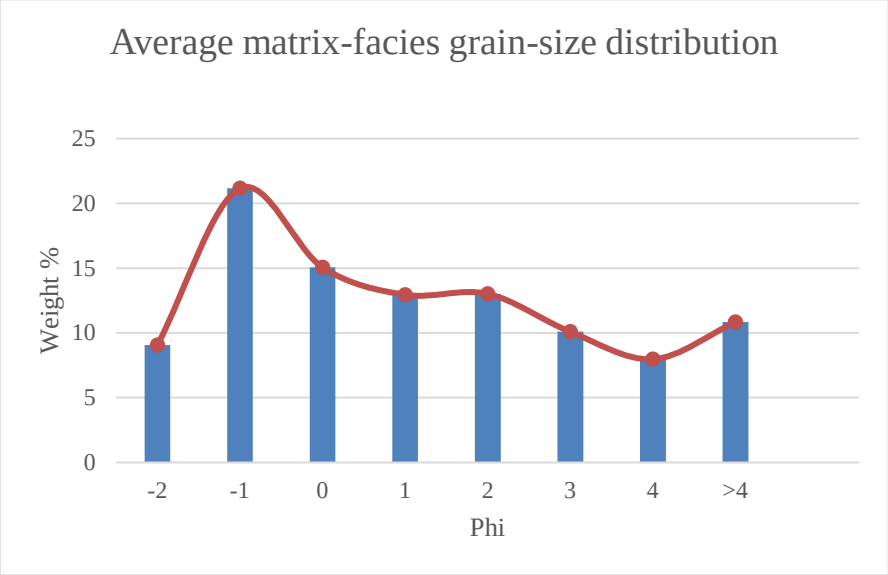

Figure 3.13. Average grain-size distribution representing all matrix facies samples. Each bar represents a bin from the phi size below to the last phi size. For example, at the -2 phi label, the bar represents the frequency or weight percent of sample that was between -2 and -4 phi. Note the multiple peaks and the positive skew. See Appendix D for complete results.

These data are partial at best and provide only a glimpse of the range in grain size between pebbles (<-4 phi) and silt (>4 phi) sizes. Sieved samples greater than -4 phi were excluded from most analysis because of bias created during the disaggregation process. A summary of statistical analysis is presented in Table 3. Outcrops contain abundant gravel of all sizes, from meter-sized to micro-sized.

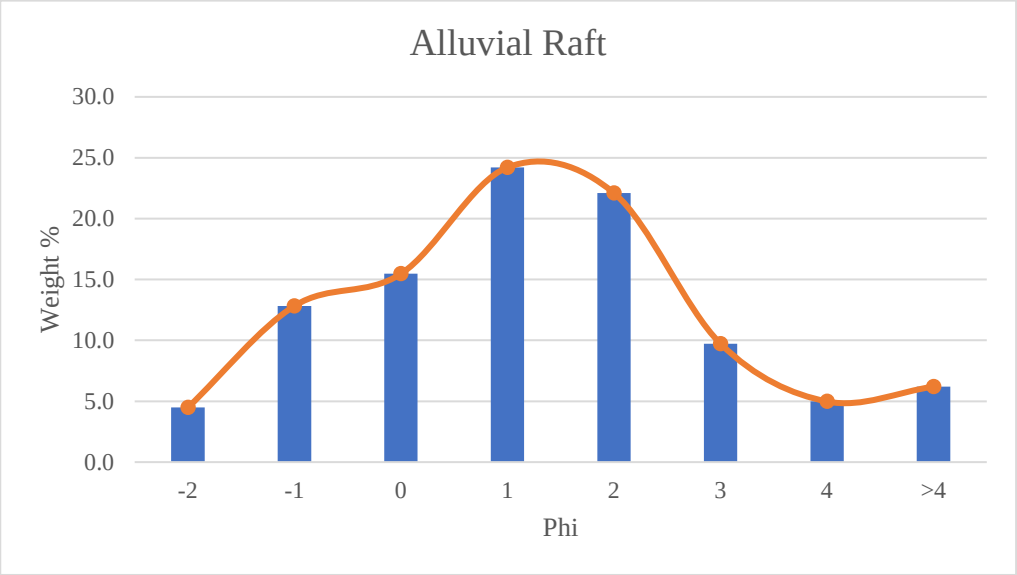

Figure 3.14. Grain-size distribution for the alluvial raft sample. The location of the raft is the western margin of the road cut at WP 0090 on U.S. 50, east of Gunnison, Colorado. The unimodal distribution suggests normal stream flow.

TABLE 3: Grain-Size Distribution Statistics Summary							
Sample (WP)	**Distance (km)**	**σ(<-4φ)**	**Sorting**	**Skew-ness**	**Skew**	**Kur-tosis**	**σ (includes > -4φ)**
205a	38.50	2.03	very poorly sorted	0.05	coarse skewed	2.38	3.10
Alluvial Raft	38.50	1.86	poorly sorted	0.31	strongly fine	3.05	2.70
164	39.70	2.02	very poorly sorted	0.56	strongly fine	2.89	2.30
217	27.80	2.30	very poorly sorted	0.29	fine	2.21	2.54
29	29.90	2.34	very poorly sorted	0.26	fine	2.09	2.73
90	38.50	2.33	very poorly sorted	0.32	strongly fine	2.12	2.82
227	29.00	2.38	very poorly sorted	0.21	fine	1.99	2.13
0089 (TP-Unmixed)	38.00	2.57	very poorly sorted	0.70	strongly fine	2.30	1.52
WP0089 (Tp-Mixed)	38.00	2.55	very poorly sorted	0.37	strongly fine	1.97	2.58
111	30.00	2.40	very poorly sorted	0.36	strongly fine	2.09	1.89
Coyote	37.40	2.35	very poorly sorted	0.13	fine	2.02	2.32
223	25.50	2.36	very poorly sorted	0.40	strongly fine	2.15	1.99
14	34.80	2.32	very poorly sorted	0.49	strongly fine	2.30	2.68
Castle Creek	8.26	2.25	very poorly sorted	0.83	strongly fine	2.91	2.13
10	34.66	2.41	very poorly sorted	0.32	strongly fine	2.08	2.58
220	26.40	2.24	very poorly sorted	0.24	fine	2.22	2.76
Samples are listed by way point or otherwise; see Appendix E for complete locations and data.							

3.5 Stream-Gravel Inventories

If the West Elk Breccia represents a volcanic debris avalanche(s) that transformed to a debris-flow(s) and incorporated, as well as deposited, sediment, there may be a statistical method for showing this based on the clast compositions. I collected lithologic and geometric data (size and rounding) for pebbles, gravel and boulders within the matrix facies of the West Elk Breccia. These data were collected by grabbing a random number of clasts within an area of no more than a square meter at an outcrop, or, if no outcrop was present, from within float. Typically, 10 or more clasts were analyzed at each location. The clasts were randomly selected, the long axis was measured, and the composition was determined from a fresh surface. Telltale sedimentary structures or compositions allowed for identification of source formations or ages, in some instances. The Gunnison Basin has seen nearly continuous non-marine deposition since Cretaceous time (Hansen, 1965). Thus, abundant alluvial gravel and paleochannel networks must have been spread across the study area. Deconstructing the sources of the alluvium may only be possible through careful study of the wide-ranging alluvium found in the area.

As discussed, uplift of the Elk and Sawatch ranges drove erosion and sedimentation into nearby parts of the Piceance Basin. Paleozoic sedimentary rocks may only have been derived from the Sawatch and Elk ranges, because these were the only places in the study area where these rocks outcropped. Paleozoic clasts should increase in abundance with distance from the volcanic source. As an example, Crandell (1989) noted that within 22 km of Mt. Shasta, the Pleistocene volcanic debris-avalanche deposit contains only Mt. Shasta derived clasts. Further, Crandell (1989) noted that there is a

decrease in Mt. Shasta rocks with distance from the volcano in the matrix facies of this deposit.

3.5.1 Results

The data suggest, on a cumulative basis, that medial-to-distal deposits decrease in volcanic-rock abundance from 50% to 27%, while Precambrian and Paleozoic rocks increase in abundance from 37% to 42%. These data are displayed in Tables 4 and 5 and graphically in Figures 3.15 and 3.16. Where precise sources were indeterminant, rocks were categorized as “sedimentary undefined” or “crystalline undefined.” All data were tabularized and graphed for each outcrop or location analyzed, and the complete results can be found in Appendix D.

Table 4: Medial Stream-Gravel Analysis		
Source	**Counts**	**%**
Precambrian	17	35
Paleozoic	1	2
Mesozoic	0	0
Tertiary intrusive	2	4
Volcanic	24	50
Sedimentary undefined	4	8
Crystalline undefined	0	0
Sum	48	100

Table 5: Distal Stream Gravel Analysis		
Source	**Counts**	**%**
Precambrian	97	36
Paleozoic	16	6
Mesozoic	9	3
Tertiary intrusive	16	6
Volcanic	74	27
Sedimentary undefined	15	5
Crystalline undefined	46	17
Sum	273	100

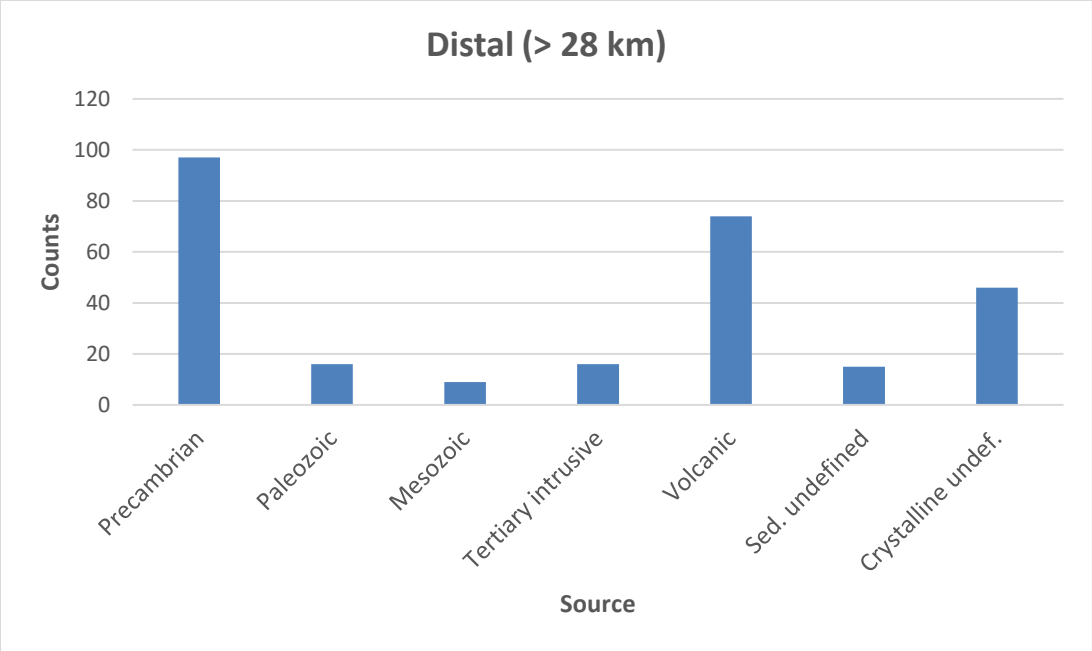

Figure 3.15. Cumulative clast-composition counts for distal gravels within the matrix facies or found as float at a stratigraphic interval that corresponds to the West Elk Breccia. Distal deposits are all those greater than 28 km from the volcanic center.

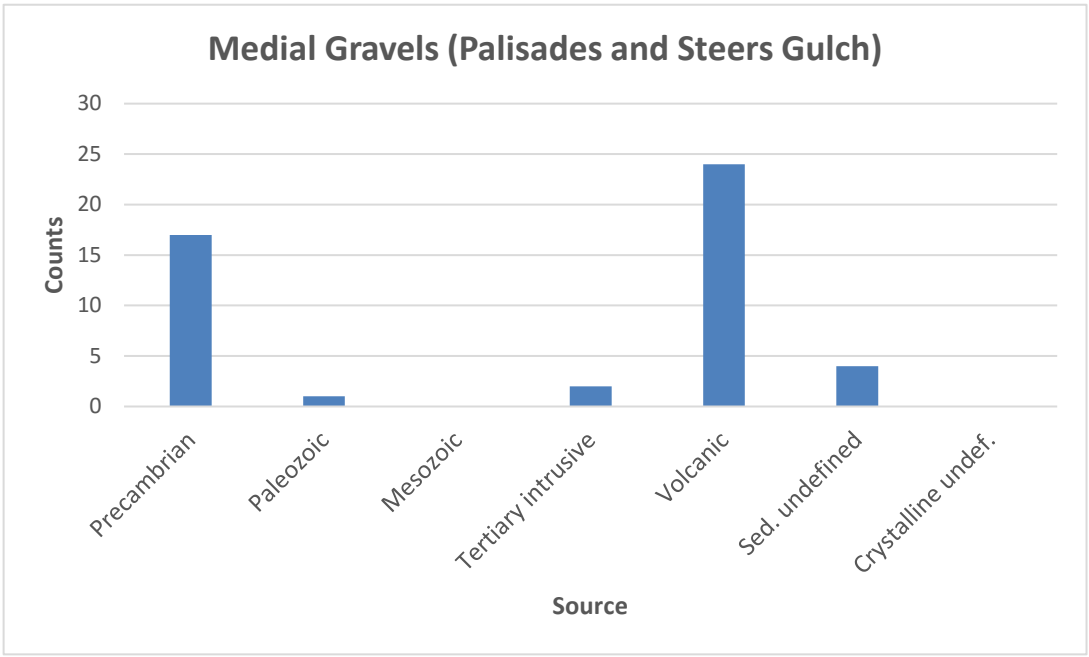

Figure 3.16. Cumulative clast-composition counts for medial gravels within the matrix facies or found as float at a stratigraphic interval that corresponds to the West Elk Breccia. Medial gravels were analyzed from the matrix facies at the Palisades and Steers Gulch.

CHAPTER 4: Interpretations

As discussed in previous parts of the study, the West Elk Breccia has been subject to many different interpretations, including tillite, laharic breccia, pyroclastic breccia, tuffaceous conglomerate, and probably several other interpretations related to various types of parabreccias (Atwood and Atwood, 1926; Hansen, 1965; Obradovich et al., 1969; Hedlund, 1974; Hedlund and Olson, 1974; Gaskill et al., 1981; Stork et al., 2006, 2007). Most of these interpretations were generated during examination of exposures in the eastern Gunnison River valley, where the outcrops are most accessible. Some of the interpretations, like that of tillite, have been firmly disproven (Van Houten, 1957). Other interpretations, however, may still be accurate for some parts of the unit, and herein lies the major problem with interpreting this unit—namely, that the formation exhibits such wide vertical and lateral stratigraphic and sedimentological variability; that parts of the formation were subject to penecontemporaneous movement from original positions both during and after deposition; and that the unit is so susceptible to weathering and erosion that what remains is like a mosaic, most parts of which have been scattered or destroyed. Although this study does not prove or disprove earlier interpretations (they may all be correct for one part or another of the unit), but it does merit another interpretation that has never been suggested based on the data collected and observations made. As has been implied by observations in early parts of the study, that interpretation is of a volcanic debris avalanche and related debris flows. Such an interpretation has not been made before, largely because most workers have never ventured much beyond the easily accessible exposures in the eastern Gunnison River valley. Even there, however, features are present that are difficult to explain without the debris-avalanche model. In gathering

evidence to support this hypothesis, I will call on three scales of evidence for support: volcano-scale evidence, outcrop-scale evidence, and smaller-scale intra-outcrop evidence.

4.1 Volcano-Scale Evidence

Debris avalanches occur as a result of volcanic sector collapses. Due to oversteepening, overloading, or a push from internal magma, all of which may be facilitated by high-pressure systems and precipitation, segments, or sectors, of a volcano may collapse (Siebert et al., 1987; de Vries and Francis, 1997) and in the process, give rise to debris avalanches, which in run-out may generate debris flows (e.g., Vallance and Scott, 1997). During their life history, most stratovolcanoes will experience multiple sector collapses, and the immediate evidence for one of these collapses is a horseshoe-shaped crater or indentation on the flank of a volcano (Fig. 4.1). Although different geologic quadrangle maps show mapped portions of what remains of the Oligocene West Elk volcano, the only geologic map to show the entire volcano is a sketch map by Gaskill et al. (1981). Interestingly, this map clearly shows a major indentation in the northern flank of the volcano, a scar into the chaotic and volcaniclastic facies that define upper parts of the volcanic cone, which reveals the underlying basal-cone facies, as well as underlying intrusive and sedimentary units that form the foundation on which the volcano sits (Fig. 4.2). I interpret this to represent some sort of late-stage sector collapse on the West Elk volcano. Although this collapse is probably not related to any of the breccia units under study, it does illustrate that sector collapses occurred on this volcano, and like other stratocones, these collapses were probably common features during its life history.

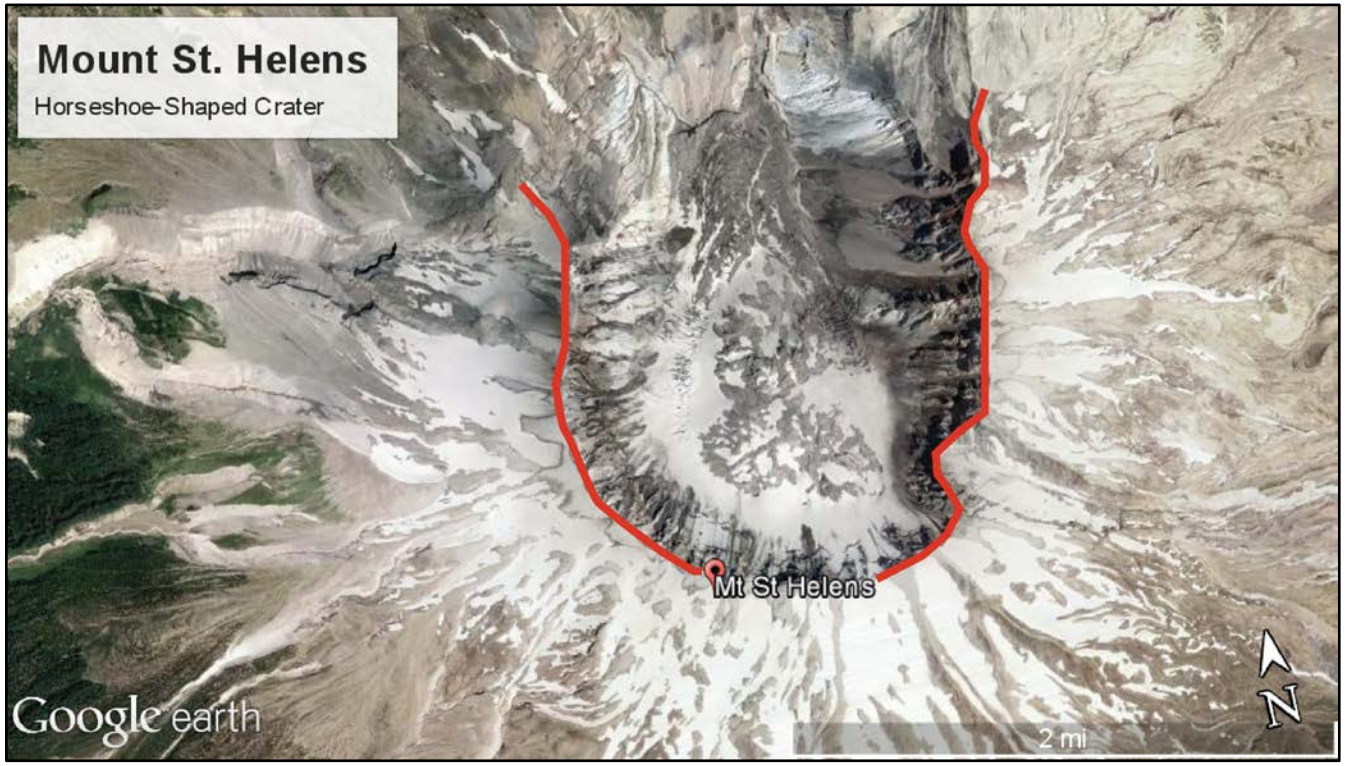

Figure 4.1. Horseshoe-shaped crater at Mt. St. Helen, Washington. Opening to the north, the crater is a result of the May 18, 1980, sector collapse and lateral blast.

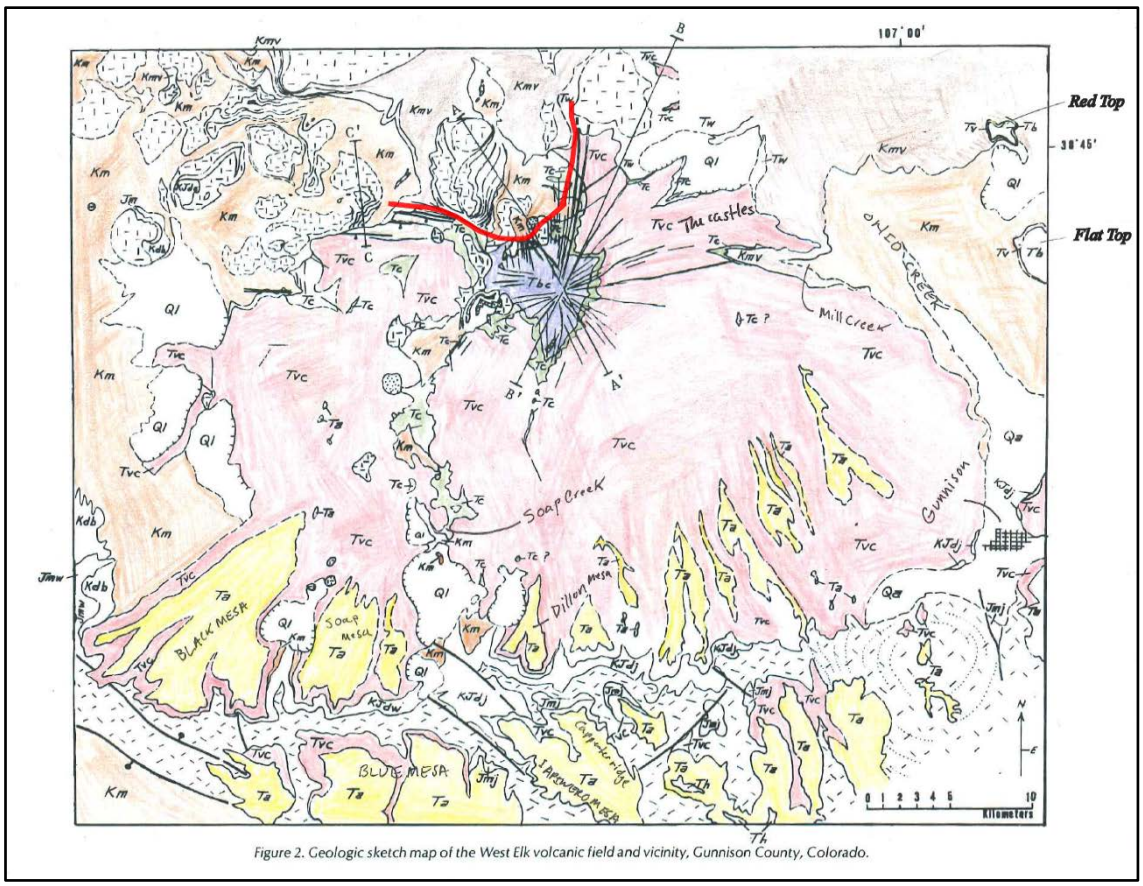

Figure 4.2. Generalized geologic map modified from Gaskill et al., (1981) to show geographic features of prominence and to show a potential horseshoe-shaped collapse scar (red line) on the northern flank of the volcano. In this sector, radial dikes are mostly absent as is the volcaniclastic facies, but present is the underlying Cretaceous Mancos Shale as well as the chaotic facies, suggesting that part of the volcano may have slid away. This absent sector may or may not have be related to the deposits in the study area, but it does show the potential for large-scale collapse.

4.2 Paleoclimate

Glaciation and snow cover can greatly affect volcanic sedimentation and contribute to edifice instability (Vallance and Scott, 1997; Pierson et al., 1990). Glaciers can contribute to instability through hydrothermal alteration and can contribute significant volumes of water to a debris avalanche that can transform the avalanche to a

debris flow (Vallance and Scott, 1997; Glicken, 1995). Therefore, it is important to explore the question: was there snow and/or ice on the West Elk Volcano that contributed to possible debris avalanches? I can model the conditions for a climate that supports snow and possibly ice, using paleoclimate data from the literature (Wolfe and Schorn, 1989; Larsen and Crossey, 2000; Barton, 2010). First, I can use empirical data from Siebert et al. (1987) to calculate the height of the West Elk Volcano. The average height-to-length ratio for volcanic debris-avalanche deposits is 0.09 (Siebert et al., 1987). Using this and the maximum runout distance for the West Elk Breccia (45 km), I calculate the height of the West Elk Volcano to have been about 13,000 feet:

$$\frac{H}{L} = 0.09$$

$$H = 0.09 * (45km) = 4.05km = 13{,}280\ ft$$

Paleoaltitudes were likely greater than estimated because of subsidence from Cenozoic extension and thermal sag following the Laramide Orogeny and Oligocene flare-up (Wolfe and Schorn, 1989). Maximum-runout distance is based on remaining outcrops of West Elk Breccia, and hence, it is likely that the West Elk Breccia extended beyond 45 km, but has since been removed by erosion. If we assume a paleo-latitude of 40° N, paleo-temperature averages in the 10°C to 4°C range (Table 1), a summit altitude of 13,280 feet or more, and fossil leaves of cedar and oak (Fig. 4.3), I interpret that the climate was likely temperate subalpine with significant precipitation primarily as snowfall and with the potential to sustain permanent snow or ice. It is likely that the paleo-West Elk volcano was snow covered and possibly glaciated.

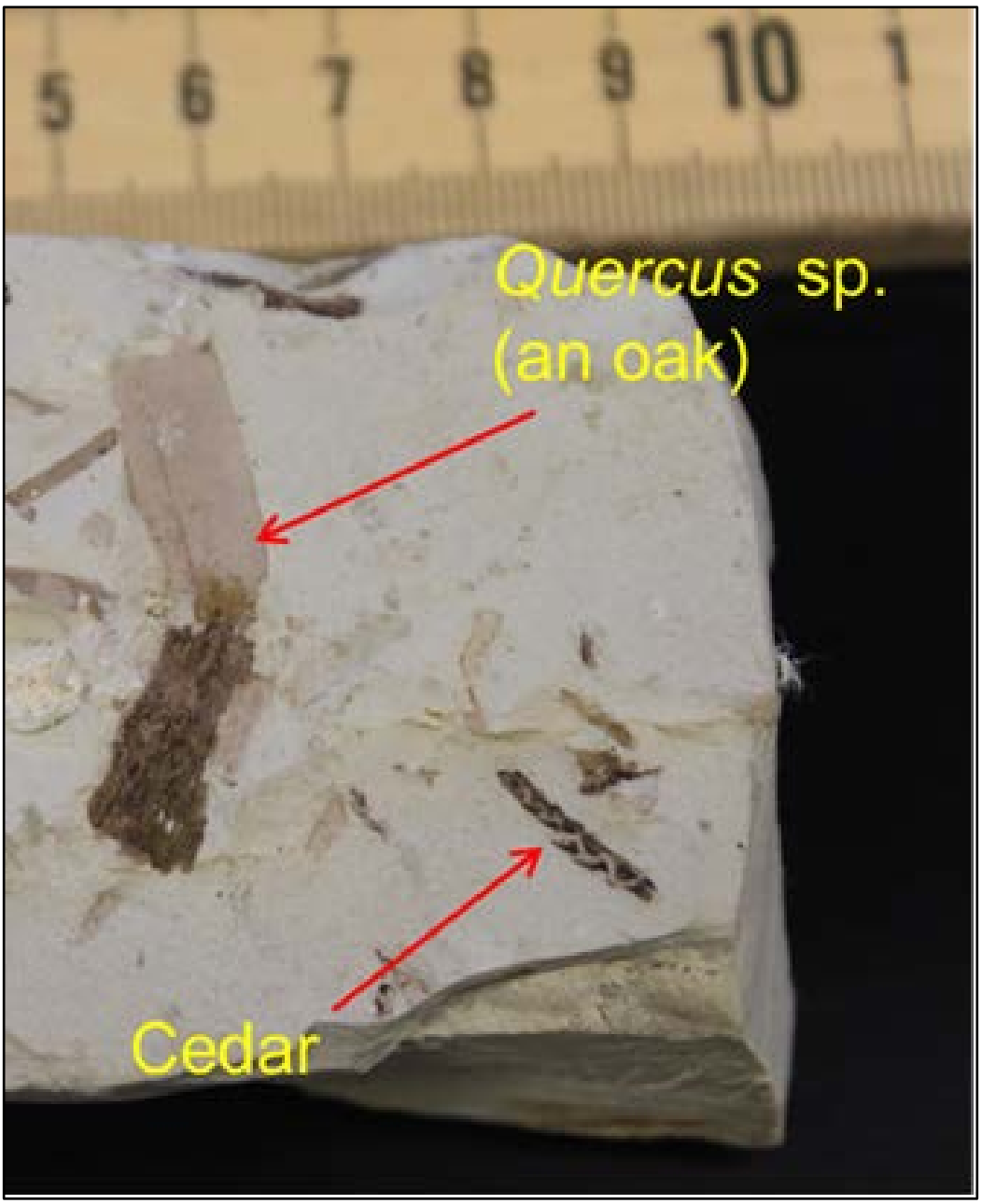

Figure 4.3. *Quercus* (oak) and cedar leaf and needle fragments in a water-laid tuff from the West Elk Breccia. These fossils corroborate paleoclimate data from Wolfe and Schorn (1989), suggesting that the West Elk volcano area was also probably temperate to subalpine.

4.3 Outcrop-Scale Evidence

As has been shown in previous sections, volcanic debris avalanches involve large volumes of material (up to 100 km^3), and as such, identifying the textural characteristics requires examining outcrops at different scales. The constituents of such voluminous mass movements are, in turn, very large and include homogeneous blocks of the original edifice surrounded by a matrix of clastic material (Siebert, 1984). The main constituents of such deposits are divided into a block facies and a matrix facies (e.g., Crandell, 1989; Malone, 1995; Roverato et al., 2014). The contacts between these facies are often sharp and highly irregular (e.g., Schneider and Fischer, 1998; Malone, 1995).

The influence of such irregular blocks of the original volcano on the local topography is referred to as hummocky topography (Figs. 2.6, 2.7). Along Ohio Creek, there is strong evidence of such topography that has been partially exhumed (Fig. 2.7). Here, the West Elk Breccia, along the western margin of Ohio Creek, is represented by blocks of resistant volcanic breccia, which are often bedded and dipping at irregular angles. Low places between the breccia blocks are often filled with tuffaceous stream gravels.

The Palisades (Fig. 4.4) is interpreted to reflect a dissected outcrop of megaclasts and matrix facies. From afar, the deposit looks like a massive, somewhat irregular cliff along the Gunnison River. A closer examination, however, reveals a heterogeneous complex of layered megablocks dipping at high angles with sharp, irregular contacts to a light-colored tuffaceous conglomerate (matrix facies) (Fig. 4.5).

The relationships between these massive megablocks and the matrix facies is especially telling (Fig. 4.6). Examination of the upper part of the main Palisades block

reveals a thick layer of matrix facies surrounding the upper portion of the block (Fig. 4.7). As in most areas, the matrix facies is highly weathered and primarily found where erosion is limited. A few hundred feet to the north of the megablock, shown in Figures 4.5 and 4.6, are dipping beds of lapilli tuff and breccia (Fig. 4.8). They too are juxtaposed with conspicuously sharp and irregular contacts to the matrix facies and massive volcanic breccia. Interestingly, the bedded breccias and lapilli tuffs are oriented differently than the previously mentioned and nearby megablock (Figs. 4.6, 4.7). Because the underlying Mesozoic rocks do not show similar orientations (Stork et al., 2006), I can conclude with some certainty that the varying orientation of these blocks is due to some sort of sliding or slumping, probably the result of avalanching.

A more obviously entrained megablock is observed two miles east of Gunnison in a roadcut (Fig. 4.8). As discussed earlier, megablocks decrease in size and abundance away from the source (Siebert, 1984). Along U.S. 50, the sizes of megaclasts decrease in the outcrops from west to east (Fig. 3.2a).

Figure 4.4. Macroscopic view of the Palisades from near the Gunnison Middle School. The black rectangle corresponds to the extent of Figure 4.5.

Figure 4.5. A close-up view of the Palisades, hinting at more complexities than what is shown in Figure 4.4. The observed area is outlined in Figure 4.4. Numbered boxes correspond to the following Figures 4.6– 4.9.

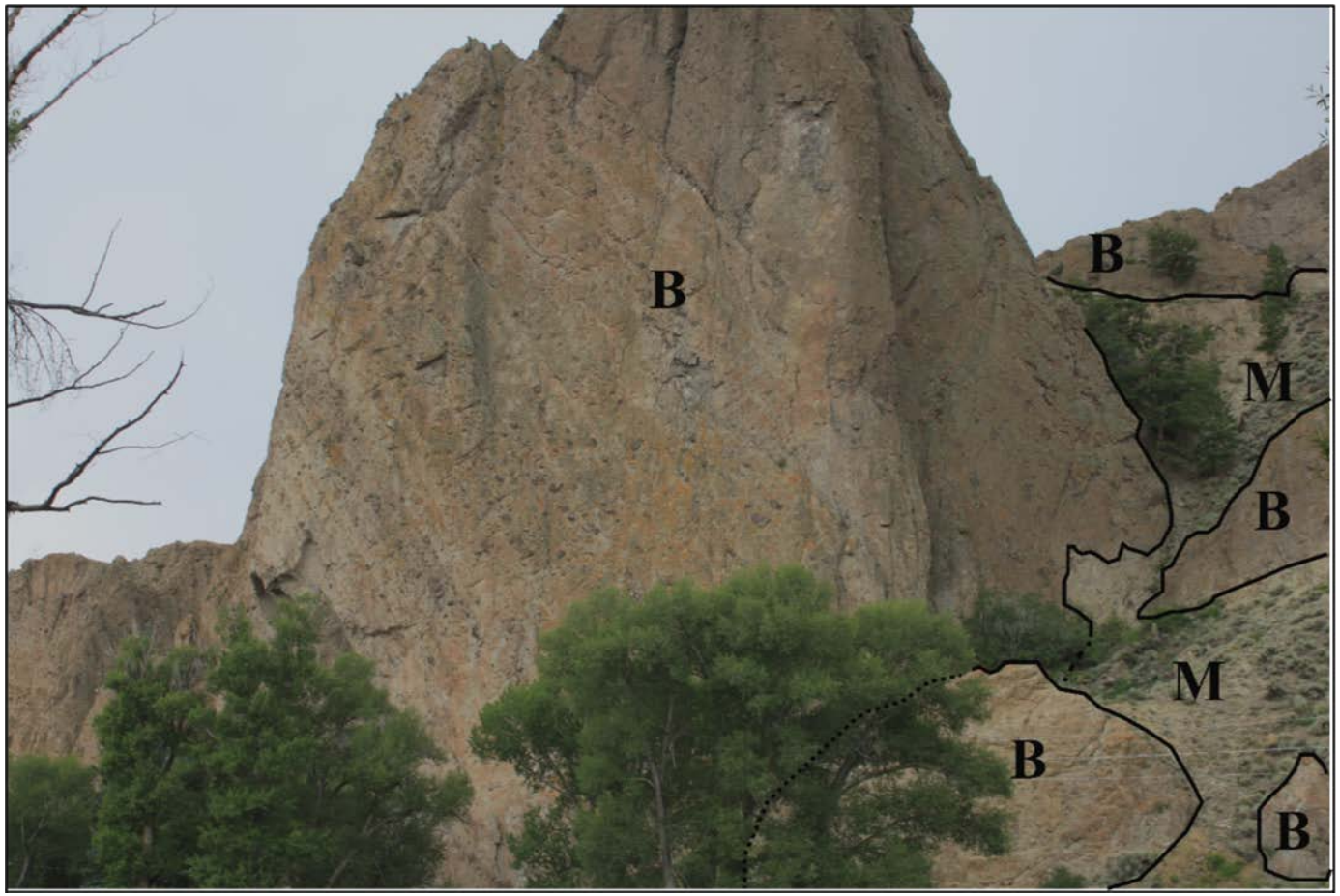

Figure 4.6. Close-up view of box 1 from Figure 4.5. Volcanic breccia megaclasts (B) are partly to wholly surrounded by matrix facies (M). The breccia has intact stratigraphic layers dipping at steep angles (about 40° NW). The light-colored matrix facies cross cuts the breccia at irregular angles and partially surrounds blocks.

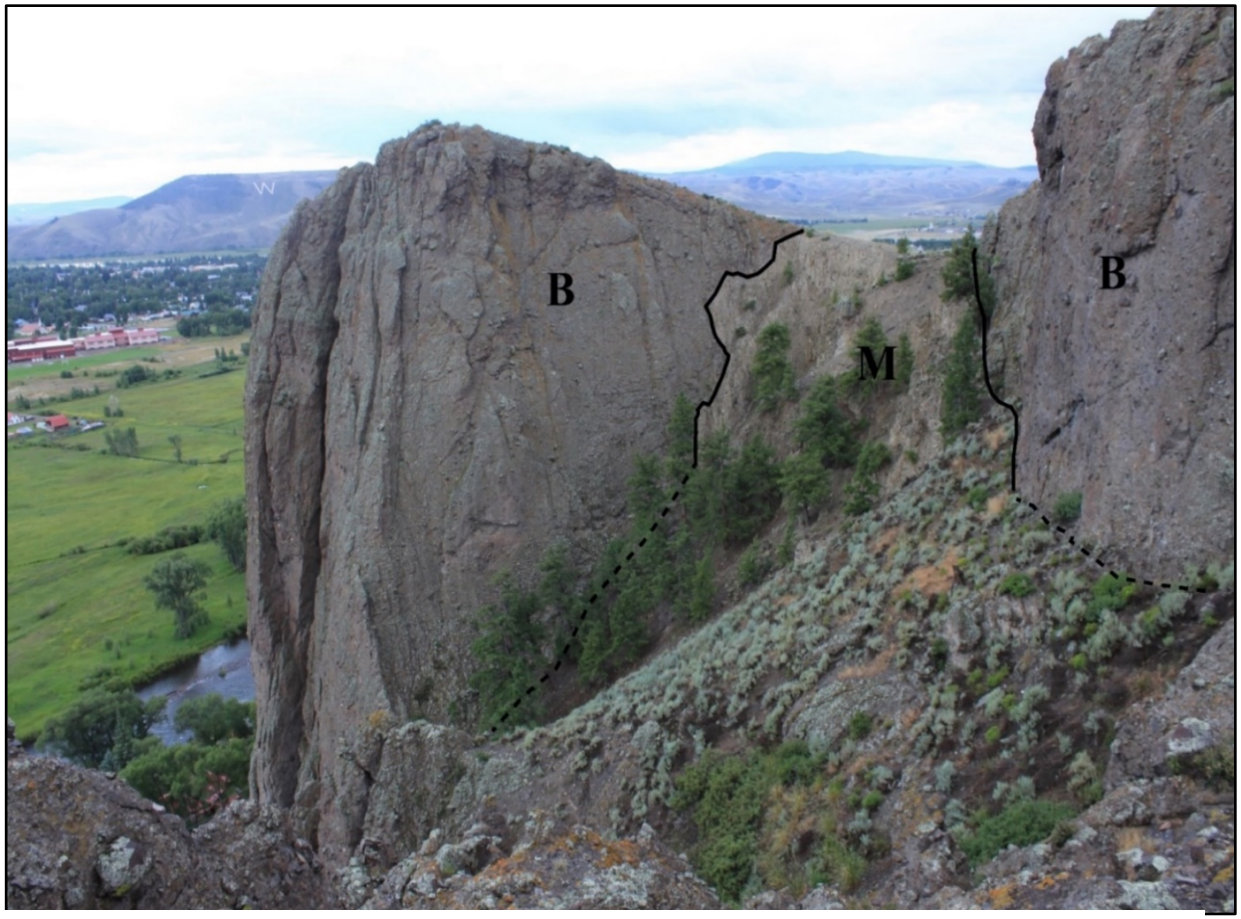

Figure 4.7. Point-of-view 3 from Figure 4.5. The back and upper part of the megablock shown in Figure 4.6. One can see the light-colored matrix extending behind and along this megaclast. Several saddles of unsorted and unstratified tuffaceous conglomerate can be found between megaclasts of volcanic breccia along the ridge that is the Palisades.

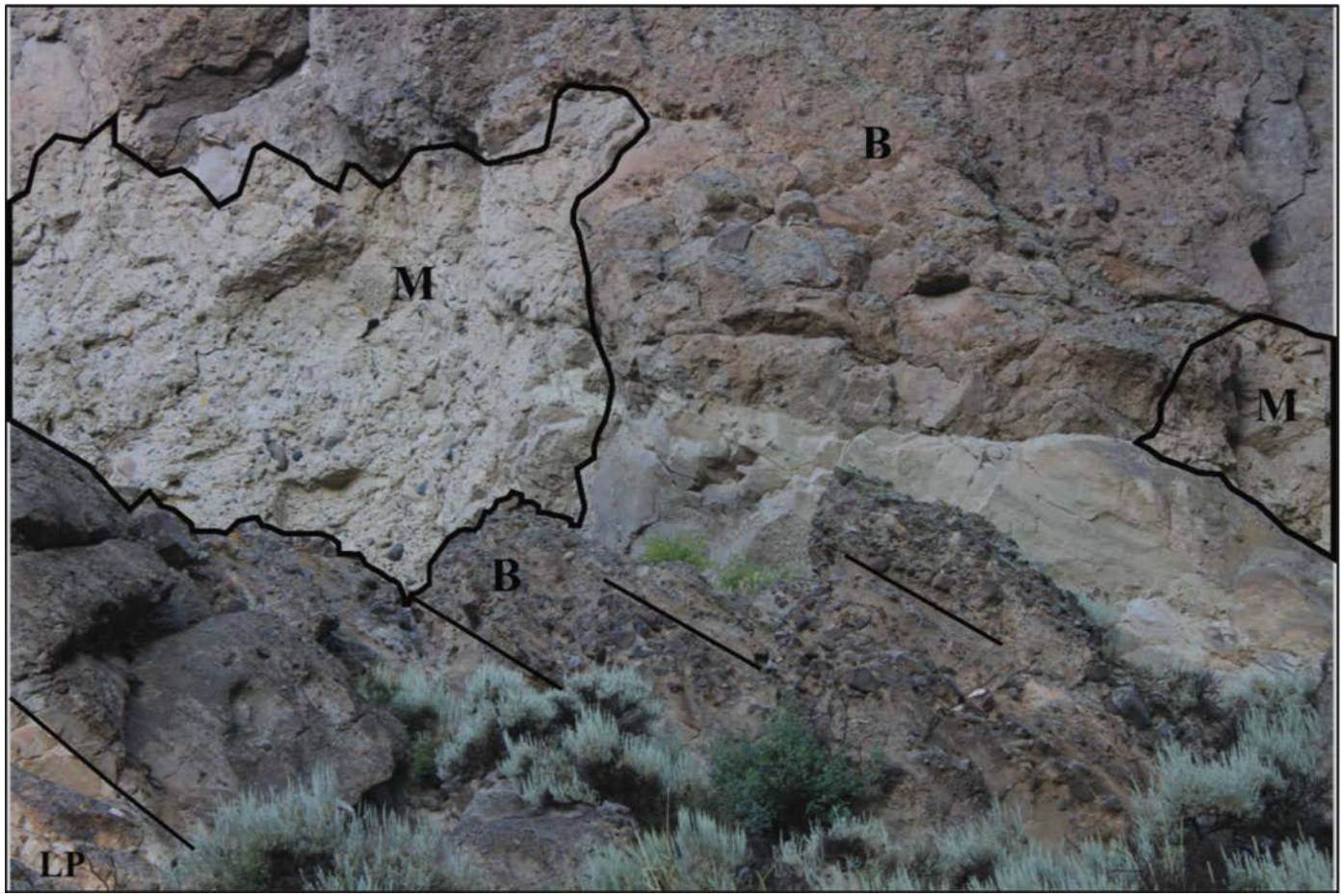

Figure 4.8. Close-up view of “box-2” from Figure 4.5. Here ‘M’ is matrix (polymict tuffaceous stream-gravel conglomerate) and ‘B’ is volcanic breccia facies. Note the inclined bedding in the lower part of the figure (N79°W, 38°NE). Also, note the orangeish lapilli tuff in the lower left corner (LP). The matrix facies on either side continues beyond the edge of the figure. These dips and contacts are highly irregular and point to a unique depositional mechanism such as a debris avalanche.

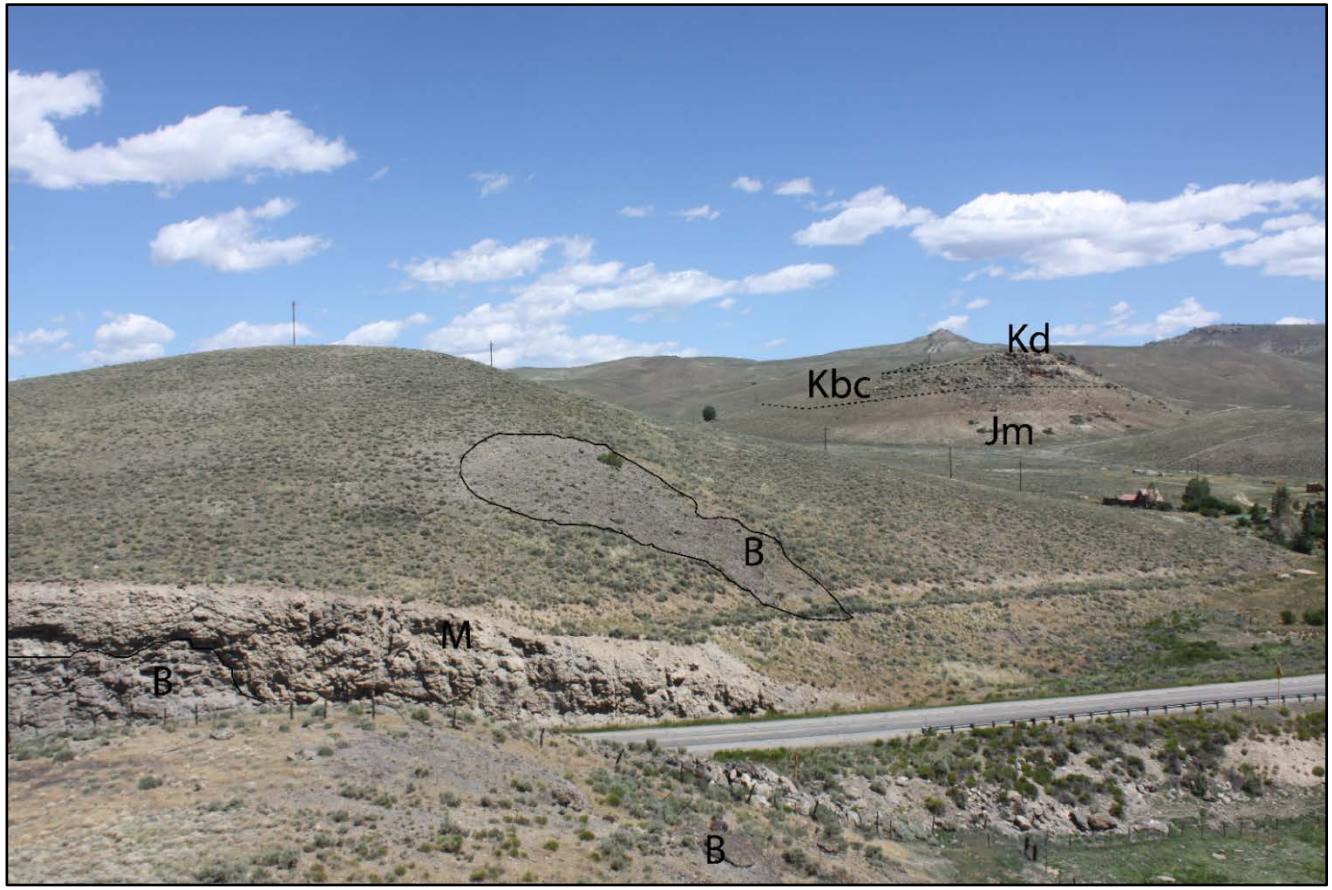

Figure 4.9. A distinct megablock of dark volcanic breccia (B) is encased in the matrix facies (M) as well as several other less distinct blocks in this outcrop about two-miles east of Gunnison. Also, note the "hogbacks" of Jurassic Morrison Formation (Jm), Cretaceous Burrow Canyon Formation (Kbc) and Dakota Sandstone (Kd). The hogbacks may have acted as a drainage divide between Elk Range drainage and the paleo-Tomichi Creek.

4.3.1 Outcrop-Scale Evidence: Origin of the Matrix Facies

Due to the lack of bedding (i.e., stratigraphic continuity) in the tuffaceous conglomerate, the irregular contacts it forms and the clast compositions it contains, I interpret it to represent an encompassing matrix facies consisting of bulked-up alluvium and comminuted volcaniclasts, reflecting the transition to a water-saturated debris flow. As the collapsed edifice avalanched onto the debris apron, the sliding mass incorporated exotic alluvium mixed with water that filled voids around megaclasts. To model this depositional processes it is necessary to understand the source of the clasts and the water that formed the matrix, as well as the paleo-drainage it occupied during the debris avalanche.

The clast compositions or "stream-gravel inventories" recorded within and around the West Elk Breccia include, among other things, Paleozoic sedimentary rocks (Appendices A and D). Gaskill et al. (1981) also reported exotic stream gravels, including Paleozoic rocks, in channels cut into the chaotic facies below the volcaniclastic facies at South Castle Creek and Mill Creek, east of the volcanic center. A significant volume of stream gravels, which include Paleozoic and Precambrian clasts, was also deposited at Flat Top (Fig 4.10), which represents probably equivalent stream drainage, now preserved due to reversal of topography. The sources of these Paleozoic and Precambrian gravels could have only been Laramide uplifts in the nearby Sawatch and Elk mountains (Fig. 4.11), which are the only places in the region where these rocks outcrop (Tweto et al., 1976). Thus, significant alluvium and water were being actively funneled into an alluvial basin from higher mountains to the east both before and during West Elk deposition.

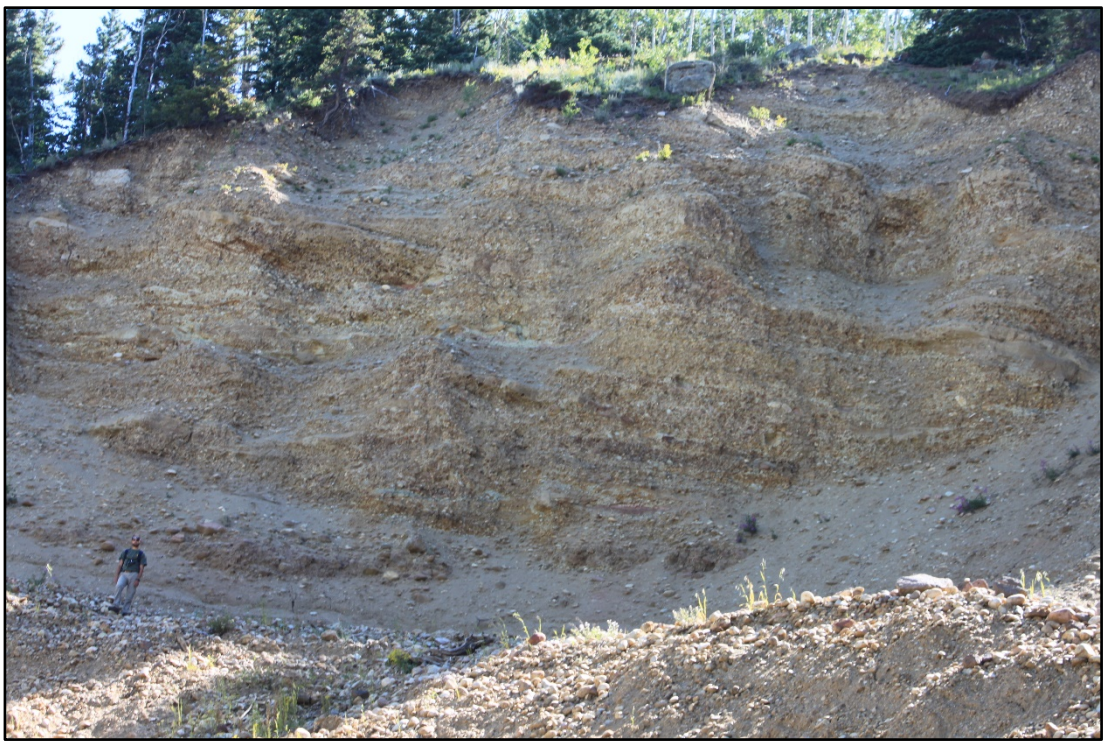

Figure 4.10. Thick fluvial gravel deposits at Flat Top are interbedded with vitric tuff and lapilli tuff sourced from the West Elk Volcano and probably related to the East Elk Creek Tuff. Stork (oral communication, 2015) has located West Elk Breccia below these gravels. These gravels almost certainly provided much of the material for the matrix facies seen in deposits at lower elevations. Elevations at this location are nearly 10,000 feet and suggest that parts of the basin were at higher elevations.

Bulking, as discussed previously, is the addition of material to a flow during transport (Vallance, 2000). Exotic alluvium from bulking has only recently been identified in debris-avalanche deposits (e.g., Crandell, 1989; Vallance and Scott, 1997; Gaylord and Neall, 2012). Typically, dry volcanic debris-avalanche matrices consist of comminuted fragments of megaclasts, or primarily volcaniclasts (Ui, 1983). Crandell (1989) noted for the Pleistocene volcanic debris-avalanche deposit originating at Mt. Shasta, that the matrix facies contains chiefly Mt. Shasta-derived clasts within 22 km of the volcano and a decrease in Mt. Shasta rocks with distance from the volcano as the

number of exotic clasts increases. Similarly, Section 3.5 shows that the number and size of West Elk megaclasts decreases while exotic clasts increase in abundance with distance from the source. Hence, both deposits suggest bulking-up on alluvium and rip-up clasts in a non-dry debris avalanche that transformed into a debris flow(s). As shown at Flat Top, large volumes of alluvium were being eroded from the recently uplifted Sawatch and Elk mountains, but what is the evidence that the paleodrainage favored bulking of exotic alluvium into West Elk debris avalanche?

The geologic record suggests that a dramatic upheaval of the alluvial plane in front of the Elk and Sawatch ranges changed the course of drainage indefinitely and had a great effect on West Elk sedimentation (Hansen, 1965; Gaskill et al., 1981). Initially, the Laramide Orogeny involved the rise of the Sawatch and Elk mountains to the east and the Gunnison Uplift to the west (Fig. 4.11). Between the Elk Mountains and the Gunnison Uplift, a shallow and northwest-southeast-elongated basin, the Piceance Basin, had formed, which by the end of Laramide time drained northward into broad lakes represented by the Green River Shale (Fig. 4.11). The Oligocene intrusion and extrusion of igneous rocks near the present-day Elk and West Elk mountains apparently cut off drainage to the north (Figs. 4.11, 4.12). Thus, drainage was diverted following Oligocene intrusion and volcanism, such that alluvial sediment and stream flow from the two highlands to the east were funneled into a prominent depocenter, centered near present-day Gunnison (Figs. 4.13). Hence, it is likely that the debris avalanches, which initiated at the West Elk Volcanic Center, had sufficient, if not abundant, water and alluvium to bulk-up on, as the Laramide highlands to the east would have been aggressively eroded in the higher, temperate-to-subalpine climates by both glacial and stream-flow regimes.

Hence, the clast compositions, paleoclimate, paleotopography, and regional geology support the interpretation that sufficient alluvium was present before and during West Elk volcanism to form a matrix that facilitated the generation of debris avalanches into the Gunnison Basin (Fig. 4.12).

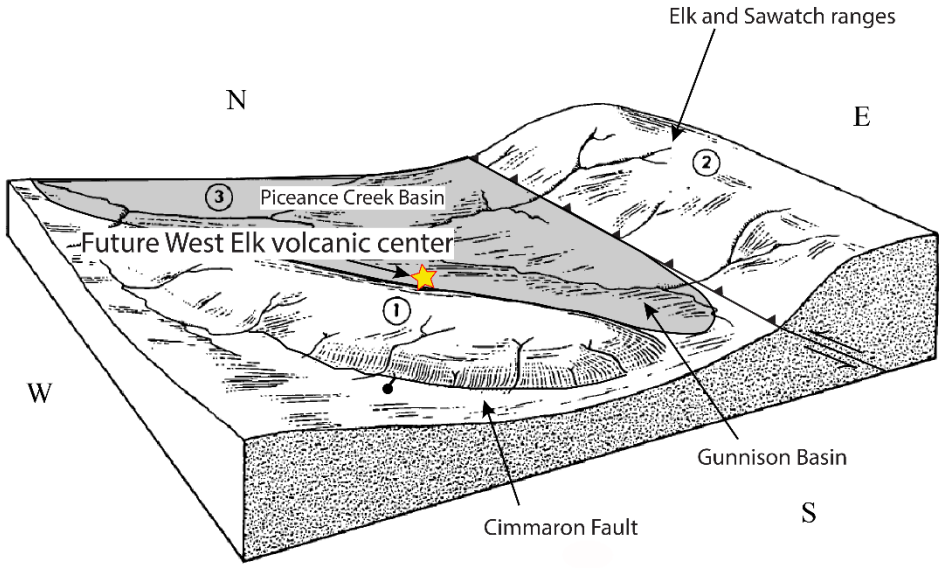

Figure 4.11. Pre-Oligocene structural model (after Hansen, 1965). The gold star represents the approximate location of the Oligocene West Elk Volcanic Center. The Gunnison Uplift (1) led to differential erosion of the Mesozoic bedrock cover in the area. The Elk and Sawatch mountains, sources of Precambrian and Paleozoic clasts, (2) drained toward the north, where sediment was deposited in large lakes to form what is now the Green River Shale (3). The fluvial deposits of this basin (the Gunnison Basin a southern extension of the Piceance Basin) are represented by sandstones and shales of the Eocene Wasatch Formation that outcrops in Ohio Creek (Cashion, 1967).

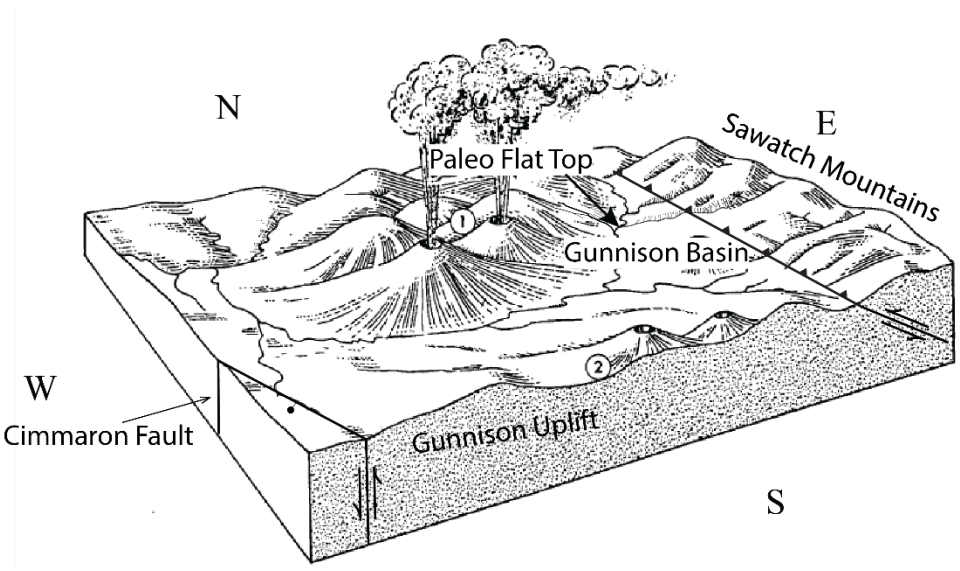

Figure 4.12. The Oligocene igneous activity of the West Elk Mountains cuts off drainage to the north and diverts it to the south into a basin centered near Gunnison (Gunnison Basin). The Oligocene tectonic setting confined drainage between the Sawatch Mountains, the Oligocene intrusives and volcanics (1), and the Gunnison Uplift (2). San Juan volcanics also entered the area from the west, overflowing the Gunnison Uplift. Flat Top Mountain is interpreted to be a relic of the paleodrainage between the Elks/Sawatch and West Elks (after Hansen, 1965).

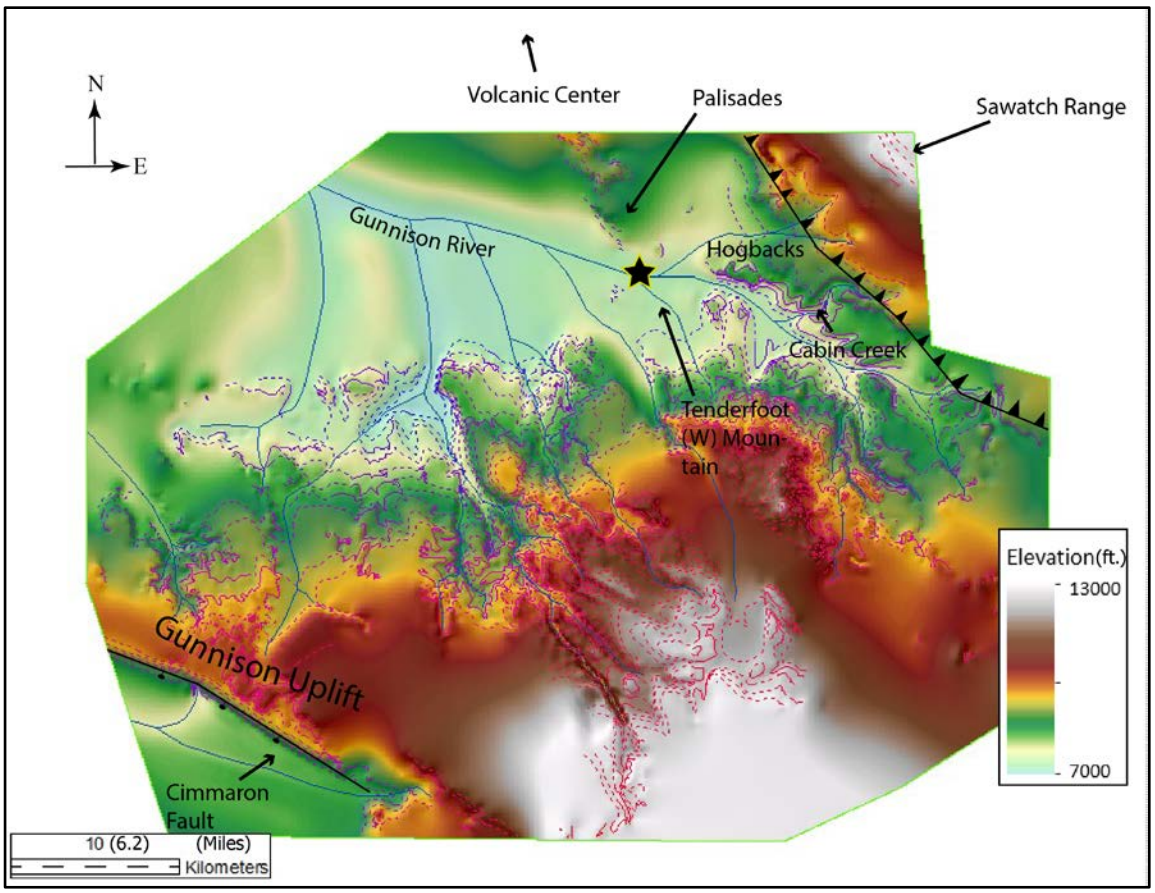

Figure 4.13. Paleogene topographic surface DEM on which the West Elk Breccia was deposited (after Stork, 2013). The black star is the approximate location of the present-day town of Gunnison. Cabin Creek is the most distal deposit of West Elk Breccia observed in this study. The West Elk Breccia moved up drainages and overran Mesozoic hogbacks in the lower paleo-Tomichi Creek. The Elk and Sawatch uplifts to the north and east are the likely sources of alluvium in the matrix facies.

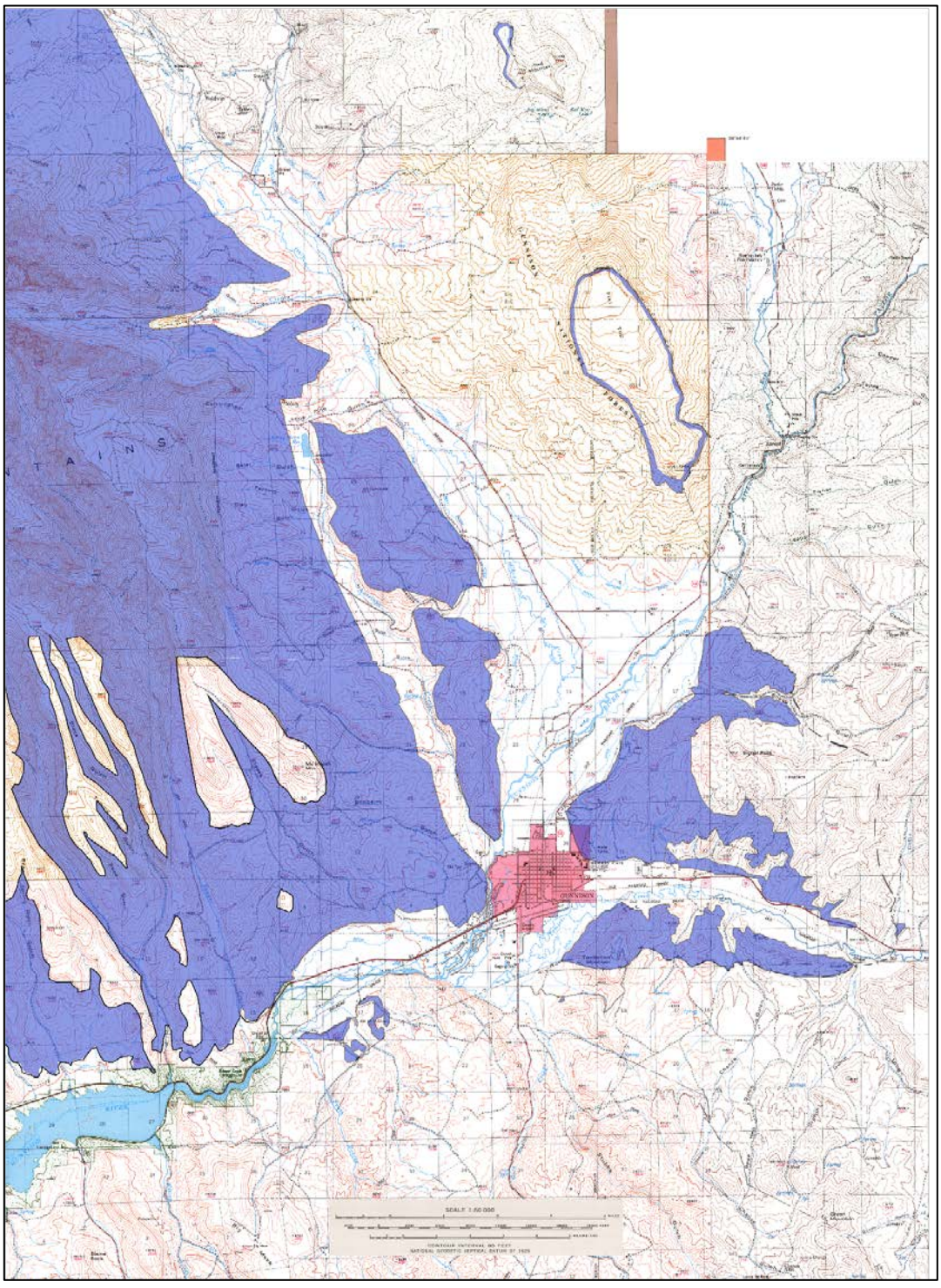

Figure 4.14. General West Elk Breccia distribution on a 1:50,000 scale county map. Purple areas represent in-place West Elk Breccia outcrops. Uncolored areas represent other rock units or slumped West Elk Breccia (Hedlund, 1974; Gaskill et al., 1986, 1987; Stork et al., 2006, 2007, and oral communication, 2015, 2016). The pink area is the town of Gunnison.

4.4 Intra-Outcrop Evidence

Other lines of evidence supporting debris-avalanche emplacement occur at the smaller intra-outcrop scale. This evidence involves small-scale features (meter-scale) seen within the deposits that suggest debris-avalanche emplacement. As observed in numerous deposits, jigsaw fractures, clastic dikes, irregular sharp contacts, and smaller megablocks, and poor sorting are some of the most conspicuous characteristics of debris avalanches (Siebert, 1984; Crandell, 1989; Malone, 1995; Glicken, 1996; Schneider and Fischer, 1998; Gaylord and Neall, 2012; Roverato et al., 2014).

Jigsaw fractures were first described by Shreve (1968) in the dry, non-volcanic debris-avalanche, the Blackhawk "landslide." Jigsaw fractures are important characteristics of debris-avalanche deposits because they indicate that the flow was laminar, that is, that the flow moved as a coherent mass without much turbulence. Jigsaw fracturing in the West Elk Breccia occurs at various scales and locations. For example, at the Palisades (Fig. 4.15) and at the first roadcut east of Gunnison, jigsaw fracturing is present in a megaclast (Fig. 2.13). Commonly associated with jigsaw fracturing is the presence of clastic dikes (e.g., Glicken, 1996; Schneider and Fischer, 1998). Schneider and Fischer (1998) suggested that these features are the result of the dilation of megaclasts and a dynamic infilling of matrix material such that the matrix fills voids that developed progressively during transport. These fracture-fills, like jigsaw fractures, are widespread in the West Elk Breccia (Figs. 4.16, 4.17).

Figure 4.15. Jigsaw-fit fractures in a clast within a megablock. The fragile edges of this rounded boulder appear to have been partially disintegrated and filled with fine material.

Also, common at the intra-outcrop scale in debris-avalanche deposits are rip-up clasts and smaller (one-meter-or-less) blocks of breccia (Figs. 4.17, 4.18). Many workers have noted such a decrease in megaclast size away from the volcanic center in other debris-avalanche deposits, reflecting increased fracturing and disaggregation (e.g., Crandell, 1989; Schneider and Fischer, 1998).

Figure 4.16. A clastic dike on U.S. 50 near WP 0010. A vertical fracture has been filled with alluvium and volcaniclasts formed in andesitic volcanic breccia. Orange oxidation may indicate permeability boundaries and that later fluids moved through this fracture.

Finally, the high variation in grain-size distribution throughout the matrix facies (Appendix E) and, hence, poor sorting therein are strong indicators of deposition by debris flows and debris avalanches. Polymodal distributions along with the degree of

rounding in cobbles and pebbles suggest that the flows bulked-up on alluvium. Such grain-size characteristics were noted by Vallance and Scott (1997) in the Osceola mudflow deposit.

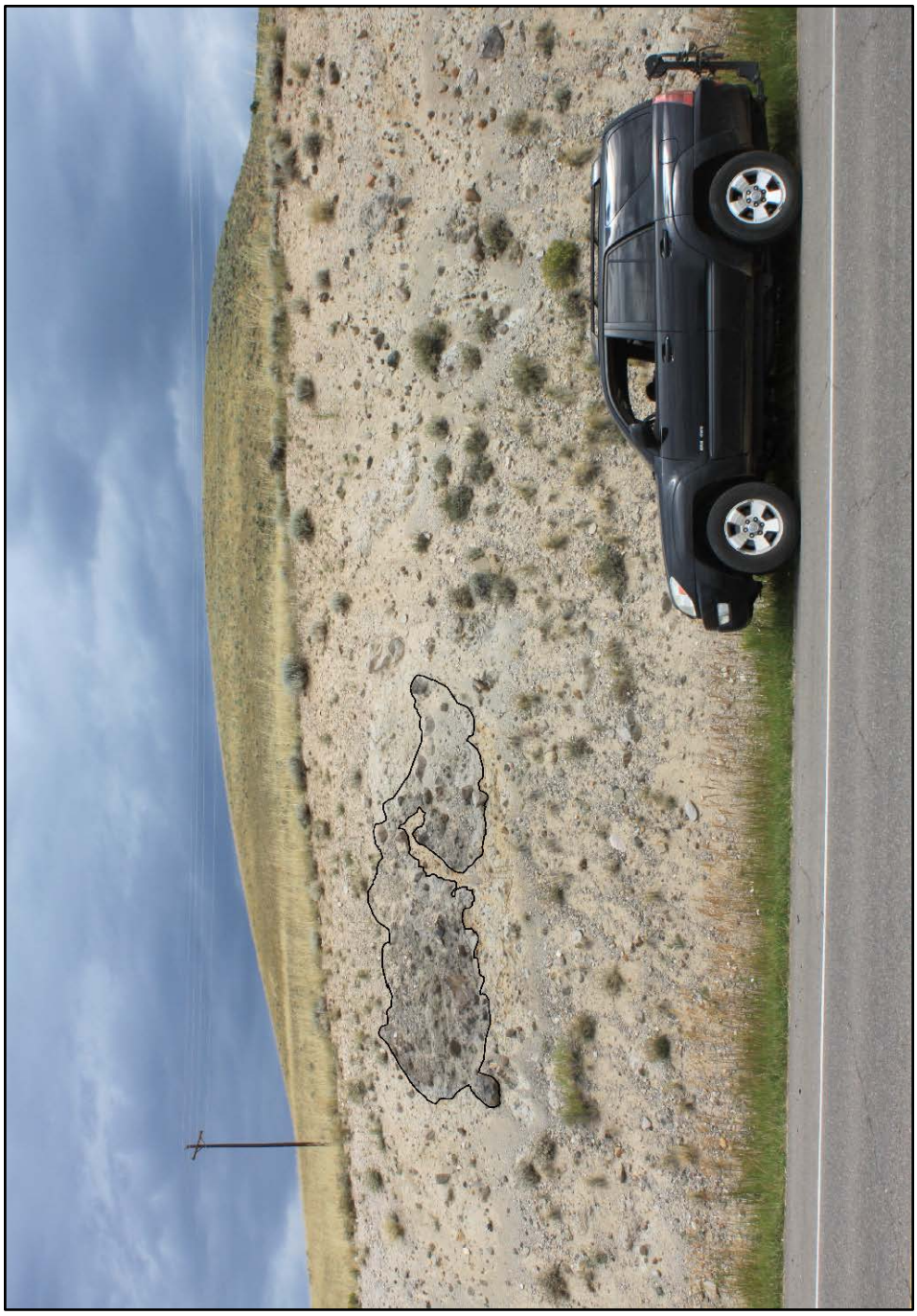

Figure 3.17. Fracture-fill in a small megaclast about 35 km from the volcanic source. Located to the east on U.S. 50 at WP 164. Megaclasts decrease in size and abundance away from the source.

Figure 4.18. Smaller megablock of breccia facies in roadcut about two-miles (3.5-km) east of Gunnison and about 21 miles (34 km) from the volcanic center (WP 0010). Small fragments are variably rounded and decrease in size away from the volcanic center.

CHAPTER 5: Conclusions

Most observed outcrops of the West Elk Breccia in the study area are best explained by a debris-avalanche model. Three broad categories of conclusions are:

5.1 Nature of the Deposits

i. Two dominant facies were identified: a well-indurated volcanic breccia and a matrix composed of primarily a tuffaceous stream-gravel conglomerate exhibiting intricate and irregular contacts with bodies of volcanic breccia. Previously unrecognized megaclasts of volcanic breccia are partly to wholly surrounded by matrix material.

ii. Geochemistry performed for this study and Ar-Ar age dates by Coven et al. (2000) corroborate the findings of Lipman et al. (1969), who suggested the West Elk Breccia is part of the early intermediate volcanic phase of San Juan volcanism.

iii. Geochemistry also confirms that the West Elk Breccia is largely andesitic in composition, with a few basaltic andesite and dacite outliers. The matrix and mixed facies are, on average, lithic tuffs. The volcanic breccia or breccia facies is on average vitric tuff, although, it is likely that the difficulty of distinguishing lithics from the surrounding matrix exaggerates the glass component within this facies.

iv. Field analysis, covering an area of nearly 100 km^2, permits an estimation for the volume of the West Elk Breccia in the field area of approximately 8.5 km^3. The

distance between the most distal deposits and the volcanic center allows for an estimation of volcano height at collapse of greater than 13,000 feet (approximately 4000 m). In comparison, the debris-avalanche deposits at Mt. Shasta and Sunrise Peak cover areas of 675 km^2 and 450 km^2 and cover areas of 45 km^3 and 100 km^3 respectively (Crandell, 1989; Malone, 1995).

5.2 Paleoclimatic and Tectonic Framework

v. Water-laid tuffs containing plant fossils of cedar and oak help to constrain a paleoclimate interpretation of temperate-to-subalpine conditions.

vi. Analysis of fossils from the nearby Oligocene Creede and Pitch Pinnacle volcanic fields corroborate the interpretations from West Elk fossils, further suggesting a temperate-to-subalpine climate capable of maintaining year-round snow, and potentially glaciers, atop the West Elk volcanic center.

vii. Preceding and contemporaneous tectonic uplift on the nearby Elk Mountain and Sawatch uplifts, combined with temperate conditions, produced larger amounts of high-level stream gravels from Precambrian, Paleozoic, and Mesozoic source areas to the east. Thick near-source deposits of these gravels, found at high elevations within the field area, provided evidence for the source of alluvium found in the matrix facies. Stream-gravel analysis supports Elk Mountain and Sawatch sources for many of the gravels.

5.3 Debris-Avalanche Evidence

viii. At the volcano scale, weathered remains of the West Elk volcano show that a large sector of the volcanic edifice is missing on the northern flank (Fig. 3.2). It is likely unrelated to the deposits observed in this study, but it shows that sector collapses did occur on the volcano and that they probably sourced debris avalanches.

ix. Observations of the Palisades and outcrops progressing northward toward Ohio Creek suggest that this ridge probably represents a partially exhumed example of hummocky topography (Fig. 2.7). Resistant volcanic breccia is partly to wholly encased in a matrix facies of volcanic ash and alluvium. Close examination reveals that the Palisades exhibits a series of megablocks, some of which are several hundred meters high. The bedding of these blocks is oriented at diverse angles, and the megablocks rest in a conglomeratic matrix on top of the Mancos Shale. Because of the diverse block orientations, it is unlikely that they represent a single continuous exposure incised by streams at various points. Rather, the Palisades outcrop string appears to represent a series of variously oriented, isolated blocks dumped into a stream valley, formed in the Mancos Shale, by a debris avalanche.

x. Jigsaw fracturing is ubiquitous in the West Elk Breccia and probably is the best evidence of debris-avalanche emplacement at the intra-outcrop scale (Figs. 2.13, 3.14). This telltale textural feature indicates that most of the West Elk avalanches and flows were non-turbulent. Another common feature observed at the intra-outcrop scale, and suggesting non-turbulent flow, are smaller megaclasts no more

than a few meters in diameter. Some of these clasts are volcanic breccia while others are exotic alluvium, consisting of meter-sized blocks of sandstone and alluvial rafts. These blocks occur almost anywhere within the deposits suggesting non-Newtonian or buoyant forces indicative of debris flows.

APPENDIX A – Measurements and Descriptions

The following appendix contains field descriptions, measured thicknesses, locations, and sample numbers. Waypoints (WP) are listed in parentheses next to the general location. A table of all waypoints with the latitude and longitude coordinates is located at the end of the document.

The Palisades, (WP 97, 101 - 106, 180 - 184)

Description	Thickness
	TOTAL 419'(128m)
Tuffaceous conglomerate; 5y 8/1; massive, non-bedded with sharp contact to adjacent and underlying breccia; dacitic ash with heterolithic stream gravel clasts (granite, schist, gneiss, sandstone, breccia clasts etc.), silt to bomb size clasts; 38°33'37.65"N, -106°56'52.14"W, sample # 07221502 b	42' (12.8m)
Polymict pyroclastic breccia; N6 and/or 5y 6/1; crudely bedded; massive-to-graded-and-inversely-graded beds; coarse andesitic to basaltic andesite ash, angular to subangular pyroclasts of basaltic andesite from silt to bomb size, some prismatically jointed; 38°33'32.46"N, -106°56'51.24"W, sample # 07221504	220' (67.1m)
Tuffaceous conglomerate; 5y 8/1 and/or 5y 7/2; massive to non-bedded fracture fill, sharp contacts with surrounding breccias; dacitic ash with heterolithologic clast compositions (quartzite, schist, gneiss, granite, quartz porphyrys, sandstones, mudstones, andesite/ basaltic andesite, pumice, etc.), from silt to boulder/bomb size, rounded to well-rounded, and poorly sorted; rip-up clasts of Cretaceous Mancos Formation; 38°33'32.61"N, -106°56'49.21"W, sample # 07221505	20' (6.1m)
Polymict tuff breccia to pyroclastic breccia; 5B 9/1; graded to inversely graded beds, thick-to-thin bedding, dip direction N11°E 38°; pyroclasts of basaltic andesite in a similar matrix; 38°33'32.61"N, -106°56'49.21"W, sample # 07221506	5' (1.5m)
Quartz biotite lapilli stone; white (N9) to orange-brown weathered; thick to very thickly bedded, sharp to gradational contacts, planar dipping beds (N60W 24 NE); felsic with lapilli clasts composed of coarse ash, biotite, and quartz, rounded and non-welded; no fossils or sedimentary structures; 38°33'32.61"N, -106°56'49.21"W, sample # 08091505	4' (1.2m)

Polymict pyroclastic breccia; 5YR 4/1, 5YR 8/1, n6; crude thick beds, gradational contacts, dipping at high angles (45°NW); pyroxene rich basaltic andesite, basaltic andesite to dacitic? Fragments of pyroclasts, from ash to bomb size fragments, mostly angular to very angular with some prismatically jointed bombs which show sub-rounding, poorly to moderately sorted, in a glassy matrix with some phenocrysts of plagioclase and pyroxene; graded to inversely graded beds; no fossils; thickness variable; tuffaceous conglomerate filling fractures (38°33'33.40"N, -106°56'46.82"W); sample #s 07201505, 07221501, 08091504	108'(33m)
Tuffaceous conglomerate ("Lower Pinnacle Stream Gravel"); 5Y 8/1; massive bedding, variable thickness, sharp contacts with clastic dikes; irregular bedding surfaces; coarse ash and sand poorly indurated, heterolithologic clast compositions (quartzite, basaltic andesite, mudstones, limestones, and granite), ranging in size from boulder to silt, rounded to well rounded, and poorly sorted in a coarse-ash cement, polypropylitized with calcite; no fossils, contains metamorphosed mudstones and calcareous sandstones?; 38°33'37.94"N, -106°56'46.38"W; sample # 08091502	20'(6.1m)

Almont Peak (WP 111-113 and 119)

Description	**Thickness**
	TOTAL 271'(83m)
Tuff and tuff breccia; 5Y 7/2; coarse andesite ash matrix contains angular clasts predominantly lapilli size to rare rounded bombs; altered to clay in places; highly variable clast content; 38°39'18.04"N, -106°53'13.33"W; Sample #s 07291505 and 07291506	20' (6.1m)
Polymict volcanic breccia; 5y 8/1; no apparent bedding; angular pyroclasts of basaltic andesite and rhyodacite? ranging in size from lapilli to boulder with a larger proportion of boulders in contrast to the lower two breccia units, less stream gravel float than below, 38°39'15.31"N, -106°53'12.63"W; sample # 07291504	91' (28 m)
Polymict volcanic breccia and conglomerate; N6; no apparent bedding; predominantly angular pyroclasts of basaltic andesite to dacite of lapilli and cobble size in an ashy matrix of similar composition; scattered outcrops	46' (14 m)

with stream gravel float of regional country rock, which is locally contained in a poorly consolidated tuffaceous matrix; 38°39'11.92"N, -106°53'13.64"W; sample # 07291503	
Volcanic breccia; N6 and N5; no apparent bedding; stream gravels in tuffaceous matrix at base but highly weathered; primarily basaltic andesite lapilli, cobbles, and rare bombs (one exceptionally large bomb several meters in diameter), well rounded; 38°39'11.92"N, -106°53'13.64"W; sample #s 07291502 and 07291501	14’(4.3 m)
Unconsolidated stream gravel; heterogeneous stream gravel mixture of quartzite, gneiss, schist, sandstone, and other country rock; rounded to subrounded; appears as float; 38°39'11.92"N, -106°53'13.64"W	Up to 100’(30.5 m)

WP 0003 and 0012 W Mountain

Description	**Thickness**
	TOTAL 452’(138m)
Tuffaceous conglomerate and stream gravel; highly weathered limited exposures, primarily float of quartz, granite, basaltic andesite, andesite, quartzite, sandstone and various intrusives; 38°32'11.73"N, -106°54'2.15"W	203’ (62m)
Polymict volcanic breccia; N6; poor exposure, no apparent bedding; angular to subrounded basaltic andesite to dacite with phenocrysts of pyroxene, primarily lapilli or gravel size to some bomb or boulders; 38°32'11.73"N, 106°54'2.15"W; sample #s 08011501 and 08011502	65’ (20m)
Volcanic breccia; 5y 8/1; poor exposure, no apparent bedding; weakly indurated yellowish volcanic matrix with angular cobbles of basaltic andesite; 38°32'11.73"N, -106°54'2.15"W;	14’ (4.3m)
Polymict volcanic breccia; N7; locally crude vertical bedding, predominantly massive, sharp contact at base with tuffaceous conglomerate; clasts are predominantly angular silt to bombs of black aphanitic andesite and basaltic andesite in a well-indurated matrix of ash and glass; local bleaching at margins, slickensides present at basal contact with tuffaceous conglomerate (bearing N43°W); 38°32'11.73"N, -106°54'2.15"W	109’ (33m)

Tuffaceous conglomerate; 5Y 7/2; no apparent bedding, fracture filling, irregular to sharp contacts with breccia above below; predominantly rounded to well-rounded clasts of granite, quartzite, amphibolite, andesite and basaltic andesite, predominantly cobbles to silt size in an ashy matrix, as well as local inclusions of breccia megaclasts (up to 13' or 4m diameter); 38°32'11.73"N, -106°54'2.15"W; sample #s 08031502	15' (0.3m)
Volcanic breccia; N7; massive-to-thin beds, gradational-to-inversely-graded and irregular contacts; angular to subangular pyroclasts of andesite and basaltic andesite in an ashy matrix of the same; 38°32'11.73"N, -106°54'2.15"W and 38°32'12.80"N106°53'30.66"W; sample #s 07191503 and 08031501	36' (11m)
Tuffaceous conglomerate; 5Y 7/2; no apparent bedding, sharp contacts with breccias above, irregular fracture fill; rounded to subrounded stream gravel (granite, gneiss, amphibolite, sandstone, andesite), varying sizes from boulders to silt, ashy matrix of primarily andesitic composition. 38°32'11.73"N, -106°54'2.15"W;	> 10' (3.1m)

Lost Canyon (WP 120 – 121)

Description	**Thickness**
	TOTAL 175' (53m)
Volcanic breccia and tuffaceous conglomerate; N7; no apparent bedding; intermingled angular breccia and rounded stream gravel, breccia is predominantly black and red aphanitic andesite and basaltic andesite, stream gravels are sandstone and granites, clasts range from silt to boulder or bomb sizes; 38°35'20.13"N, -106°51'22.98"W; sample # 07301503	105' (32m)
Volcanic breccia; 5Y 8/1 to 10yr 5/4; no apparent bedding, highly weathered and scattered outcrops of breccia and intermingled stream grave; angular to rounded silt-to-bomb-size clasts of basaltic andesite and pyroxene andesite pyroclasts in an ashy matrix of the same, some pumice in poorly indurated matrix with stream gravel; polypropylitized with calcite overgrowths; 38°35'20.13"N, -106°51'22.98"W; sample # 07301502	36' (11m)
Volcanic breccia and tuffaceous conglomerate; 5Y 6/1; no apparent bedding, poorly exposed; highly variable clast composition primarily andesite and dacite? intermingled stream gravel of country rock, angular to	> 34.2' (10.4m)

rounded, poorly indurated; 38°35'20.13"N, -106°51'22.98"W; Sample # 07301501	

Measured Section at Sapinero Wildlife Preserve (Waypoints 174 – 178)

Description	**Thickness**
	TOTAL 392’ (119 m)
Volcanic breccia and stream gravel; poorly consolidated with no apparent bedding; angular to subrounded clasts of volcanics and crystalline stream gravel	49’ (15 m)
Covered	71’ (22 m)
Lapilli tuff; white to brown; no apparent bedding	14.25’ (4.3 m)
Tuff; 5y 7/2; no apparent bedding; equigranular, subrounded to subangular breccia; clasts scarce; overlain by gravels of quartzite, granite, sandstone, and dacitic? volcaniclasts; sample # 07181502 and 08081504; 38.4911 N, -107.135964 W	40’ (12 m)
Volcanic breccia; light brown to tannish gray weathered, light gray fresh; vague bedding; sand to bomb sized clasts of light gray “dacite” and dark gray basaltic andesite, fine grained matrix; sample # 07181501; 38.491011N, -107.136305 W	57’ (17 m)
Incompetent stream gravel conglomerate; 5y 7/6; massive to no apparent bedding of stream gravels, but vague bedding of breccia above gravels; fine sand, silt, and coarse ash matrix, minor hornblende, plagioclase and quartz crystals present, mostly lapilli size subrounded to subangular; sample# 08081503, 07181501; 38.491011N, -107.136305 W	63’ (19 m)
Fossiliferous tuff and gravel;5y 6/4, 5y 6/1, 5y 7/2 colors from lowest stratigraphic unit to highest; thinly bedded to laminae, horizontal, possibly gradational contacts; mud to clay sized grains at base above gravels becomes silt in upper tuff; soft, middle layer may contain varves; fossils (Oak leaves and cedar needles); samples #08081502 a and b (where a is middle and b is upper portion of unit); 38.491048N, -107.136383W	23’ (7 m)
Fine tuff, gravel, and lapilli tuff; 5y 7/2, 5y 8/4, 10y 8/2; thinly bedded to laminae in tuff, unconsolidated gravel	30’ (9 m)

fining upward, sand and pumice? at base of fine tuff; andesitic – dacitic ash? fine ash to silt size, poorly cemented, alteration to clay? stream gravels include Precambrian quartzite and granite as well as volcaniclastics; sample # 08081501 a, b, c; 38.490957 N, -107.136492 W	
Fine tuff and unconsolidated stream gravel; 5y 8/1; thinly bedded to laminae of planar horizontal ash; non-bedded stream gravel; flaggy and fissile tuff; sample # 08081505; 38°29'27.16"N, 107° 8'12.26"W	>45’ (14 m)

East of WSCU WP 138 - 142

Description	**Thickness**
	TOTAL 225’ (69 m)
Volcanic Breccia; n6; no apparent bedding; angular to subrounded clasts of basaltic andesite and andesite, some dark colored clasts show vesicularity? sample # 08051503; 38.55476N, 106.91697 W	98’ (30 m)
Tuff breccia and tuffaceous conglomerate; 5Y 7/2; angular to subrounded volcaniclasts; maybe mixing with stream gravels; sample # 08051502; 38.55410 N, -106.91703 W	46’ (14 m)
Volcanic breccia and tuffaceous conglomerate; 5y 7/2; no bedding; basaltic andesite, sub angular to sub rounded; stream gravel fills fractures? Composed of a poorly consolidated tuffaceous matrix of lithic fragments and glass, gravels are rounded cobbles to rare boulders of sandstones, volcaniclastics, quartz porphyrys, schist, and gneiss; excellent exposure of tuffaceous conglomerate behind water towers (WP 142); sample # 08051501; 38.55333 N, -106.91748 W	81’ (24 m)

Almont Peak (WP 150 -148)

Description	**Thickness**
	TOTAL 148’ (45 m)
Tuff, tuff breccia, and volcanic breccia; 5y 6/4; poor exposure, no bedding, highly weathered; clasts are cobble to lapilli sized fragments of basaltic andesite to dacite? In a coarse ash matrix with lithics, quartz and	17’ (5.2 m)

mafic minerals; sample # 08061501; 38.65939 N, -106.878423 W	
Volcanic breccia; 5y 7/2; no apparent bedding, hoodoo outcrop morphology; red rhyodacite to basaltic andesite clasts in a coarse ash, lithic and possibly glass matrix, some quartz and mafic minerals present; angular to subrounded, increasing rounding with size; sample # 08061502; 38.658895 N, -106.878165 W	34’ (10.4 m)
Poorly consolidated to unconsolidated stream gravels; no bedding, only float; gravels include predominantly rounded chert, quartz porphyry, alkali granite, schist, gneiss, rhyodacite? pyroxene andesite? and quartzite, from gravel (< 2 cm) to boulder sizes (35 cm); 38.657969 N, -106.877287 W	197’ (60 m)

Cooper Ranch and Never Sink Trail areas (WP 0023 and 0024)

Description	**Thickness**
	TOTAL 148’ (45 m)
Volcanic breccia; milky brown gray fresh, brown to gray weathered; hoodoo forming outcrops with massive bedding, no sorting or grading apparent; clasts of basaltic andesite, andesite; sample # 6271503; 38.527982 N, -107.030165 W	314’ (96m)
Talus slope; white weathering, chalky brown fresh; planar and undulatory beds?; clasts of andesite, dacite, and basaltic andesite, red rhyolite breccia, rounded to subrounded quartzite; poorly consolidated; 38.514483 N, -107.021159 W	38’ (12 m)
Volcanic breccia; purplish red fresh and blue gray weathered; thick- to thin-bedded; angular clasts of rhyolite, dacite and andesite, varying sizes from sand to boulder; sample # 06271502; 38.514483 N, -107.021159 W	31’ (9.5 m)

Master Waypoint List

Waypoint	Latitude	Longitude
0001	38.531413	-106.916049
0002	38.535816	-106.908692
0003	38.536592	-106.900596
0004	38.694538	-107.078326
0005	38.695233	-107.094184
0006	38.7005	-107.116362
0007	38.490237	-107.2324
0008	38.485926	-107.228532
0009	38.48773	-107.225615
0010	38.543827	-106.882213
0011	38.510428	-106.911029
0012	38.53688889	-106.89185
0013	38.59116	-106.857851
0014	38.58938	-106.856468
0015	38.588994	-106.856082
0016	38.590146	-106.855829
0017	38.59076	-106.8561
0018	38.654827	-106.879884
0019	38.65491	-106.880815
0020	38.652836	-106.88278
0021	38.468974	-107.089217
0022	38.468876	-107.088385
0023	38.514483	-107.021159
0024	38.527982	-107.030165
0025	38.521439	-107.039784
0026	38.659341	-106.929535
0027	38.664959	-106.930877
0028	38.660303	-106.926956
0029	38.656784	-106.891044
0030	38.664301	-106.893665
0031	38.661056	-106.899509
0032	38.653206	-106.883667
0033	38.650519	-106.882922
0034	38.657016	-106.879266
0035	38.657732	-106.878948
0036	38.658798	-106.878295
0037	38.661816	-106.877757
076	38.772431	-107.060749
087	38.552877	-106.917635

088	38.490718	-107.137443
089	38.53727778	-106.8474667
090	38.53552	-106.84042
091	38.521125	-106.823699
092	38.520763	-106.826526
093	38.520803	-106.826513
094	38.522379	-106.831891
095	38.53516	-106.901648
096	38.560814	-106.955201
097	38.559277	-106.94634
101	38.560695	-106.953852
102	38.560459	-106.947817
103	38.560592	-106.954566
104	38.560092	-106.950948
105	38.559925	-106.947541
106	38.559017	-106.947567
107	38.557764	-106.946714
108	38.55834	-106.94912
109	38.559698	-106.951123
111	38.65331	-106.887122
112	38.65425278	-106.8868417
113	38.65501111	-106.8870361
114	38.656059	-106.892727
116	38.656104	-106.892071
117	38.656751	-106.891104
118	38.657866	-106.889651
119	38.65642	-106.888439
120	38.588925	-106.856384
121	38.5891	-106.855602
122	38.535771	-106.901909
123	38.535378	-106.902665
124	38.533601	-106.903791
125	38.533868	-106.901337
126	38.533784	-106.895129
127	38.534151	-106.889623
128	38.534192	-106.864157
129	38.530772	-106.864854
130	38.527877	-106.864078
131	38.528002	-106.863569
132	38.527385	-106.864229
133	38.524756	-106.862141

134	38.522492	-106.862004
135	38.522314	-106.856033
136	38.523573	-106.853224
137	38.528834	-106.859557
138	38.553324	-106.917479
139	38.554104	-106.917056
140	38.554764	-106.91697
141	38.554699	-106.915092
142	38.552584	-106.915722
143	38.553104	-106.913945
144	38.555536	-106.91188
145	38.559086	-106.909999
146	38.562376	-106.911439
147	38.557139	-106.916072
148	38.65939	-106.878423
149	38.658895	-106.878165
150	38.657969	-106.877287
151	38.658354	-106.87645
152	38.661407	-106.876596
153	38.664155	-106.875226
154	38.662707	-106.878028
155	38.66415	-106.876233
156	38.664324	-106.876059
157	38.664548	-106.87567
158	38.676569	-106.879801
159	38.676573	-106.88184
160	38.530719	-106.807508
161	38.530436	-106.806868
162	38.530064	-106.806535
163	38.529893	-106.806408
164	38.53208611	-106.8297583
165	38.532928	-106.829957
166	38.534057	-106.829911
167	38.537732	-106.848774
168	38.537117	-106.848874
169	38.587822	-106.886612
170	38.58545833	-106.8867
171	38.585147	-106.886716
172	38.584237	-106.886255
173	38.578699	-106.884056
174	38.490957	-107.136492

175	38.491048	-107.136383
176	38.491011	-107.136305
177	38.4911	-107.135964
178	38.490878	-107.13674
179	38.560551	-106.947812
180	38.560539	-106.946218
181	38.559155	-106.946971
182	38.559059	-106.947003
183	38.558983	-106.947491
184	38.560007	-106.947587
185	38.706145	-106.919937
186	38.706044	-106.919579
187	38.706216	-106.919312
188	38.708403	-106.917753
189	38.708667	-106.91446
190	38.709046	-106.914355
191	38.709121	-106.91479
192	38.70846	-106.914246
193	38.520231	-107.147074
194	38.519291	-107.148499
195	38.519996	-107.147944
196	38.472808	-106.951929
197	38.762029	-106.944178
198	38.767607	-106.939996
199	38.488119	-107.16597
200	38.488	-107.1657611
201	38.48801944	-107.1650083
202	38.488071	-107.165982
203	38.538514	-106.853979
204	38.536344	-106.842785
205	38.533088	-106.835214
206	38.53592	-106.897706
207	38.536267	-106.902144
208	38.536	-106.90478
209	38.53597	-106.904781
210	38.536028	-106.906311
211	38.535206	-106.908205
212	38.533573	-106.905667
213	38.533311	-106.909751
214	38.532424	-106.908862
215	38.574225	-106.893702

216	38.708495	-106.914105
217	38.531656	-106.987515
218	38.538176	-106.989442
219	38.538165	-106.993272
220	38.538508	-106.995107
221	38.536268	-106.98842
222	38.53728	-106.988503
223	38.546176	-107.002944
224	38.54699	-107.003872
225	38.653968	-106.880243
226	38.653505	-106.882063
227	38.654258	-106.881582
456	38.539052	-106.833286
7/25/16_p26	38.73481204	-107.1560242
07/23/2016_Palisades	38.57290445	-106.9505113
07-21-2016Description	38.55292115	-106.8473573
Coyote	38.54387928	-106.8388298
Description_7-25-16	38.73861516	-107.1421199
gaskill_measured_section	38.73888611	-107.1570444
Lapilli Tuff	38.60689466	-106.9705015
Lost_Canyon_7/24/16_SG_Unit	38.58959568	-106.8556384
MancosWEBcontact	38.61979109	-106.9663863

APPENDIX B – Geochemistry

Bulk-Rock Geochemical Calculations

Sample	SiO2	Fe2O3	Al2O3	K2O	Na2O	CaO	MgO	P2O5	TiO2	Total	LOI	Lat	Long	WP
7191501	60.8	5.2	17.1	2.0	2.3	4.5	2.5	0.4	0.9	95.7	4.28	38°32'39.12"N	106°52'54.63"W	10
7191502	57.6	7.2	15.0	2.3	2.4	6.3	3.6	0.6	0.8	95.9	4.14	38°32'11.73"N	106°54'2.15"W	3
7201503	61.5	2.8	16.2	3.1	3.2	4.2	1.8	0.2	0.4	93.5	6.49	38°32'14.20"N	106°50'50.88"W	89
7201505	54.1	8.3	12.7	2.2	2.1	9.9	2.8	0.5	0.8	93.5	6.53	38°33'33.40"N	106°56'46.82"W	97
7221503	59.4	7.3	17.2	2.7	2.9	6.4	2.2	0.7	0.8	99.7	0.33	38°33'35.73"N	106°56'51.15"W	105
7221504	58.4	7.2	15.3	2.5	2.4	8.0	2.4	0.6	0.7	97.5	2.51	38°33'32.46"N	106°56'51.24"W	106
7221505	60.1	5.6	15.0	2.5	1.9	5.7	3.0	0.3	0.8	94.9	5.08	38°33'32.46"N	106°56'51.24"W	106
7291501	57.2	7.5	16.5	1.9	2.7	7.4	2.2	0.6	1.1	96.9	3.05	38°39'11.92"N	106°53'13.64"W	111
7291502	58.2	6.5	16.0	2.2	2.6	6.2	2.2	0.5	1.0	95.4	4.65	38°39'11.92"N	106°53'13.64"W	111
7291503	57.6	7.3	15.3	2.4	2.5	6.1	2.2	0.6	0.9	94.9	5.08	38°39'11.92"N	106°53'13.64"W	111
7291504	58.1	7.8	14.7	2.1	2.4	6.9	2.1	0.6	0.8	95.4	4.58	38°39'15.31"N	106°53'12.63"W	112
7301502	62.7	3.8	16.5	2.8	2.8	4.3	1.6	0.4	0.7	95.6	4.45	38°35'20.13"N	106°51'22.98"W	120
8011501	58.5	8.9	14.4	2.2	2.1	6.9	2.2	0.6	0.9	96.7	3.32	38°32'11.73"N	106°54'2.15"W	3
8011502	56.7	7.7	14.4	2.1	2.2	7.4	2.3	0.6	0.8	94.4	5.62	38°32'11.73"N	106°54'2.15"W	3
8031502	57.4	6.6	11.7	2.2	1.7	6.6	3.2	0.3	0.7	90.4	9.60	38°32'12.80"N	106°53'30.66"W	12
8051501	61.1	7.0	14.9	2.0	1.9	5.4	2.0	0.7	1.1	96.0	4.03	38°33'11.97"N	106°55'2.92"W	138
8051505	58.6	3.9	16.5	2.8	2.6	5.7	1.7	0.6	0.9	93.3	6.67	38°33'25.70"N	106°54'57.86"W	147
8061505	59.7	7.4	15.4	2.1	2.5	5.0	2.3	0.4	0.8	95.6	4.37	38°39'51.57"N	106°52'33.81"W	156
8071504	60.5	4.3	14.7	2.6	2.0	6.6	2.6	0.3	0.7	94.3	5.71	38°31'55.51"N	106°49'47.13"W	164
8071507	58.5	5.5	15.6	2.3	2.8	5.9	2.3	0.5	0.6	94.0	5.99	38°35'16.16"N	106°53'11.80"W	169
8071508	58.6	7.4	15.6	2.5	2.5	6.3	2.7	0.6	0.9	97.2	2.81	38°35'7.65"N	106°53'12.12"W	170
8091502	62.2	3.3	16.3	2.3	2.1	4.8	3.1	0.3	0.9	95.4	4.63	38°33'37.94"N	106°56'46.38"W	180
8091506	58.5	8.0	15.2	2.3	2.3	6.5	2.5	0.6	0.8	96.6	3.36	38°33'36.03"N	106°56'51.31"W	184
8111504	60.1	5.4	14.4	2.4	2.0	5.2	1.5	0.6	1.3	93.1	6.90	38°29'17.23"N	107° 9'57.49"W	199
8111505	60.2	4.9	14.1	2.3	1.3	3.3	2.0	0.3	0.9	89.3	10.68	38°29'16.80"N	107° 9'56.74"W	200
8111506	59.5	5.7	14.8	2.0	1.2	3.5	2.0	0.2	1.0	90.0	10.03	38°29'16.87"N	107° 9'54.03"W	201
8111507	66.4	1.7	16.2	5.0	1.4	1.2	2.0	0.1	0.4	94.5	5.52	38°29'16.87"N	107° 9'54.03"W	201
072215-02b	61.9	4.5	15.5	2.4	2.0	5.8	2.5	0.4	0.8	95.6	4.45	38°33'37.65"N	106°56'52.14"W	102
08111502 a	61.5	4.6	16.6	1.4	1.1	5.0	4.1	0.2	0.7	95.3	4.70	38°46'3.39"N	106°56'23.99"W	198

Bulk-Rock Geochemical Calculations											
	SiO2	**Fe2O3**	**Al2O3**	**K2O**	**Na2O**	**CaO**	**MgO**	**P2O5**	**TiO2**	**Total**	**LOI**
AGV-1	58.86	6.933362	16.23357	2.835365	3.9294	4.89166	1.717145	0.505301	1.058258	96.96	3.04
AGV-2	61.06	7.061194	17.16789	2.890151	4.142213	5.245843	1.946902	0.484819	1.06153	101.07	-1.07
AMH-1	60.34	5.642437	16.94121	1.139067	4.211928	5.889944	2.104577	0.161908	0.790876	97.22	2.78
BCR-2	52.70	13.13119	11.85629	1.663335	2.933916	7.157935	2.294999	0.338409	2.266665	94.35	5.65
MGL-AND	59.80	5.355793	17.05286	2.349052	4.556159	5.607807	3.592101	0.254993	0.6774	99.25	0.75
MGT-1	72.39	1.338065	15.71129	4.71517	4.124973	0.95092	1.291666	0.143933	0.225692	100.89	-0.89
OU-10	66.92	5.616423	12.42118	1.452083	2.229192	2.483388	2.752675	0.100982	0.536928	94.52	5.48
Sarm 41	60.24	5.271561	14.577	1.415766	1.184122	1.623782	8.156839	0.052936	0.598865	93.12	6.88
										95.34	4.66
Max	72.387	13.13119	17.22845	5.008845	4.556159	9.948574	8.156839	0.704739	2.266665		
Min	52.70408	1.338065	11.65053	1.139067	1.145259	0.95092	1.291666	0.052936	0.225692		
Average	59.92266	6.072939	15.23605	2.38818	2.47297	5.456515	2.528061	0.415675	0.842839		
STD	3.385989	2.16025	1.383024	0.737863	0.854996	1.847459	1.122179	0.185643	0.319382		

Master Sample List

Sample #	Waypoint	T.S. (y/n)	WDXRF (y/n)	latitude	longitude
7181501	WP 088	no	no		
7181502	WP 088	no	no		
7181503	WP 088	no	no		
7181504		no	no		
7181505	WP 090	no	no		
7181506		no	no		
7191501		yes	yes	38°32'39.12"N	106°52'54.63"W
7191502	WP 0003	yes	yes	38°32'11.73"N	106°54'2.15"W
7191503	wp 0003	yes	no	38°32'11.73"N	106°54'2.15"W
7191504	wp 095	no	no		
7201501	WP 89	no	no		
7201502	wp 89	no	no		
7201503	wp 89	no	yes	38°32'14.20"N	106°50'50.88"W
7201505	wp 97	yes	yes	38°33'33.40"N	106°56'46.82"W
7201506	wp 97	no	no		
7221501	wp101	no	no		
7221501	wp 103	no	no		
7221502	WP 103	no	no		
7221503	Wp 105	no	yes	38°33'35.73"N	106°56'51.15"W
7221504	WP 106	yes	yes	38°33'32.46"N	106°56'51.24"W
7221505	WP 106	no	yes	38°33'32.46"N	106°56'51.24"W
7221506	WP 106	no	no		
7291501	WP 111	no	yes	38°39'11.92"N	106°53'13.64"W
7291502	WP 111	yes	yes	38°39'11.92"N	106°53'13.64"W
7291503	WP 111	no	yes	38°39'11.92"N	106°53'13.64"W
7291504	WP 112	yes	yes	38°39'15.31"N	106°53'12.63"W
7291505	Wp 113	no	no	38°39'18.04"N	106°53'13.33"W
7291506	WP 119	no	no		
7301502	WP 120	no	yes	38°35'20.13"N	106°51'22.98"W
7301503	WP 121	no	no		
8011503	WP 125	no	no		
8031501	Wp 0012	no	no		
8031502	WP 0012	yes	yes	38°32'12.80"N	106°53'30.66"W
8041504	Wp 128	no	no		
8041505	WP 130	no	no		
8041506	WP 131	yes	no	38°31'40.81"N	106°51'48.85"W
8041507	WP 133	yes	no	38°31'29.12"N	106°51'43.71"W

Sample #	Waypoint	T.S. (y/n)	WDXRF (y/r	latitude	longitude
8041508	WP 137	no	no		
8051501	Wp 138	yes	yes	38°33'11.97"N	106°55'2.92"W
8051502	Wp 139	no	no		
8051503	WP 140	no	no		
8051504	Wp 142	no	no		
8051505	WP 147	yes	yes	38°33'25.70"N	106°54'57.86"W
8061503	WP 148	no	no		
8061504	Wp 154	no	no		
8061501	WP 148	no	no		
8061502	WP 149	no	no		
8061505	wp 156	yes	yes	38°39'51.57"N	106°52'33.81"W
8071501	WP 161	yes	no	38°31'49.57"N	106°48'24.72"W
8071503	wp 164	yes	no	38°31'55.51"N	106°49'47.13"W
8071504	wp 164	yes	yes	38°31'55.51"N	106°49'47.13"W
8071505	WP 164	no	no		
8071506	WP 165	no	no		
8071507	WP 169	yes	yes	38°35'16.16"N	106°53'11.80"W
8071508	WP 170	yes	yes	38°35'7.65"N	106°53'12.12"W
8081503	WP 176	no	no		
8081504	WP 177	no	no		
8081505	wp 178	no	no		
8091501	WP 179	no	no		
8091502	wp 180	yes	yes	38°33'37.94"N	106°56'46.38"W
8091503	wp 180	no	no		
8091504	WP 180	yes	no	38°33'37.94"N	106°56'46.38"W
8091505	WP 181	no	no		
8091506	Wp 184	no	yes	38°33'36.03"N	106°56'51.31"W
8101501	WP 185	no	no		
8101502	Wp 186	no	no		
8101503	Wp 189	no	no		
8101504	WP 193	no	no		
08111502c	WP 198	yes	no	38°46'3.39"N	106°56'23.99"W
8111503	WP 198	yes	no	38°46'3.39"N	106°56'23.99"W
8111504	WP 199	yes	yes	38°29'17.23"N	107° 9'57.49"W
8111505	WP 200	yes	yes	38°29'16.80"N	107° 9'56.74"W
8111506	WP 201	yes	yes	38°29'16.87"N	107° 9'54.03"W
8111507	WP 201	yes	yes	38°29'16.87"N	107° 9'54.03"W

Sample #	Waypoint	T.S. (y/n)	WDXRF (y/n)	latitude	longitude
8011501	WP 0003	yes	yes	38°32'11.73"N	106°54'2.15"W
8011502	WP 0003	yes	yes	38°32'11.73"N	106°54'2.15"W
8031503		no	no		
07221502 b	WP 102	yes	yes	38°33'37.65"N	106°56'52.14"W
07301501 (1)		no	no		
08081501 a,b,c	WP 174	no	no		
08111502 a,b,c	WP 198	yes(a)	yes	38°46'3.39"N	106°56'23.99"W
08081502 a&b	WP 175	no	no		

T.S. = Thin-Section data; W.D.X.R.F.= Wavelength-dispersive x-ray fluorescence data

Bibliography of Standards

Sarm-41

South African Committee for Certified Reference Materials (1992) Catalogue of certified reference materials. South Africa Bureau of Standards, private Bag x191, Pretoria, Transvaal 0001, South Africa. 36 pp.

AMH -1, AGV-2, AGV-1

Skeen C.J., and Crandell, W.B., 1989, Computerized spectrographic data for two new USGS rocks, AMH-1 and DTS-2:U.S. Geological Survey Open File Report 89-183

MGT-1

Webb P.C., Thompson M.,Potts P. J. and Batjargal B., 2007, GEOPT21 – AN INTERNATIONAL PROFICIENCY TEST FOR ANALYTICAL GEOCHEMISTRY LABORATORIES – REPORT ON ROUND 21 / July 2007 (Granite, MGT-1): GeoPT21 Report International Association of Geoanalysts.

MGL – And

Webb P.C., Thompson M.,Potts P. J. and Batjargal B., 2007, GeoPT27 – AN INTERNATIONAL PROFICIENCY TEST FOR ANALYTICAL GEOCHEMISTRY LABORATORIES – REPORT ON ROUND 27 (Andesite, MGL-AND) / July 2010: GeoPT21 Report International Association of Geoanalysts.

OU-10

Webb P.C., Thompson M.,Potts P. J. and Watson, J. S., 2009, GeoPT24 – AN INTERNATIONAL PROFICIENCY TEST FOR ANALYTICAL GEOCHEMISTRY LABORATORIES – REPORT ON ROUND 24 (Longmyndian greywacke, OU-10) / Jan 2009: GeoPT21 Report International Association of Geoanalysts.

BCR-2

Plumlee, G., 1998, PRELIMINARY - U.S. Geological Survey Certificate of Analysis

BCR-2

Basalt, Columbia River,

http://crustal.usgs.gov/geochemical_reference_standards/basaltbcr2.html#certinfo

APPENDIX C – Petrography

See Chapter 2.4 for discussion of petrographic methods and results

Summary of framework components					
Facies	**Sample**	**Lithics (%)**	**Crystals (%)**	**Glass (%)**	**Sum (%)**
mixed	8071501	33	27	40	100
breccia	7221504	23	23	55	100
matrix	8091502	41	34	25	100.25
EEC TUFF	8111507	1	4	95	100
mixed	8051505	39	31	30	99.5
matrix	7221502b	39	31	30	99.5
breccia	7201505	60	26	15	100
breccia	7291504	35	35	30	100
breccia	8041506	27	33	40	100
lava	8041507	0	50	50	100
breccia	8071508	16	64	20	100
breccia	8091504	18	22	60	100
mixed	8051501	48	12	40	100
mixed	8061505	25	46	30	100
EEC Tuff	8111505	10	30	60	100
EEC TUFF	08111502c	28	12	60	100
EEC TUFF	8111506	6	54	40	100
breccia	8011501	42	28	30	100
breccia	8011502	70	10	20	100
matrix	7191501	36	29	35	100
matrix	8031502	48	32	20	100
breccia	7191502	17	39	45	100
mixed	8111504	38	47	15	100
Hinsdale	8111503	21	60	19	100
breccia	7291502	20	30	50	100
lava	7191503	0	60	40	100
breccia	8071507	30	30	40	100
breccia	8071503	20	30	50	100
	Averages	28	33	39	
breccia		31	31	38	
matrix		41	32	28	
mixed		36	33	31	
EEC TUFF		11	25	64	

Shorthand notation and abbreviations recorded on petrographic report forms

OPX – Orthopyroxene
CPX – Clinopyroxene
Plag. – Plagioclase Feldspar
Hbl. – Hornblende
Xtal – Crystal
SA – Subangular
VR – Very well-rounded
SR – Subrounded
A – Angular
R – Rounded
VA – Very Angular

Sample Name or No.: 08011502

Plane-Polarized Light

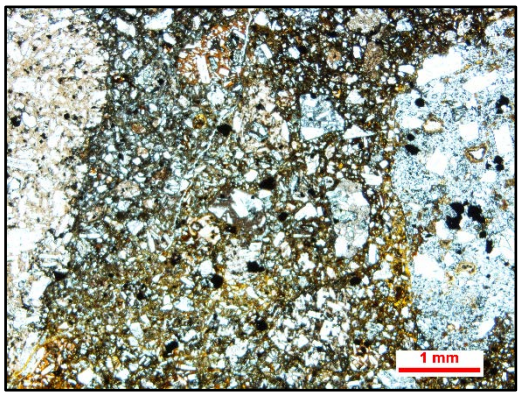

Framework grain composition(%)

Quartz: 0-1%
Feldspar: 20-25%
Lithic Fragments: >70%
Other common minerals: Hornblende, CPX

Percent composition of rock

Matrix (%): 40 **Composition:** Glass
Cement (%): 60 **Composition:** Calcite (secondary)
Apparent Grain Rounding: Angular – Subangular
Grain Size (approx. range): 1cm or less
Sorting (description): poor

Other comments/Observations

Jigsaw fracturing
Varying volcaniclasts w/ plagioclase phenocrysts
Comminuted grains

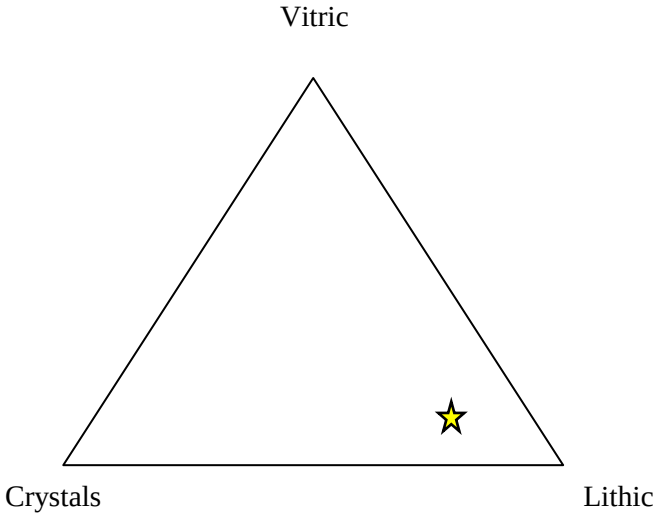

Rock Type: Lithic Tuff

Plane-Polarized Light
08011502

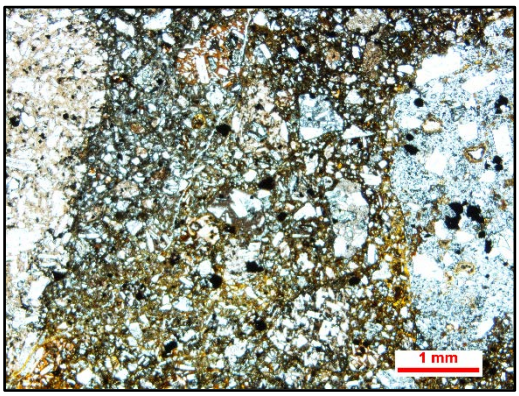

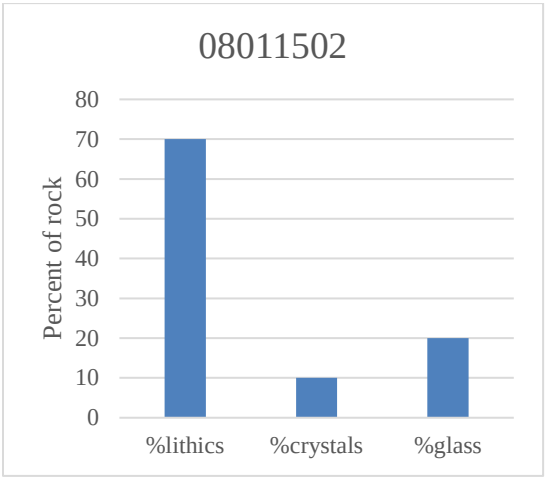

Sample Name or No.: 08111503

Cross-Polarized Light

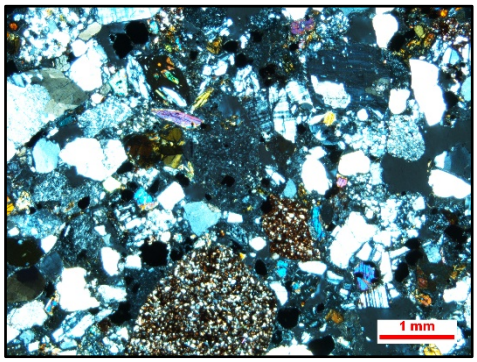

Framework grain composition (%)

Quartz: 40-45%
Feldspar: 10-15%
Lithic Fragments: 35-40%
Other common minerals:
Hbl + CPX (5%) Opaques (10%)

Percent composition of rock

Matrix (%): 65 **Composition:** comminuted minerals and glass
Cement (%): 35 **Composition:** silica?
Apparent Grain Rounding: Very Angular to subrounded
Grain Size (approx. range): ?
Sorting (description): moderate

Other comments/Observations

10% porosity
Volcaniclasts, sandstones, and high number of quartz grains

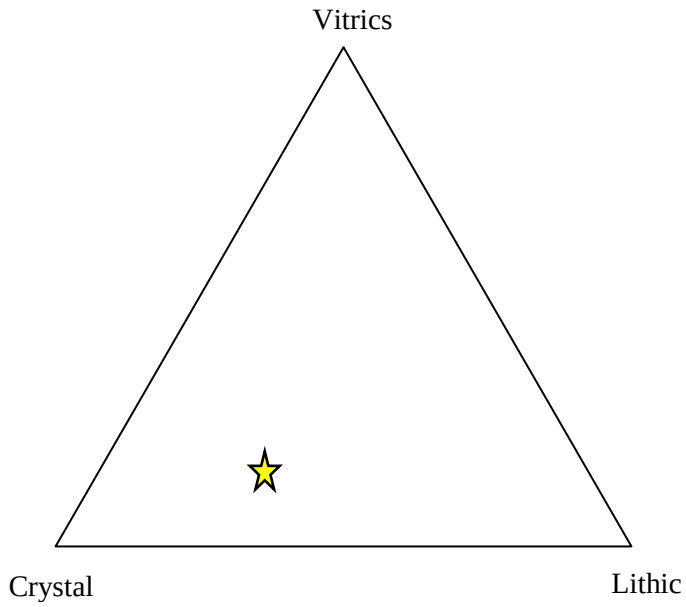

Rock Type: Crystal Tuff

Cross-Polarized Light

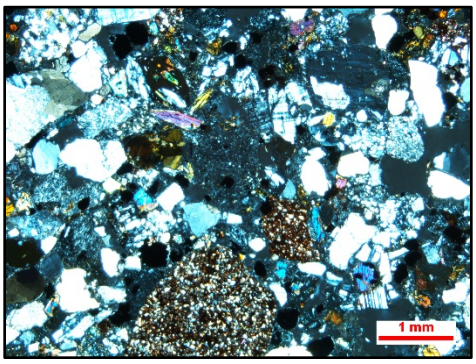

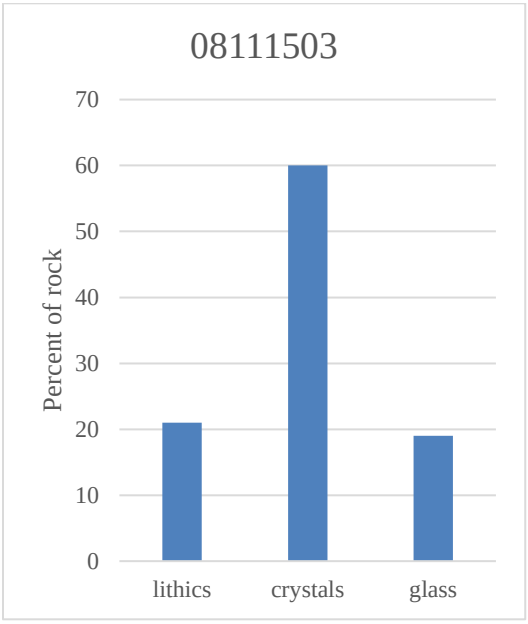

Plane-Polarized Light

Sample Name or No.: 08051505

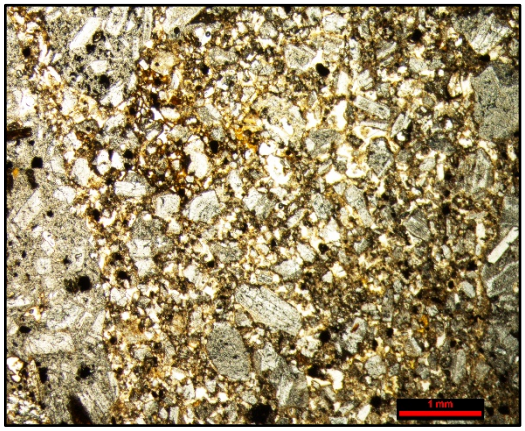

Framework grain composition (%)

Quartz: 0-1%
Feldspar: 40-45%
Lithic Fragments: 50-55%
Other common minerals:
Opaques, CPX, Hornblende

Percent composition of rock

Matrix (%): 80 **Composition:** Quartz+Feldspar
Cement (%): 20 **Composition:** Quartz+Feldspar+Hematite
Apparent Grain Rounding: Very Angular - Subrounded
Grain Size (approx. range): 2 cm - <1mm
Sorting (description): Poor

Other comments/Observations

Pleochroic ratty hornblende? in some lava fragments
High Porosity (35-40%)
Pleochroic augite
Clasts have low relief blend in with matrix
Jigsaw fracturing seen in feldspar crystals
No exotic clasts; all are volcanic
Image above is from cross-polarized light

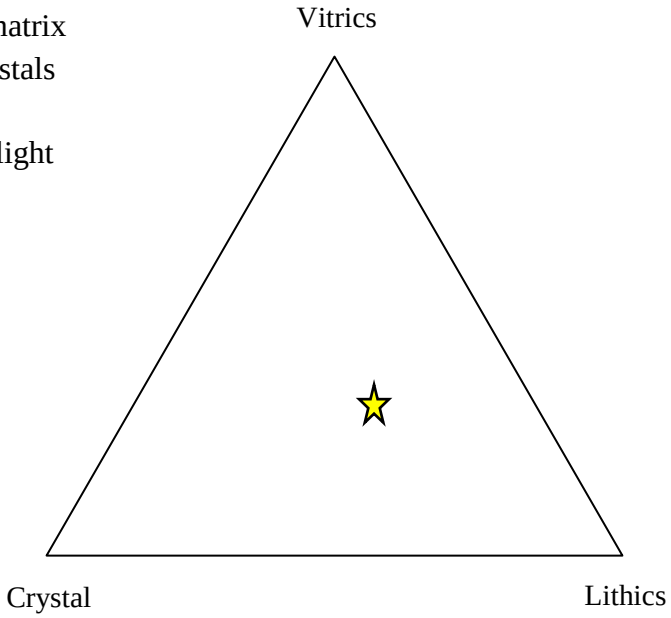

Rock Type: Lithic Tuff

Plane-Polarized Light
08051505

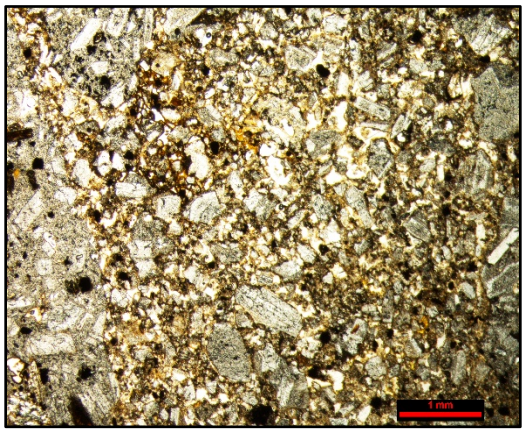

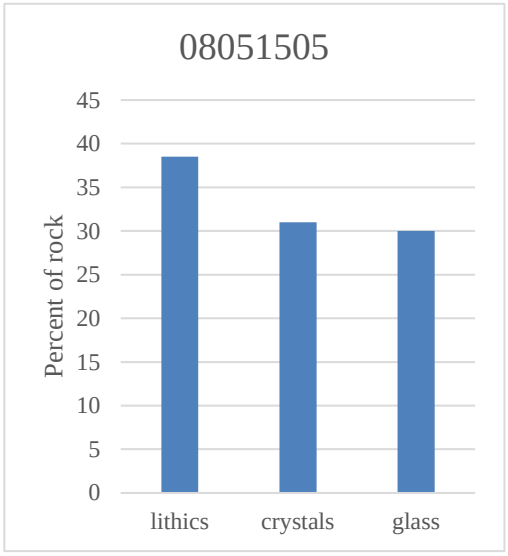

Sample Name or No.: 07221502b

Plane-Polarized Light

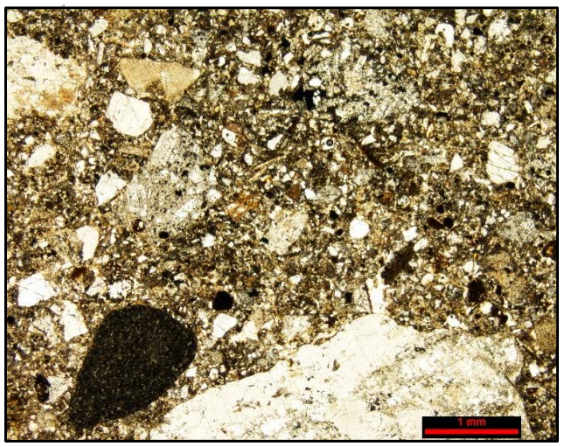

Framework grain composition(%)

Quartz: 40-45%
Feldspar: 5-10%
Lithic Fragments: 50-55%
Other common minerals: Biotite?

Percent composition of rock

Matrix (%): 85 **Composition:** Glass?
Cement (%): 15 **Composition:** Calcite, silica? and hematite?
Apparent Grain Rounding: Subangular – well-rounded
Grain Size (approx. range): 1 cm or less
Sorting (description): Poor

Other comments/Observations

Rounded sandstone, mudstone, schist? and volcaniclasts
Abundant rounded quartz grains with undulatory ext.

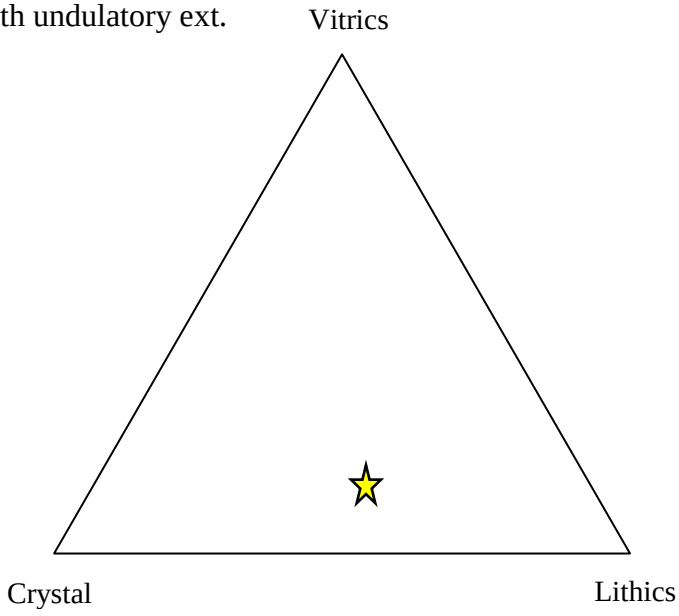

Rock Type: Lithic Tuff

Plane-Polarized Light
07221502b

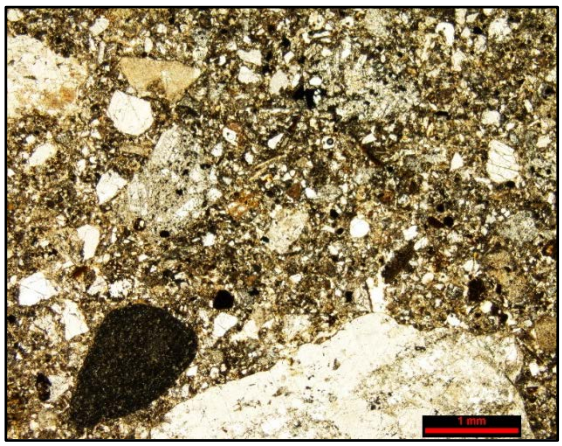

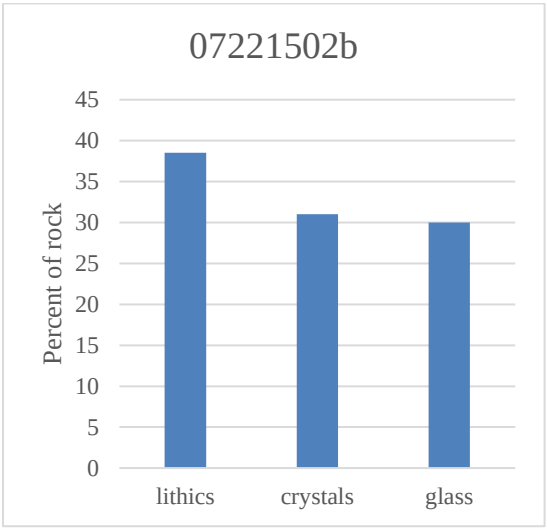

Sample Name or No.: 08091502

Cross-Polarized Light

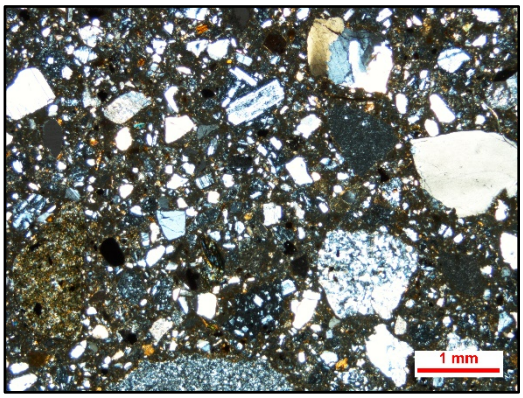

Framework grain composition(%)

Quartz: 30-35%
Feldspar: 5-10%
Lithic Fragments: 50-55%
Other common minerals: Opaques, hematite

Percent composition of rock

Matrix (%): 85 **Composition:** Silica Glass
Cement (%): 15 **Composition:** Silica
Apparent Grain Rounding: Rounded - subangular
Grain Size (approx. range): <10-15mm
Sorting (description): poor

Other comments/Observations

Abundant subangular to subrounded volcaniclasts and pumice

Exotic clasts include quartzite and chlorite schist

Jigsaw fracturing seen in feldspar crystals

Fracture porosity

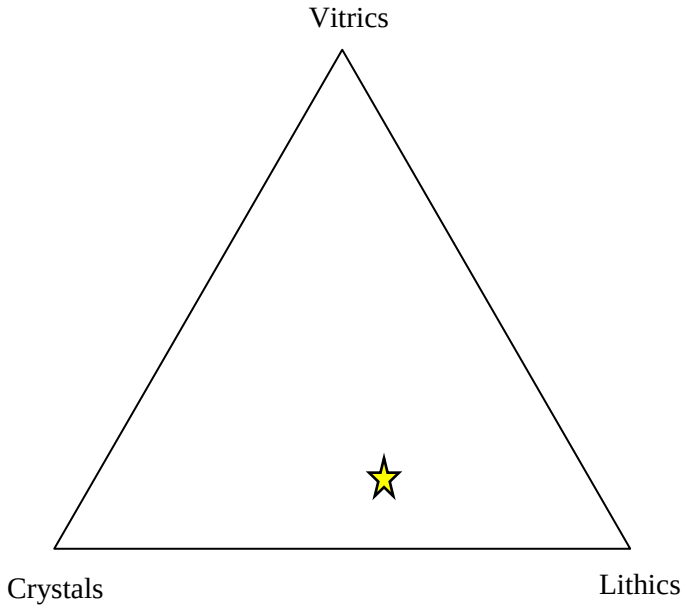

Rock Type: Lithic Tuff

Cross-Polarized Light
08091502

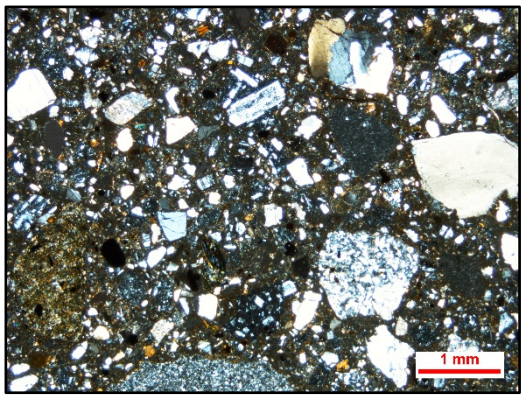

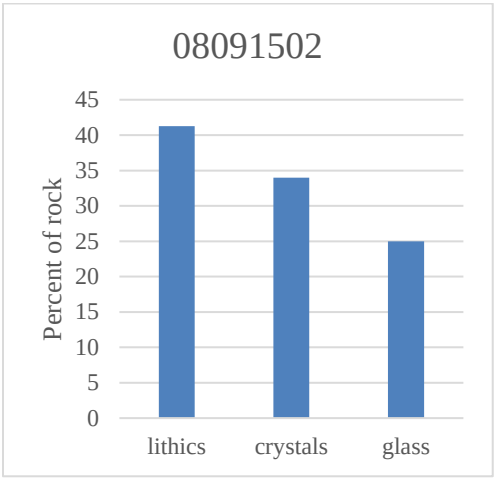

Sample Name or No.: 08031502

Cross-Polarized Light

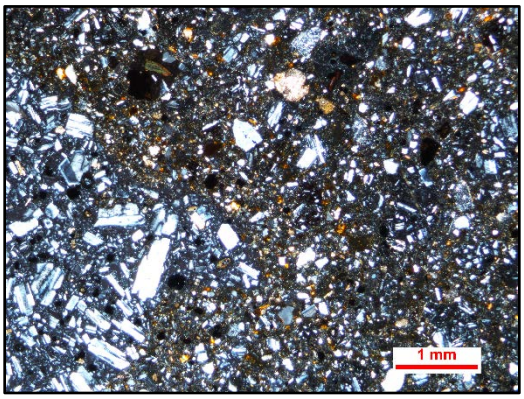

Framework grain composition (%)

Quartz: 10-15%
Feldspar: 25-30%
Lithic Fragments: 55-60%
Other common minerals: Hornblende

Percent composition of rock

Matrix (%): 80 **Composition:** Glass, opaques, and hematite
Cement (%): 20 **Composition:** silica and calcite
Apparent Grain Rounding: n/a
Grain Size (approx. range): fine sand to gravel greater than 1 cm
Sorting (description): poor

Other comments/Observations

Exotic clasts of sandstone and hornblende schist
Trachyitic hornblende andesite (1 cm in size)
Rounded mudstone lithics
Rounded metamorphic quartzite

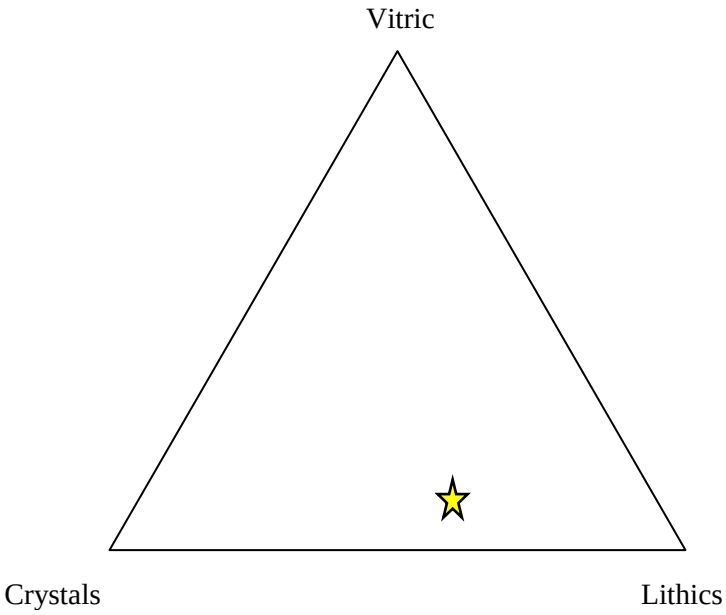

Rock Type: Lithic Tuff

Cross-Polarized Light
08031502

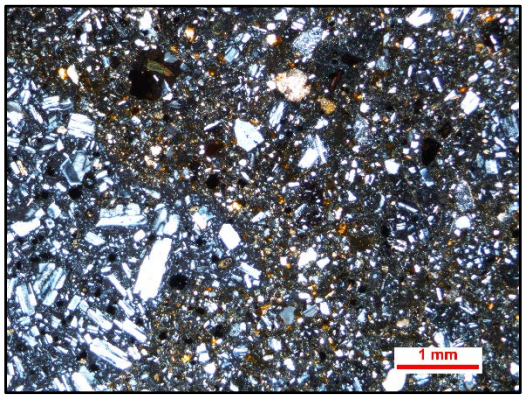

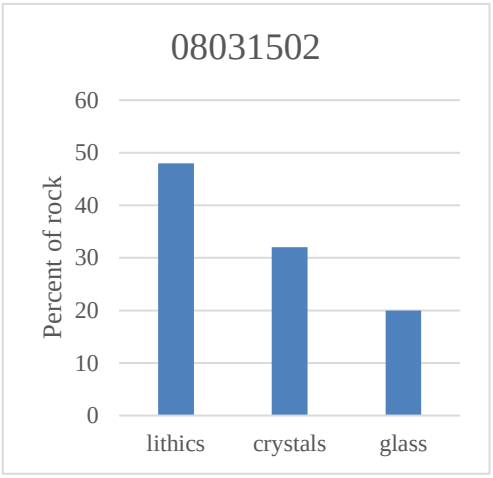

Sample Name or No.: 07191501

Framework grain composition (%)

Cross-Polarized Light

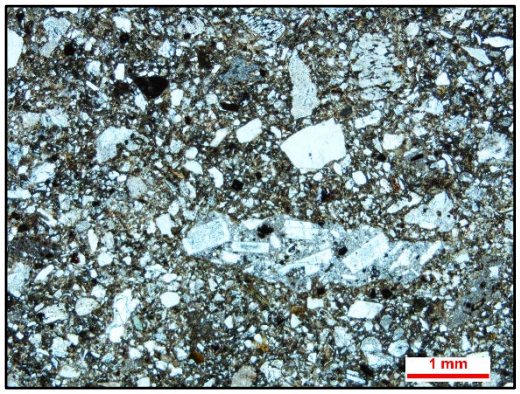

Quartz: 15-20%
Feldspar: 25-30%
Lithic Fragments: 50-55%
Other common minerals:
Hornblende, CPX, opaques

Percent composition of rock

Matrix (%): 50 **Composition:** Glass
Cement (%): 50 **Composition:** silica
Apparent Grain Rounding: n/a
Grain Size (approx. range): 20 mm or less
Sorting (description): poor to moderate

Other comments/Observations

Low porosity

Lithics of metasedimentary rocks ± sandstone?

Rounded minerals with high interference colors

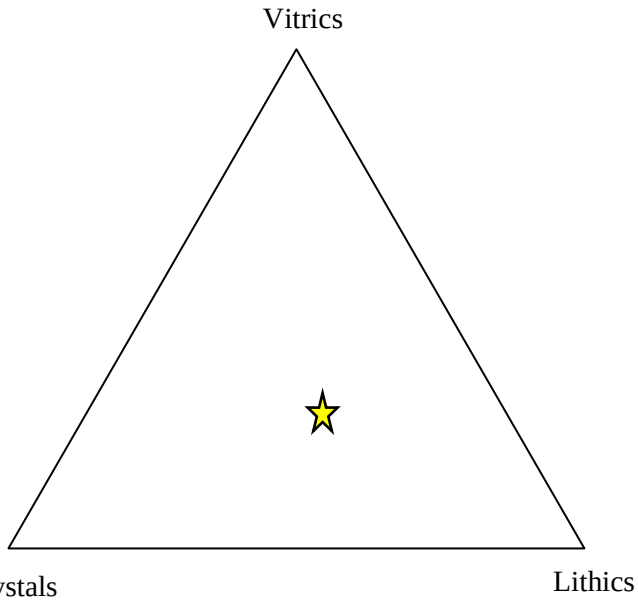

Rock Type: Lithic tuff

Cross-Polarized Light
07191501

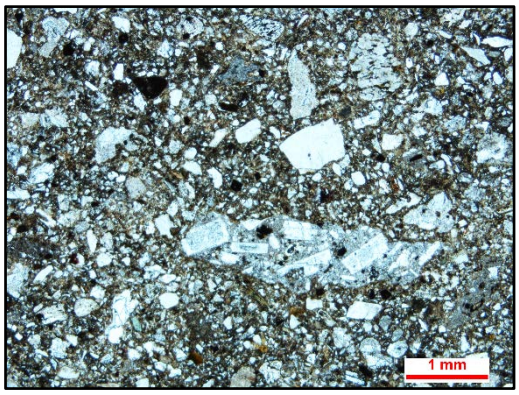

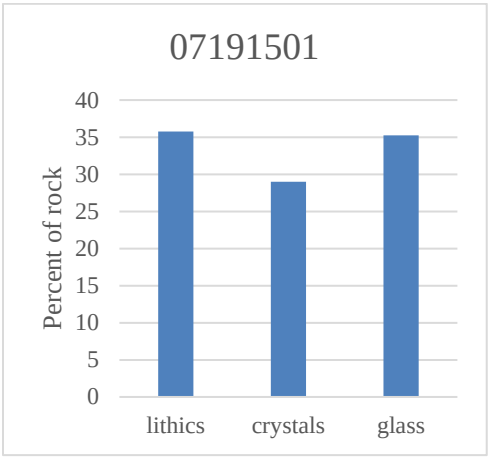

Sample Name or No.: 07191502

Framework grain composition (%)

Cross-Polarized Light

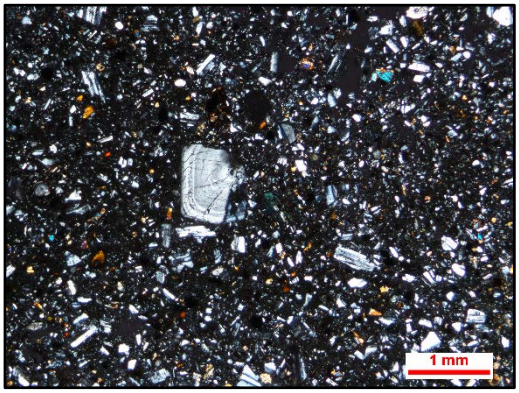

Quartz: 5-10%
Feldspar: 65-70%
Lithic Fragments: 25-30%
Other common minerals:
Hornblende, CPX, and opaques

Percent composition of rock

Matrix (%): n/a **Composition:** Glass
Cement (%): n/a **Composition:** Silica
Apparent Grain Rounding:
Grain Size (approx. range): fine-very fine less than 1 mm
Sorting (description): moderate

Other comments/Observations

Very fine grained and moderately to well sorted

Pockets of very well comminuted material?

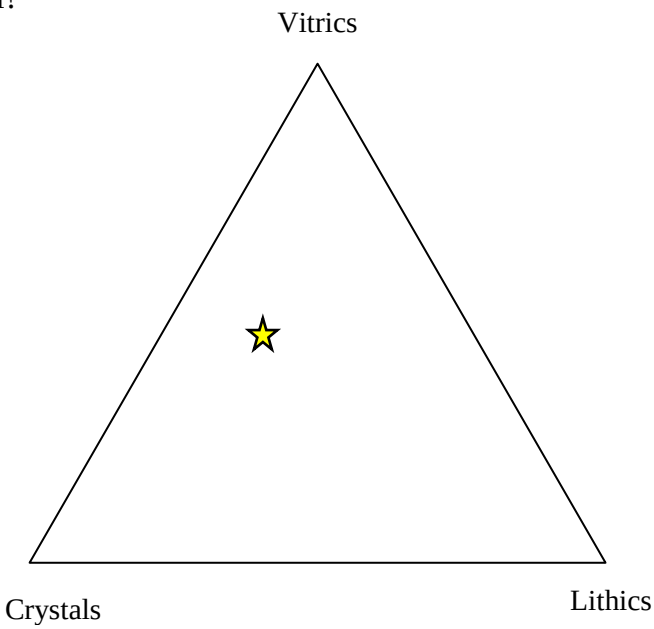

Rock Type: Crystal-to-vitric tuff

Cross-Polarized Light
07191502

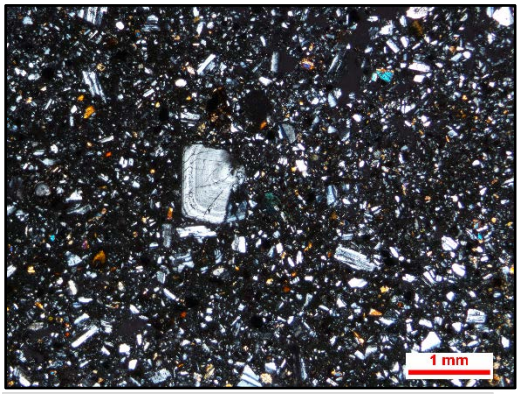

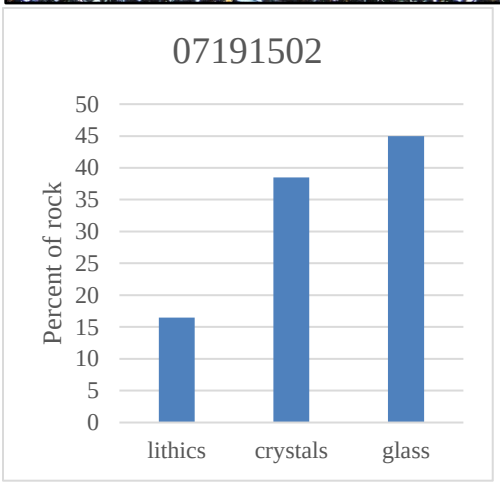

Sample Name or No.: 08071501

Framework grain composition (%)

Plane-Polarized Light

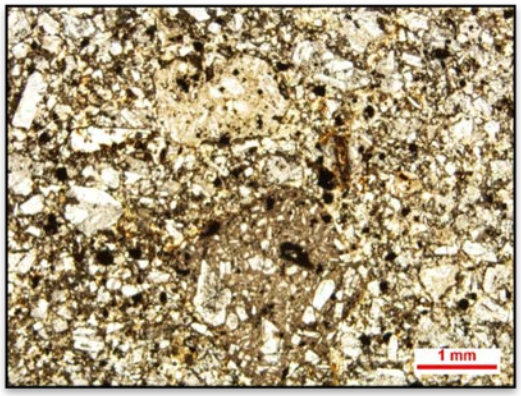

Quartz: 0-1%
Feldspar: 40-45%
Lithic Fragments: 55-60%
Other common minerals: Opaques

Percent composition of rock

Matrix (%): 40 **Composition:** Glass
Cement (%): 60 **Composition:** n/a
Apparent Grain Rounding: SA - R
Grain Size (approx. range): one grain greater than 1 cm
Sorting (description): Moderate to poor

Other comments/Observations

Minor olivine? Or anomalous interference in plag.

Some clasts show porosity, total porosity approx. 10%

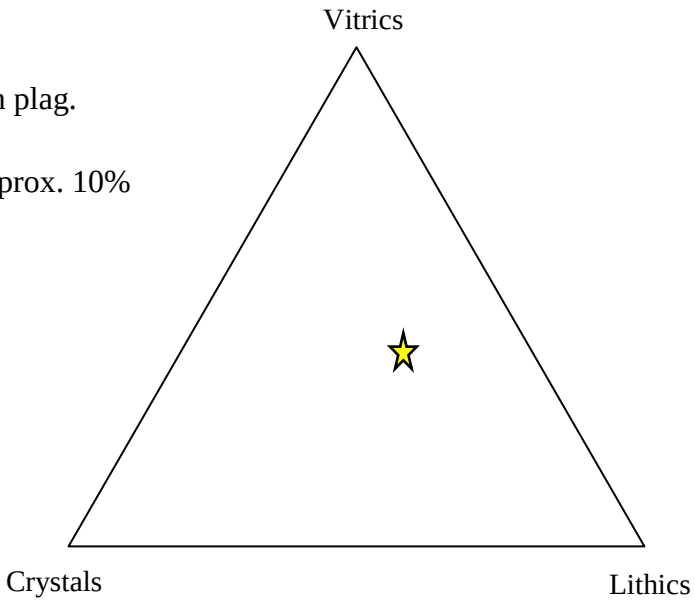

Rock Type: Vitric tuff

Plane-Polarized Light
08071501

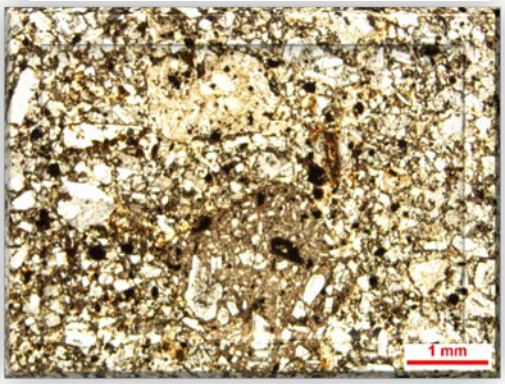

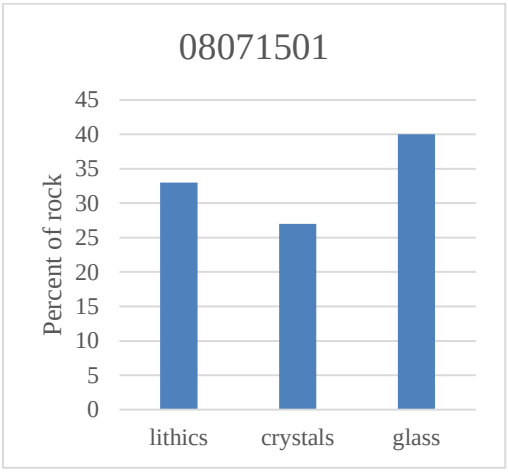

Sample Name or No.: 08111504

Plane-Polarized Light

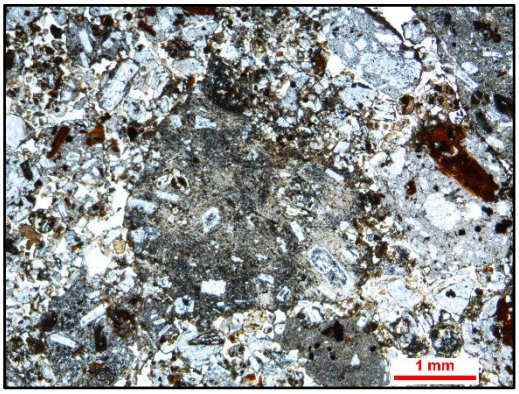

Framework grain composition (%)

Quartz: 5-10%
Feldspar: 40-45%
Lithic Fragments: 45-50%
Other common minerals: Opaques

Percent composition of rock

Matrix (%): n/a **Composition:** Opaques, glass
Cement (%): n/a **Composition:** silica
Apparent Grain Rounding: Angular – Rounded
Grain Size (approx. range): less than 60 mm
Sorting (description): poor to moderate

Other comments/Observations

Highly altered with many hornblende crystals oxidized deep red

Volcaniclasts of hornblende andesite?

No exotic clasts

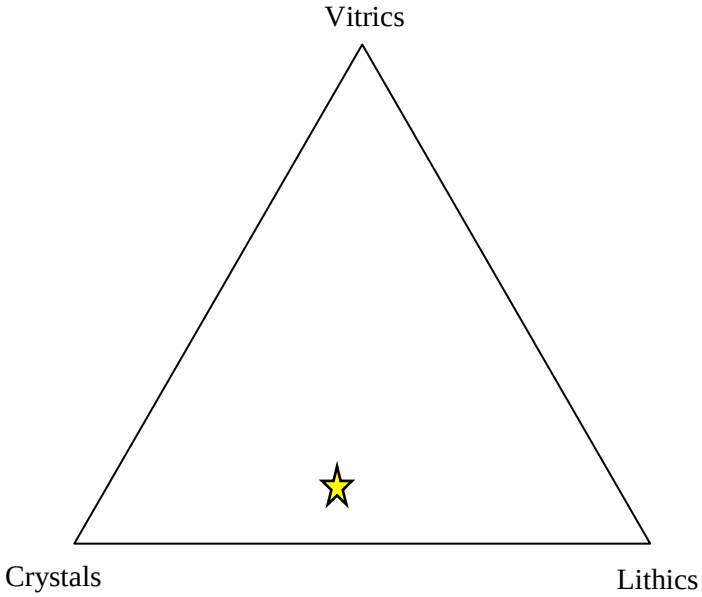

Rock Type: Crystal tuff

Plane-Polarized Light
08111504

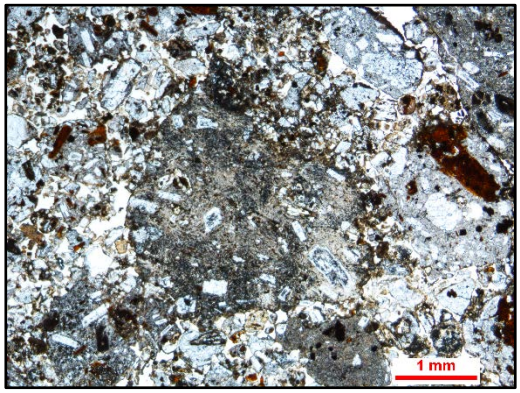

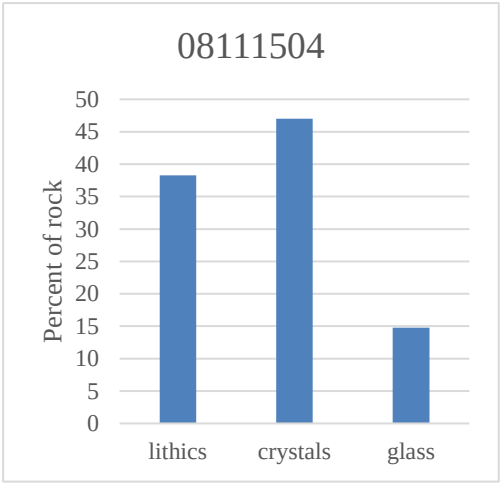

Sample Name or No.: 07291502

Cross-Polarized Light

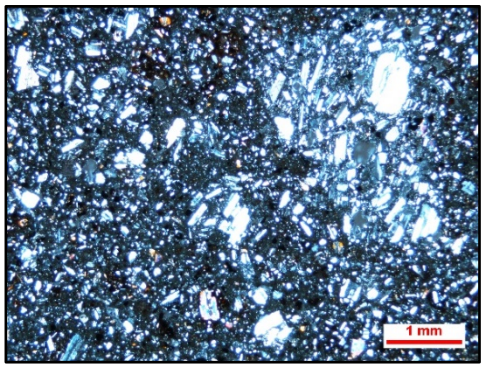

Framework grain composition (%)

Quartz: 5-10%
Feldspar: 50-55%
Lithic Fragments: 40-45%
Other common minerals:
Augite and Hornblende

Percent composition of rock

Matrix (%): 50 **Composition:** Glass and fine xtals
Cement (%): 50 **Composition:** glass?
Apparent Grain Rounding:
Grain Size (approx. range): mostly 10-20 mm (exceptional grain 1cm)
Sorting (description): poor

Other comments/Observations

Composed primarily of volcaniclasts in a glassy matrix

Some exotic clasts of schist? And quartzite

3-4% porosity

Some volcaniclasts contain other volcanics

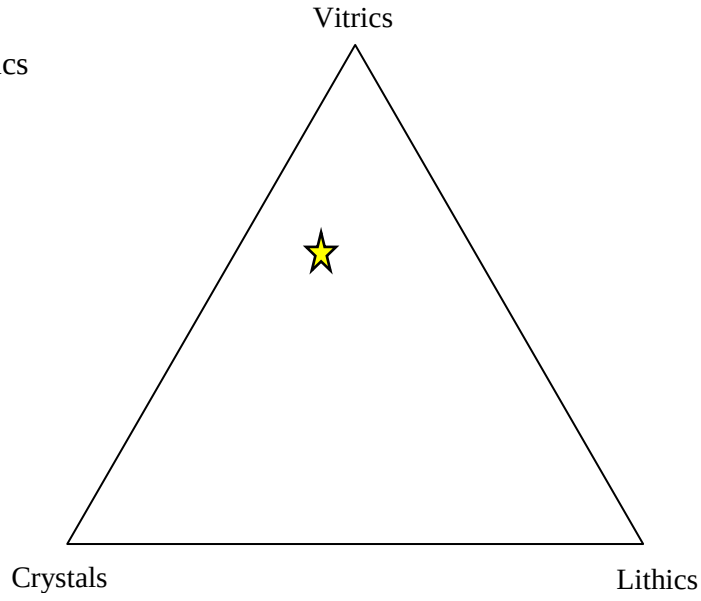

Rock Type: Vitric tuff

Cross-Polarized Light
07291502

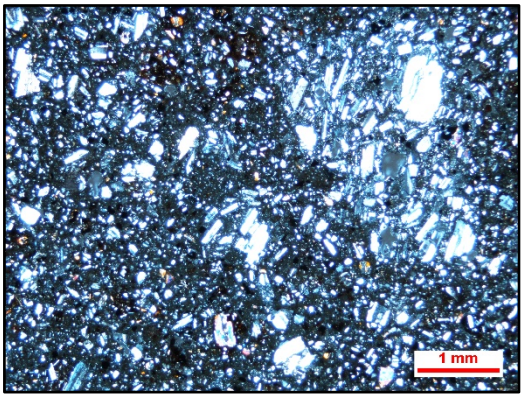

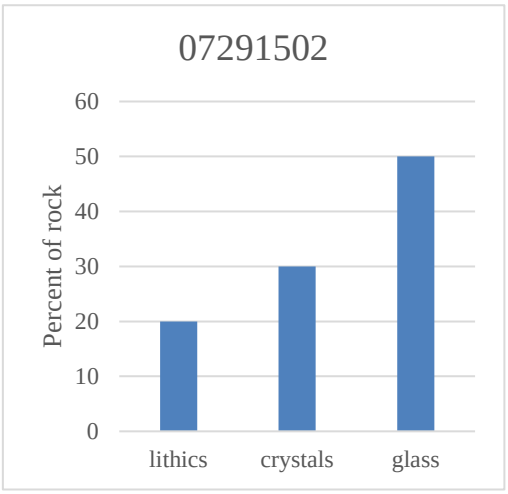

Sample Name or No.: 08011501

Framework grain composition (%)

Cross-Polarized Light

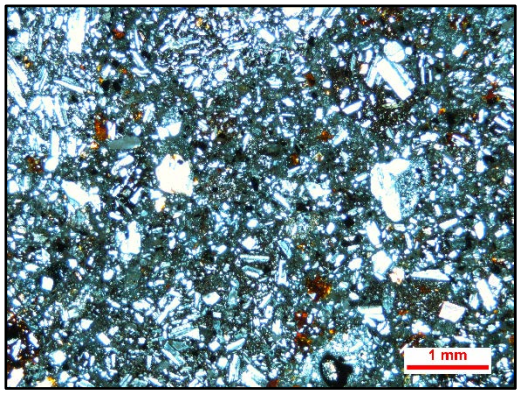

Quartz: 1-5%
Feldspar: 35-40%
Lithic Fragments: 60-65%
Other common minerals:
Hornblende, CPX, and Hematite

Percent composition of rock

Matrix (%): n/a **Composition:** feldspar, silica, and glass
Cement (%): n/a **Composition:** calcite and silica
Apparent Grain Rounding: rounded-to-mostly angular
Grain Size (approx. range): most clasts less than 10 mm one clast 1cm
Sorting (description):

Other comments/Observations

Plag. Altering to calcite?

Glassy matrix binding volcaniclasts

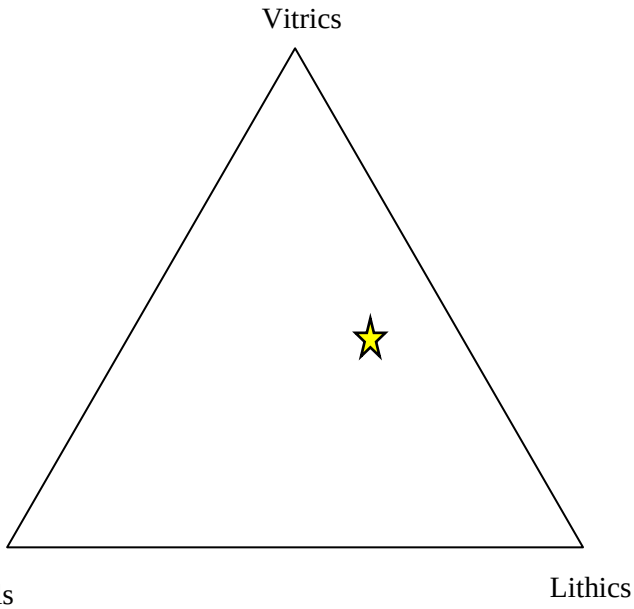

Rock Type: Lithic tuff

Cross-Polarized Light
08011501

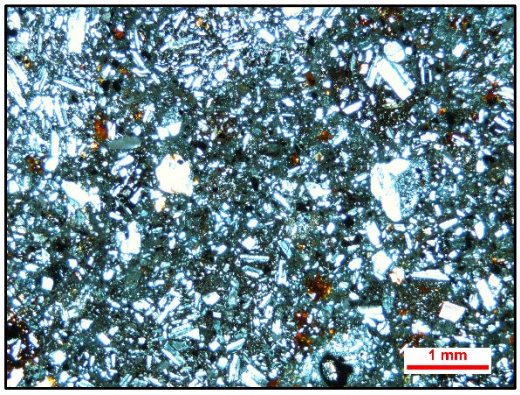

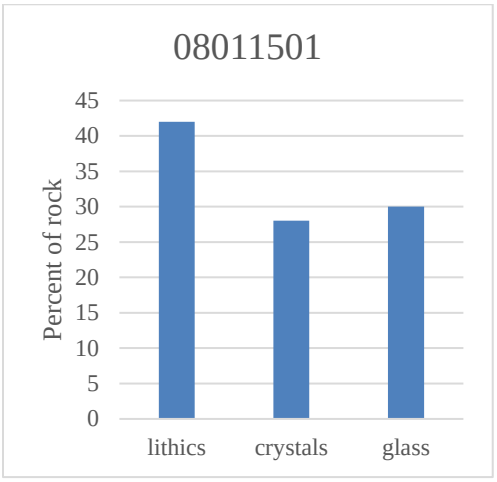

Sample Name or No.: 08111506

Framework grain composition(%)

Plane-Polarized Light

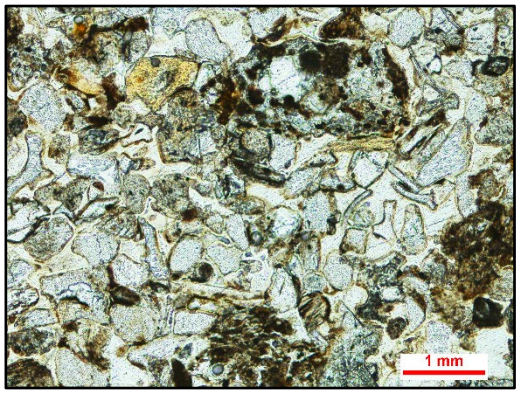

Quartz: 60-65%
Feldspar: 30-35%
Lithic Fragments: 5-10%
Other common minerals:
Feldspar, opaques, hematite

Percent composition of rock

Matrix (%): 90 **Composition:** Glass
Cement (%): 10 **Composition:** silica
Apparent Grain Rounding: very angular to subangular
Grain Size (approx. range): fine to medium
Sorting (description): moderate to well

Other comments/Observations

Elongate, curved glass

Lithics are pumice?

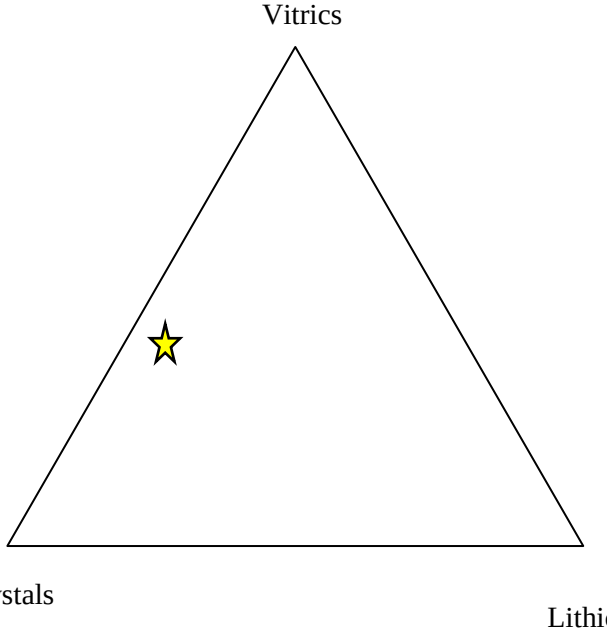

Rock Type: Crystal tuff

Plane-Polarized Light
08111506

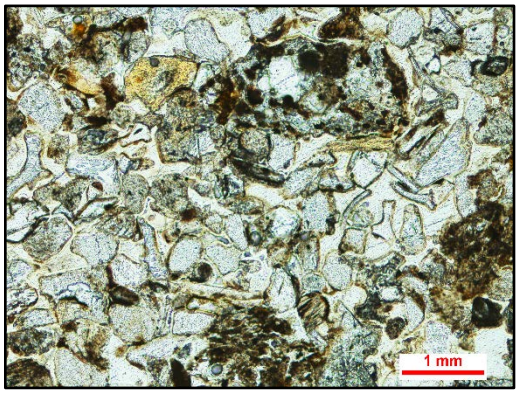

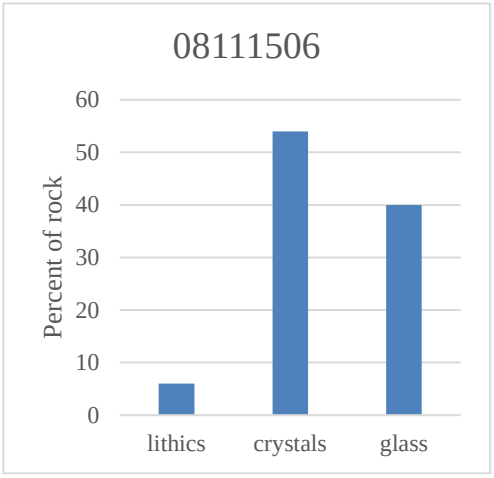

Sample Name or No.: 08111507

Plane-Polarized Light

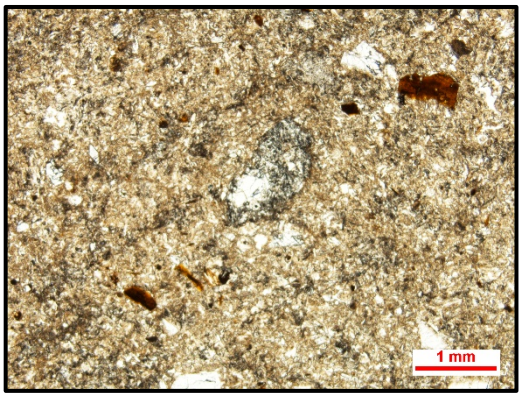

Framework grain composition (%)

Quartz: 65-70%
Feldspar: 0-1%
Lithic Fragments: 0-1%
Other common minerals:
Biotite and opaques

Percent composition of rock

Matrix (%): 95 **Composition:** Siliceous glass
Cement (%): 5 **Composition:** sericite
Apparent Grain Rounding: angular–subangular
Grain Size (approx. range): sand–silt (medium–coarse ash)
Sorting (description): none

Other comments/Observations

Some porosity
Some oxidation
Very fine, glass matrix with obvious glass shards

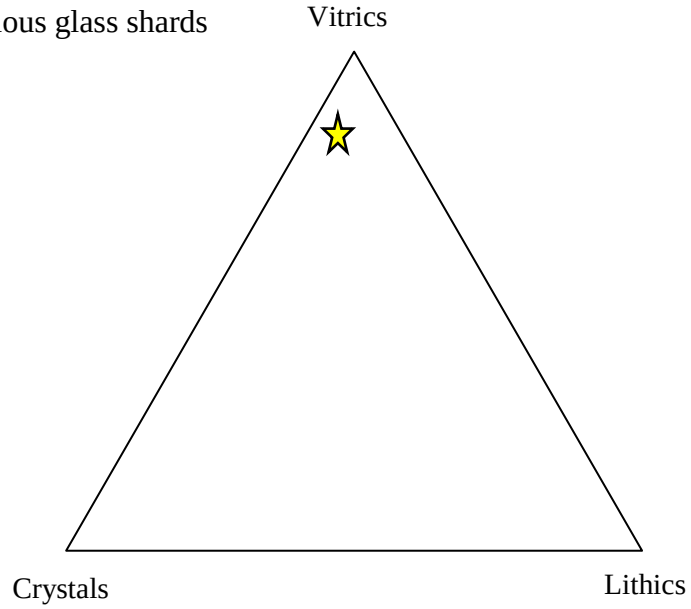

Rock Type: Vitric tuff

Plane-Polarized Light
08111507

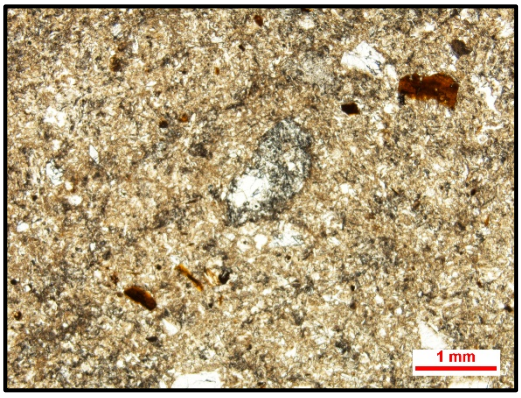

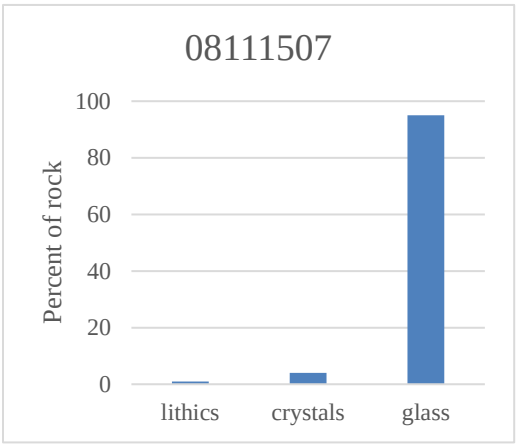

Sample Name or No.: 08111502c

Cross-Polarized Light

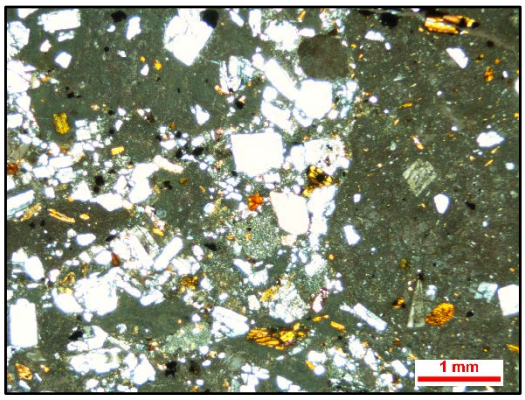

Framework grain composition (%)

Quartz: 10-15%
Feldspar: 15-20%
Lithic Fragments: 65-70%
Other common minerals: Hornblende, cpx?

Percent composition of rock

Matrix (%): 85 **Composition:** Glass (plag. And quartz)
Cement (%): 15 **Composition:** calcite + silica?
Apparent Grain Rounding: SA - VR
Grain Size (approx. range): less than 50 mm
Sorting (description): very poorly

Other comments/Observations

Heterogenous mixture of volcaniclasts sandstone
Appears to be reworked by water
Post lithification conchoidal fracture
Some cubic opaques (pyrite)

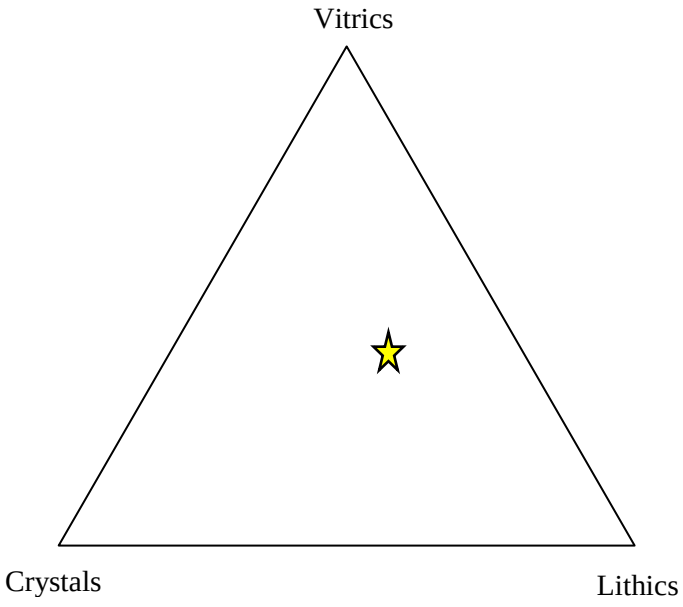

Rock Type: vitric tuff

Cross-Polarized Light
08111502c

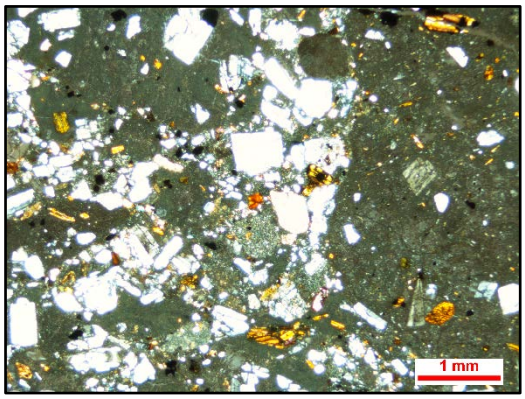

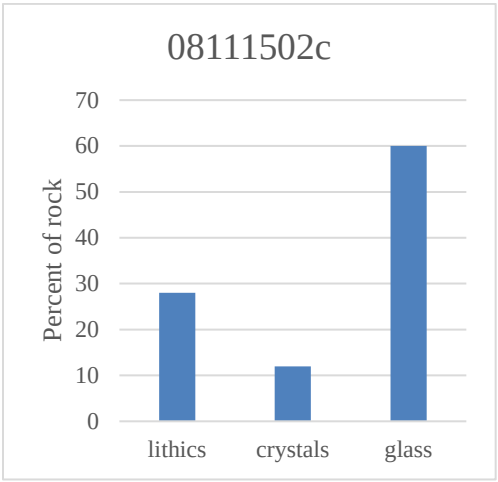

Sample Name or No.: 08111505

Plane-Polarized Light

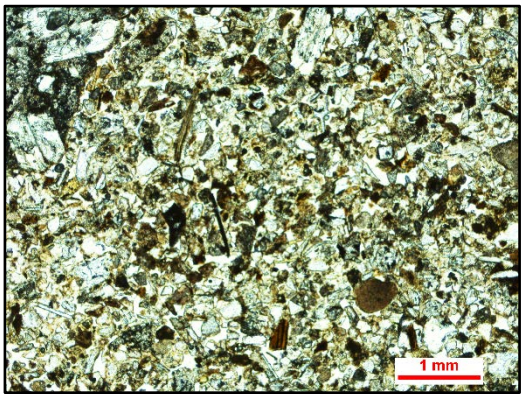

Framework grain composition (%)

Quartz: 40-45%
Feldspar: 30-35%
Lithic Fragments: 20-25%
Other common minerals:
Hornblende, cpx?

Percent composition of rock

Matrix (%): 85 **Composition:** Glass (plag. And quartz)
Cement (%): 15 **Composition:** calcite + silica?
Apparent Grain Rounding: angular to subrounded
Grain Size (approx. range): less than 10-15mm
Sorting (description): Moderate

Other comments/Observations

Appears to be graded?

Devitrified glass?

Porosity of approx. 50%

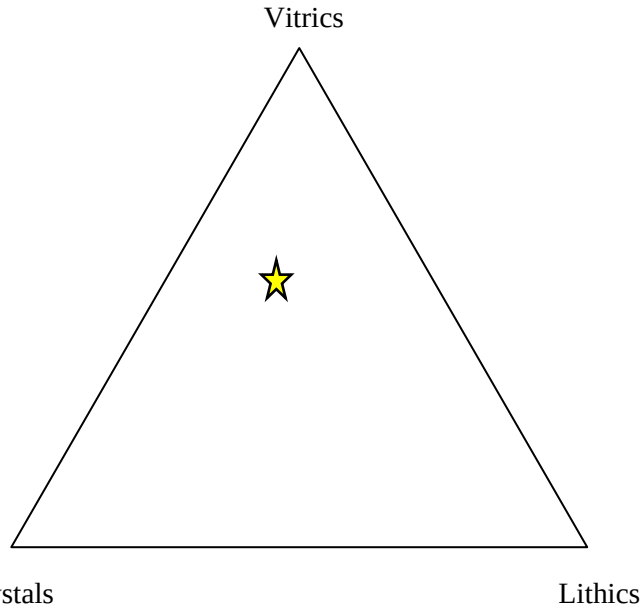

Rock Type: Vitric tuff

Plane-Polarized Light
08111505

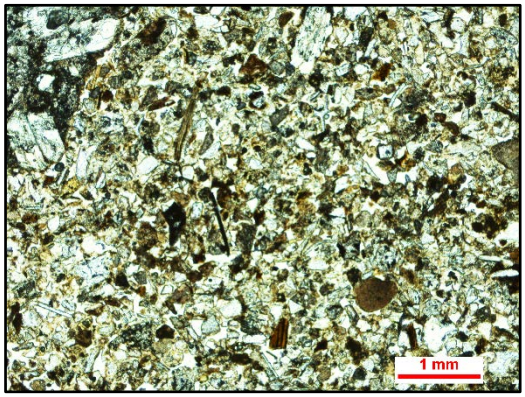

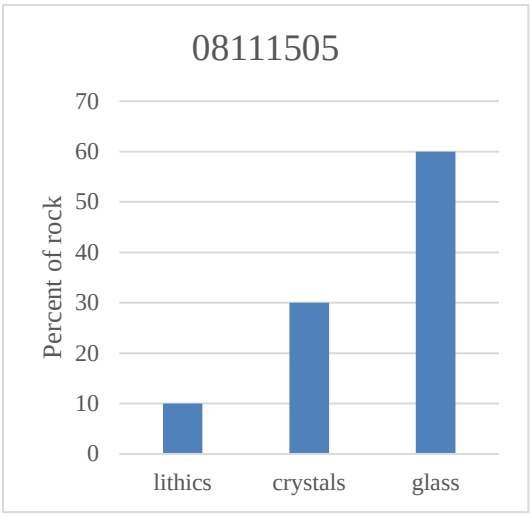

Sample Name or No.: 08061505

Cross-Polarized Light

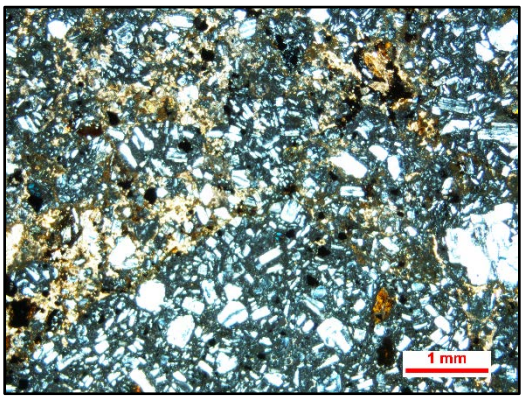

Framework grain composition(%)

Quartz: 25-30%
Feldspar: 40-45%
Lithic Fragments: 40-45%
Other common minerals:

Percent composition of rock

Matrix (%): 90 **Composition:** Plag. and quartz
Cement (%): 10 **Composition:** calcite + silica?
Apparent Grain Rounding: angular to subrounded
Grain Size (approx. range):
Sorting (description): Poor

Other comments/Observations

Calcite cement; matrix is comminuted glass and xtals

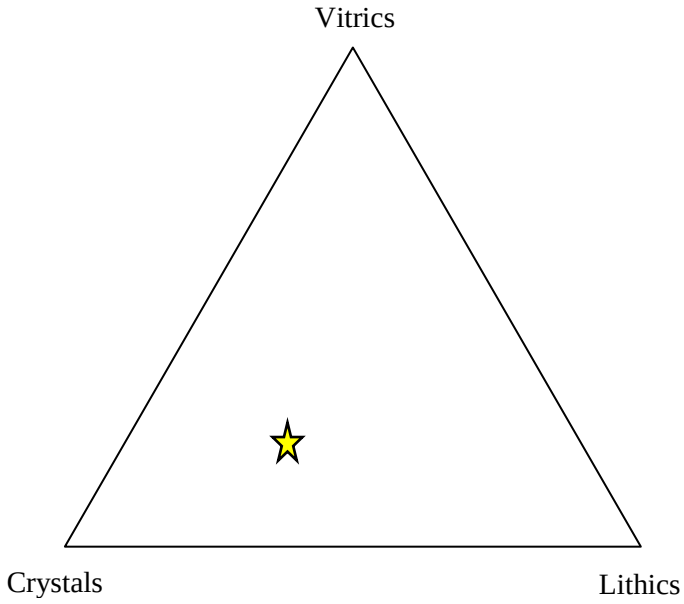

Rock Type: crystal tuff

Cross-Polarized Light
08061505

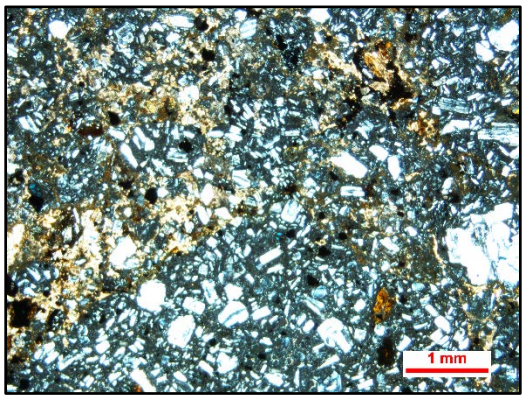

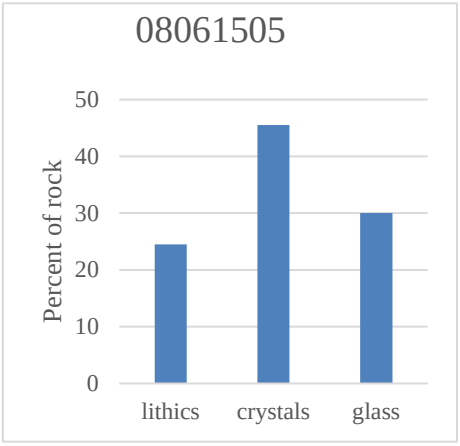

Sample Name or No.: 08051501

Framework grain composition (%)

Cross-Polarized Light

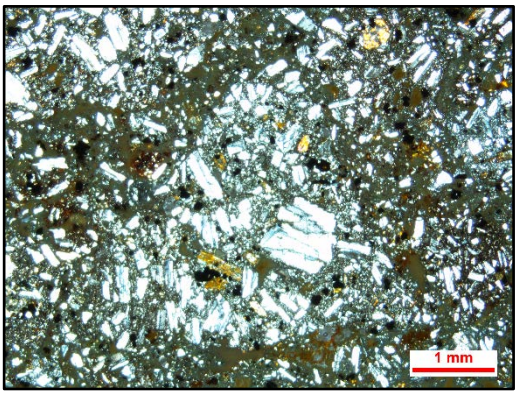

Quartz: 1-5%
Feldspar: 15-20%
Lithic Fragments: >70%
Other common minerals: hematite opaques

Percent composition of rock

Matrix (%): 40 **Composition:** Glass
Cement (%): 60 **Composition:** Silica
Apparent Grain Rounding: VA - SA
Grain Size (approx. range): Max 2 cm
Sorting (description): Poor

Other comments/Observations

Jigsaw fracturing

Solely volcaniclastic

Hematite cement?

Altered plag. and CPX?

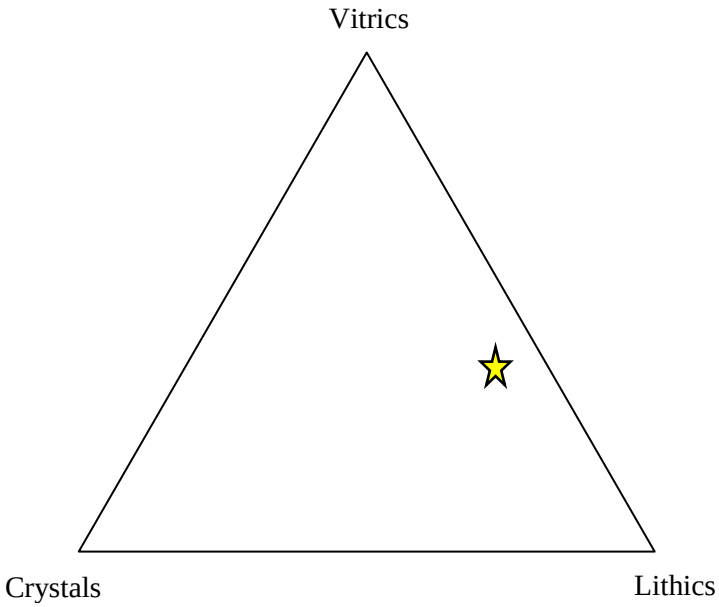

Rock Type: Lithic Tuff

Cross-Polarized Light
08051501

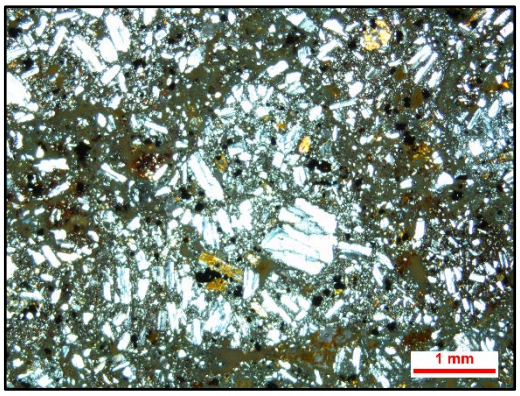

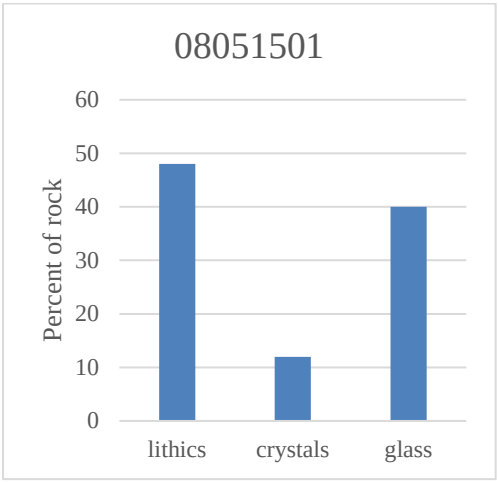

Sample Name or No.: 08091504

Plane-Polarized Light

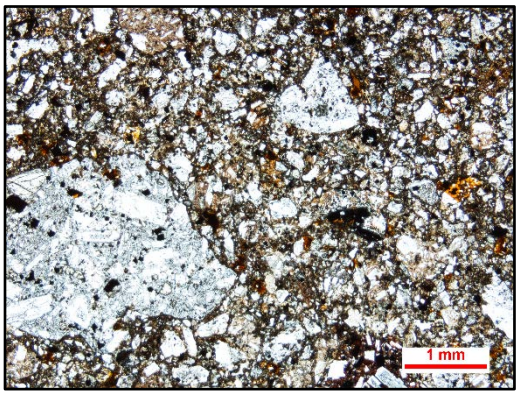

Framework grain composition (%)

Quartz: 0-1%
Feldspar: 40-45%
Lithic Fragments: 40-45%
Other common minerals:
Hematite, biotite, OPX

Percent composition of rock

Matrix (%): 100 **Composition:** Glass + Plag.
Cement (%): ? **Composition:**
Apparent Grain Rounding: A - SR
Grain Size (approx. range):
Sorting (description): Poor

Other comments/Observations

Subangular clasts of andesite with subhedral plag phenos

Some clasts have brown (in PPL) glass matrix

Some rounded and preferentially weathered clasts

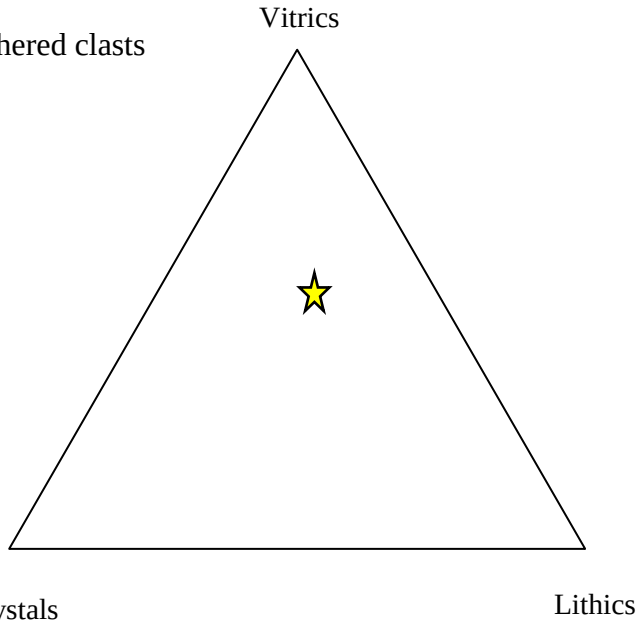

Rock Type: Vitric tuff

Plane-Polarized Light
08091504

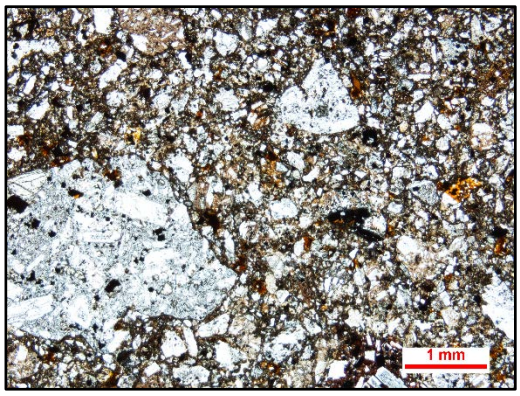

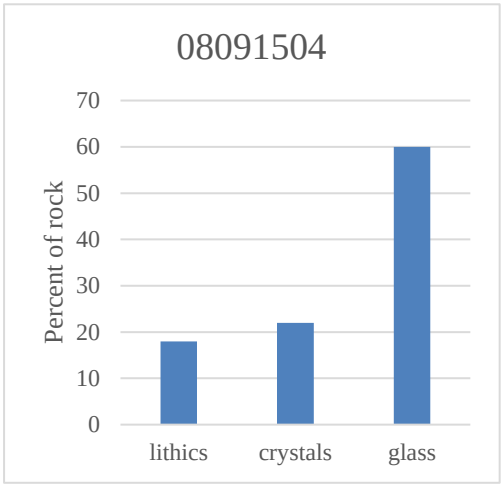

Sample Name or No.: 08071508

Plane-Polarized Light
08071508

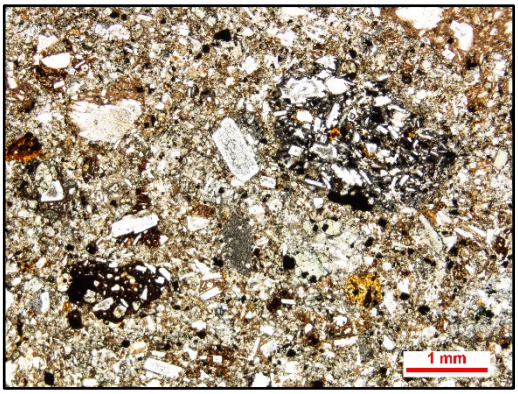

Framework grain composition (%)

Quartz: 30-35%
Feldspar: 30-35%
Lithic Fragments: 10-15%
Other common minerals: Augite

Percent composition of rock

Matrix (%): 55 **Composition:** > 50% glass
Cement (%): 15 **Composition:** Silica
Apparent Grain Rounding: R to SA
Grain Size (approx. range): ?
Sorting (description): Poor

Other comments/Observations

Glassy matrix
Rounded volcaniclasts

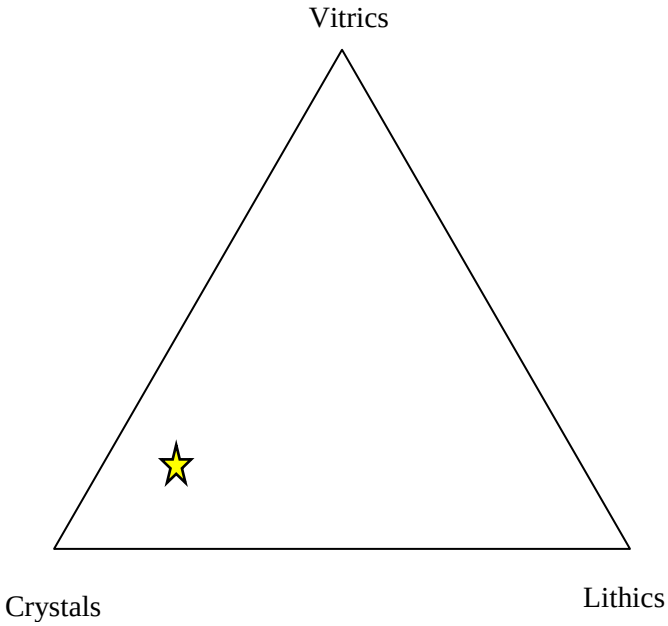

Rock Type: Crystal Tuff

Plane-Polarized Light
08071508

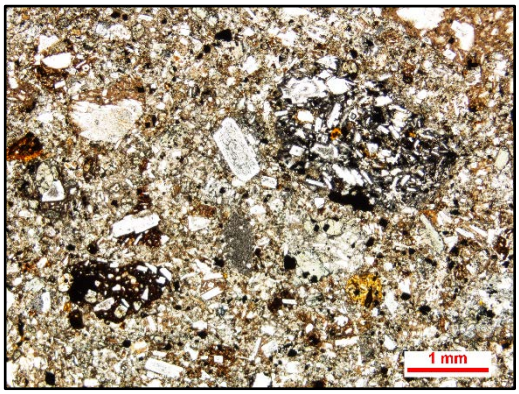

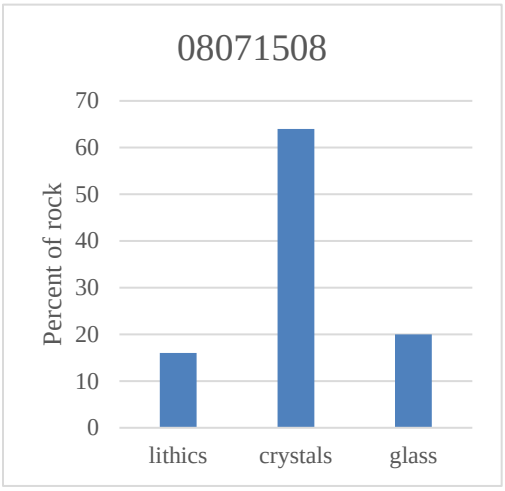

Sample Name or No.: 07221504

Plane-Polarized Light

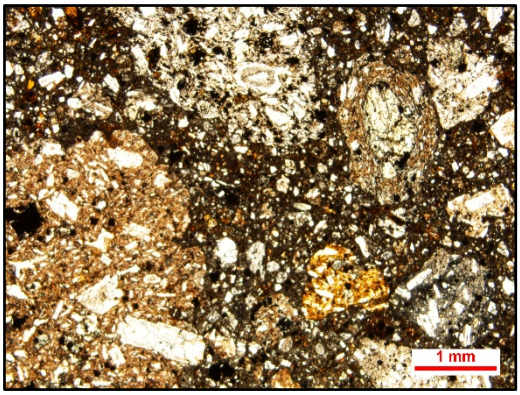

Framework grain composition (%)

Quartz: 0-1%
Feldspar: 50-55%
Lithic Fragments: 50-55%
Other common minerals: CPX, Hornblende

Percent composition of rock

Matrix (%): 100 **Composition:** Glass, Plag.
Cement (%): 15 **Composition:** silica
Apparent Grain Rounding: R - SA
Grain Size (approx. range): ?
Sorting (description): Very poor

Other comments/Observations

Clasts from various sources

Some clasts show trachyitic texture

Opaques 2-3% pyrite? Or needle-like pyrrhotite?

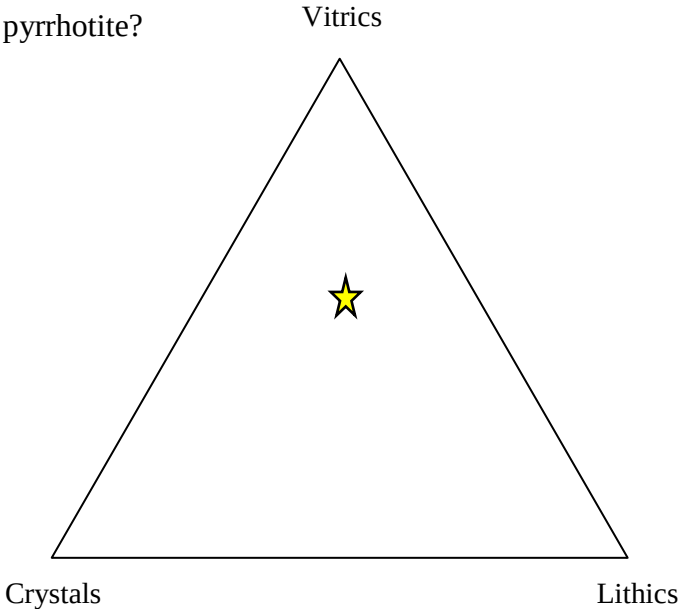

Rock Type: Vitric tuff

Plane-Polarized Light
07221504

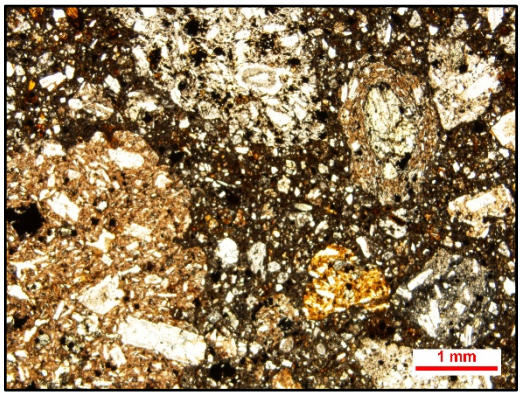

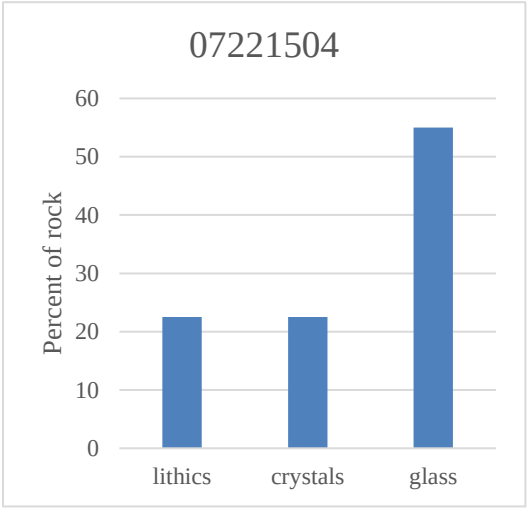

Sample Name or No.: 08041507

Cross-Polarized Light

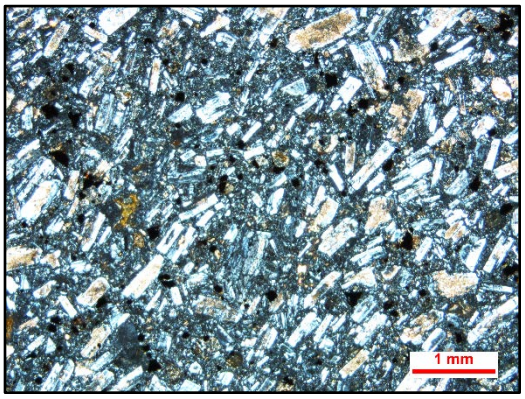

Framework grain composition (%)

Quartz: 10-15%
Feldspar: >70%
Lithic Fragments: 0-1%
Other common minerals:
Hornblende and CPX

Percent composition of rock

Matrix (%): n/a **Composition:**
Cement (%): 100 **Composition:** quartz glass? And hematite?
Apparent Grain Rounding: n/a
Grain Size (approx. range): n/a
Sorting (description): n/a

Other comments/Observations

Clast of lava from breccia

Trachyitic texture parallel to long axis of the slide

Altered, opaque (hematite?) and sericite?

Subhedral to euhedral plag. crystals

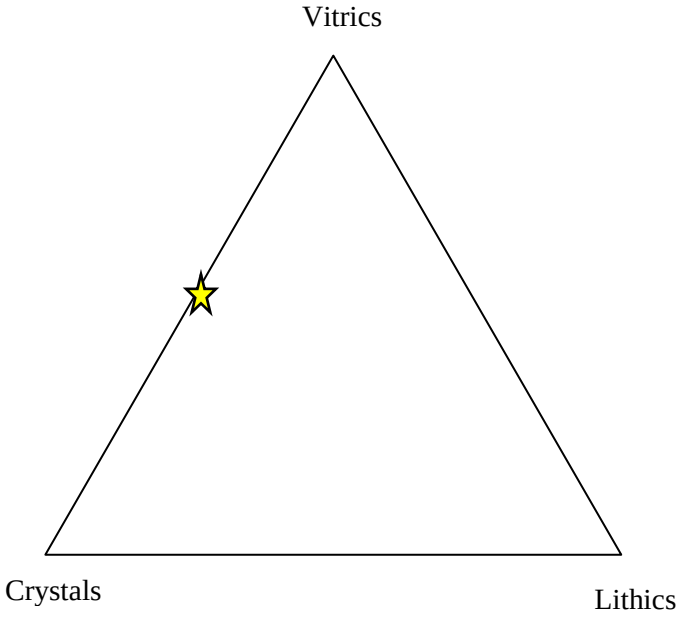

Rock Type: Hornblende andesite

Cross-Polarized Light
08041507

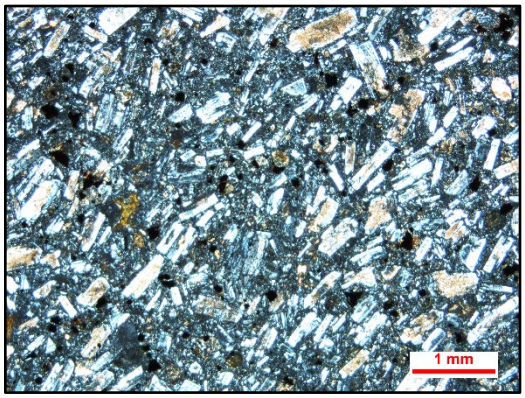

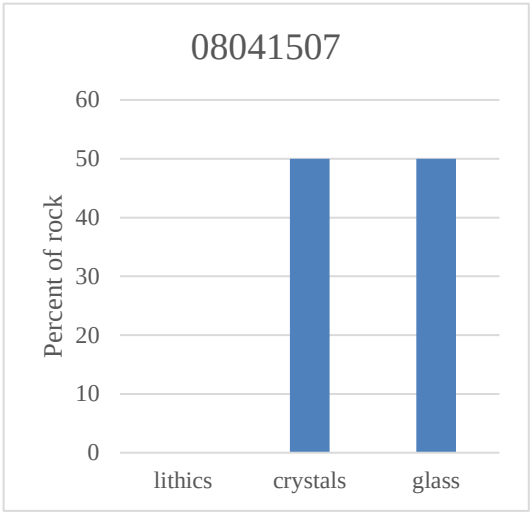

Sample Name or No.: 08041506

Plane-Polarized Light

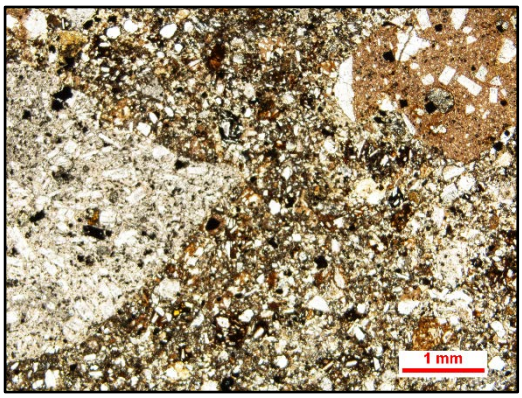

Framework grain composition (%)

Quartz: 15-20%
Feldspar: 30-35%
Lithic Fragments: 45-50%
Other common minerals:
Hornblende and CPX

Percent composition of rock

Matrix (%): 60 **Composition:** Glass and opaques
Cement (%): 40 **Composition:** hematite and silica
Apparent Grain Rounding: A to VR
Grain Size (approx. range): 1cm or less
Sorting (description): very poor

Other comments/Observations

Has abundant plagioclase crystals in the matrix

Very different than 08031502

Many volcaniclasts show iron oxide staining

Larger clasts show angularity

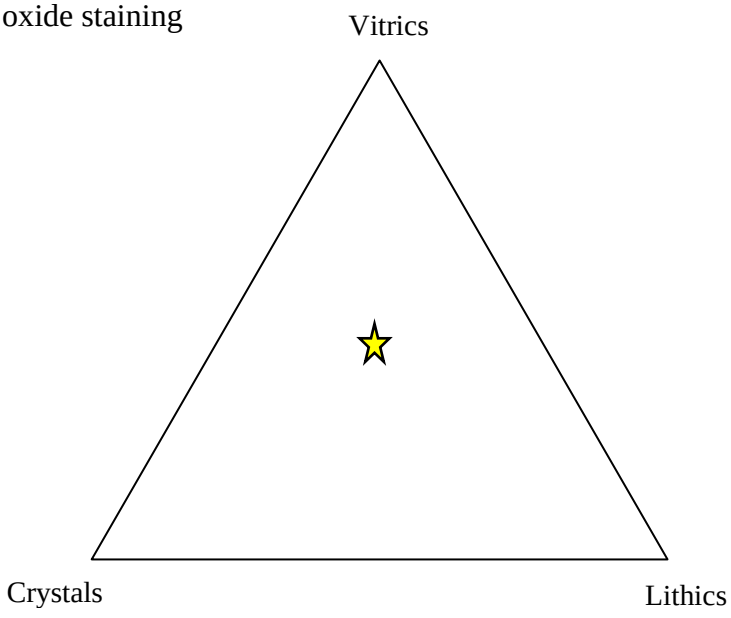

Rock Type: vitric tuff

Plane-Polarized Light
08041506

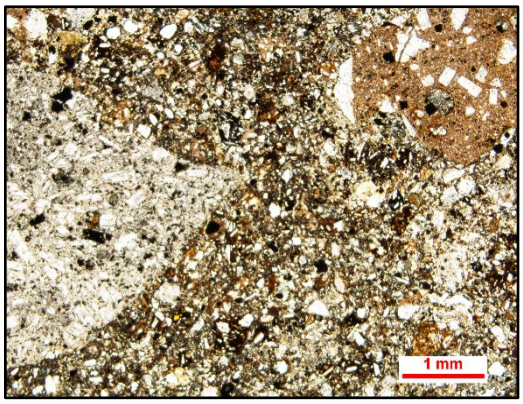

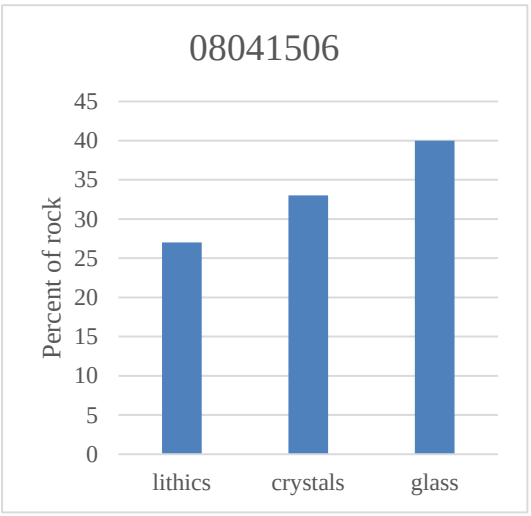

Sample Name or No.: 07291504

Framework grain composition (%)

Plane-Polarized Light

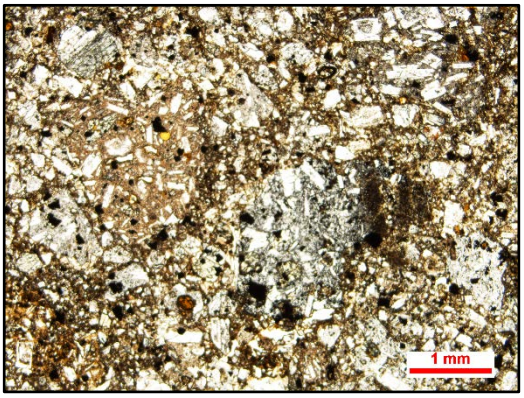

Quartz: 5-10%
Feldspar: 40-45%
Lithic Fragments: 45-50%
Other common minerals:

Percent composition of rock

Matrix (%): 25 **Composition:** Glass + Plag.
Cement (%): 75 **Composition:** silica
Apparent Grain Rounding: SA to SR
Grain Size (approx. range): 1 cm or less
Sorting (description): Poor

Other comments/Observations

Jigsaw Fracturing

Some pyroxene/hornblende andesite

Clasts show vesicularity

Matrix has limited vesicularity

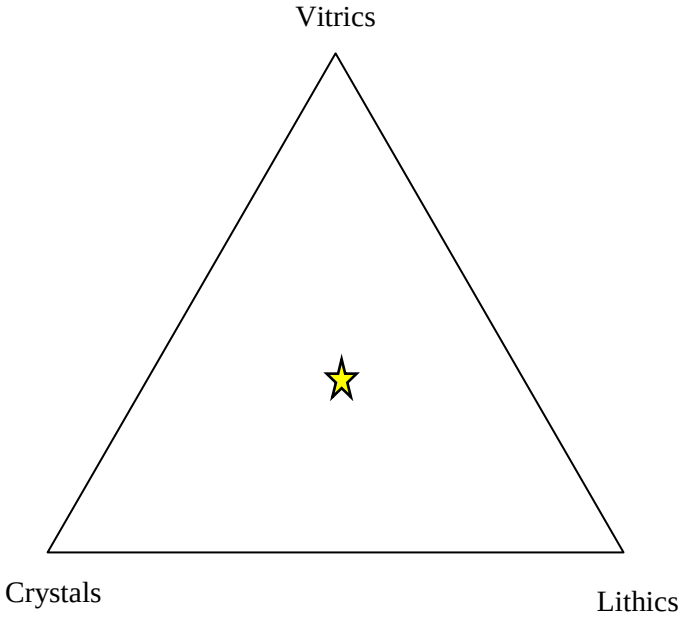

Rock Type: Crystal-lithic tuff

Plane-Polarized Light
07291504

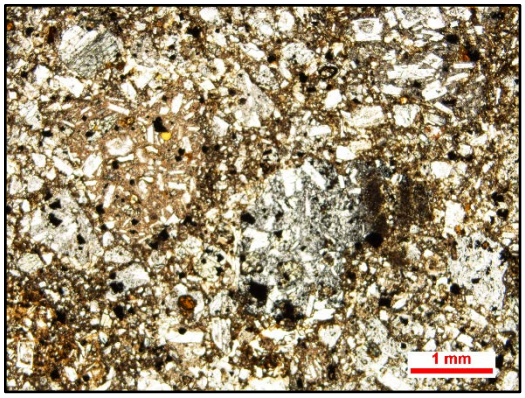

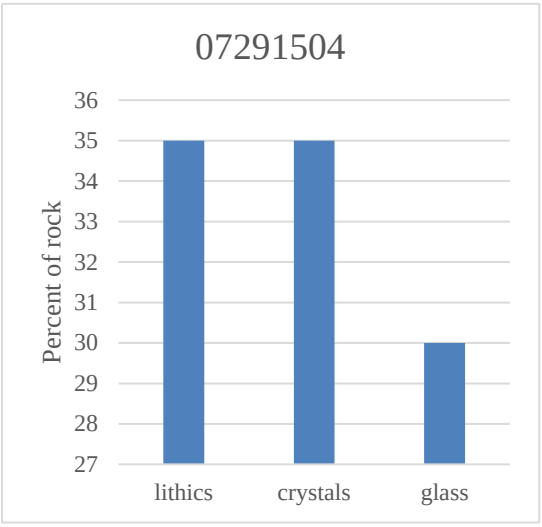

Sample Name or No.: 08071507

Plane-Polarized Light

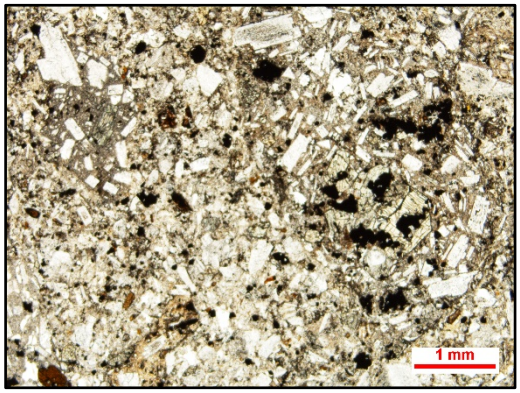

Framework grain composition(%)

Quartz: 0-1%
Feldspar: 50-55%
Lithic Fragments: 50-55%
Other common minerals: Hornblende, CPX

Percent composition of rock

Matrix (%): 50 **Composition:** Feldspar and silica glass
Cement (%): 50 **Composition:** Silica
Apparent Grain Rounding: SA - R
Grain Size (approx. range): ?
Sorting (description): Poor

Other comments/Observations

Partially devitrified glass – plag?

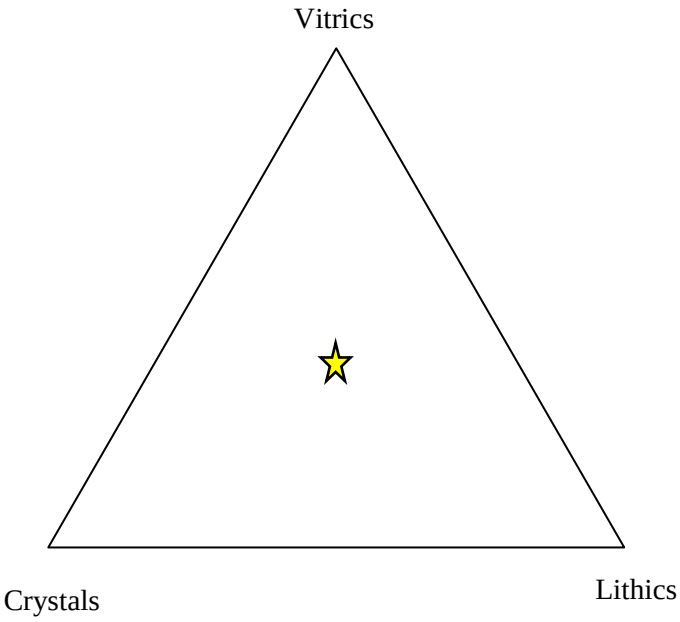

Rock Type: vitric tuff

Plane-Polarized Light
08071507

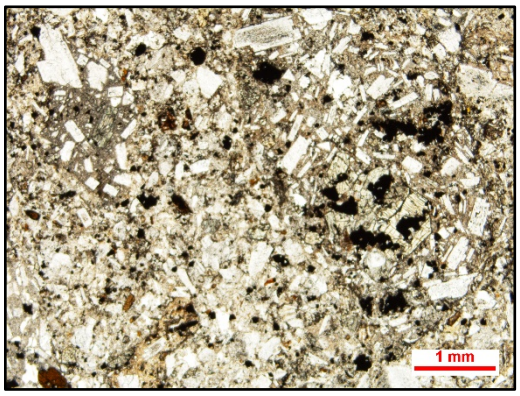

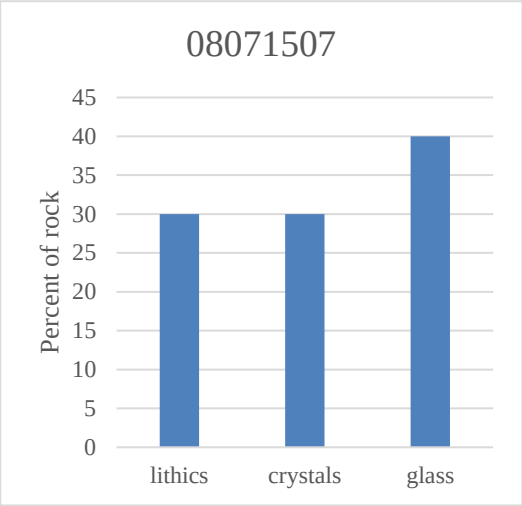

Sample Name or No.: 08071503

Cross-Polarized Light

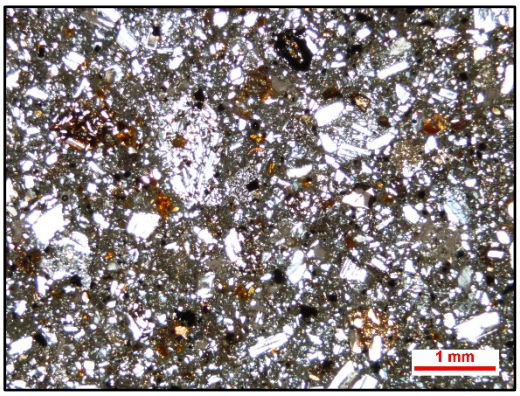

Framework grain composition(%)

Quartz: 0-1%
Feldspar: 55-60%
Lithic Fragments: 40-45%
Other common minerals: Hornblende, CPX

Percent composition of rock

Matrix (%): 80 **Composition:** Glass, Opaques
Cement (%): 10-20 **Composition:** Hematite, silica
Apparent Grain Rounding: SA - SR
Grain Size (approx. range): 10-15 mm or less
Sorting (description): Poor-moderate

Other comments/Observations

Jigsaw fracturing

subhedral hornblende phenocrysts (volcaniclasts)

Pore space 10%

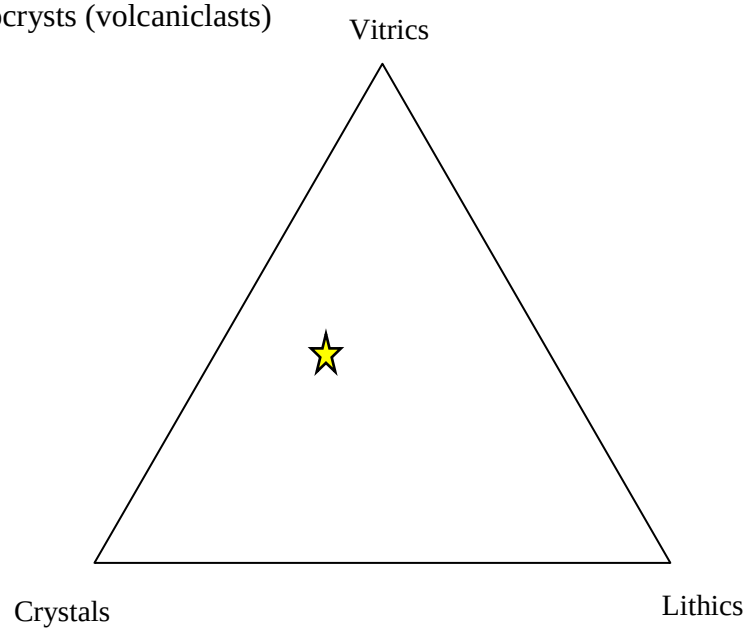

Rock Type: Vitric tuff

Cross-Polarized Light
08071503

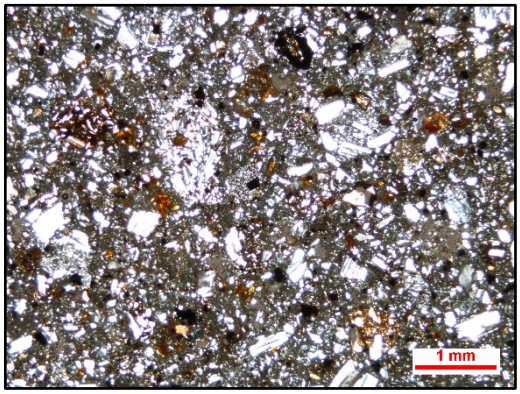

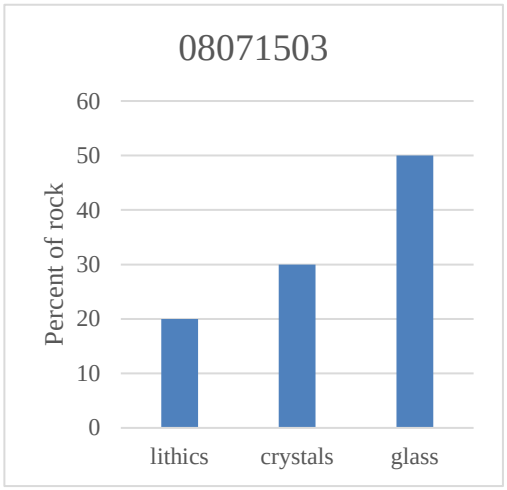

Sample Name or No.: 07201505

Plane-Polarized Light

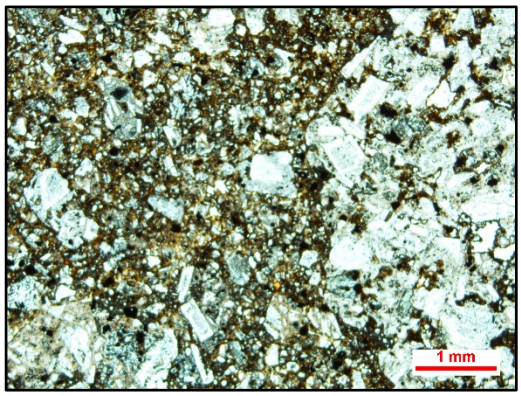

Framework grain composition (%)

Quartz: 0-1%
Feldspar: 20-25%
Lithic Fragments: >70%
Other common minerals: Augite, Hornblende

Percent composition of rock

Matrix (%): 90 **Composition:** Quartz glass
Cement (%): 10 **Composition:** sericite?
Apparent Grain Rounding: VA - SR
Grain Size (approx. range): Large clast greater than 2 cm majority less
Sorting (description): Poor

Other comments/Observations

Comminuted lithic clast framework; jigsaw fractures

Difficult to distinguish some of the larger clasts

Heavy alteration (hematite); opaques square

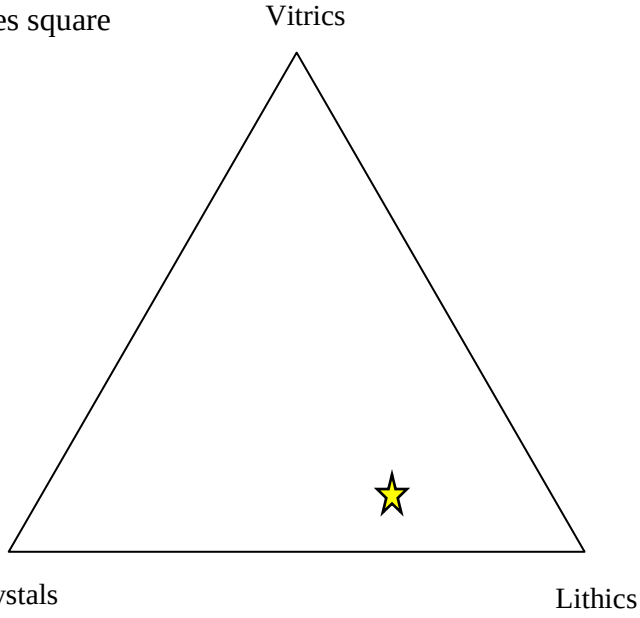

Rock Type: Lithic tuff

Plane-Polarized Light
07201505

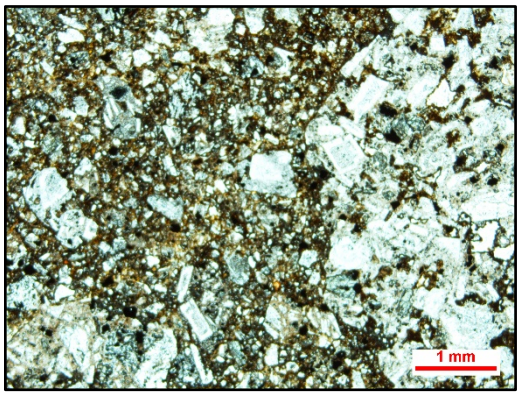

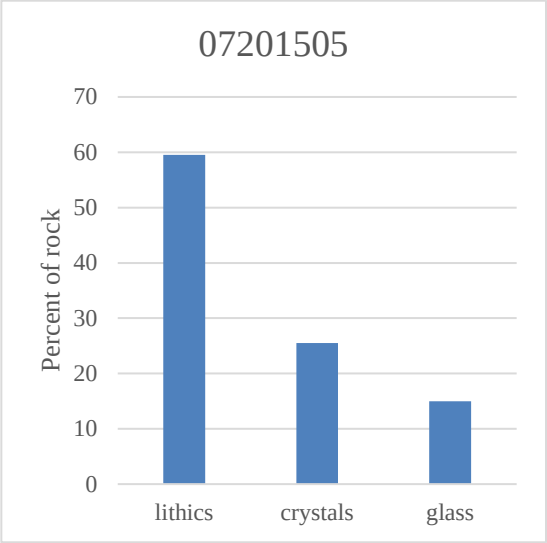

Sample Name or No.: 07191503

Plane-Polarized Light

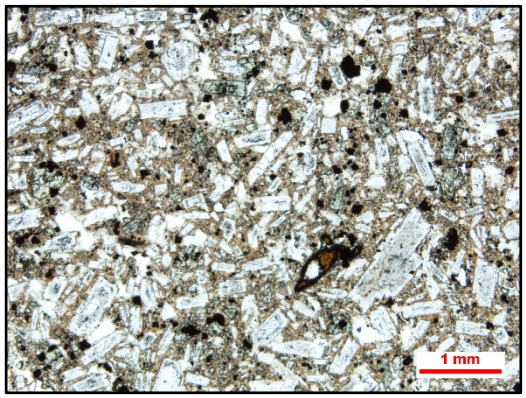

Framework grain composition (%)

Quartz: 0-1%
Feldspar: >70%
Lithic Fragments: 0-1%
Other common minerals:
Hornblende and CPX

Percent composition of rock

Matrix (%): 15 **Composition:** Glass + Plag.
Cement (%): 85 **Composition:** silica
Apparent Grain Rounding: n/a
Grain Size (approx. range): n/a
Sorting (description): n/a

Other comments/Observations

Vesicular?

Subhedral to euhedral plagioclase crystals

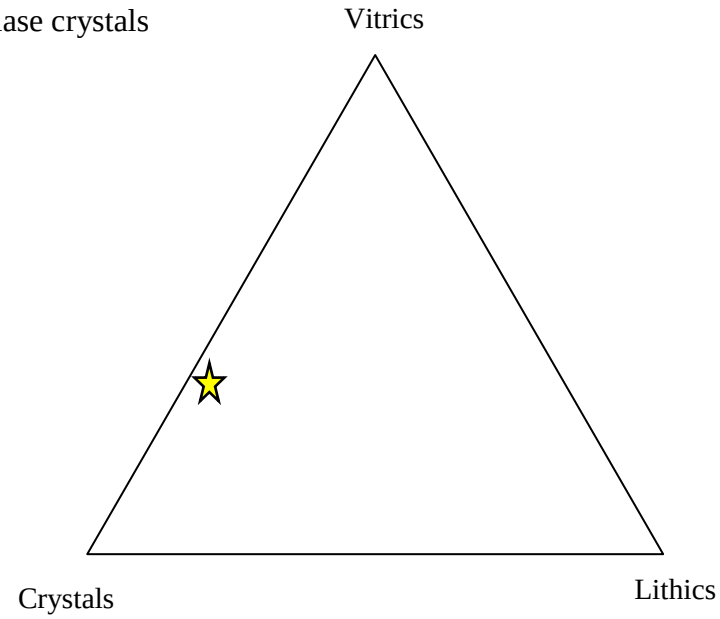

Rock Type: hornblende-pyroxene andesite

Plane-Polarized Light
07191503

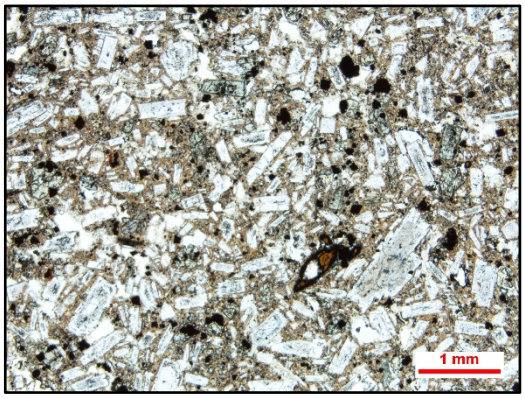

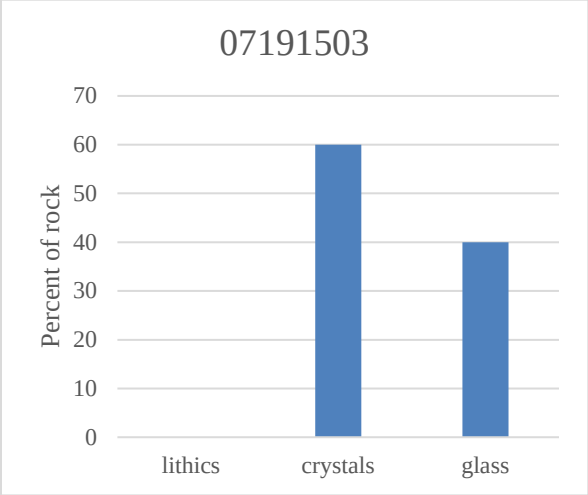

APPENDIX D – Stream-Gravel Inventory

Shorthand and abbreviations used in stream-gravel inventories

To – Tertiary Oligocene

Km – Cretaceous Mancos Formation

Kd – Cretaceous Dakota Sandstone

Kbc – Cretaceous Burro Canyon Formation

Jm – Jurassic Morrison Formation

Jjc – Jurassic Junction Creek Sandstone

Pz – Paleozoic undifferentiated

pC – preCambrian undifferentiated

qtzite – Quartzite

qtz – quartz

s.s. – sandstone

k-granite – Alkali feldspar granite

Location	Rock #	Size (in. unless otherwise noted)	Rounding	Composition
Wp 150 E. of Almont Pk	1	0.75	angular	chert
	2	2	subrounded	quartz Porphyry
	3	2.5	subrounded	alkali granite
	4	3.5	rounded	schist/gneiss
	5	2.25	subangular	volcanic; rhyodacite
	6	1	subrounded	quartzite
	7	2.5	rounded	alkali granite
	8	2.25	subrounded	volcanic; hornblende andesite

	9	2.5	subrounded	hornblende andesite
	10	2.5	subrounded	quartzite
	11	1.25	rounded	granodiorite
	12	4	rounded	andesite
	13	5	rounded	gneiss
	14	13.5	subrounded	granite
WP 158 NE of Almont Pk	1	7	rounded	weathered granodiorite
	2	1.75	subangular	quartzite or limestone?
	3	1	subrounded	quartzite (Jjc)
	4	1	rounded	pC quartzite
	5	1.5	subangular	limestone
	6	2	subrounded	quartz porphyry
	7	2.25	rounded	quartz latite
	8	7	subrounded	limestone
	9	6.5	rounded	quartz arenite (Kbc?)
	10	4.5	subrounded	coarse grained, quartz arenite (Maroon Fm.?)
	11	3	Subangular	conglomeratic sandstone (Gothic?)
	12	13	rounded	granite
WP 114 W. Side Almont Pk.	1	8	rounded	hornblende-biotite andesite (gray - white)
	2	10	rounded	orange black metased
	3	?	rounded	black aphanitic metabasalt or quartzite
	4	?	rounded	black aphanitic metabasalt or quartzite
	5	6	rounded	plag. rhyodacite
	6	6	rounded	biotite granite
	7	6	rounded	biotite granite
	8	?	rounded	sawatch
~WP 122 at I-Bar (W. Mountain)	1	2.75	subrounded	biotite-alkali granite
	2	4.5	rounded	quartzite (black pC)

	3	5	angular	dacite-andesite (To) aphanitic lava
	4	3.25	rounded	granodiorite (pC?)
	5		rounded	amphibolite (pC)
	6	0.5	rounded	alkali Granite
	7	2.25	subrounded/subangular	andesite?
	8	1	rounded	quartz (pC)
	9	1.5	rounded	quartz (pC)
	10	0.5	rounded	quartz (pC)
	11	2.5	rounded	qtzite (pC)
	12	2.25	subangular	amphibolite (pc)
	13	2.75	subrounded	fine s.s. qtzite (pC?)
	14	2.5	rounded	tonalite
	15	1.75	rounded	qtzite (pC?)
	16	1.75	rounded	granite (K-spar)
	17	1.5	subrounded/sub-angular	breccia (I-Bar)
	18	1.5	subangular	andesite
	19	2.5	subrounded	granite
WP 124 High on W. Mountain	1	5	rounded	hblende andesite/ dacite (maybe biotite)
	2	3	rounded	quartz
	3	6.5	rounded	dacite-andesite (To) aphanitic lava
	4	3.5	subangular	amphibolite (pC)
	5	6	rounded	dacite–andesite (To) aphanitic lava
	6	3.5	rounded	rhyolite
	7	2.5	rounded	granodiorite
	8	1	subrounded	qtz
	9	2	subrounded	dacite-andesite (To) aphanitic lava
	10	4	rounded	qtzite (pc, black)
	11	2.5	subrounded	qtzite (white Pz?)
	12	>1m	bomb	andesite
WP 0012	1	5.5	rounded	qtz. monzonite
p. 50 FB 2	2	2	subrounded	amphibolite or quartzite
UNIT 4	3	2.5	subangular to subrounded	basaltic andesite

East of I-Bar	4	1.75	subrounded	andesite
	5	2.25	subangular	hblende scoria
	6	1.5	angular	brecciated lava basaltic
	7	0.5	subangular	qtzite
	8	10.5	subrounded	qtzite/amphibolite (pC)
~WP127	1	0.75	rounded	milky qtz
BASE OF UNIT 3	2	0.75	rounded	granite (tonalite?)
Above 0012	3	2.5	subrounded	qtzite
Field Book 2 p. 53	4	3	subrounded	aplite?
	5	2.5	rounded	qtzite
	6	3	subrouned	s.s.
	7	5.5	subrounded (platy)	s.s. (Kbc)
	8	5	rounded	s.s. -qtzite
	9	3	subangular	qtzite
	10	3.5	subrounded	qtzite
	11	3.5	subrounded	granite (tonalite?)
	12	7.75	angular	pC Qtzite
	13	10.5	subrounded	Monzo diorite?
	14	13.5	rounded	qtzite
WP127	1	3	subrounded	qtzite/s.s.
top OF UNIT 3	2	3	subangular	qtz
Above 0012	3	2.75	subrounded	tonalite
Field Book 2 p. 53	4	2.25	rounded	qtzite
	5	2.25	subrounded	basaltic andesite?
	6	3	subangular-subrounded	schist
	7	1.75	subrounded	qtzite
	8	2	very well rounded	basaltic andesite
	9	3.75	subrounded	granodiorite
	10	5.25	angular	granite (alkaline)
	11	8.25	rounded	qtzite
	12	12	subangular	tuff (To?)
	13	43	subrounded	tuff (To?)
WP 134	1	8.25	rounded	granodiorite
Unit 3 ?	2	3.25	subrounded	qtzite

Chance Gulch	3	2.25	subangular	qtz monzonite
	4	2.5	subrounded	granite
	5	2.5	subrounded	qtzite
	6	2.5	rounded	sand stone
	7	1.5	angular	qtzite (pC) black
	8	1.25	angular	basaltic andesite?
	9	2.25	angular	volcaniclast (altered)
	10	3.5	rounded	hblende andesite?
	11	4	subrounded	qtzite
	12	5.25	subrounded	blue-gray andesite
	13	4	subangular–angular	diorite
WP 146	1	2.5	rounded	sandstone
Unit 3	2	2.75	subrounded	volcanic - dacite
Behind wscu	3	2.75	subrounded	intrusive latite?
south of signal peak	4	1.5	rounded	basaltic andesite
Field book 2 p. 60–61	5	3	rounded	extrusive andesite
	6	4	rounded	diorite
	7	2.5	subrounded	granite
	8	3.5	subrounded	quartzite
	9	1.5	subrounded	preCambrian
	10	2.25	rounded	basaltic andesite
	11	2.5	subangular	basaltic andesite
	12	1.75	angular	basaltic andesite
	13	1	subrounded	sandstone/quartzite
	14	2	angular	quartzite
	15	9.5	subrounded	quartzite
	16	9.5	rounded	quartz porphyry
WP 163	1	5.5	rounded	quartz porphyry (quartzite?)
Cabin Creek	2	2.5	subrounded	quartz porphyry
	3	3.75	subrounded	porphyry/quartzite
	4	3.5	rounded	porphyry/quartzite
	5	2.25	subangular	quartz
	6	1.5	subrounded	porphyry/quartzite
	7	1.75	subrounded	porphyry/quartzite
	8	1	subangular	chert
	9	0.75	subrounded	metasedimentary
	10	1	subangular	quartzite

	11	9.5	rounded	sandstone (Jjc?)
	12	8	rounded	porphyry/quartzite
WP 166	1	0.75	angular	granite
HWY 50 and CO 42	2	0.75	subangular	quartz
	3	2.25	subrounded	limestone
	4	2.25	rounded	hornblende andesite
	5	3	rounded	schist/gneiss
	6	3.25	angular	dacite-andesite (To) aphanitic lava
	7	2.5	subrounded	porphyry/quartzite
	8	2	rounded	granite
	9	3.5	rounded	limestone?
	10	5	rounded	quartz porphyry
	11	16.75	subrounded	basalt?
	12	8	subrounded	rhyodacite
WP 173	1	1.75	sub angular	mudstone
Field Book 3 p. 11	2	2.75	subrounded	quartz monzonite
	3	1	subrounded	quartzite
	4	1	rounded	diorite
	5	4.5	rounded	gneiss
	6	4	subrounded	quartzite
	7	5	subrounded	quartzite
	8	3.5	rounded	granite
	9	7	rounded	s.s.
	10	5.75	rounded	quartzite
	11	5	rounded	s.s.
	12	5	subrounded	intrusive diorite
WP 179	1	2.25	rounded	granodiorite
The Palisades	2	2.5	subrounded	quartzite
Upper Pinnacle S.g.	3	1.25	rounded	basaltic andesite
Matrix sample	4	2.25	rounded	quartz porphyry/quartzite
8091501	5	6	rounded	gneiss
	6	7	rounded	rhyodacite
	7	3	rounded	basaltic andesite
	8	4	rounded	andesite
	9	3.5	rounded	basaltic andesite
	10	7	rounded	basalt
	11	4	rounded	basaltic andesite

	12	1	subrounded	granite
Near WP 103	1	3.75	rounded	granite
West Side of The Palisades	2	3.75	subrounded	diorite
	3	5.5	angular	basalt
	4	4	angular	aphanitic
	5	3	subrounded	gneiss
	6	4.25	rounded	Hbl andesite
	7	3	rounded	dacite-andesite (To) aphanitic lava
	8	2.75	rounded	quartzite
	9	2.25	rounded	quartzite
	10	1.75	rounded	Hbl andesite
	11	3.5	subrounded	aphanitic basalt
	12	5	rounded	andesite
	13	3.5	rounded	sandstone
	14	6.75	rounded	basaltic andesite
	15	5.75	rounded	Hbl andesite
		Length (cm)	Rounding	Classification
WP 187 FLAT TOP PROPER	1	6.5	rounded	schist
8/10/2015	2	11.5	rounded	dolomite
	3	6.5	rounded	k-granite
	4	5.5	rounded	dolomite
	5	4	rounded	granodiorite
	6	7	subrounded	diorite
	7	4.5	rounded	granodiorite
	8	13	rounded	quartz porphyry
	9	11	rounded	quartz monzonite
	10	16.5	rounded	welded tuff (Carp. Ridge Fm.?)
	11	18.5	subrounded	tertiary conglomerate
	12	7.5	subrounded	pegmatitic granite
WP 188 - Flat Top		Length (cm)	Rounding	Classification
	1	12.5	subrounded	Kd (Dakota Fm.)
	2	6	subangular	s.s. Jjc?
	3	8	subangular	diorite
	4	9	subrounded	basaltic andesite
	5	9	subangular	granite
	6	11.5	subrounded	porphyry/quartzite

	7	15	subrounded	k-granite
	8	12.5	rounded	dacite-andesite (To) aphanitic lava
	9	6	subrounded	dirty s.s.
	10	5	subrounded	diorite
	11	16.5	subrounded	andesite
	12	19.25	subrounded	quartzite
	13	4.5	subrounded	monzonite
	14	9.75	rounded	quartz porphyry
	15	18.25	subangular	dolomite
NEAR WP 189		Length (cm)	Rounding	Classification
Flat Top	1	6.5	subrounded	diorite
	2	16	subrounded	arkose arenite
	3	6.5	subrounded	qtzite (Jjc?)
	4	8.5	subrounded	qtzite (Jjc?)
	5	3.5	subrounded	qtz
	6	10	subangular	diorite
	7	5	rounded	gabbro (metavolcanic?)
	8	4	rounded	tuff (or rhyolite)
	9	4	rounded	rhyolite
	10	7.5	subrounded	metavolc
	11	6.5	subangular	rhyolite
	12	6.5	subangular	rhyodacite?
	13	8.5	subrounded	rhyolite
	14	8.5	subrounded	granodiorite
	15	6.5	subrounded	qtz arenite
WP 192	1	3.25	subrounded	rhyodacite
North side of Flat Top	2	3.5	subrounded	rhyodacite
	3	0.75	subrounded	rhyodacite
Unit Below	4	1.75	subrounded	rhyolite
East Elk Creek Tuff	5	1.75	subrounded	hbl andesite
Unit Above	6	1	subrounded	basaltic andesite
Tmhb	7	1	subangular	rhyodacite
	8	0.75	subangular	rhyodacite
	9	3.5	angular	basalt
	10	3.5	subangular	rhyolite
	11	5.5	subrounded	rhyodacite
	12	2.5	subangular	granite
	13	2	subangular	granite

	14	2.25	subangular	granite
	15	4.5	subrounded	rhyolite
WP 0010, Hillslope above northern roadcut		Length (cm)	Color	Classification
	1	8	black	“salty” (plag phenos) basaltic andesite
	2	?	black	“salty” (plag phenos) basaltic andesite
	3	?	black	“salty” (plag phenos) basaltic andesite
	4	10.5	black	quartzite
	5	4	black	quartzite or schist
	6	6	black	pyroxene andesite
	7	6	blue–gray	pyroxene andesite
	8	12	white	quartzite
	9	3	blue–gray	pyroxene andesite
	10	5	blue–gray	“”
	11	4	blackish plag phenos	granite
	12	15	blue–gray	pyroxene andesite
	13	6.5	black	diorite
	14	5.5	white	qtz. latite porphyry
	16	5	gray, hornblende?	qtzite
WP 0010 within northern roadcut		Length (cm)	Color	Classification
	1	11	black	qtzite
	2	8.5	white	qtzite
	3	4.5	black	basaltic andesite
	4	9.5	black	“salty” basaltic andesite
	5	5.5	black	pyroxene basaltic andesite
	6	6	tan (biotite?)	quartz latite porphyry
	7	4.5	black-brown	basaltic andesite
	9	10.5	blue gray	pyroxene andesite
	10	0.5	pink	k-spar granite
	11	1.5	black	qtzite

	12	9	white–tan	quartz latite porphyry
	13	3.5	black	basaltic andesite
	14	4	black	basaltic andesite
	15	16	blue-gray	pyroxene andesite
	16	17.5	black	basaltic andesite
	17	10	black	schist
WP 206		Length (cm)	Color	Classification
p. 34 Field book 4	1	7.5	black (aphanitic)	basaltic andesite
	2	6.5	Gray – green	quartzite
	3	4	Blue gray	pyroxene andesite
	4	3.5	Reddish gray	pyroxene andesite
	5	14.5	black aphanitic	basaltic andesite
	6	2.5	“”	basaltic andesite
	7	6	black green	granodiorite
	8	7.5	greenish gray	quartzite
	9	5.5	pink white	k-spar granite
	10	3.5	grayish red	basaltic andesite
	11	6	greenish black	basaltic andesite
	12	10	black aphanitic	basaltic andesite
	13	8.5	blackish red	basaltic andesite
	14	6.5	green	quartzite
WP 191 F.T. proper		Length (cm)	color	Classification
Below EEC Tuff	1	8.5	pink	granite
	2	8	gray	andesite
	3	9	maroon	quartzite
	4	10.5	maroon	quartzite
	5	8.5	gray weathered to brown fresh	sandstone
	6	11.5	tan	granite
	7	7	white	granite
	8	5.5	greenish black	granodiorite
	9	6.5	tan	sandstone
	10	14	orange	granite
	11	4	white	granite
	12	2.5	pinkish – black	granite
	13	17	pink	granite
	14	12.5	orange	sandstone
	15	5.5	maroon	conglomerate
	16	9	white – brown	muscovite granite

	17	3	greenish black	biotite granodiorite
	18	5	brownish green	dolomite or dolomitic s.s.
	19	9.5	green to white	muscovite granite
	20	6	tan – brown	“sucrosic” limestone
	21	1.5	white	sandstone
WP 220		Length (cm)	Color	Classification
Steers Gulch	1	10.5	Very light gray	quartz latite
Field book 5 p. 5–6	2	12.5	Blue gray	porphyritic pyroxene andesite
	3	5	Dark blue	chert
	4	6	Blackish green	schist?
	5	7.5	Black	pyroxene basaltic andesite
	6	6	Black	basaltic andesite
	7	5	Gray greenish	pyroxene andesite
	8	4	Black pin	granite
	9	5	White	quartz porphyry
WP 224		Length (cm)	Color	Classification
Field book 5 7/16 p. 9–10	1	6.5	black (amphibolite?)	schist
	2	12.5	pink	k-granite
	3	8.5	pink	k-granite
	4	5.5	gray Aphanitic	andesite
	5	5	salmon	granite
	6	8.5	white–orange	quartz latite porphyry
	7	4.5	black	schist
	8	11	black	pyroxene basaltic andesite
	9	6	black–pink	granodiorite
	10	6.5	black–pink	granodiorite
	11	5.5	brown	dolomite
	12	8	gray	pyroxene andesite(coarse)
	13	5.5	black	mudstone
	14	4.5	black	basaltic andesite
	15	4	white	sandstone

Possible source formations are abbreviated in parentheses.

Graphical clast-composition data

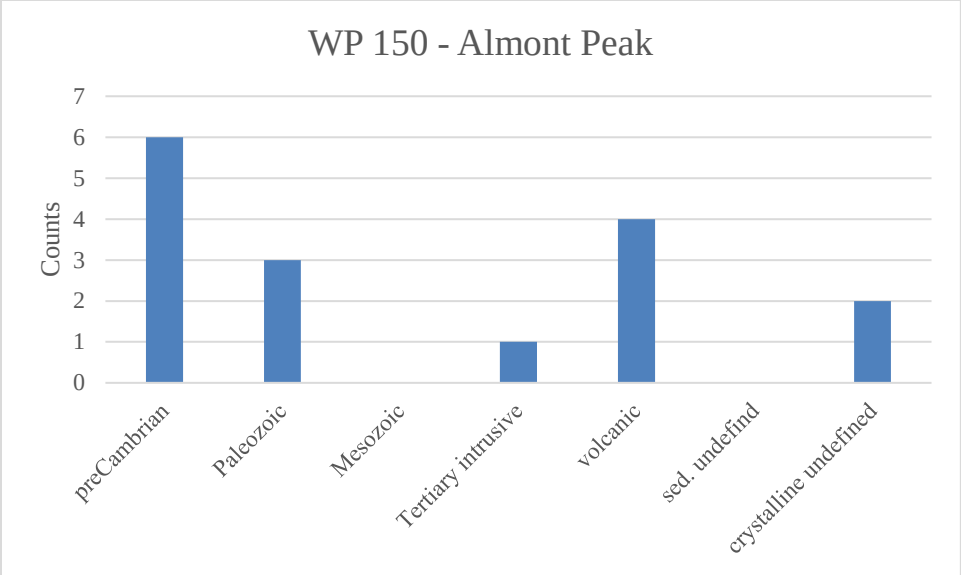
WP 150 - Almont Peak
Counts
7
6
5
4
3
2
1
0
preCambrian
Paleozoic
Mesozoic
Tertiary intrusive
volcanic
sed. undefind
crystalline undefined

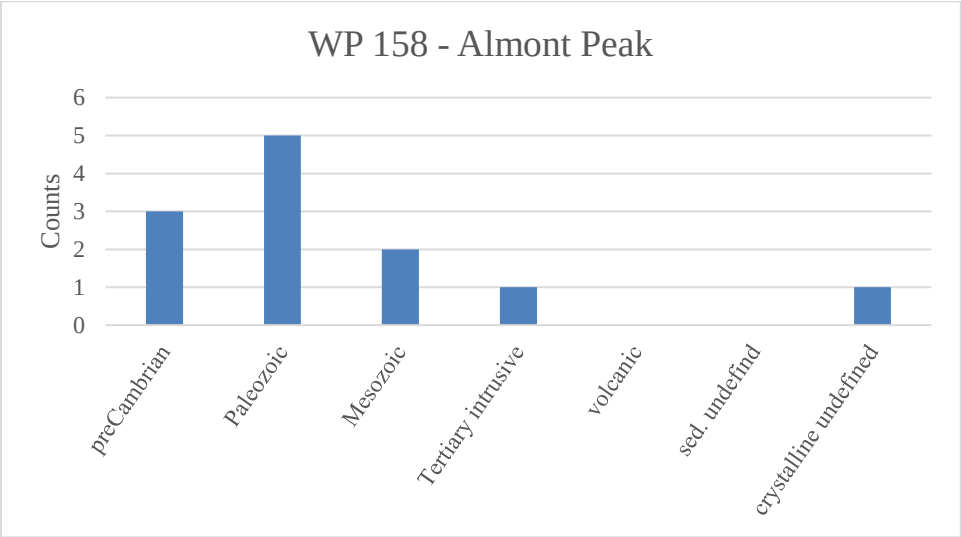
WP 158 - Almont Peak
Counts
6
5
4
3
2
1
0
preCambrian
Paleozoic
Mesozoic
Tertiary intrusive
volcanic
sed. undefind
crystalline undefined

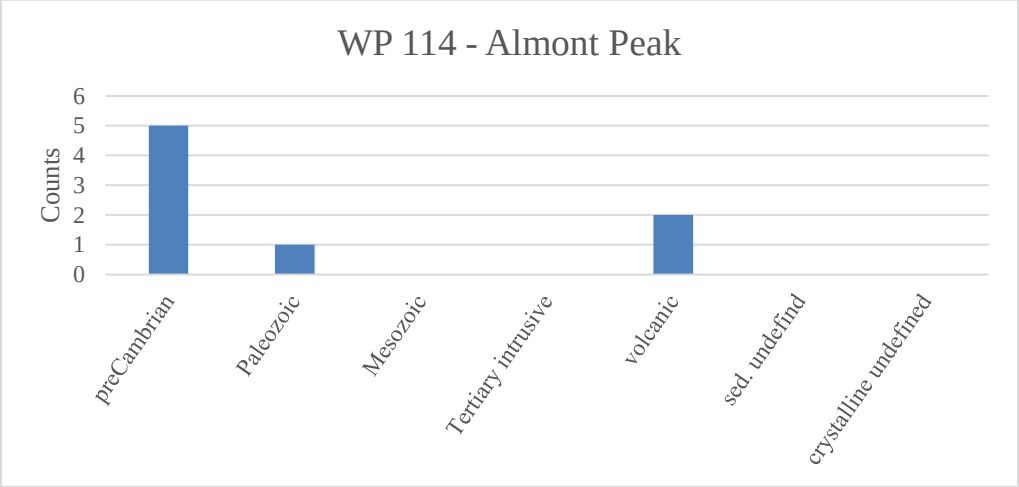
WP 114 - Almont Peak
Counts
6
5
4
3
2
1
0
preCambrian
Paleozoic
Mesozoic
Tertiary intrusive
volcanic
sed. undefind
crystalline undefined

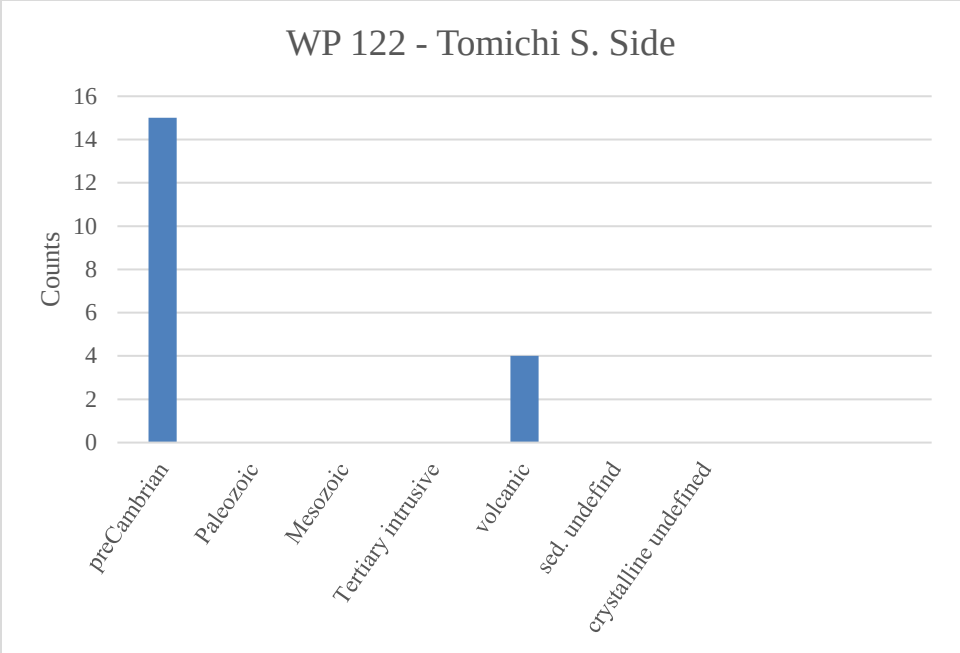
WP 122 - Tomichi S. Side
Counts
16
14
12
10
8
6
4
2
0
preCambrian
Paleozoic
Mesozoic
Tertiary intrusive
volcanic
sed. undefind
crystalline undefined

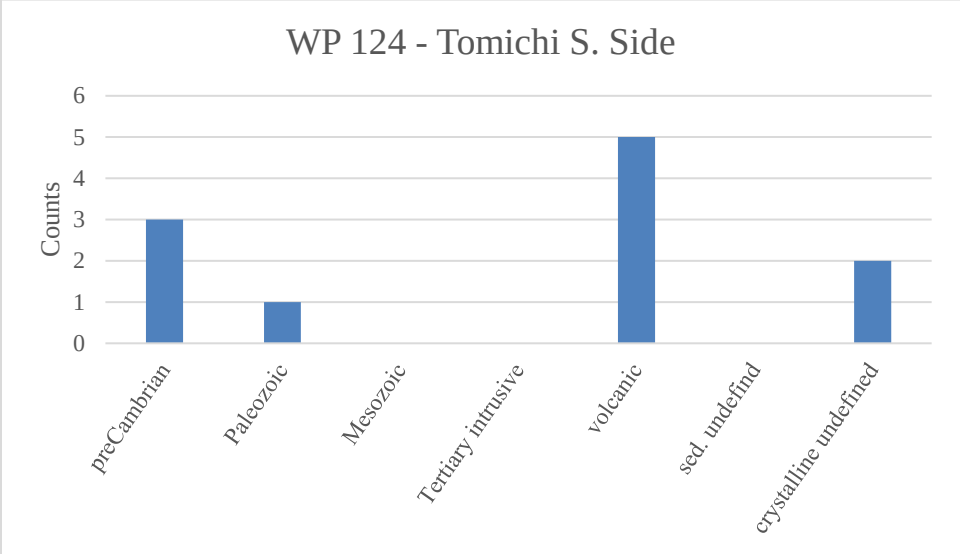
WP 124 - Tomichi S. Side
Counts
6
5
4
3
2
1
0
preCambrian
Paleozoic
Mesozoic
Tertiary intrusive
volcanic
sed. undefind
crystalline undefined

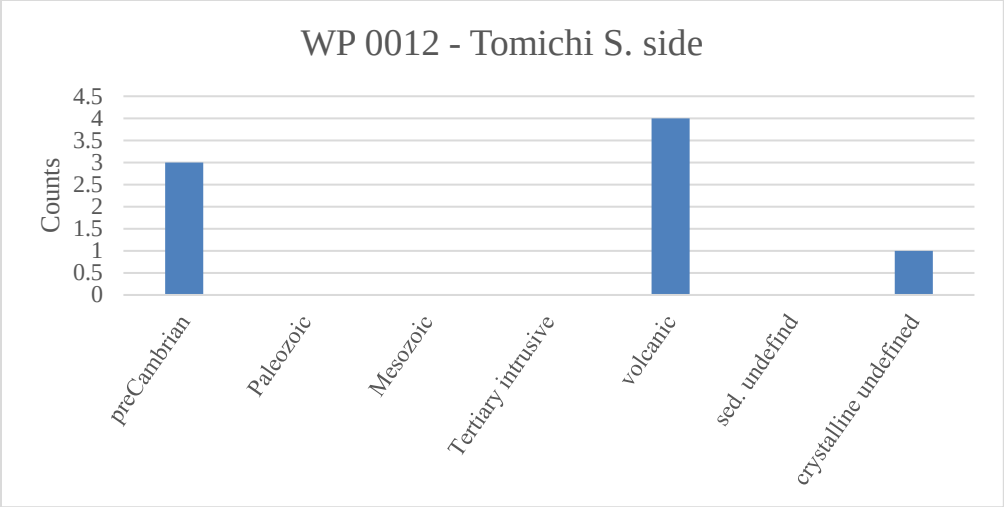
WP 0012 - Tomichi S. side
Counts
4.5
4
3.5
3
2.5
2
1.5
1
0.5
0
preCambrian
Paleozoic
Mesozoic
Tertiary intrusive
volcanic
sed. undefind
crystalline undefined

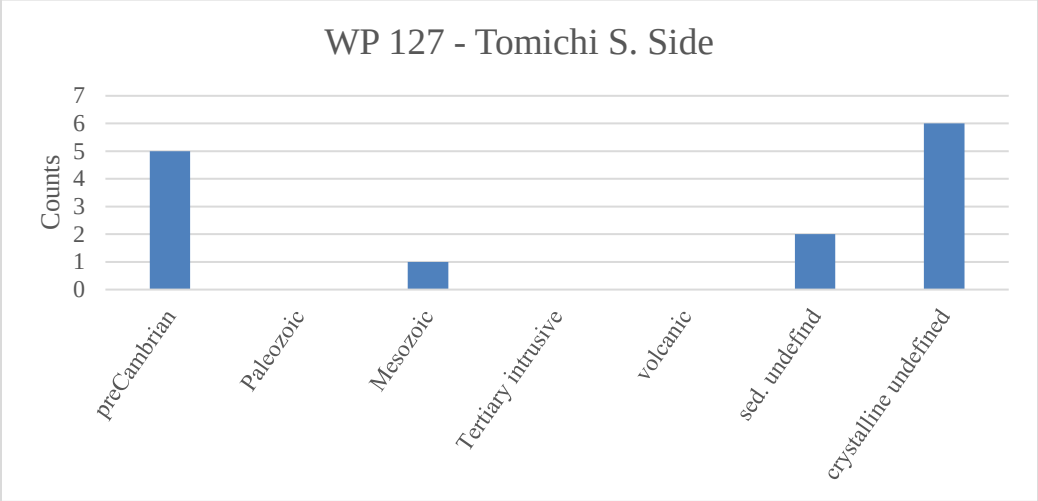
WP 127 - Tomichi S. Side
Counts
7
6
5
4
3
2
1
0
preCambrian
Paleozoic
Mesozoic
Tertiary intrusive
volcanic
sed. undefind
crystalline undefined

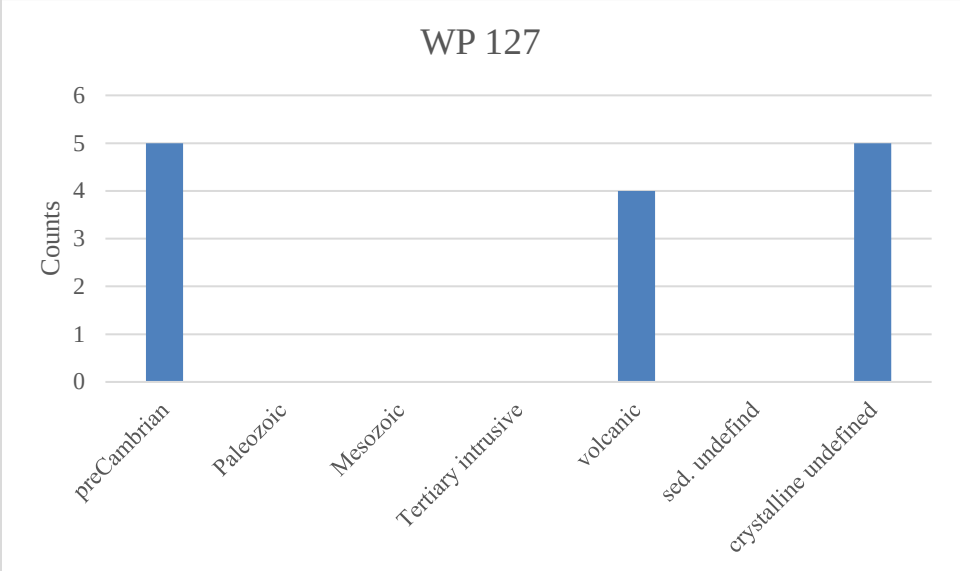
WP 127
Counts
6
5
4
3
2
1
0
preCambrian
Paleozoic
Mesozoic
Tertiary intrusive
volcanic
sed. undefind
crystalline undefined

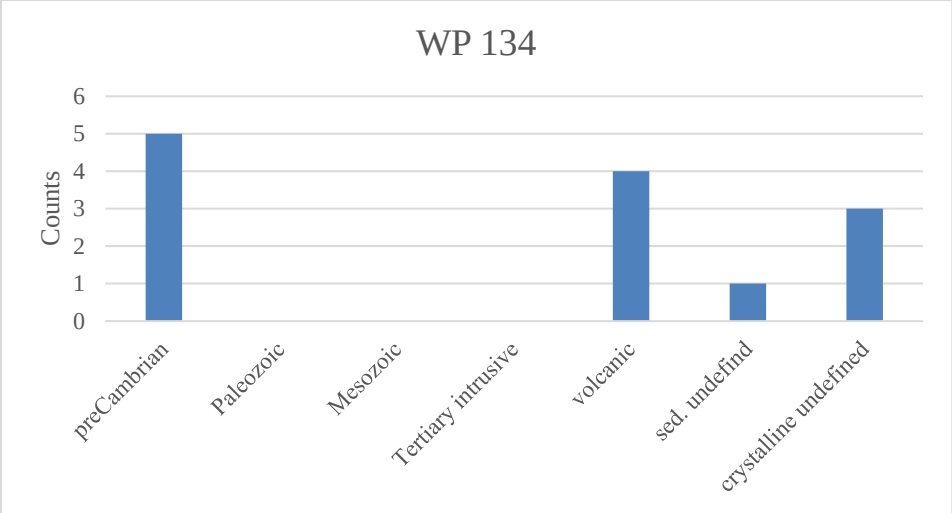
WP 134
Counts
6
5
4
3
2
1
0
preCambrian
Paleozoic
Mesozoic
Tertiary intrusive
volcanic
sed. undefind
crystalline undefined

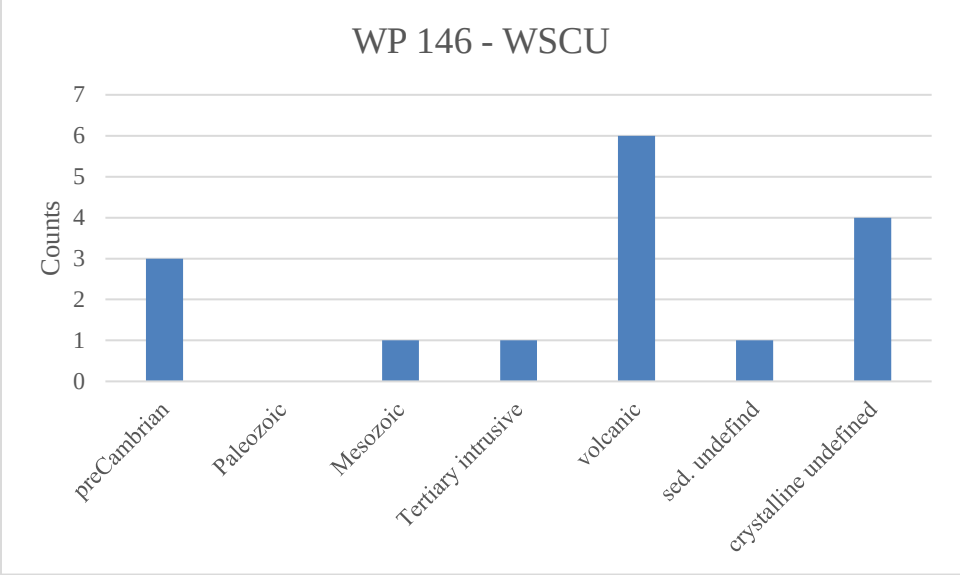
WP 146 - WSCU
Counts
7
6
5
4
3
2
1
0
preCambrian
Paleozoic
Mesozoic
Tertiary intrusive
volcanic
sed. undefind
crystalline undefined

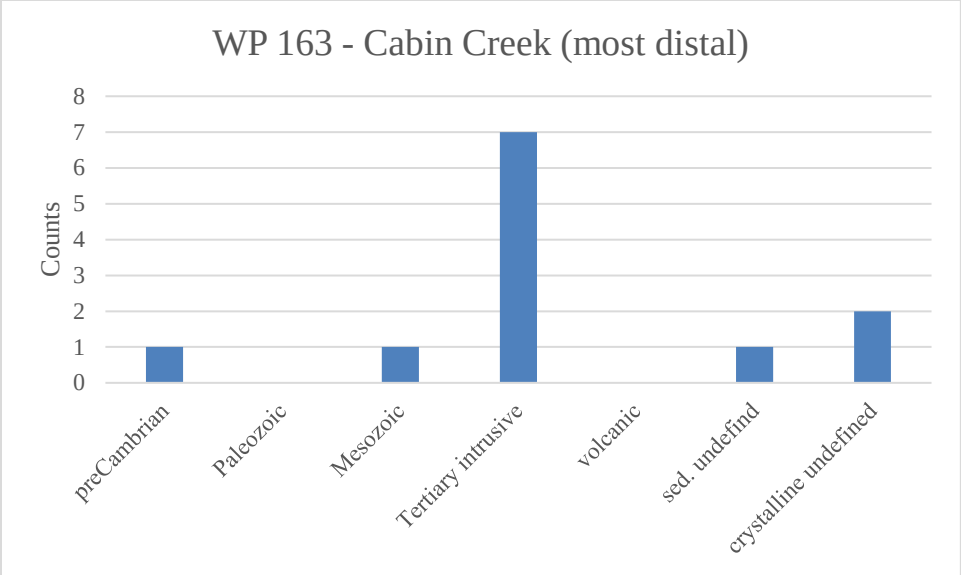
WP 163 - Cabin Creek (most distal)
Counts
8
7
6
5
4
3
2
1
0
preCambrian
Paleozoic
Mesozoic
Tertiary intrusive
volcanic
sed. undefind
crystalline undefined

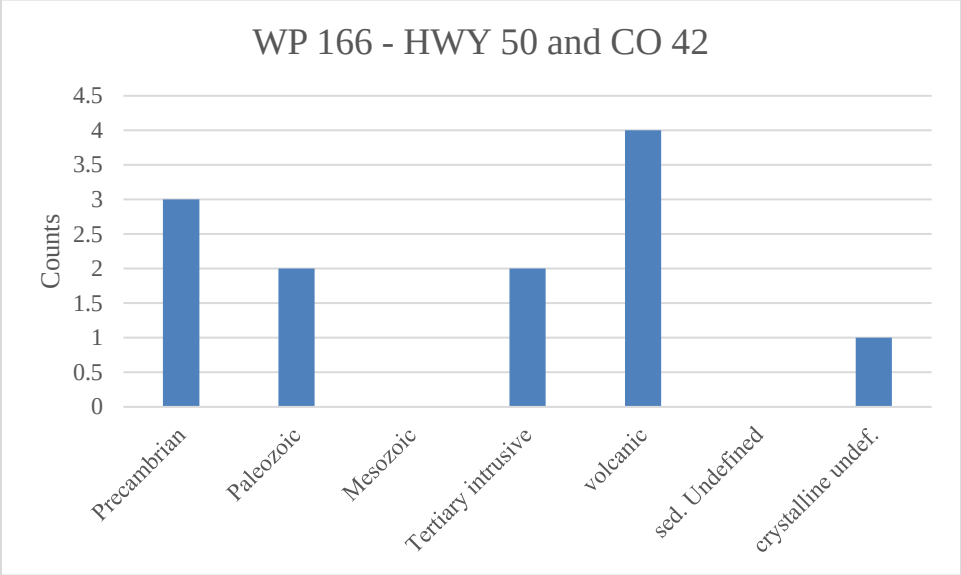
WP 166 - HWY 50 and CO 42
Counts
4.5
4
3.5
3
2.5
2
1.5
1
0.5
0
Precambrian
Paleozoic
Mesozoic
Tertiary intrusive
volcanic
sed. Undefined
crystalline undef.

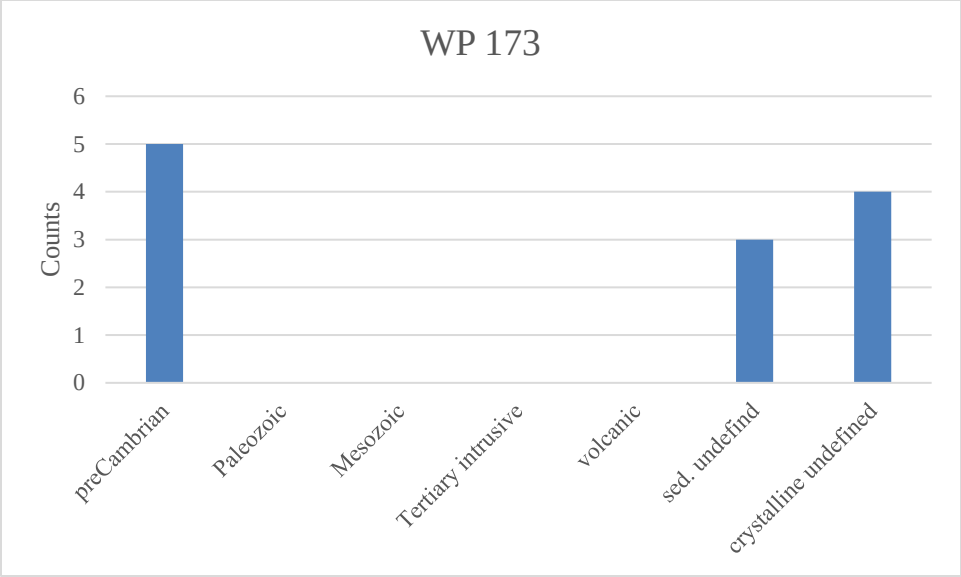
WP 173
Counts
6
5
4
3
2
1
0
preCambrian
Paleozoic
Mesozoic
Tertiary intrusive
volcanic
sed. undefind
crystalline undefined

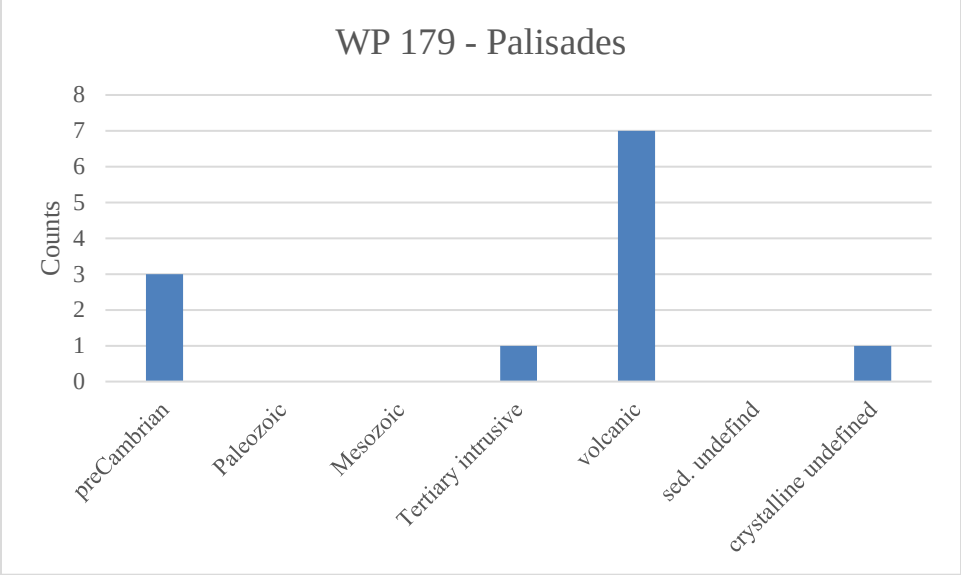
WP 179 - Palisades
Counts
8
7
6
5
4
3
2
1
0
preCambrian
Paleozoic
Mesozoic
Tertiary intrusive
volcanic
sed. undefind
crystalline undefined

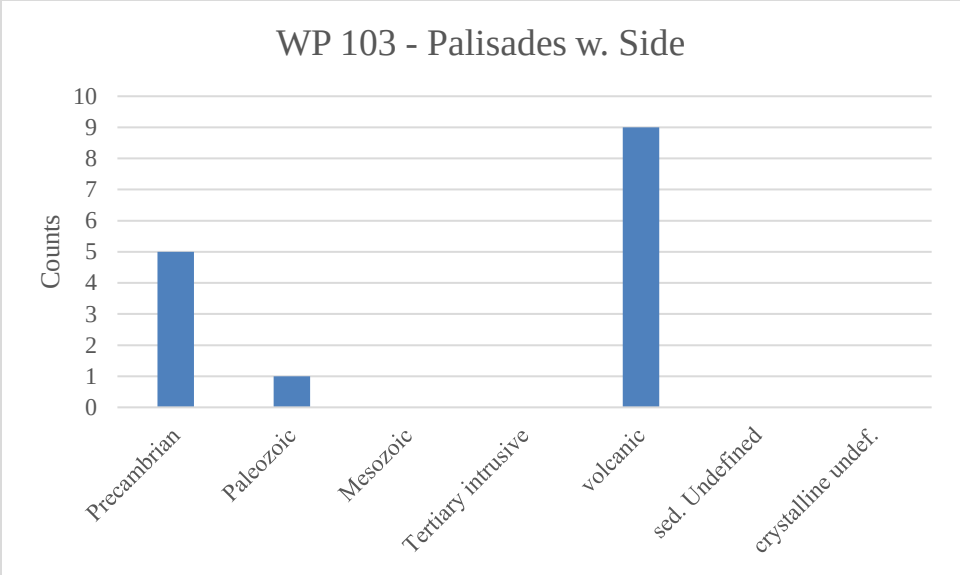
WP 103 - Palisades w. Side
Counts
10
9
8
7
6
5
4
3
2
1
0
Precambrian
Paleozoic
Mesozoic
Tertiary intrusive
volcanic
sed. Undefined
crystalline undef.

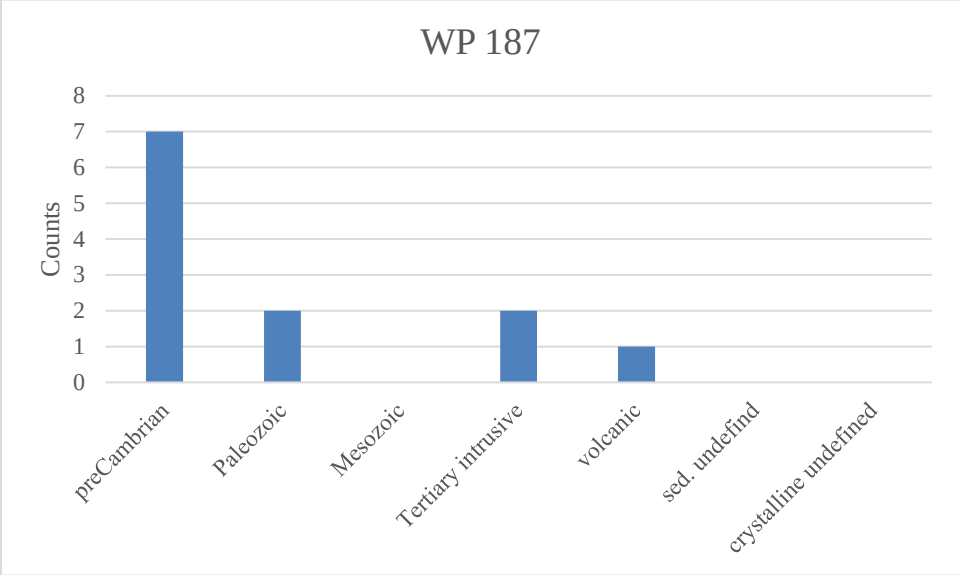
WP 187
Counts
8
7
6
5
4
3
2
1
0
preCambrian
Paleozoic
Mesozoic
Tertiary intrusive
volcanic
sed. undefind
crystalline undefined

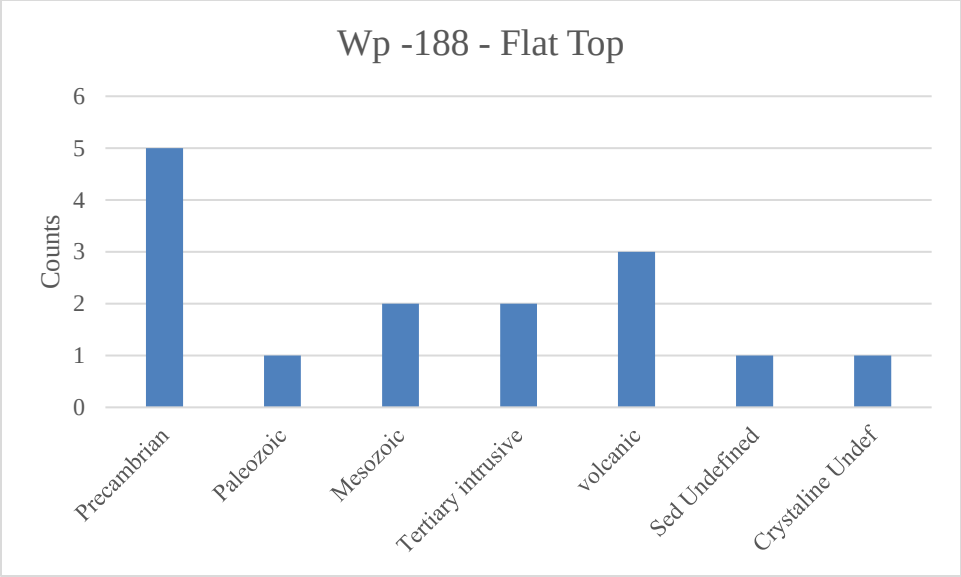
Wp -188 - Flat Top
Counts
6
5
4
3
2
1
0
Precambrian
Paleozoic
Mesozoic
Tertiary intrusive
volcanic
Sed Undefined
Crystaline Undef

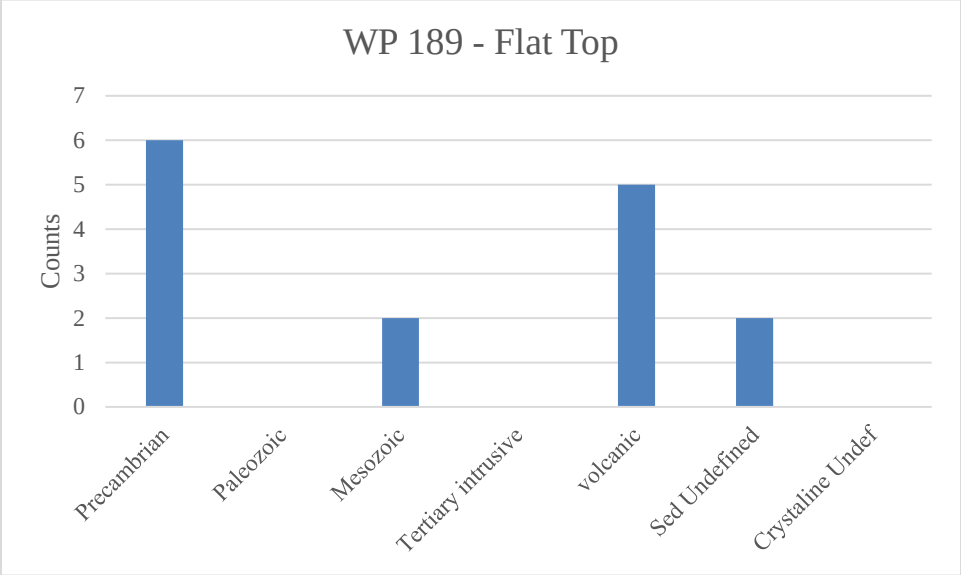
WP 189 - Flat Top
Counts
7
6
5
4
3
2
1
0
Precambrian
Paleozoic
Mesozoic
Tertiary intrusive
volcanic
Sed Undefined
Crystaline Undef

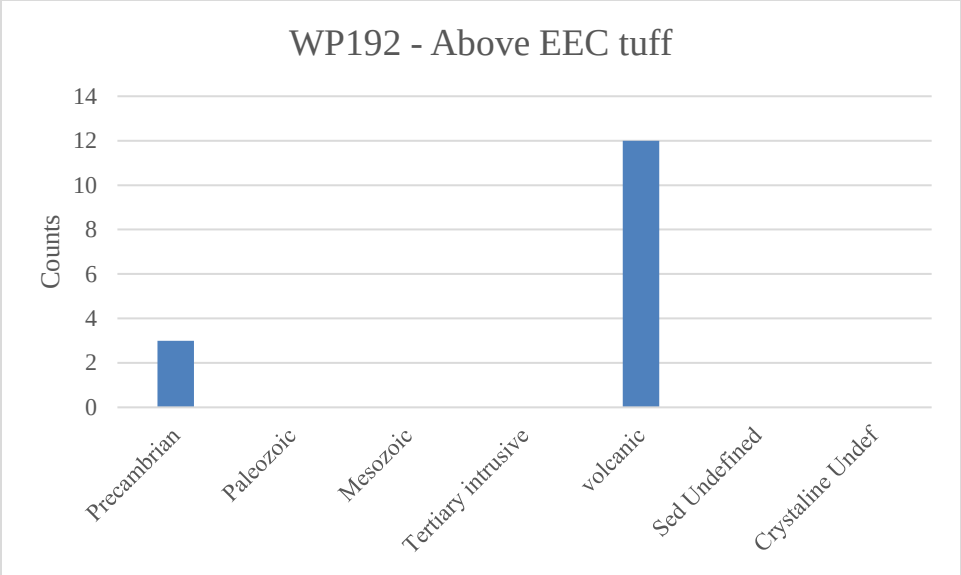
WP192 - Above EEC tuff
Counts
14
12
10
8
6
4
2
0
Precambrian
Paleozoic
Mesozoic
Tertiary intrusive
volcanic
Sed Undefined
Crystaline Undef

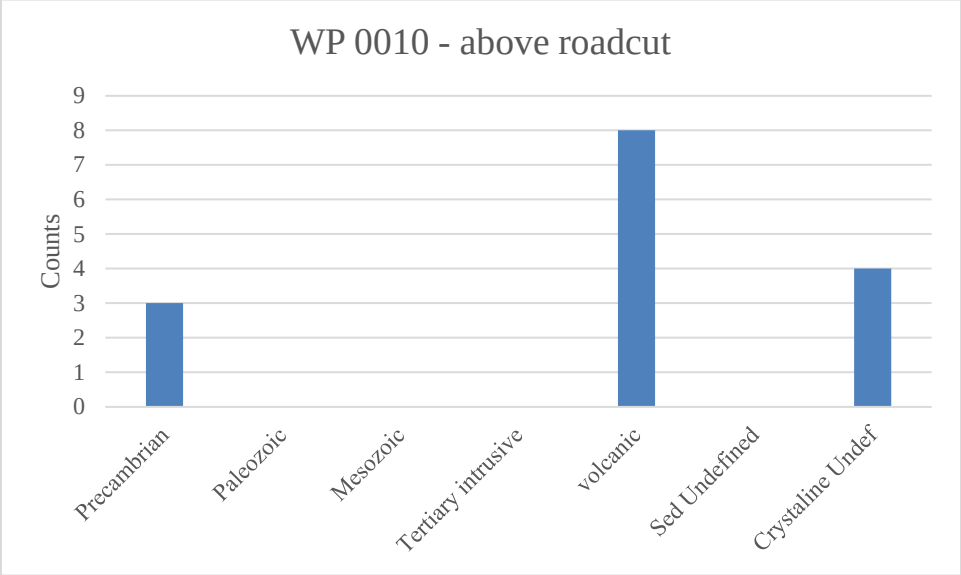
WP 0010 - above roadcut
Counts
9
8
7
6
5
4
3
2
1
0
Precambrian
Paleozoic
Mesozoic
Tertiary intrusive
volcanic
Sed Undefined
Crystaline Undef

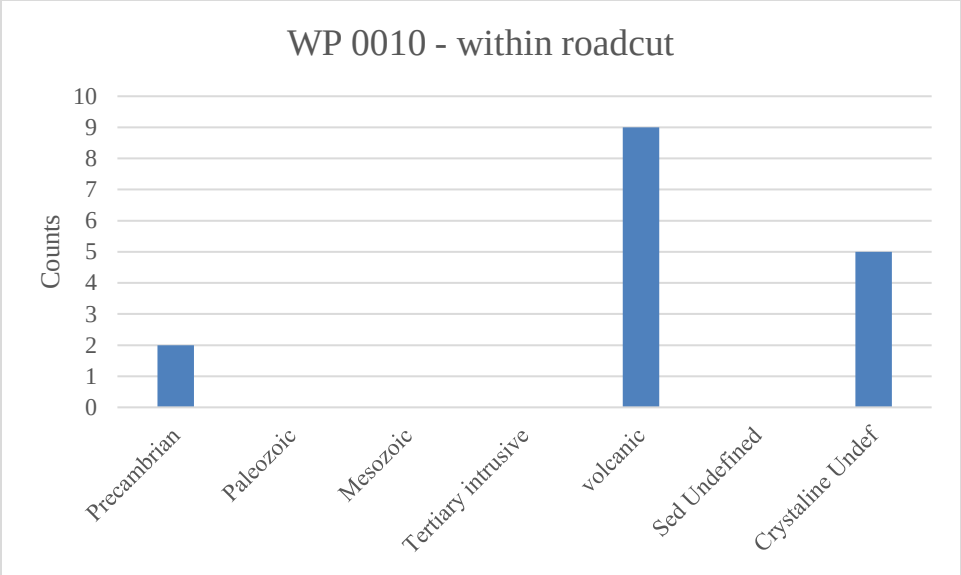
WP 0010 - within roadcut
Counts
10
9
8
7
6
5
4
3
2
1
0
Precambrian
Paleozoic
Mesozoic
Tertiary intrusive
volcanic
Sed Undefined
Crystaline Undef

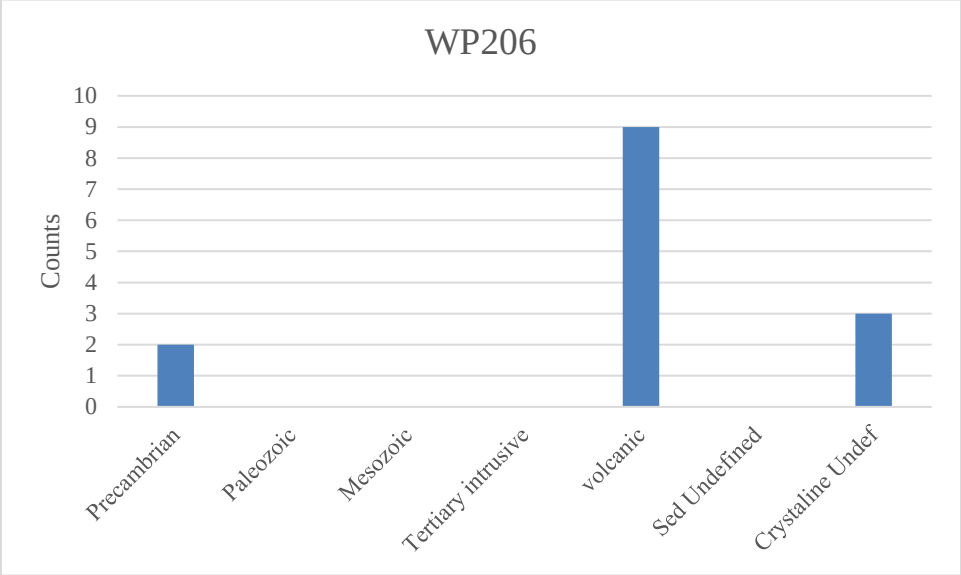
WP206
Counts
10
9
8
7
6
5
4
3
2
1
0
Precambrian
Paleozoic
Mesozoic
Tertiary intrusive
volcanic
Sed Undefined
Crystaline Undef

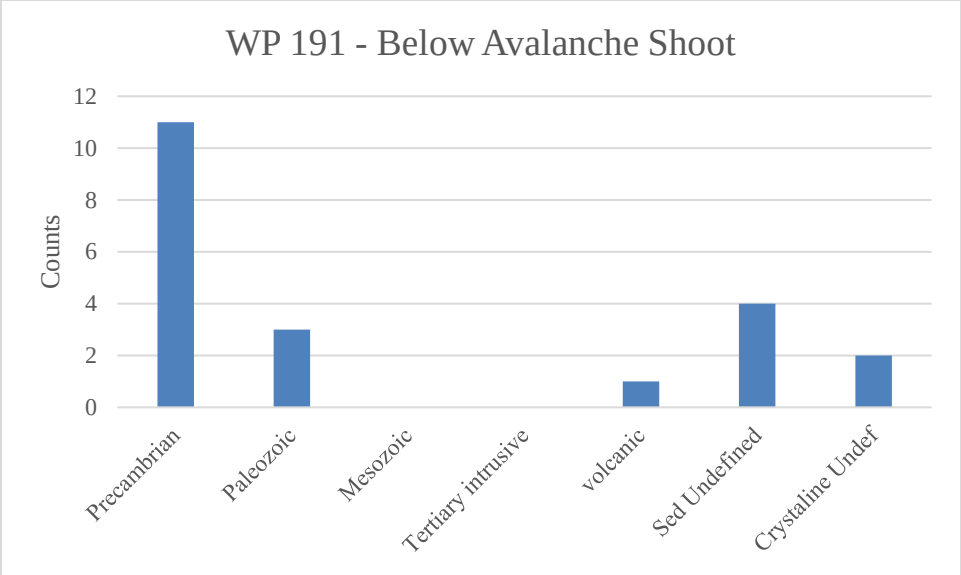
WP 191 - Below Avalanche Shoot
Counts
12
10
8
6
4
2
0
Precambrian
Paleozoic
Mesozoic
Tertiary intrusive
volcanic
Sed Undefined
Crystaline Undef

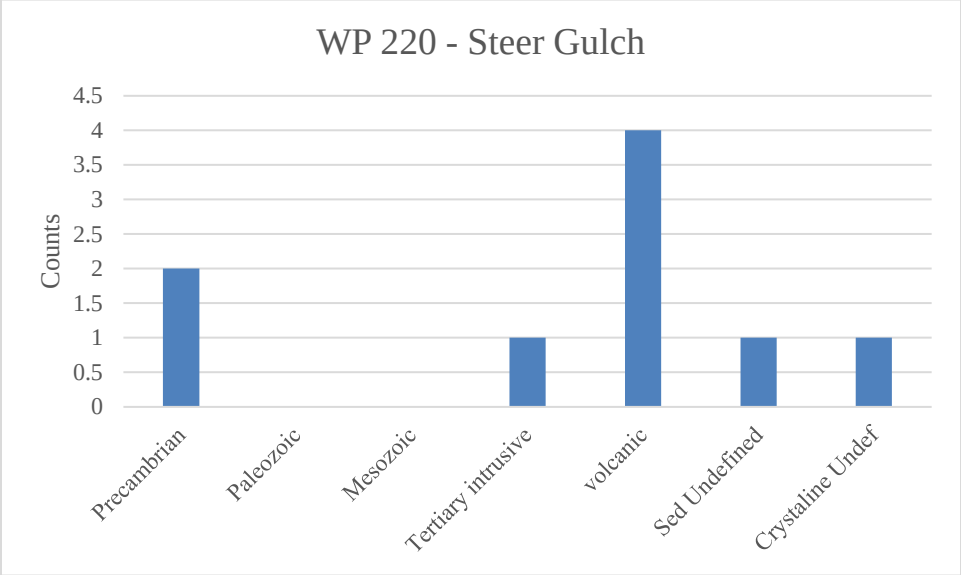
WP 220 - Steer Gulch
Counts
4.5
4
3.5
3
2.5
2
1.5
1
0.5
0
Precambrian
Paleozoic
Mesozoic
Tertiary intrusive
volcanic
Sed Undefined
Crystaline Undef

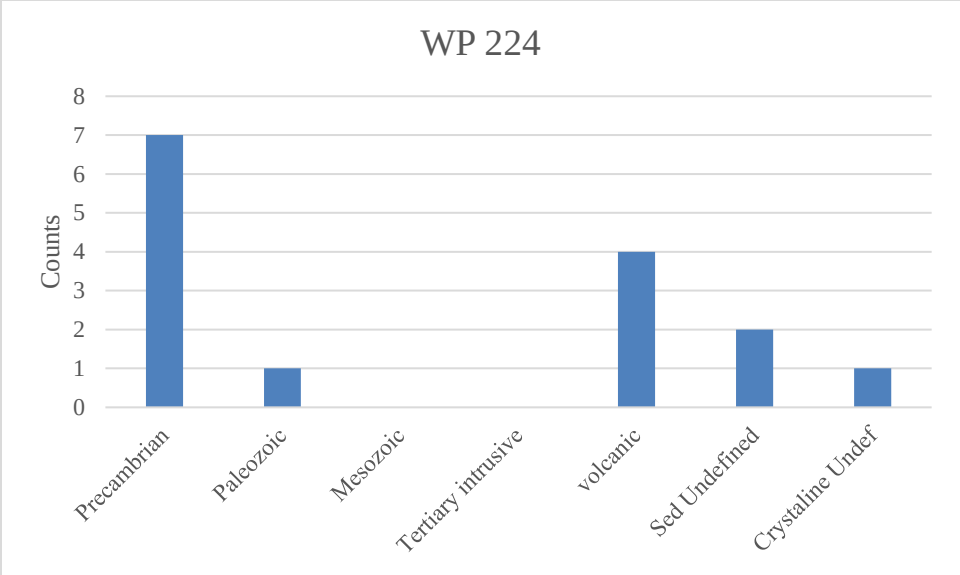

Statistics of stream-gravel analysis

TOTALS for Medial deposits (Palisades and Steers Gulch)	Count	%
Precambrian	17	35
Paleozoic	1	2
Mesozoic	0	0
Tertiary intrusive	2	4
volcanic	24	50
sed. Undefined	4	8
crystalline undefined	0	0
Sum	48	100

TOTALS for Distal (> 28 km from volcanic center)	Count	%
Precambrian	97	36
Paleozoic	16	6
Mesozoic	9	3
Tertiary intrusive	16	6
volcanic	74	27
Sed. Undefined	15	5
Crystalline Undefined	46	17
sum	273	100

APPENDIX E – Grain-Size Analysis

Raw and graphed data from dry sieving. Latitude and longitude data for way points are listed in Appendix A.

WP 220			
Sample weight(g)	Weight%	Phi	Wentworth-Size Classification
	0.0	-4	Pebble/cobble
56.5	7.5	-2	Pebble
140	18.5	-1	Granule
109.2	14.5	0	Very Coarse Sand
108.6	14.4	1	Coarse Sand
114.8	15.2	2	Medium Sand
89.9	11.9	3	Fine Sand
65.1	8.6	4	Very Fine Sand
71	9.4	>4	
755.1	100.0		

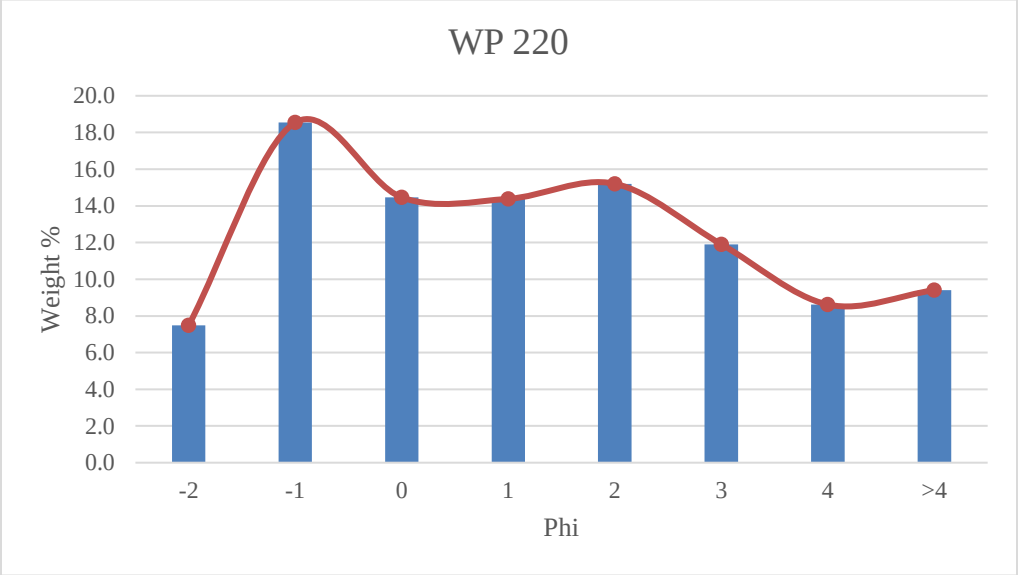

WP 0010			
Sample weight(g)	Weight%	Phi	Wentworth-Size Classification
	0.0	-4	Pebble/cobble
56.9	9.0	-2	Pebble
132.3	21.0	-1	Granule
91.8	14.6	0	Very Coarse Sand
75	11.9	1	Coarse Sand
82.3	13.1	2	Med. Sand
63.7	10.1	3	Fine Sand
49.3	7.8	4	Very Fine Sand
78.4	12.5	>4	
629.7	100.0		

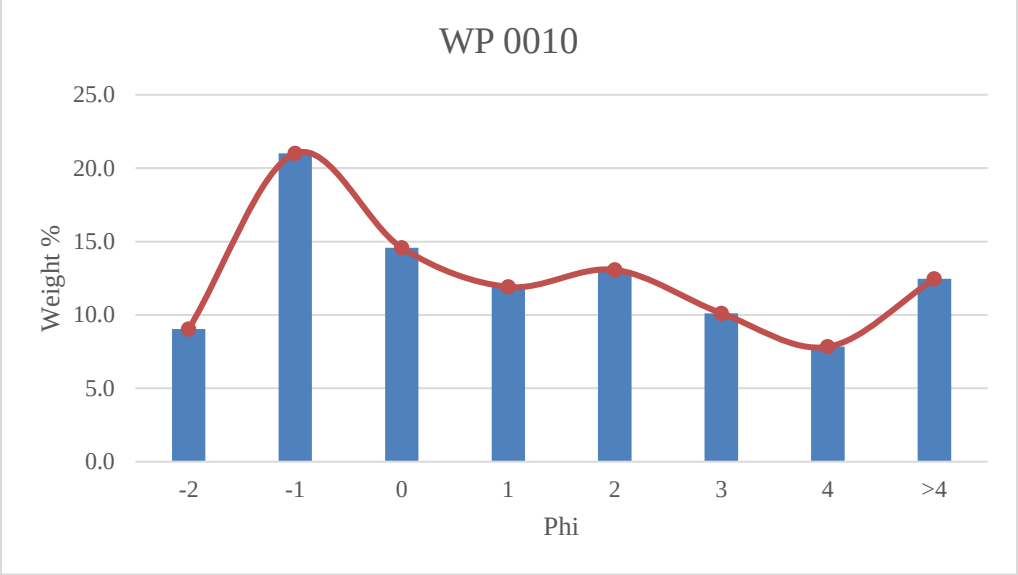

Castle Creek (38.740897°, -107.153728°)			
Sample weight(g)	Weight%	Phi	Wentworth-Size Classification
	0.0	-4	Pebble/cobble
113.8	16.8	-2	Pebble
207.4	30.7	-1	Granule
112.1	16.6	0	Very Coarse Sand
66	9.8	1	Coarse Sand
60.3	8.9	2	Medium Sand
39.5	5.8	3	Fine Sand
30.3	4.5	4	Very Fine Sand
46.9	6.9	>4	
676.3	100.0		

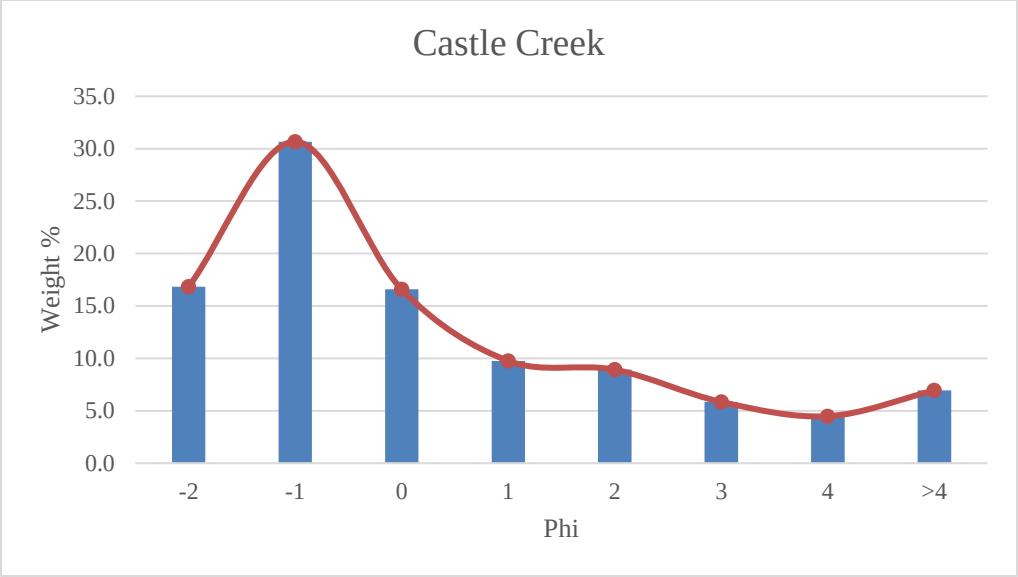

WP 0014 (Lost Canyon)			
Sample weight(g)	Weight%	Phi	Wentworth-Size Classification
	0.0	-4	Pebble/cobble
95.6	11.6	-2	Pebble
203.7	24.8	-1	Granule
131.2	16.0	0	V. Coarse Sand
93.2	11.4	1	Coarse Sand
92.1	11.2	2	Med. Sand
78	9.5	3	Fine Sand
57.8	7.0	4	V. Fine Sand
69.3	8.4	>4	
820.9	100.0		

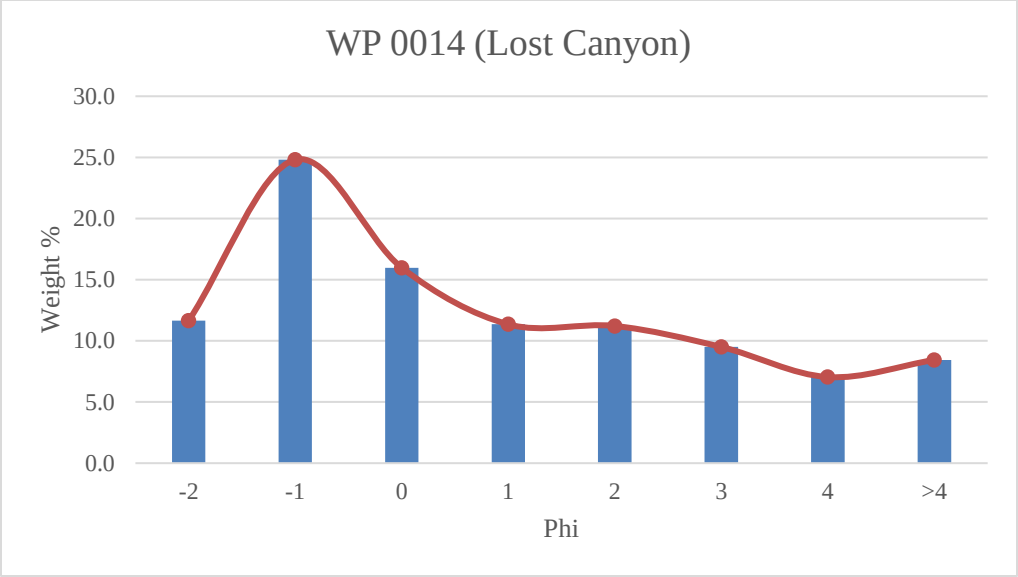

WP 223			
Sample weight(g)	Weight%	Phi	Wentworth-Size Classification
	0.0	-4	Pebble/cobble
34.3	8.7	-2	Pebble
90.7	23.0	-1	Granule
61	15.5	0	V. Coarse Sand
48.5	12.3	1	Coarse Sand
46.6	11.8	2	Med. Sand
37.1	9.4	3	Fine Sand
32.4	8.2	4	V. Fine Sand
43.2	11.0	>4	
393.8	100.0		

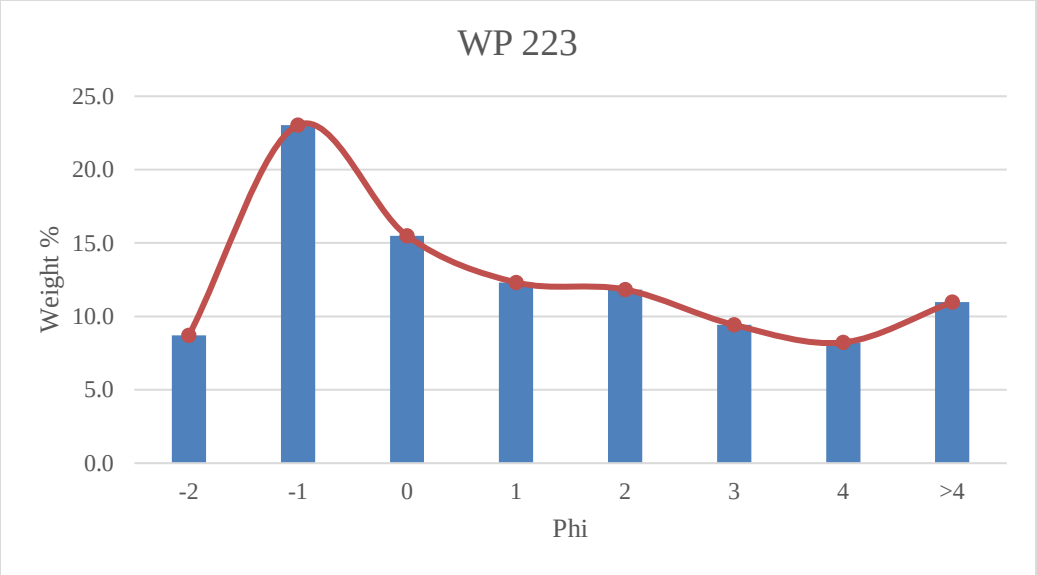

Coyote (38.544203°, -106.839576°)			
Sample weight(g)	Weight%	Phi	Wentworth-Size Classification
	0.0	-4	Pebble
35	7.7	-2	Pebble
80.4	17.8	-1	Granule
60.7	13.4	0	V. Coarse Sand
55	12.2	1	Coarse Sand
63.5	14.1	2	Med. Sand
51.5	11.4	3	Fine Sand
55.6	12.3	4	V. Fine Sand
50.1	11.1	>4	
451.8	100.0		

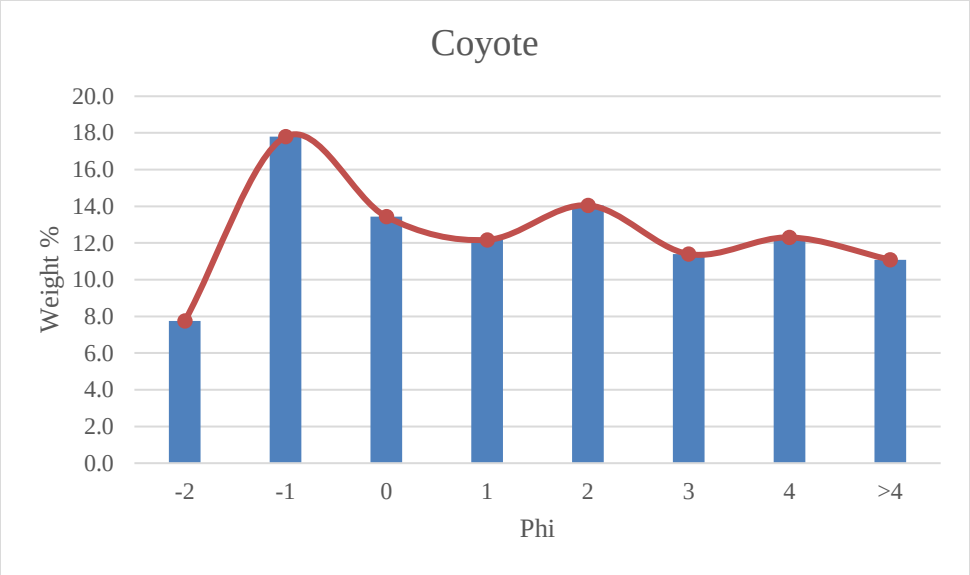

WP 0089 (Trailer Park)			
Sample weight(g)	Weight%	Phi	Wentworth-Size Classification
	0.0	-4	Pebble
18.5	8.3	-2	Pebble
45.3	20.4	-1	Granule
33.9	15.2	0	V. Coarse Sand
29.3	13.2	1	Coarse Sand
30.7	13.8	2	Med. Sand
9.7	4.4	3	Fine Sand
12.5	5.6	4	V. Fine Sand
42.5	19.1	>4	
222.4	100.0		

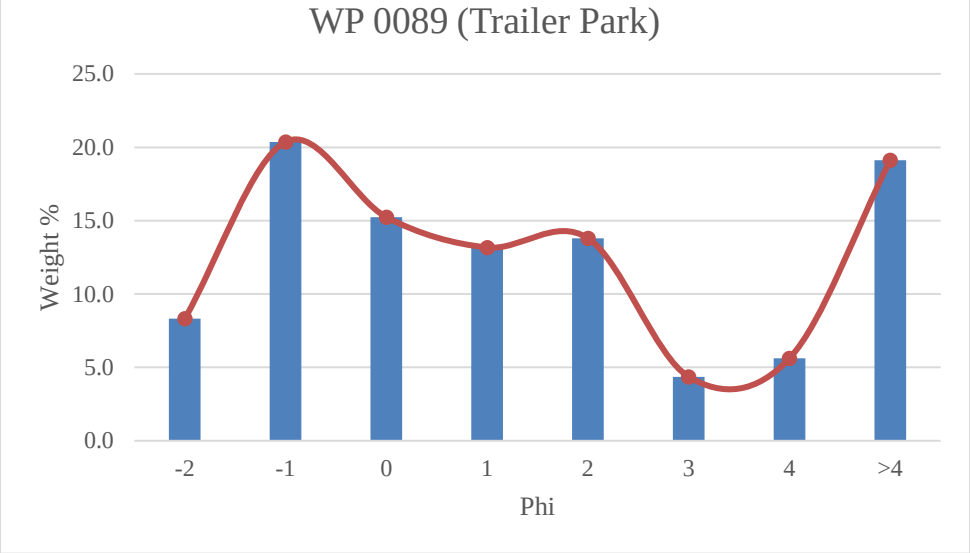

Samples below partially disaggregated with metal table spoon for 10 minutes. Samples above partially disaggregated with ultra-sonic homogenizer for 10 minutes.

Trailer Park (WP0089) -			
Sample weight(g)	Weight%	Phi	Wentworth-Size Classification
458.6	368.9	-4	Pebble
21.9	17.6	-2	Pebble
36.8	29.6	-1	Granule
16.7	13.4	0	Very Coarse Sand
10.2	8.2	1	Coarse Sand
9.2	7.4	2	Medium Sand
7.1	5.7	3	Fine Sand
7.1	5.7	4	Very Fine Sand
15.3	12.3	>4	
124.3	100.0		

WP 111			
Sample weight(g)	Weight%	Phi	Wentworth-Size Classification
	0.0	-4	Pebble
30	9.1	-2	Pebble
74.6	22.6	-1	Granule
50.1	15.2	0	V. Coarse Sand
36.9	11.2	1	Coarse Sand
39.5	12.0	2	Med. Sand
34.1	10.3	3	Fine Sand
26.6	8.1	4	V. Fine Sand
38.5	11.7	>4	
330.3	100.0		

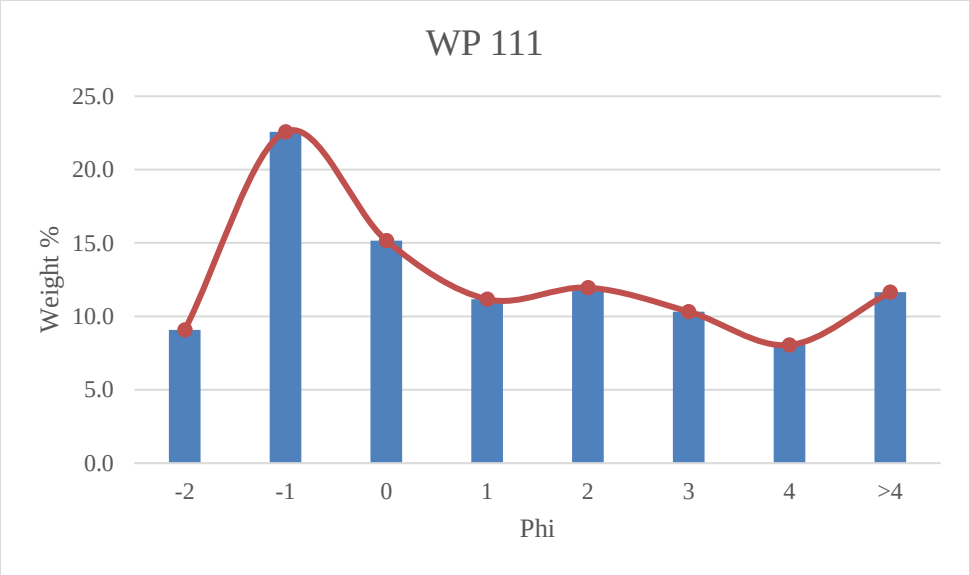

WP 227			
Sample weight(g)	Weight%	Phi	Wentworth-Size Classification
	0.0	-4	Pebble
25.5	6.8	-2	Pebble
71.5	19.2	-1	Granule
54.8	14.7	0	V. Coarse Sand
44.4	11.9	1	Coarse Sand
47.3	12.7	2	Med. Sand
43.3	11.6	3	Fine Sand
37.1	9.9	4	V. Fine Sand
49.2	13.2	>4	
373.1	100		

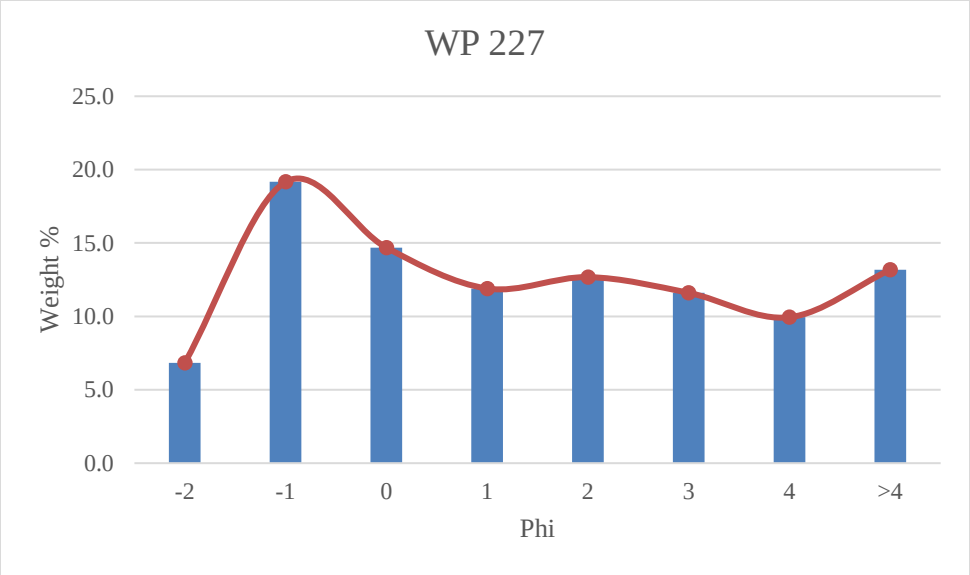

WP 0090			
Sample weight(g)	Weight%	Phi	Wentworth-Size Classification
	0.0	-4	Pebble
46.2	6.9	-2	Pebble
135.6	20.2	-1	Granule
106.6	15.8	0	V. Coarse Sand
86	12.8	1	Coarse Sand
90.4	13.4	2	Med. Sand
72.3	10.7	3	Fine Sand
54.4	8.1	4	V. Fine Sand
81.3	12.1	>4	
672.8	100		

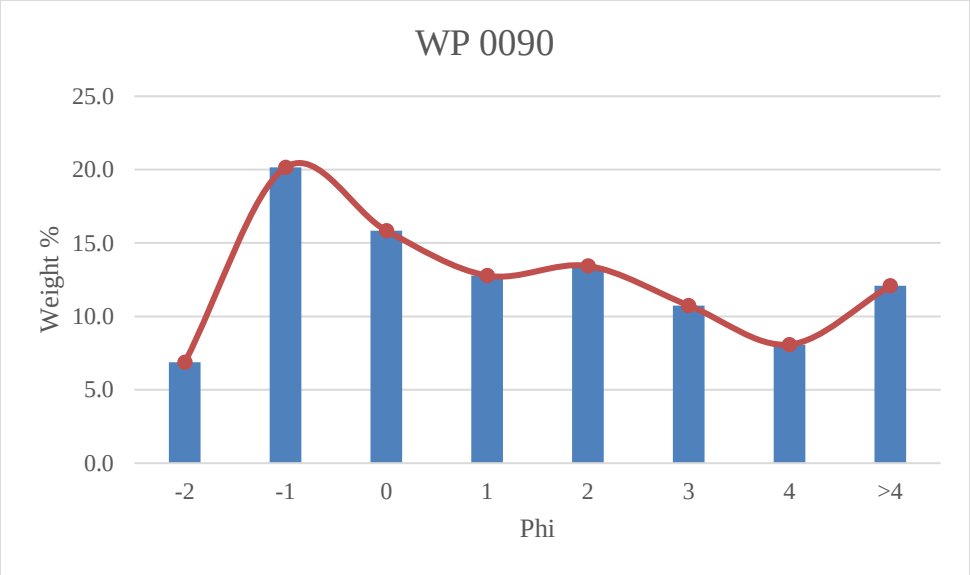

WP 0029			
Sample weight(g)	Weight%	Phi	Wentworth-Size Classification
	0.0	-4	Pebble
42.2	6.5	-2	Pebble
122.3	18.7	-1	Granule
97	14.8	0	V. Coarse Sand
89.5	13.7	1	Coarse Sand
89.5	13.7	2	Med. Sand
72.5	11.1	3	Fine Sand
56.3	8.6	4	V. Fine Sand
84.4	12.9	>4	
653.7	100		

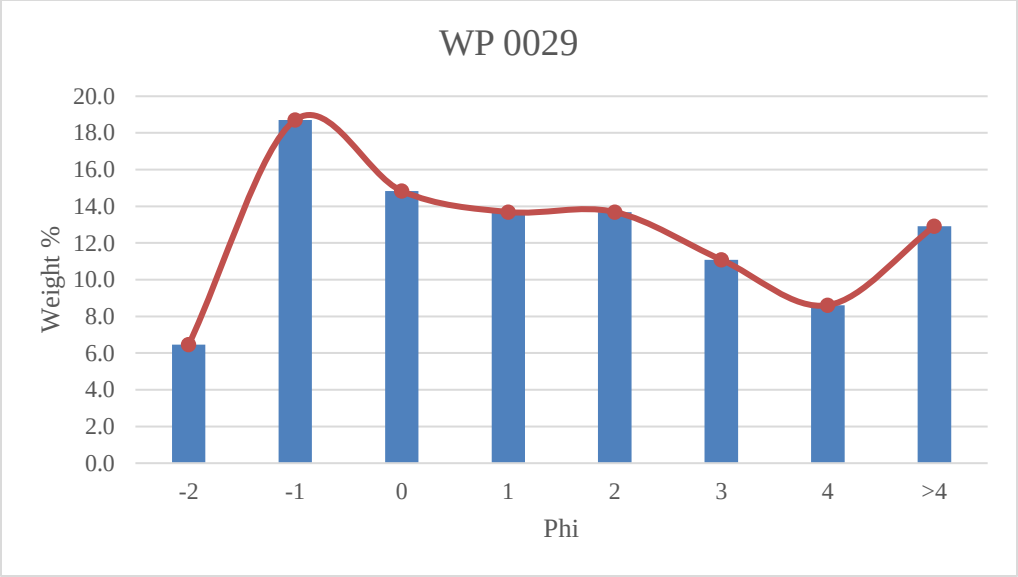

WP 217			
Sample weight(g)	Weight%	Phi	Wentworth-Size Classification
405.4	64.9	-4	Pebble
43.6	7.0	-2	Pebble
110.8	17.7	-1	Granule
95.5	15.3	0	V. Coarse Sand
96.2	15.4	1	Coarse Sand
90.8	14.5	2	Med. Sand
63.9	10.2	3	Fine Sand
48	7.7	4	V. Fine Sand
75.5	12.1	>4	
624.3	100.0		

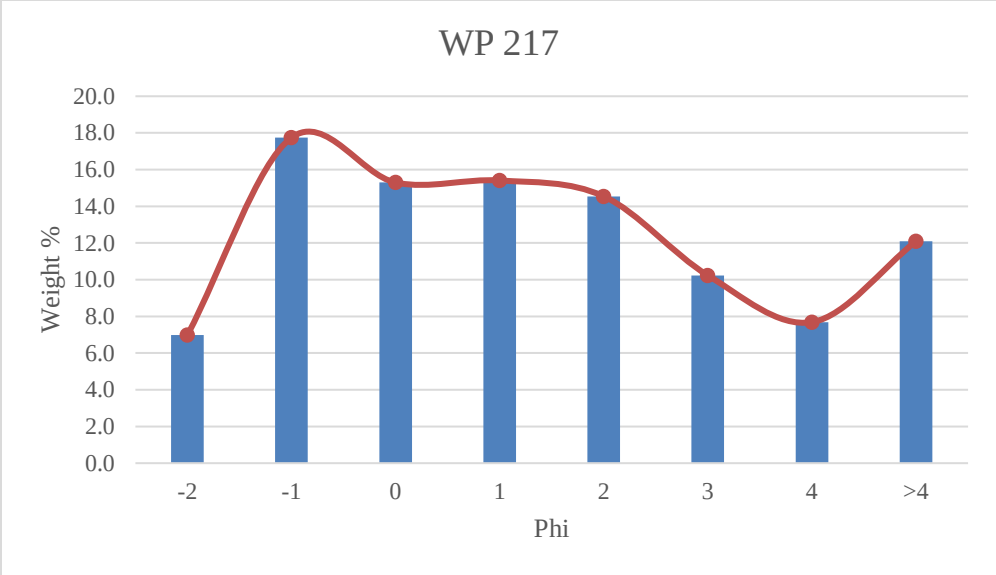

WP 164			
Sample weight(g)	weight%	Phi	Wentworth-Size Classification
405.4	107.2	-4	Pebble
34.4	9.1	-2	Pebble
87.3	23.1	-1	Granule
69.8	18.5	0	V. Coarse Sand
67.6	17.9	1	Coarse Sand
52.9	14.0	2	Med. Sand
28.4	7.5	3	Fine Sand
16.9	4.5	4	V. Fine Sand
20.9	5.5	>4	
378.2	100.0		

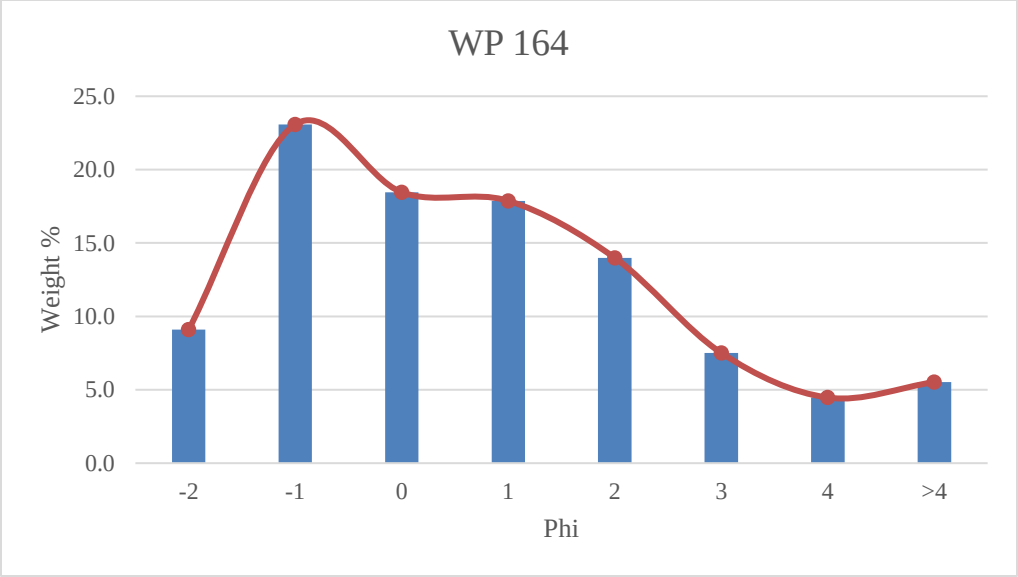

Alluvial Raft (WP 0090)			
Sample weight(g)	Weight%	Phi	Wentworth-Size Classification
192.6	63.5	-4	Pebble
13.6	4.5	-2	Pebble
38.9	12.8	-1	Granule
46.9	15.5	0	V. Coarse Sand
73.4	24.2	1	Coarse Sand
67	22.1	2	Med. Sand
29.5	9.7	3	Fine Sand
15.1	5.0	4	V. Fine Sand
18.8	6.2	>4	
303.2	100.0		

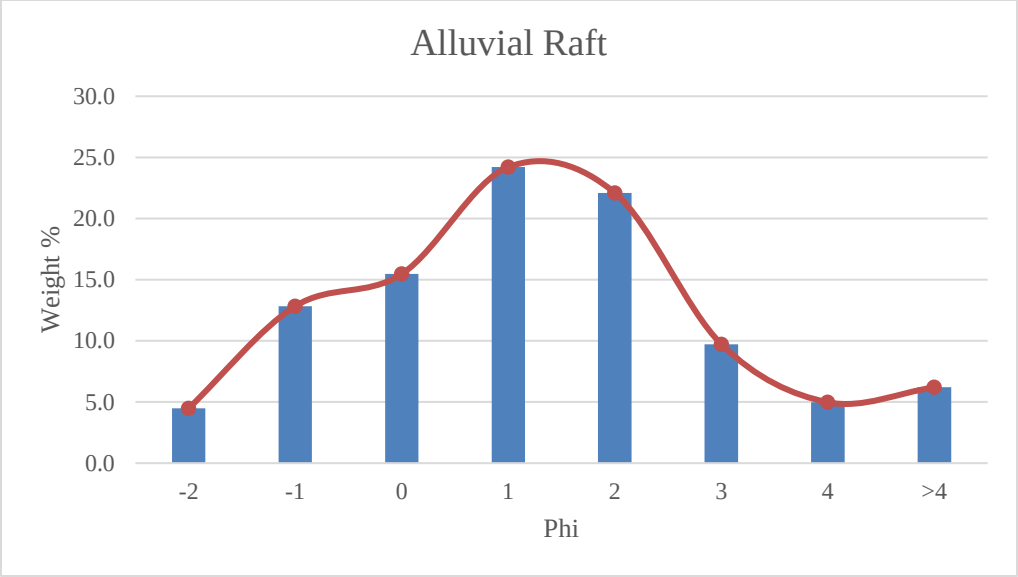

For data labeled 205A and 205B the only difference is the number of sieves used.

WP 205A			
Sample weight (g)	Weight %	Phi	Wentworth-Size Classification
	0	-4	Pebble
21.2	2	-2	Pebble
79.4	9	-1	Granule
107.6	13	0	V. Coarse Sand
140.1	16	1	Coarse Sand
173.1	20	2	Med. Sand
135.6	16	3	Fine Sand
90.4	11	4	V. Fine Sand
107.5	13	>4	
854.9	100		

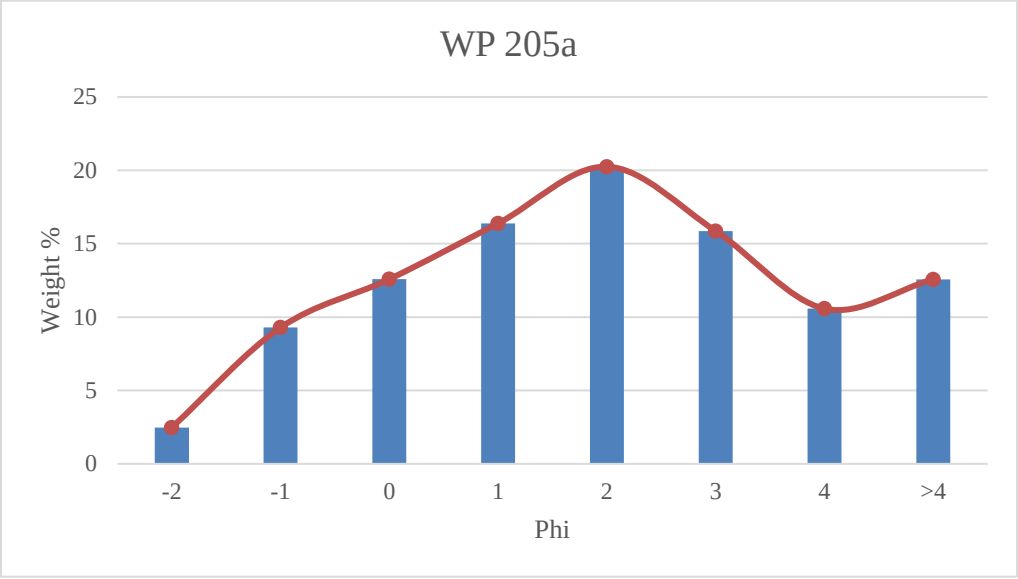

WP 205			
Sample weight	Weight %	Phi size	Wentworth-Size Classification
		-4	Pebble
26.9	6.242747737	-2	Pebble
25.6	5.941053609	-1.75	
16.6	3.852401949	-1.5	
18.7	4.339754003	-1.25	
21.8	5.059178464	-1	Granule
22.8	5.29125087	-0.75	
21.2	4.91993502	-0.5	
24.6	5.708981202	-0.25	
23.1	5.360872592	0	Very Coarse Sand
29.3	6.799721513	0.25	
29.3	6.799721513	0.5	
32	7.426317011	0.75	
24.8	5.755395683	1	Coarse Sand
35.5	8.238570434	1.25	
29.9	6.938964957	1.5	
25.1	5.825017405	1.75	
26.1	6.057089812	2	Medium Sand
27.3	6.3355767	2.25	
16.1	3.736365746	2.5	
20.9	4.850313298	2.75	
1	0.232072407	3	Fine Sand
37.4	8.679508006	3.25	
18.5	4.293339522	3.5	
11.5	2.668832676	3.75	
3.2	0.742631701	4	Very Fine Sand
13.7	3.17939197	4.25	
17.1	3.968438153	4.5	
31	7.194244604	<4.5	

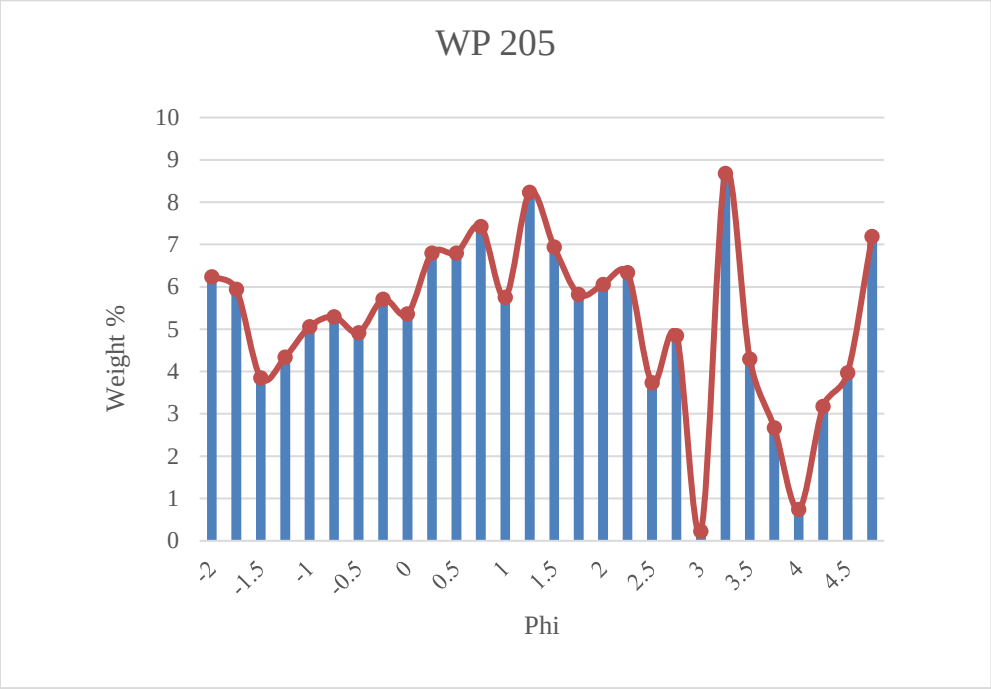
WP 205
Weight %
10
9
8
7
6
5
4
3
2
1
0
-2
-1.5
-1
-0.5
0
0.5
1
1.5
2
2.5
3
3.5
4
4.5
Phi

Sam-ple	Dis-tance (km)	σ (<4φ)	Sorting	Skew-ness	Skew	Kurto-sis	σ (include s > 4φ)	Sort-ing
205a	38.50	2.03	very poorly sorted	0.05	coarse skewed	2.38	3.10	very poorly sorted
Alluvi-al Raft	38.50	1.86	poorly sorted	0.31	strongly fine	3.05	2.70	very poorly sorted
164	39.70	2.02	very poorly sorted	0.56	strongly fine	2.89	2.30	very poorly sorted
217	27.80	2.30	very poorly sorted	0.29	fine	2.21	2.54	very poorly sorted
29	29.90	2.34	very poorly sorted	0.26	fine	2.09	2.73	very poorly sorted
90	38.50	2.33	very poorly sorted	0.32	strongly fine	2.12	2.82	very poorly sorted
227	29.00	2.38	very poorly sorted	0.21	fine	1.99	2.13	very poorly sorted
WP008 9 (“Traile r Park”)	38.00	2.55	very poorly sorted	0.37	strongly fine	1.97	2.58	very poorly sorted
111	30.00	2.40	very poorly sorted	0.36	strongly fine	2.09	1.89	poorly sorted
coyote	37.40	2.35	very poorly sorted	0.13	fine	2.02	2.32	very poorly sorted
223	25.50	2.36	very poorly sorted	0.40	strongly fine	2.15	1.99	poorly sorted
14	34.80	2.32	very poorly sorted	0.49	strongly fine	2.30	2.68	very poorly sorted
Castle Creek	8.26	2.25	very poorly sorted	0.83	strongly fine	2.91	2.13	very poorly sorted
10	34.66	2.41	very poorly sorted	0.32	strongly fine	2.08	2.58	very poorly sorted
220	26.40	2.24	very poorly sorted	0.24	fine	2.22	2.76	very poorly sorted

References

Atwood, W.W., and Atwood, W.R., 1926, Gunnison Tillite of Eocene Age: The Journal of Geology, Vol. 34, p. 612–622.

Baars, D. L., and Stevenson, G. M., 1981, Tectonic evolution of western Colorado and eastern Utah, *in* Western Slope Colorado: New Mexico Geological Society, 32nd, Field Conference Guidebook, p. 105–112.

Barton, M. A., 2010, Floral diversity and climate change in central Colorado during the Eocene and Oligocene [M.S. Thesis], Boulder, University of Colorado, 2911 p.

Bird, P., 1998, Kinematic history of the Laramide orogeny in latitudes 35–49 N, western United States: Tectonics, Vol. 17(5), p. 780–801.

Carrivic, J. L., 2011, Jökulhlaups: geological importance, deglacial association and hazard management: The Geologists' Association & The Geological Society of London, Geology Today, Vol. 27, No. 4, p. 133–140.

Cashion, W. B., 1967, Geology and fuel resources of the Green River Formation, southeastern Uinta basin, Utah and Colorado, USA: Geological Survey Professional Paper, Vol. 548, 48 p.

Chenoweth, W. L., 1982, The Hayden Survey in the Elk Mountains, Grand Junction Geological Society, Southern Piceance Basin Field Trip Guidebook, p. 95-97.

Chronic, H., and Williams, F., 2002, Roadside Geology of Colorado (second edition): Hong Kong, Mountain Press, 398 p.

Chronic, H., and Williams, F., 2014, Roadside Geology of Colorado (third edition): Hong Kong, Mountain Press, 416 p.

Coven, B., Panter K., and Stork A., 1999, Ar/Ar age of the West Elk Volcano, Gunnison and Delta Counties, Colorado (abs.): Geological Society America Abstracts with Program, Vol. 31, no. 7, p. 478

Crandell, D. R., 1989, Gigantic debris avalanche of Pleistocene age from ancestral Mount Shasta volcano, California, and debris-avalanche hazard zonation: U.S. Geological Survey Bulletin 1861, 32 p.

Crandell, D.R., Miller, C.D., Glicken, H.X., Christiansen, R.L., and Newhall, C.G., 1984, Catastrophic debris avalanche from ancestral Mount Shasta volcano, California: Geology, Vol. 12, p. 143–146.

Crossey, L.J., Karlstrom, K.E., Springer, A., Newell, D., Hilton, D., and Fischer, T., 2009, Degassing of mantle-derived CO2 and He from springs in the southern Colorado Plateau region: neotectonic connections and implications for groundwater systems. Geological Society of America Bulletin, Vol. 121, p. 1034–1053.

Davies, T., McSaveney, M., and Kelfoun, K., 2010, Runout of the Socompa volcanic debris avalanche, Chile: a mechanical explanation for low basal shear resistance: Bulletin of Volcanology, Vol. 72(8), p. 933-944.

Francis, P.W., and Self, S., 1987, Collapsing volcanoes: Scientific American, Vol. 278, p. 90–99.

Fillmore, R., 2011, Geological Evolution of the Colorado Plateau of Eastern Utah and Western Colorado, Including the San Juan River, Natural Bridges, Canyonlands,

Arches, and the Book Cliffs: Salt Lake City, Utah, U.S.A., University of Utah Press, 524 p.
Fisher, R. V., and Schmincke, H. U., 1984, Pyroclastic rocks: Berlin, Springer-Verlag, 472 p.
Gaskill, D.L., Mutschler, F.E., and Bartleson B.B., 1981, West Elk Volcanic Field, Gunnison and Delta Counties, Colorado, *in* Epis, R.C., and Callender, J.F., eds, Western Slope Colorado, Western Colorado and Eastern Utah: New Mexico Geological Society Thirty Second Field Conference Guide Book, p. 305-315.
Gaskill, D.L., Colman, S.M., Delong, J.E., and Robinson, C.H., 1986, Geologic map of the Crested Butte quadrangle, Gunnison County, Colorado: U.S. Geological Survey, Geologic Quadrangle Map GQ-1580, scale 1:24,000.
Gaskill, D.L., Delong, J.E., and Cochran, D.M., 1987, Geologic map of the Mt. Axtell quadrangle, Gunnison County, Colorado: U.S. Geological Survey, Geologic Quadrangle Map GQ-1604, scale 1:24,000.
Gaylord, D.R., and Neall, V.E., 2012, Subedifi ce collapse of an andesitic stratovolcano: The Maitahi Formation, Taranaki Peninsula, New Zealand. Geological Society of America Bulletin, Vol. 124, p. 181–199.
Glicken, H.X., 1996, Rockslide-debris avalanche of May 18, 1980, Mt. St. Helens volcano, Washington: U.S. Geological Survey Open-file Report 96–677, p. 90.
Hansen, W.R., 1965, The Black Canyon of the Gunnison: Today and yesterday: U.S. Geological Survey Bulletin 1191, 76 p.
Hayden, F.V., 1874, (seventh) Annual Report of the United States Geological and Geographical Survey of the Territories, Embracing Colorado: Being a report of progress of the exploration for the year 1873*:* US Government Printing Office, Washington, D.C., 718 p.
Hedlund, D.C., 1974, Geologic map of the Big Mesa quadrangle, Gunnison County, Colorado: U.S. Geological Survey Geologic Quadrangle Map GQ-1153, scale 1:24,000.
Hedlund, D.C., and Olson J.C., 1974, Geologic map of the Iris NW quadrangle, Gunnison and Saguache Counties, Colorado: U.S. Geological Survey Geologic Quadrangle Map GQ1134, scale 1:24,000.
Larsen, D., 2000, Upper Eocene and Oligocene lacustrine deposits of the southwestern United States with emphasis on the Creede and Florissant Formations, in E. H. Gierlowski-Kordesch and K. R. Kelts, eds., Lake basins through space and time: AAPG Studies in Geology, Vol. 46, p. 425–438.
Larsen, D., and Crossey, L.J., 2000, Sedimentary petrology and authigenic mineral distributions in the Oligocene Creede Formation, Colorado, United States, *in* Bethke, P.M., and Hay, R.L., eds., Ancient Lake Creede: Its Volcano-Tectonic Setting, History of Sedimentation, and Relation to Mineralization in The Creede Mining District: Geological Society of America Special Paper 346, p. 179–208.
Larsen, E. S., Jr and Cross, W., 1956, Geology and petrology of the San Juan region, southwestern Colorado: U.S. Geological Survey Professional Paper 258, 303 p.
Le Maitre et al., 2002, R.W. Le Maitre, A. Streckeisen, B. Zanettin, M.J. Le Bas, B. Bonin, P. Bateman, G. Bellieni, A. Dudek, S. Efremova, J. Keller, J. Lameyre, P.A. Sabine, R. Schmid, H. Sørensen, A.R. Woolley, Igneous Rocks: A

Classification and Glossary of Terms: Recommendations of the International Union of Geological Sciences (second edition): Subcommission on the Systematics of Igneous Rocks Cambridge University Press, Cambridge, England, 2002, 236 p.

Lipman, P. W., 1969, Alkalic and tholeiitic basaltic volcanism related to the Rio Grande depression, southern Colorado and northern New Mexico: Geol. Soc. America Bull., Vol. 80, p. 1343–1353.

Lipman, P.W., Doe, B., and Hedge, C., 1978, Petrologic evolution of the San Juan volcanic field, southwestern Colorado: Pb and Sr isotope evidence: Geological Society of America Bulletin, Vol. 89, p. 59–82.

Lipman, P. W., Prostka, H. J., and Christiansen, R. L., 1972, Cenozoic volcanism and plate-tectonic evolution of the western United States. I. Early and Middle Cenozoic: Philosophical Transactions of the Royal Society of London, Mathematical, Physical and Engineering Sciences, Vol. 271(1213), p. 217–248.

Lipman, P. W., Steven, T. A., and Mehnert, H. H., 1970, Volcanic history of the San Juan Mountains, Colorado, as indicated by potassiumargon dating: Geological Society of America Bulletin., Vol. 81, p. 2329–2352.

Malone, D.H., 1995, A very large debris-avalanche deposit within the Eocene volcanic succession of the northeastern Absaroka Range, Wyoming: Geology, Vol. 23, p. 661–664.

Naranjo, J.L., Sigurdsson, H., Carey, S.N. and Fritz, W., 1986. Eruption of Nevado del Ruiz volcano, Colombia, on 13 November 1985: Tephra fall and lahars, Science, Vol. 233 (4767), p. 961–963.

Nemec, W., And Steel, R. J., 1984, Alluvial and coastal conglomerates: Their significant features and some comments on gravelly mass flow deposits, *in* Koster E. H., and Steel R. J., eds., Sedimentology of Gravels and Conglomerates: Canadian Society of Petroleum Geologists Memoir 10, p. 1–31.

Obradovich, J. D., Mutschler, F. E., and Bryant, Bruce, 1969, Potassium-argon ages bearing on the igneous and tectonic history of the Elk Mountains and vicinity, Colorado—A preliminary report: Geologic Society of America Bulletin, Vol. 80, no. 9, p. 1749-1756.

Pierson, T. C., Janda, R. J., Thouret, J. C., and Borerro, C. A., 1990, Perturbation and melting of snow and ice by the 13 November 1985 eruption of Nevado del Ruiz, Colombia, and consequent mobilization, flow, and deposition of lahars: Journal of Volcanology and Geothermal Research, Vol. 41, p. 17–66.

Roverato, M., Cronin, S., Procter, J., and Capra, L., 2014, Textural features as indicators of debris avalanche transport and emplacement, Taranaki volcano: Geological Society of America Bulletin 127 (1-2), p. 3–18.

Schneider, J.L., and Fisher, R. V., 1998, Transport and emplacement mechanisms of large volcanic debris avalanches: evidence from the northwest sector of Cantal Volcano (France): Journal of Volcanology Geothermal Research, Vol. 83, p. 141–165.

Shreve, R. L, 1968, The Blackhawk landslide: Geological Society of America Special Papers 108, p. 1–48.

Siebert, L., 1984, Large volcanic debris avalanches: Characteristics of source areas, deposits, and associated eruptions: Journal of Volcanology and Geothermal Research, Vol. 22, p. 163–197.
Siebert, L., Glicken, H., and Ui, T., 1987,Volcanic hazards from Bezymianny- and Bandai-type eruptions: Bulletin of Volcanology, Vol. 49, p. 435–459.
Smith, G.A., 1991, Facies sequences and geometries in continental volcaniclastic sediments, *in* Fisher, R.V. and Smith, G.A., eds., Sedimentation in Volcanic Settings: SEPM, Special Publication 45, p. 109–122.
Smith, G.A., and Fritz,W. J., 1989,Volcanic influences on terrestrial sedimentation: Geology, Vol. 17, p. 375–376.
Smith, G. A., and Lowe, D. R., 1991, Lahars: Volcano-hydrologic events and deposition in the debris flow–hyperconcentrated flow continuum, *in* Fisher, R. V., and Smith, G. A., eds., Sedimentation in volcanic settings: Society for Sedimentary Geology (SEPM) Special Publication 45, p. 59–70.
Stoeber, M., and Filmore, R., 2003, The composition of modern Gunnison River Basin gravels, Gunnison County, Colorado: http://www.western.edu/academics/undergraduate/geology/geology-student-research (accessed accessed January 2017).
Stork, A., 2013, Paleogene Topography Of The Gunnison Area, Gunnison County, Colorado, Geological Society of America Meeting, Rocky Mountain Section, Vol.45, No. 5, p.8.
Stork, A., Coogan, J. C., Csar, A., and Wentz, R., 2006, Geologic Map of the Gunnison Quadrangle, Gunnison County, Colorado: Colorado Geological Survey, Open-File Report OF-06-04, scale 1:24,000.
Stork, A., Coogan, J. C., Fillmore, R., Brunkal, H., Nicolette, J., and Payton, A., 2007, Geologic Map of the Signal Peak Quadrangle, Gunnison County, Colorado: Colorado Geological Survey, Open-File Report OF-07-03, scale 1:24,000.
Tost, M., Cronin, S. J., Procter, J. N., Smith, I. E. M., Neall, V. E., and Price, R. C., 2015, Impacts of catastrophic volcanic collapse on the erosion and morphology of a distal fluvial landscape: Hautapu River, Mount Ruapehu, New Zealand: Geological Society of America Bulletin, Vol. 127 (1–2), p. 266–280.
Tweto, Ogden, Steven, T.A., Hail, W.J., and Moench, R.H., 1976, Preliminary geologic map of the Montrose 1 degree x 2 degrees quadrangle, northwestern Colorado: U.S. Geological Survey, Miscellaneous Field Studies Map MF-761, scale 1:250,000.
Ui, T., 1983, Volcanic dry avalanche deposits—Identification and comparison with nonvolcanic debris stream deposits: Journal of Volcanology and Geothermal Research, Vol. 18, p. 135–150.
Ui, T., and Glicken, H., 1986, Internal structural variations in a debris-avalanche deposit from ancestral Mount Shasta, California, USA: Bulletin of volcanology, Vol. 48(4), p. 189–194.
Ui, T., Takarada, S., and Yoshimoto, M., 2000, Debris avalanches, *in* Sigurdsson, H., Houghton, B., Rymer, H., and Stix, J., eds., Encyclopedia of Volcanoes: San Diego, California, Academic Press, 1389 p. 617–626.

Ui, T., Yamamoto, H. and Suzuki-Kamata, K., 1986, Characterization of debris avalanche deposits in Japan. Journal of Volcanology Geothermal Research, Vol. 29, p. 231-243.

Van Houten, F. B., 1957, Appraisal of Ridgway and Gunnison "Tillites," Southwestern Colorado: Geological Society of America Bulletin, Vol. 68(3), p. 383–388.

Vallance, J. W., 2000, Lahars. *in* Sigurdsson, H., Houghton, B., Rymer, H., and Stix, J., eds., Encyclopedia of Volcanoes: New York, New York, Academic Press, p. 601–616.

Vallance, J. W., and Scott K. M., 1997, The Osceola Mudflow from Mount Rainier: Sedimentology and hazard implications of a huge clay-rich debris flow: Geological Society of America Bulletin, Vol. 109(2), p. 143–163.

de Vries, B. V., and Francis, P. W., 1997, Catastrophic collapse at stratovolcanoes induced by gradual volcano spreading: Nature, Vol. 387(6631), p. 387–390.

Wadge, G., Francis, P. W., and Ramirez, C. F., 1995, The Socompa collapse and avalanche event: Journal of Volcanology and Geothermal Research, Vol. 66(1), p. 309–336.

Walton, A. W., and Palmer B. A., 1988, Lahar facies of the Mount Dutton Formation (Oligocene-Miocene) in the Marysvale volcanic field, southwestern Utah: Geological Society of America Bulletin, Vol. 100(7), p. 1078–1091.

Waresback, D. B., and Turbeville B., 1990, Evolution of a Plio-Pleistocene volcanogenic-alluvial fan: the Puye Formation, Jemez Mountains, New Mexico: Geological Society of America Bulletin, Vol. 102(3), p. 298–314.

Wentworth, C. K., 1922, A Scale of Grade and Class Terms for Clastic Sediments: The Journal of Geology, Vol. 30(5), p. 377–392.

Wolfe, J., and Schorn, H., 1989, Paleocologic, Paleoclimatic, and Evolutionary Significance of the Oligocene Creede Flora, Colorado: Paleobiology, Vol. 15(2), p. 180–198.

Wolfe, J. A., Forest, C. E., and Molnar, P., 1998, Paleobotanical evidence of Eocene and Oligocene paleoaltitudes in midlatitude western North America: Geological Society of America Bulletin, Vol. 110(5), p. 664–678.

Zernack, A.V., Procter, J.N., and Cronin, S.J., 2009, Sedimentary signatures of cyclic growth and destruction of stratovolcanoes: A case study from Mt Taranaki, New Zealand: Sedimentary Geology, Vol. 220, p. 288–305.

VITA

Patrick J. Whalen
Lexington, KY

EDUCATION

M.S. Geology: University of Kentucky – May 2017, Expected (GPA: 3.9)
Thesis Title: The Oligocene West Elk Breccia: Evidence for Massive Volcanic Debris Avalanches in the Eastern Gunnison River Valley, West-Central Colorado, USA
B.S. Geology: University of Kentucky, Department Honors (GPA: 3.1)

PROFESSIONAL EXPERIENCE

National Association of Geoscience Teachers Internship May–Aug. 2014
U.S.G.S, Cascade Volcano Observatory, Vancouver, Washington

PRESENTATIONS AND PUBLICATIONS

Whalen, P. J., and Ettensohn, F.E., 2016, Evaluating Pyroclastic Sedimentary Rocks: Examples from the Oligocene of Central Colorado: Geological Society of America Southeastern Section meeting, Abstracts with Programs Vol. 48, No. 3.

Whalen, P. J., and Ettensohn, F.E., 2016, The West Elk Breccia: Evidence of a Massive Volcanic Debris Avalanche in the Eastern Gunnison River Valley, West-Central Colorado, USA: Abstract V43E-3181 presented at 2016 Fall Meeting, AGU, San Francisco, California, 12–16 December.